

University of Alberta

Stepwise Activation of E–H (E = Si, Ge) Bonds at Adjacent Rhodium
and Iridium Centres

by

Md Hosnay Mobarok

A thesis submitted to the Faculty of Graduate Studies and Research in partial
fulfillment of the requirements for the degree of

Doctor of Philosophy

Department of Chemistry

©Md Hosnay Mobarok
Fall 2012
Edmonton, Alberta

Permission is hereby granted to the University of Alberta Libraries to reproduce single copies of
this thesis and to lend or sell such copies for private, scholarly or scientific research purposes only.
Where the thesis is converted to, or otherwise made available in digital form, the University of
Alberta will advise potential users of the thesis of these terms.

The Author reserves all other publication and other rights in association with the copyright in the
thesis and, except as herein before provided, neither the thesis nor any substantial portion thereof
may be printed or otherwise reproduced in any material form whatsoever without the author's
prior written permission.

Abstract

Transition metal-mediated E–H (E = Si, Ge) bond activation plays a pivotal role in industrially important processes, such as hydrosilylation and dehydrogenative coupling of organosilanes. Activation of these bonds by mono-metallic complexes is well studied, however, E–H bond activations in bimetallic complexes, especially complexes containing two different metals, and their subsequent reactivities, have been less well studied. This thesis probes the activation of Si–H and Ge–H bonds in a variety of organosilanes and organogermanes by bimetallic complexes involving Rh/Ir metal combination.

The second and third Chapters of this thesis explore the reactivity and mechanistic details of incorporation of multiple units of silicon- (Chapter 2) and germanium-containing (Chapter 3) functionalities in dppm-bridged (dppm = Ph₂PCH₂PPh₂) complexes of Rh/Ir via stepwise activation of Si–H and Ge–H bonds. A number of intermediates are characterized either *in situ* (by low-temperature NMR spectroscopy) or isolated during these transformations. The subsequent reactivity of one cationic germylene-bridged complex has also been demonstrated in Chapter 3.

A synthetic protocol is outlined in Chapter 4 for the selective incorporation of two different μ -silylene units, and the influence of the substituents and π -stacking interactions on the Si---Si distance (determined by X-ray crystallography) in this series and the implications related to the nature of the Si---Si interactions are discussed. By using a similar synthetic strategy a series of (μ -silylene)/(μ -germylene) complexes have also been synthesized.

Finally in Chapter 5, Si–H bond activations of silanes have been studied in a Rh/Ir complex bridged by an electronically rich and less-sterically hindered bridging ligand, depm (dep_m = Et₂PCH₂PEt₂).

Acknowledgements

First, I would like to thank my supervisor Professor Martin Cowie for being an excellent mentor and a great teacher throughout my Ph.D. research. Thanks Marty, for everything that you did for me during my stay in your laboratory.

I have been fortunate to work with a wonderful group of people during my time in the Cowie group: Matt Zamora, Lindsay Hounjet, Mike Slaney, Tiffany MacDougall, Rahul Samant and Kyle Wells. Thank you guys for your support and cooperation. Special thanks goes to Mike for making me familiar with Cowie chemistry during first few months.

Many thanks go to two exceptional crystallographers across the hall: Dr. Robert McDonald and Dr. Michael Ferguson for solving numerous crystal structures for this work. I also would like to thank Dr. Albin Otter, Mark Miskolzie and Nupur Dabral for their assistance and insights during numerous NMR studies.

I would like to thank Dr. Norman Gee and Dr. Jason Cooke for their helpful attitude during the teaching assistantship.

I am grateful to my friends Rashedul Islam, Shafiu Azam, Delwar shikder, Abu Kausar, Nikolai Sinkov, and Azizur Rahman for their support in various stage of my stay at university of Alberta. Specially, Ibrahim Al-Rafia, with whom I spent hours discussing chemistry, politics, philosophy and religion. Thanks Rafi for your stimulating company.

I am particularly indebted to my parents, Mr. Alam and Mrs. Alam, for all the contributions they made in my life. I am indebted to my wife Momataj for her

continuous support and encouragement throughout my Ph. D. study. I am also indebted to my beautiful daughter whose smile is enough to make my day.

Finally and foremost, I thank almighty Allah for His unbound blessings in my life.

Hosnay Mobarok
Edmonton

Table of Contents

Chapter 1 – Introduction.....	1
Section 1.1 – Organometallic Chemistry.....	1
Section 1.2 – Inorganometallic Complexes and Their Applications	2
Section 1.3 – Silicon and Germanium.....	7
Section 1.4 – Interactions of Silicon and Germanium with Transition Metals.....	10
Section 1.5 – Synthetic Routes to Metal-silicon and Metal-germanium Complexes.....	14
Section 1.6 – E–H Bond Activation at Transition Metals.....	16
Section 1.7 – Interactions of Silicon and Germanium with Bimetallic Complexes.....	19
Section 1.8 – Motivations for this Research.....	25
Section 1.9 – Objectives of this Thesis.....	29
Section 1.10 – References.....	32
Chapter 2 – Multiple Silicon–Hydrogen Bond Activations at Adjacent Rhodium and Iridium Centers....	40
Section 2.1 – Introduction.....	40
Section 2.2 – Experimental.....	42
Section 2.2.1 – General Comments.....	42
Section 2.2.2 – Preparation of Compounds.....	43
Section 2.3 – X-ray Data Collection and Structure Determination	59
Section 2.3.1 – General Considerations.....	59
Section 2.3.2 – Special refinement conditions.....	60
Section 2.4 – Results and Compound Characterization.....	62
Section 2.4.1 – Reactions of [RhIr(CO) ₃ (dppm) ₂] with Primary Silanes.....	62
Section 2.4.1.1 – Mono-silylene-bridged products.....	62
Section 2.4.1.2 – Bis-silylene-bridged products.....	72

Section 2.4.2 – Reactions of $[\text{RhIr}(\text{CO})_3(\text{dppm})_2]$ with Secondary Silanes.....	80
Section 2.4.3 – Reactions of $[\text{RhIr}(\text{CH}_3)(\text{CO})_2(\text{dppm})_2][\text{CF}_3\text{SO}_3]$ with Secondary Silanes.....	87
Section 2.5 – Discussion.....	94
Section 2.6 – Conclusions.....	99
Section 2.7 – References.....	99
Chapter 3 – Germyl and Germylene-bridged Complexes of Rh/Ir and Subsequent Chemistry of a Bridging Germylene Group.....	106
Section 3.1 – Introduction.....	106
Section 3.2 – Experimental.....	108
Section 3.2.1 – General Comments.....	108
Section 3.2.2 – Preparation of Compounds.....	109
Section 3.3 – X-ray Data Collection and Structure Determination	123
Section 3.3.1 – General Considerations.....	123
Section 3.3.2 – Special refinement conditions.....	124
Section 3.4 – Results and Characterization of Compounds.....	127
Section 3.4.1 – Reactions of $[\text{RhIr}(\text{CO})_3(\text{dppm})_2]$ with Primary and Secondary Germanes.....	127
Section 3.4.2 – Reactions of $[\text{RhIr}(\text{CH}_3)(\text{CO})_2(\text{dppm})_2][\text{CF}_3\text{SO}_3]$ with Primary & Secondary Germanes.....	141
Section 3.4.3 – Reactivity of the Cationic Germylene- Bridged Complex.....	146
Section 3.5 – Discussion.....	154
Section 3.6 – References.....	160

Chapter 4 – Mixed <i>Bis</i>(μ-Silylene) and (μ-Silylene)/(μ-Germylene) Complexes at a Rh/Ir Core: Influence of Substituent and π-Stacking Effects on the Si---Si Separation.....	165
Section 4.1 – Introduction.....	165
Section 4.2 – Experimental.....	170
Section 4.2.1 – General Comments.....	170
Section 4.2.2 – Preparation of Compounds.....	171
Section 4.3 – X-ray Data Collection and Structure Determination	180
Section 4.3.1 – General Considerations.....	180
Section 4.3.2 – Special refinement conditions.....	181
Section 4.4 – Results and Characterization of Compounds.....	182
Section 4.4.1 – Mixed <i>bis</i> (μ -silylene) Complexes.....	182
Section 4.4.2 – (μ -silylene)/(μ -germylene) Complexes.....	186
Section 4.5 – Discussion.....	189
Section 4.6 – References.....	195
Chapter 5 – Multiple Si–H Bond Activations in a Bis(diethylphosphino)methane-bridged Complex of Rh and Ir: Synthesis of an Unusual <i>Bis</i>(silyl)/(μ-silylene) Complex.....	200
Section 5.1 – Introduction.....	200
Section 5.2 – Experimental.....	202
Section 5.2.1 – General Comments.....	202
Section 5.2.2 – Preparation of Compounds.....	203
Section 5.3 – X-ray Data Collection and Structure Determination	209
Section 5.3.1 – General Considerations.....	209
Section 5.3.2 – Special refinement conditions.....	210
Section 5.4 – Results and Compound Characterization.....	211
Section 5.5 – Discussion.....	220
Section 5.6 – References.....	222

Chapter 6 – Conclusions.....	225
Section 6.1 – Concluding Remarks.....	225
Section 6.1.1 – Roles of metals in Si–H bond activation.....	225
Section 6.1.2 – Nature of Si--Si interaction.....	231
Section 6.1.3 – Ge–H bond activation.....	232
Section 6.1.4 –Effect of a bridging ligand on Si–H bond activation	236
Section 6.2 – Future directions.....	238
Section 6.3 – References.....	239
Appendices	241
Appendix I – For Chapter 2.....	242
Appendix II – For Chapter 3.....	251
Appnedix III – For Chapter 4.....	264
Appendix IV – For Chapter 5.....	276
Appendix V – Crystallographic Data.....	283
Appendix VI – Drying Agents for Solvents.....	284
Appendix VII – Acknowledgements.....	285

List of Tables

Chapter 2

Table 2.1.....	74
----------------	----

Appendix I

Table A.1 Crystallographic Experimental Details for Compounds 4 , 5 and 12	242
Table A.2 Crystallographic Experimental Details for Compounds 8a , 8b and 8c	243
Table A.3 Selected bond distances of 4	244
Table A.4 Selected bond angles of 4	244
Table A.5 Selected bond distances of 5 (molecule A).....	245
Table A.6 Selected bond angles of 5 (molecule A).....	245
Table A.7 Selected bond distances of 5 (molecule B).....	245
Table A.8 Selected bond angles of 5 (molecule B).....	246
Table A.9 Selected bond distances of 8c	246
Table A.10 Selected bond angles of 8c	246
Table A.11 Selected bond distances of 12	247
Table A.12 Selected bond angles of 12	247

Appendix II

Table A.13 Crystallographic Experimental Details for Compounds 20 , 21 and 23	251
Table A.14 Crystallographic Experimental Details for Compounds 24 , 25 and 28	252
Table A.15 Crystallographic Experimental Details for Compounds 29 , 30 and 31	253
Table A.16 Selected bond distances of 20	254
Table A.17 Selected bond angles of 20	254
Table A.18 Selected bond distances of 21	255
Table A.19 Selected bond angles of 21	255
Table A.20 Selected bond distances of 23	255

Table A.21 Selected bond angles of 23	255
Table A.22 Selected bond distances of 24	256
Table A.23 Selected bond angles of 24	256
Table A.24 Selected bond distances of 25	256
Table A.25 Selected bond angles of 25	256
Table A.26 Selected bond distances of 28	257
Table A.27 Selected bond angles of 28	257
Table A.28 Selected bond distances of 29	257
Table A.29 Selected bond angles of 29	257
Table A.30 Selected bond distances of 30	258
Table A.31 Selected bond angles of 30	258
Table A.32 Selected bond distances of 31	258
Table A.33 Selected bond angles of 31	258

Appendix III

Table A.34 Crystallographic Experimental Details for Compounds 34, 35 and 36	264
Table A.35 Crystallographic Experimental Details for Compounds 37 and 39	265
Table A.36 Crystallographic Experimental Details for Compounds 41 and 42	266
Table A.37 Selected bond distances of 34	267
Table A.38 Selected bond angles of 34	267
Table A.39 Selected bond distances of 35	267
Table A.40 Selected bond angles of 35	267
Table A.41 Selected bond distances of 36	268
Table A.42 Selected bond angles of 36	268
Table A.43 Selected bond distances of 37	268
Table A.44 Selected bond angles of 37	268
Table A.45 Selected bond distances of 39	269
Table A.46 Selected bond angles of 39	269

Table A.47 Selected bond distances of 41	269
Table A.48 Selected bond angles of 41	269
Table A.49 Selected bond distances of 42	270
Table A.50 Selected bond angles of 42	270

Appendix IV

Table A.51 Crystallographic Experimental Details for Compounds 48, 49 and 51	276
Table A.52 Selected bond distances of 48	277
Table A.53 Selected bond angles of 48	277
Table A.54 Selected bond distances of 49	277
Table A.55 Selected bond angles of 49	277
Table A.56 Selected bond distances of 51	278
Table A.57 Selected bond angles of 51	278

List of Figures

Chapter 1

Figure 1.1 Mechanism of metal-mediated olefin metathesis and two well-established catalysts for olefin metathesis.....	1
Figure 1.2 A nickel catalyst for the dehydrogenative polymerization of silanes.....	7
Figure 1.3 Different coordination modes of silicon to mono- and bimetallic complexes.....	10
Figure 1.4 Illustration of orbitals or orbital interactions in (a) free silylene (b) metal-silylene complex and (c) base-stabilized metal-silylene complex.....	11
Figure 1.5 Base-stabilized (a, b) and base-free (c, d) silylene and germylene complexes.....	12
Figure 1.6 Orbital interactions between silylene or germylene fragments in a bimetallic core.....	14
Figure 1.7 Sequential coordination of Si–H bond leading to oxidative cleavage.....	16
Figure 1.8 Crystallographically characterized examples of η^1 -silane and η^2 -silane complexes.....	17
Figure 1.9 Orbital interactions during Si–H bond activation in late transition metals.....	18
Figure 1.10 Examples of E–E interaction or E–E bond formation in a multimetallic core.....	20
Figure 1.11 Planar multimetallic core stabilized by bridging-silylene and -germylene ligands.....	21
Figure 1.12 A heterobimetallic Ti/Rh catalyst for the hydrosilylation of acetophenone.....	23
Figure 1.13 Complexes of interest for E–H bond activations.....	29
Figure 1.14 Steric differences between dppm and depm.....	31

Chapter 2

Figure 2.1 ^{31}P NMR spectra of complex 4	63
Figure 2.2 The metal-hydride region of the ^1H -NMR spectrum of complex 4	64
Figure 2.3 Molecular view of compound 5	66
Figure 2.4 Molecular views of compounds 8a and 8b	73
Figure 2.5 Molecular view of compound 8c	75
Figure 2.6 Molecular view of compound 12	83
Figure 2.7 Coupling constants of 10 and 11 obtained from spectral simulation of the $^{31}\text{P}\{^1\text{H}\}$ NMR spectra.....	86
Figure 2.8 ^1H -NMR resonance of the Si-H moiety for 15	90

Chapter 3

Figure 3.1 Molecular views of compounds 20 and of 21	132
Figure 3.2 Molecular view of compound 23	136
Figure 3.3 Molecular view of compound 24	138
Figure 3.4 Molecular view of compound 25	140
Figure 3.5 Molecular view of compound 28	142
Figure 3.6 $^1\text{H}\{^{31}\text{P}\}$ NMR spectra of high-field regions for complexes 26 and 27	144
Figure 3.7 Molecular view of compound 29	149
Figure 3.8 Molecular view of compound 31	153

Chapter 4

Figure 4.1 Molecular views of compounds 34 , 35 , 36 and 37	185
Figure 4.2 Molecular views of compound 39 , 41 and 42	189
Figure 4.3 Representations of the bis(μ -silylene) complexes showing the separation between the parallel aryl rings and of Si atoms.....	192

Chapter 5

Figure 5.1 Molecular view of compound 48	214
Figure 5.2 Molecular view of compound 49	216
Figure 5.3 Molecular view of compound 51	219

Appendix I

Figure A.1 Molecular views of compound 4	244
Figure A.2 ^1H -NMR spectrum of 4 at $-50\text{ }^\circ\text{C}$	248
Figure A.3 STD-NMR spectrum of complex 4 at $-50\text{ }^\circ\text{C}$	248
Figure A.4 Selected NMR spectra of compound 2 at $-80\text{ }^\circ\text{C}$	249
Figure A.5 $^{31}\text{P}\{^1\text{H}\}$ NMR of complex 8a and 8b	250

Appendix II

Figure A.6 Molecular view of the complex cation of 30	254
Figure A.7 Selected NMR spectra of compound 20	259
Figure A.8 $^{31}\text{P}\{^1\text{H}\}$ NMR spectra of Compound 21	259
Figure A.9 $^{31}\text{P}\{^1\text{H}\}$ NMR spectrum of Compound 23	260
Figure A.10 ^1H NMR spectrum of Compound 23	260
Figure A.11 $^{31}\text{P}\{^1\text{H}\}$ NMR spectrum of Compound 25	261
Figure A.12 ^1H NMR spectrum of Compound 25	261

Figure A.13 $^{31}\text{P}\{^1\text{H}\}$ NMR spectrum of Compound 28	262
Figure A.14 ^1H NMR spectrum of Compound 28	262
Figure A.15 Variable temperature $^{31}\text{P}\{^1\text{H}\}$ NMR and selected region of ^1H NMR spectrum of complex 29	263
Figure A.16 Hydride region of ^1H NMR spectrum of complex 29	263

Appendix III

Figure A.17 Selected NMR spectra for compound 34	271
Figure A.18 Selected NMR spectra for compound 35	272
Figure A.19 Selected NMR spectra for compound 36	273
Figure A.20 Selected NMR spectra for compound 37	274
Figure A.21 Selected NMR spectra for compound 38	275

Appendix IV

Figure A.22 Selected NMR spectra for compound 47	279
Figure A.23 Selected NMR spectra for compound 48	280
Figure A.24 Selected NMR spectra for compound 51	281
Figure A.25 Selected NMR spectra for compound 51	282

List of Schemes

Chapter 1

Scheme 1.1	3
Scheme 1.2.....	3
Scheme 1.3.....	4
Scheme 1.4.....	5
Scheme 1.5.....	15
Scheme 1.6.....	15
Scheme 1.7.....	16
Scheme 1.8.....	22
Scheme 1.9.....	22
Scheme 1.10.....	23
Scheme 1.11.....	24
Scheme 1.12.....	24
Scheme 1.13.....	25
Scheme 1.14.....	26
Scheme 1.15.....	26
Scheme 1.16.....	28

Chapter 2

Scheme 2.1.....	62
Scheme 2.2.....	70
Scheme 2.3.....	71
Scheme 2.4.....	72
Scheme 2.5.....	78
Scheme 2.6.....	78
Scheme 2.7.....	79
Scheme 2.8.....	80
Scheme 2.9.....	88

Scheme 2.10.....	95
------------------	----

Chapter 3

Scheme 3.1.....	128
Scheme 3.2.....	135
Scheme 3.3.....	137
Scheme 3.4.....	141
Scheme 3.5.....	147
Scheme 3.6.....	150
Scheme 3.7.....	151
Scheme 3.8.....	157

Chapter 4

Scheme 4.1.....	183
Scheme 4.2.....	187
Scheme 4.3.....	188
Scheme 4.4.....	191

Chapter 5

Scheme 5.1.....	211
Scheme 5.2.....	215

Chapter 6

Scheme 6.1.....	227
Scheme 6.2.....	228

List of Abbreviations and Their Meanings

Symbols	Meaning
{X}	decoupled-nucleus X
1D	one-dimensional
2D	two-dimensional
Å	Angström
Anal. Cald.	Analytical calculation
bp	Boiling point
BAr ^F ₄	tetrakis(3,5-bis(trifluoromethyl)phenyl)borate
BPh ₄	tetraphenylborate
<i>ca.</i>	approximately
COE	cyclooctene
dep _m	<i>bis</i> (diethylphosphino)methane
dpp _m	<i>bis</i> (diphenylphosphino)methane
Equiv	Equivalent
Et	ethyl
FT	Fourier transform
g	gram
gCOSY	gradient-enhanced correlation spectroscopy
gHMBC	gradient heteronuclear multiple bond correlation
gHMQC	gradient heteronuclear multiple quantum coherence
gHSQC	gradient heteronuclear single quantum coherence
h	hour
Hz	hertz
IR	infrared
kJ	kilojoule
Me	methyl
Mes	mesityl
mg	milligram

MHz	megahertz
min	minute
mL	millilitre
mmol	millimole
mol	mole
${}^nJ_{AB}$	n-bond AB coupling constant
NMR	Nuclear magnetic resonance
NOE	Nuclear Overhauser effect
°C	degree Celcius
ORTEP	Oak Ridge Thermal Ellipsoid Plot
OTf	triflate
Ph	phenyl
ppm	parts per million
RT	room temperature
s	second
SST	spin saturation transfer
STD	saturation transfer difference
${}^t\text{Bu}$	<i>tert</i> -butyl
<i>tert</i>	tertiary
THF	tetrahydrofuran
TMS	tetramethylsilane
vs.	versus
δ	partial charge or chemical shift in ppm
μ	micro
$\mu-$	bridging
ν_{AB}	A–B bond stretching frequency

Chapter 1

Introduction

1.1 Organometallic Chemistry

Transition metal (TM) complexes, by definition, contain a transition metal coordinated to a number of ligands through metal-element bonds, in which the elements are usually from the *p*-block of the Periodic Table. Organometallic chemistry is a sub-discipline of coordination chemistry in which metal-complexes contain metal-carbon (M-C) bonds. Organometallic complexes have a wide variety of applications in industry¹ as catalysts in processes such as olefin hydroformylation,² olefin polymerization,³ olefin metathesis,⁴ cross-coupling reactions,⁵ alkene hydrogenation,⁶ etc. For instance, industrially important olefin metathesis reactions are catalyzed by alkylidene complexes usually involving ruthenium, as in Grubbs' catalysts,^{4a} or molybdenum and tungsten as in the Schrock catalysts^{4b} (Figure 1.1), in which fragments of alkenes are redistributed by the scission and regeneration of the C=C bonds through a metallacyclobutane intermediate as shown in Figure 1.1.

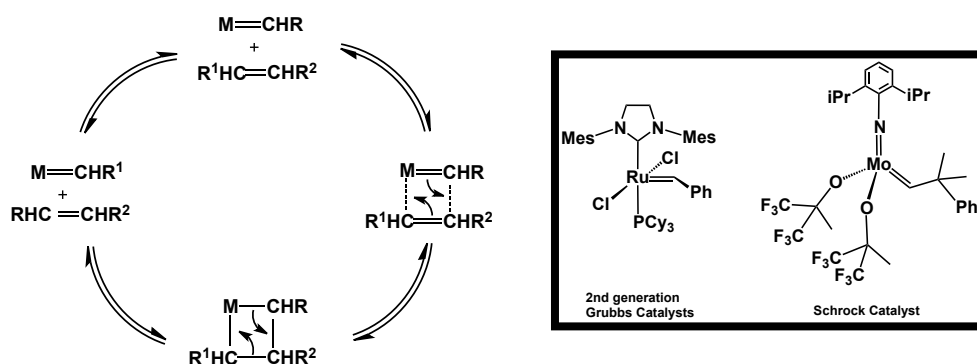


Figure 1.1: Mechanism of metal-mediated olefin metathesis (left) and two well-established catalysts for olefin metathesis (inset).

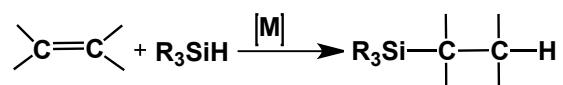
1.2 Inorganometallic Complexes and Their Applications

Other than M–C bonds, organometallic complexes also contain other M–E bonds (where E represents an element from the *p*-block, excluding carbon) in which these other groups generally act as ancillary ligands. In organometallic catalysts, ancillary ligands allow modulation of catalytic properties of a specific complex through fine-tuning of the electronic and steric parameters or by creating the necessary coordinative unsaturation for substrate activation and subsequent transformation based on the lability of these ligands. However, these ancillary ligands usually do not take part in the ensuing product transformations and thereby are dubbed “innocent” ligands. Phosphorus- and nitrogen-containing ligands, such as phosphines and amines, are ubiquitous as innocent ligands. However, E-containing ligands can also be non-innocent, taking an active part in transition-metal-mediated transformations.

The study of such interactions of main group elements (E) with transition metals (M) is a fascinating area of research and comprises an important class of compounds sometimes dubbed “*Inorganometallic complexes*”.⁷ These compounds (containing M–E bonds), although clearly different from organometallic species, nevertheless can play a similar role of active catalysts, particularly in transformations involving the *p*-block elements such as silicon, boron, etc.^{7,8a} In the same way that M–C bonds play a pivotal role in the chemistry of organic transformations, M–E bonds involving the heavier Group 14 elements are also important in a range of transformations involving these elements.^{8a}

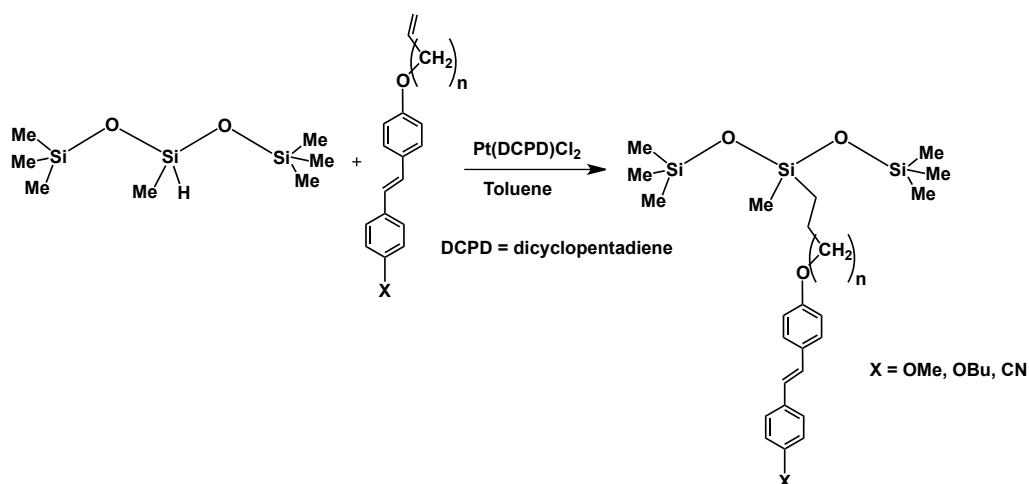
Compounds containing Group 14 elements (E = Si, Ge, Sn) bonded to transition metals have been widely investigated, as these complexes often give rise to unique reactivities in industrially important catalytic processes, such as in E–C and E–E bond-forming reactions.^{7,8} Metal catalyzed E–C bond formation, especially for E = Si, (known as hydrosilylation reaction when a Si–H bond is added across an unsaturated bond; Scheme 1.1) has attracted the most attention due to its importance in industry.⁹ For example, side-chain liquid-crystalline

Scheme 1.1



siloxanes, which are important in the electronics industry, due to their importance in the manufacture of displays for electronic devices, are prepared via the hydrosilylation of mesogens with methylhydrosiloxane as shown in Scheme 1.2.¹⁰

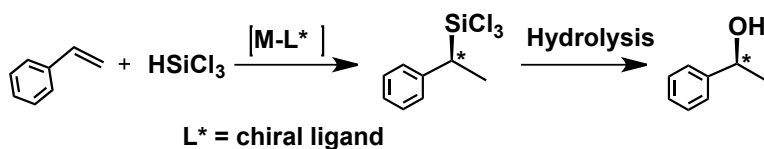
Scheme 1.2



Furthermore, catalytic asymmetric hydrosilylation is extensively used in organic synthesis for the generation of asymmetric centres (Scheme 1.3), which is particularly important in the synthesis of pharmaceuticals.^{9c} One of the big

advantages in this case is the availability of relatively simple methods for the removal of silyl groups from the organosilyl compounds to generate new derivatives.

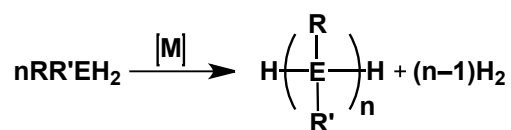
Scheme 1.3



Wilkinson and coworkers reported the first silicon-containing transition-metal complex, $[\text{Cp}(\text{CO})_2\text{FeSiMe}_3]$ in 1956.¹¹ The desire to understand the nature of the interaction between the metal and silicon or another heavier element as compared to a $\text{M}-\text{C}$ σ bond was the initial reason behind the synthesis of such complexes. Later, following the discovery of transition-metal catalyzed hydrosilylation of olefins,¹² a plethora of Si-containing metal complexes, ranging from early to late metals, were reported and many of these are effective in hydrosilylation.^{13,9a,9c} Although not as well studied as hydrosilylation, transition-metal catalyzed hydrogermylation (involving $\text{Ge}-\text{C}$ bond formation)¹⁴ and hydrostannylation (involving $\text{Sn}-\text{C}$ bond formation)¹⁵ are also known. Other reactions in this class ($\text{E}-\text{C}$ bond formation) include, dehydrogenative silylation (to produce a vinylsilane)¹⁶ and the addition of two Group 14 elements to carbon-carbon unsaturated substrates (known as double silylation, double germylation or double stannylation).^{8a}

The discovery of Group 4 metal-catalyzed dehydrogenative coupling of primary silanes to produce polysilanes, by Harrod *et al.*¹⁷ sparked investigation into a dehydrocoupling route for E–E bond formation to give polysilane, polygermane and polystannane compounds (Scheme 1.4). Unlike organic polymers, which contain mainly carbon backbones, heavier inorganic polymers

Scheme 1.4



containing group-14 elements as backbones have proven to be difficult to synthesize. The main reason is that stable unsaturated E=E species, analogues of the vinyl precursors to organic polymers, can be prepared only when sterically bulky substituents are present,^{17c,18} which understandably inhibits their polymerization.

Silicon–silicon, germanium–germanium, or tin–tin bond forming reactions are traditionally carried out by the reduction of element-halide bonds, such as in the Wurtz-type coupling, using alkali metals.^{17d} Although this procedure is prevalent in industry for the formation of small molecules and high-molecular weight polymers with Group 14 backbones, it suffers from many synthetic limitations such as: (1) functional group intolerance in the presence of highly reactive alkali metals; (2) problems with reproducibility, accompanied by a high percentage of cyclic oligomerization; (3) the formation of byproducts such as di- and polysiloxanes; and (4) potential hazards involved in the large-scale operation

of these processes. The development of catalytic processes for the formation of E–E bonds have been mainly driven by interest in high molecular-weight polymers having Si, Ge, or Sn backbones, for their chemical and electronic properties which result from electron delocalization through the σ -bond framework (also known as σ -conjugation) of the polymer backbone.^{17d} In addition, these Group 14-containing polymers are known to absorb in the ultraviolet spectral region, with absorption maxima dependent both on the main-chain substituents and on chain length, providing a route for fine-tuning the electronic properties of the materials. As a result, these materials have potential applications as photoconductors, photoresists in microelectronics, photoinitiators for radical reactions, and precursors to “SiC” ceramic materials.¹⁷

As mentioned above, the most promising catalysts to date for dehydrogenative coupling to generate E–E bonds are derivatives of Group 4 metallocenes.^{8b} In contrast, late transition-metal catalysts are generally sluggish in performing these transformations and produce substantial redistribution of substituents on silanes by competing Si–C bond activation at the metal centre.¹⁹ However, some recent investigations have shown that a few complexes involving late transition-metals can be effective for silane oligomerization and polymerization.²⁰ One such example was reported by Abu-Omar and coworkers in which the efficiency of a dinuclear nickel hydride complex (Figure 1.2) as a catalyst for the formation of polysilanes from primary and secondary silanes has been demonstrated.^{20a} Surprisingly, this catalyst produces polysilanes with molecular weights and “linear-to-cyclic polymer ratios” that are comparable to

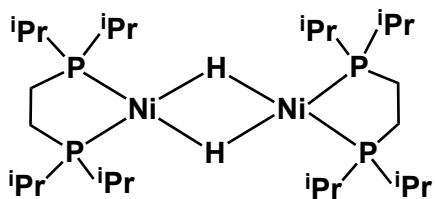


Figure 1.2: A nickel catalyst for dehydrogenative polymerization of silanes.

those obtained using Group 4 metallocene catalysts.

Silicon-containing transition-metal complexes have also been widely investigated for the generation of Si–O and Si–N bonds. Among the important reactions in this class are silane alcoholysis for the synthesis of alkoxy silanes – a reaction that provides a convenient method for the protection of hydroxyl groups in organic synthesis and for the synthesis of silyl ethers,²¹ hydrosilylation of carbonyl-containing compounds,²² and hydrosilylation of nitrogen-containing substrates such as nitriles,²³ and imines.²⁴ All of these reactions are most often catalyzed by late transition metals.

1.3 Silicon and Germanium

Among the “Group 14 element-transition metal” complexes, those containing Si have been most extensively studied owing to their industrial importance as mentioned above. In contrast, germanium- and tin-containing species are less frequently studied, presumably a result of the expense of the former and toxicity of the latter. As a result, our understanding of the bonding and reactivities of these main-group transition-metal complexes are based mainly on studies on silicon-containing metal analogues. An important factor favouring studies involving Si is the presence of the NMR-active ²⁹Si nucleus with a natural abundance of 4.67 %, which, despite having a negative gyromagnetic ratio, can

easily be detected in NMR spectroscopy by using different population transfer pulse sequences such as DEPT (distortionless enhancement by polarization transfer) or INEPT (insensitive nuclei enhanced by polarization transfer) if silicon is directly attached to a more sensitive nucleus such as hydrogen or fluorine.^{9b} A final advantage of Si chemistry is that silicon precursors, such as organosilanes, are inexpensive and readily available. In this work, we will focus on the coordination chemistry and reactivities of two of the Group 14 elements, silicon and germanium, with complexes containing two adjacent Rh/Ir centres, as will be explained in what follows.

Although as a Group 14 element, silicon is expected to have a reactivity similar to that of its lighter congener, carbon, these two elements, in fact, have very different reactivity patterns. Due to the electronegativity difference between carbon (2.5) and hydrogen (2.1), the C–H bond is more polarized toward carbon resulting in a protic hydrogen, whereas the lower electronegativity of Si (1.8) than hydrogen (2.1), results in a hydridic hydrogen in Si–H containing compounds. Silicon is also significantly larger than carbon as seen in the covalent radii of the two (Si : 1.17 Å and C: 0.77 Å) and one of the consequences of the larger size of silicon is its ability to support higher coordination numbers than carbon. Also, Si has more diffuse valence orbitals than carbon, which leads to poorer overlap especially during the formation of π -bonds. As a result, while unsaturated compounds of carbon (e.g., alkenes, alkynes, ketones) are common, reports of disilenes, the silicon analogues of alkenes, did not appear until 1981^{18a} while disilynes were first reported in 2004.^{18b} Although some donor-stabilized silanones

are known, stable silanones (containing Si=O moieties analogous to ketones), in the absence of donors such as N-heterocyclic carbenes, are still elusive.²⁵ The bond energy for a C–C bond (334 kJ/mol in CH₃–CH₃) is similar to a C–O bond (340 kJ/mole in Me₃C–OH), while the Si–O bond (536 kJ/mole in Me₃Si–OH) is significantly stronger than the Si–Si bond (308 kJ/mole in SiH₃–SiH₃) owing to the greater electronegativity difference between Si–O and C–O.^{8a,9b} This difference is obvious in the chemistry of silicon versus carbon compounds. While catenation (the ability to form a chain-like structure involving the same element via a series of covalent bonds) is a common occurrence in carbon chemistry, it is not the case for silicon. Si–Si bonds are more reactive (due to the availability of low-lying antibonding orbitals and the weaker Si–Si bond) than their C–C analogues and reluctant to form catenation products. Instead, polymers of silicon are predominantly comprised of Si–O chains owing to the strength of these bonds.²⁶ Carbon exhibits a maximum coordination number of 4 as dictated by the “Effective Atomic Number (EAN) Rule”. In contrast, Si often disobeys the EAN rule and exhibits coordination numbers higher than 4 in many cases. Although this behaviour was initially attributed to the use of vacant low-lying *d* orbitals, in which the involvement of *dsp*³ or *d*²*sp*³ hybrid orbitals allowed electron counts greater than that dictated by the EAN rule; more recent calculations show that *d* orbital involvement is not significant since these orbitals are too high in energy to contribute significantly in bonding. Instead, hypervalent silicon is better described by the formation of 3-centre molecular orbitals.^{26, 27}

The electronegativity (1.9) and size of germanium (1.22 Å) are not

significantly different from those of silicon. Like silicon, germanium can form hypervalent compounds and is reluctant to form catenation products due to the weaker Ge–Ge bond strength (188 kJ/mole). Compounds containing germanium-germanium multiple bonds, like their silicon counterpart, can also be synthesized by using bulky substituents.^{28a} Very recently the first stable germanone containing the Ge=O moiety has been reported.^{28b}

1.4 Interactions of Silicon and Germanium with Transition Metals

Silicon- and germanium-containing groups can coordinate to metals in a variety of coordination modes. Some of the commonly encountered fragments and their coordination modes in mono- and bimetallic complexes are shown below in Figure 1.3.¹³ When bonded to a single metal, silicon and germanium are most

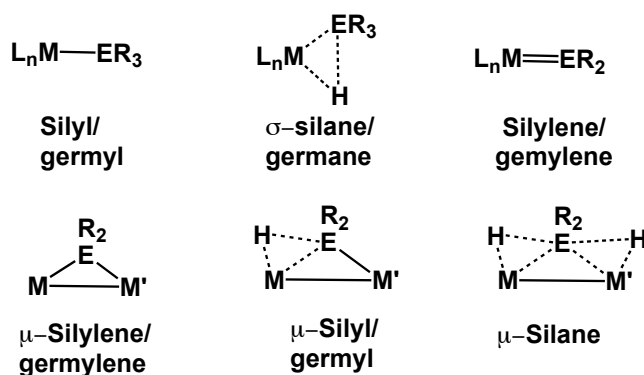


Figure 1.3: Different coordination modes of silicon to mono- and bimetallic complexes.

commonly found as *silyl* or *germyl*-type species, whereas in a bimetallic environment *silylene* or *germylene* units (bridging two metals) are more common. The silyl or germyl ligand-type is directly analogous to an alkyl group and is

considered formally as a two-electron donor having a charge of -1 . The less common coordination modes involving σ -silane, μ -silane and μ -silyl groups are the result of incomplete oxidative addition of Si–H bonds to the metal. In these coordination modes the E–H moiety forms a σ -complex to a metal, and this moiety is considered to be neutral, formally donating the 2 electrons from the E–H bond to the metal.

The silylene ($:\text{SiR}_2$) or germylene ($:\text{GeR}_2$) ligand is analogous to a carbene or alkylidene group. However, silylenes and germylenes show significantly different reactivity patterns than carbenes. While carbenes can exhibit either singlet ($\sigma^2\pi^0$) or triplet ($\sigma^1\pi^1$) ground-state electronic configurations, with very few exceptions silylenes or germylenes exhibit only a singlet electronic ground state, with an empty p orbital and a doubly occupied σ orbital (Figure 1.4a). Compared to carbon, the np valence electrons (in which, $n > 2$) in heavier Group 14 elements are energetically more separated from ns valence electrons (due to

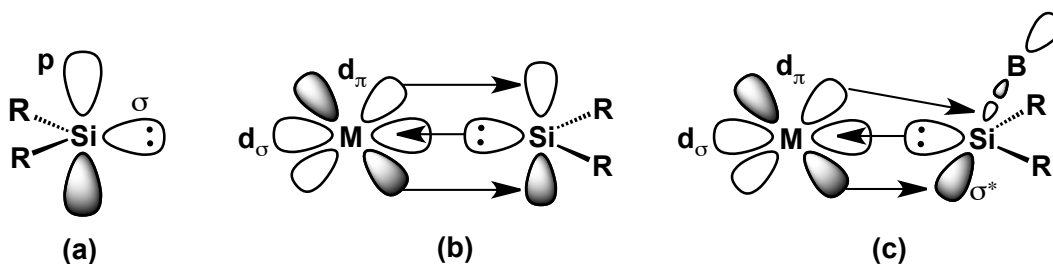


Figure 1.4: Illustration of orbitals or orbital interactions in (a) free silylene (b) metal-silylene complex and (c) base-stabilized metal-silylene complex.

Pauli repulsion with the $(n-1)p$ electrons in the inner shells). Therefore, hybridization is less likely between ns and np orbitals of heavier atoms. As a result, the singlet-triplet energy separation of carbenes is fairly low ($\Delta E_{s-t} \sim 11.2$

kcal/mole) while for the heavier analogues of carbenes this energy separation is remarkably high ($\Delta E_{s-t} \sim 21.0$ kcal/mole for silylene and $\Delta E_{s-t} \sim 23.0$ kcal/mole for germylene).²⁹ Due to the availability of the unoccupied p -orbital, silylenes or germylenes are more prone to react with Lewis bases, which can donate their free lone pair into the empty Si or Ge p orbital, while at the same time, the Si or Ge lone pair can donate to Lewis acids.³⁰ Theoretically this donor/acceptor interaction should lead to stable metal-silylene or metal-germylene complexes through a synergic σ -donor and π -acceptor interactions, in which the lone pair of electrons on silicon or germanium can be donated to the empty σ -symmetry metal orbital and back-donation from the filled $d\pi$ metal orbitals to the empty p orbital of the silylene or germylene to create a bonding pattern directly analogous to Fischer-carbenes (Figure 1.4b). However, until relatively recently, complexes containing terminal metal-silylene or metal-germylene interactions were rare, and were only stable in the presence of a coordinating base; these were referred to as “base-stabilized silylene or germylene complexes” (Figure 1.5a and 1.5b).^{31,32} This apparent instability of complexes containing a pure metal-element double-bond can be attributed to weaker back-donation (compared to the carbene

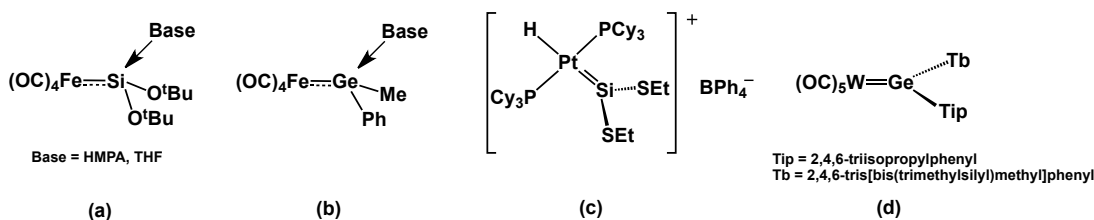


Figure 1.5: Base-stabilized (a,b) and base-free (c, d) silylene and germylene complexes.

complexes) from the $d\pi$ metal orbitals to the p orbital of the elements (Si or Ge) making the metal–element double bond strongly polarized toward the metal, $M^{\delta-} = E^{\delta+}$. As a consequence, silicon or germanium becomes highly electron-deficient and a coordinating base is required to stabilize these species (Figure 1.4c).³² In 1993, Tilley and coworkers reported the first base-free silylene complex (Figure 1.5c).³³ In the following year Okazaki and his group reported the first base-free germylene complex (Figure 1.5d).³⁴ In both cases steric bulk was introduced around Si and Ge to protect these centres from nucleophilic attack.

Silylene or germylene fragments are more stable when coordinated in a bridging fashion in bimetallic complexes (known as μ -silylene or μ -germylene complexes) and are much more commonly observed than their monometallic counterparts with a terminal metal–element double bond.^{13,35} This is in part because the electron-deficient silylene- or germylene-groups are more effectively protected in a bimetallic environment (by the ancillary ligands on the two metals) from nucleophilic attack. Although most of the silylene- or germylene-bridged complexes can be viewed as the replacement of two σ -bonded groups in organosilanes and organogermanes by transition-metal fragments, this is not necessarily suggestive that metal-element bonds in these complexes are just composed of sp^3 -hybridized silicon or germanium σ -bound to the two transition metals. In reality, μ -silylene or μ -germylene bimetallic complexes with accompanying metal-metal bonds possess very acute M–E–M angles (58° to 77°).^{13,35} As a result, a more appropriate representation of the interaction between silylene and germylene fragments with the bimetallic core involves σ - and π -type

orbital interactions between the sp^2 -hybridized silylene or germylene ligand and the symmetry adapted molecular orbitals of the bimetallic unit, shown in Figure 1.6. This description is supported by the spectroscopic and structural properties,

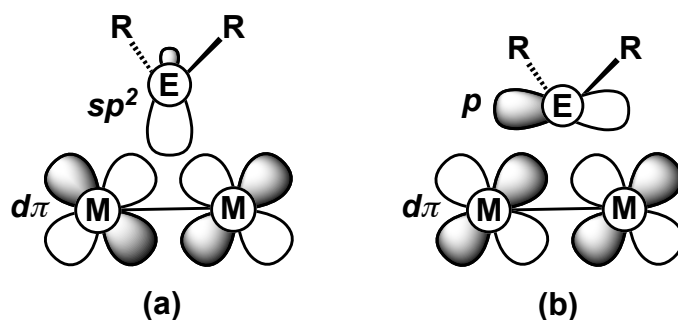


Figure 1.6: Orbital interactions between silylene or germylene fragments in bimetallic core.

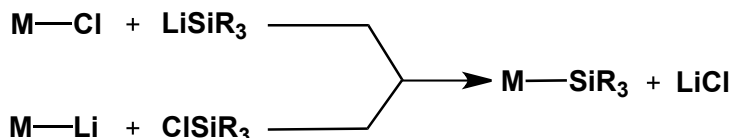
including the large downfield shift of the ^{29}Si NMR resonances of silylene ligands (although not as far downfield as is generally observed for mononuclear silylene complexes).^{31,35} However, silylene- and germylene-bridged bimetallic complexes without an accompanying metal-metal bond are generally accompanied by large M–E–M angles in which case silicon and germanium centres can be regarded as sp^3 -hybridized; as such they differ from terminal silylene or germylene complexes in having no low-lying empty p -orbital on the atom, rendering it less vulnerable to nucleophilic attack.³⁵

1.5 Synthetic Routes to Metal-silicon and Metal-germanium Complexes

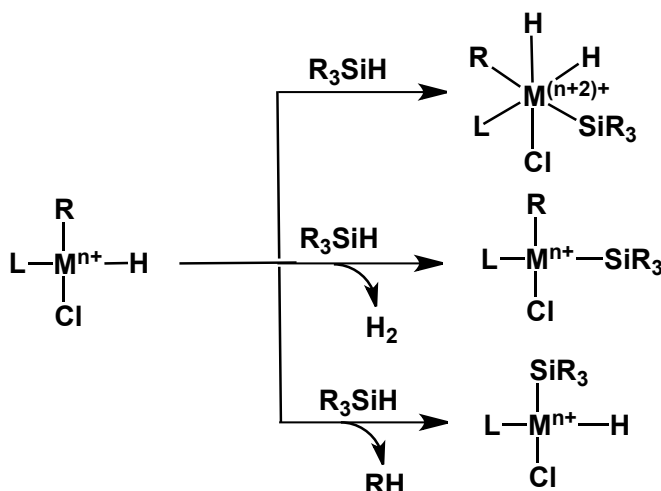
Although there are a variety of synthetic routes available for the preparation of complexes containing a metal-silicon bond, the two most commonly used routes involve: 1) salt elimination, in which either a silylmetallic reagent is

reacted with a metal halide (a transmetallation reaction) or an anionic metal species is reacted with a silicon halide (Scheme 1.5); and 2) the oxidative addition of Si–H bonds of an organosilane to a transition-metal centre (Scheme 1.6).¹³

Scheme 1.5



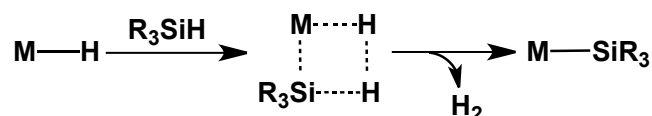
Scheme 1.6



Of these two methods, the latter has been more prominent, in which the complete cleavage of a Si–H bond results in an increase in the metal’s formal oxidation state. Often however, oxidative addition is accompanied by the elimination of small molecules such as H₂, CH₄, HCl, etc. from the metal, in which case the silicon-containing complex undergoes no overall change in oxidation state of the metal. Metal-silyl complexes can also be formed through metathesis between M–H and Si–H units (Scheme 1.7). This case is often

observed in early- transition metal complexes in high oxidation states in which

Scheme 1.7



the metal (usually d^0) cannot undergo oxidative addition.^{8c} Most germanium-containing metal complexes are prepared by similar salt-elimination or oxidative-addition pathways, similar to the methods noted above for the synthesis of metal-silicon complexes.³⁵

1.6 E–H Bond Activation at Transition Metals

Although silicon is a heavier analogue of carbon, the Si–H bond complexation to metals has a much closer resemblance to H–H bond coordination rather than to C–H bond complexation, so much so that a Si–H bond of a hydrosilane is sometimes described as a “fat” H_2 molecule.³⁶ Like H_2 , the interaction of silanes with a metal centre begins in a non-classical fashion in which the Si–H bond is not completely broken, but instead interacts with the metal in a side-on manner in which the unit donates two σ -electrons to the metal, generating a three-centre ($\text{M} \cdots \text{H} \cdots \text{Si}$) two-electron interaction (Figure 1.7).

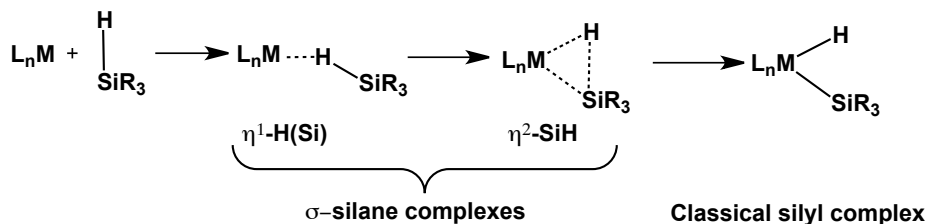


Figure 1.7: Sequential coordination of Si–H bond leading to oxidative cleavage.

However, the electronegativity difference between silicon and hydrogen, results in the non-classical interaction of silanes with a metal centre being somewhat different than that of dihydrogen. Since, hydrogen is more electronegative than silicon the bonding $\sigma(\text{Si-H})$ orbital is more localized on hydrogen while the antibonding orbital (σ^*) is more localized on silicon.³⁶ As a result, when a silane approaches a metal, the initial interaction is formed via the hydrogen atom of the Si-H bond in an η^1 -fashion (Figure 1.7), followed by pivoting of the Si-H bond around H to bring the silicon atom into closer proximity to the metal. Examples of η^1 -silane³⁷ and η^2 -silane³⁸ complexes are sketched in Figure 1.8.

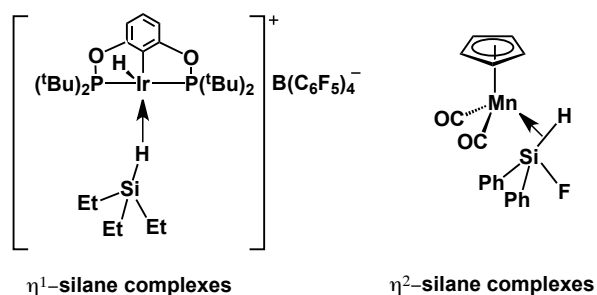


Figure 1.8: Crystallographically characterized examples of η^1 -silane and η^2 -silane complexes.

This bonding picture of H_2 or R_3SiH with a metal is analogous to the well-known Dewar-Chatt-Duncanson model,³⁹ was originally put forward to describe the bonding in metal-olefin complexes. In the case of a silane, donation from the occupied Si-H σ -bond into an empty metal orbital is accompanied by back donation from an occupied metal orbital into the Si-H σ^* orbital (Figure 1.9). Compared to dihydrogen, Si-H bonds are more basic with a higher energy Si-H

bonding orbital and a lower lying σ^* (Si–H) antibonding orbital, which consequently makes silanes better σ -donor to metals and also better π -acceptors.¹³

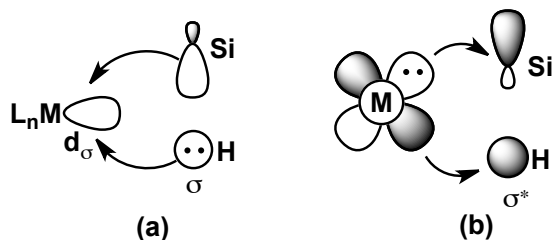


Figure 1.9: Orbital interactions during Si–H bond activation in late transition metals.

This factor makes the metal-promoted activation of Si–H bonds more facile than both C–H and H–H bond activation despite the comparable bond dissociation energies (350-430¹ kJ/mole for Si–H, 435 kJ/mole for H–H and 335-485¹ kJ/mole for C–H bond).^{13a} The strength of back-donation determines the fate of the Si–H unit, as related to its oxidative addition. In general, when the σ -donation from a Si–H bond is stronger, with minimal back-donation, a non-classical type of bonding mode prevails, whereas stronger π -back-donation from the metal to the antibonding Si–H orbital favours the complete cleavage of the Si–H bond, and the resulting oxidative addition yielding hydride and silyl groups on the metal. Another important factor that needs to be taken into consideration during the interaction of Si–H bonds with metals is the effect of substituents on silicon. Generally, electron-donating groups on silane increase the σ -donation from σ (Si–H) to the metal but decrease π -back-donation from the metal to σ^* (Si–H) orbitals

¹ Depends on the substituents

since both bonding and antibonding orbitals of Si–H go higher in energy in the presence of such groups. In contrast, electron-withdrawing substituents on silicon decrease σ -donation and increase back-donation components by stabilizing the energy of both the bonding and antibonding orbitals of the Si–H bond.³⁶ Since the extent of oxidative addition of a Si–H bond to the metal depends on the degree of back-donation from the metal, any factor that decreases this component will tend to favour the non-classical bonding mode.³⁶

1.7 Interactions of Silicon and Germanium with Bimetallic Complexes.

Inspired by the success of monometallic silicon- and germanium-containing complexes in a variety of chemical transformations, many bimetallic systems (mostly homobimetallic), containing these elements were developed in which the silicon- and germanium-containing fragments generally bridge both metals (Figure 1.3). Interest in such complexes has been largely triggered by the search for unique reactivity that might be achieved by the cooperative involvement of the adjacent metals. Cooperative bimetallic reactivity is an important phenomenon in inorganic chemistry,⁴⁰ and is based on the idea that two metals, when in close proximity, may interact in a cooperative manner to enable transformations that are either inaccessible or not easily accessible to single metal centres. Nature exploits a number of bimetallic protein complexes that carry out a unique set of catalytic transformations, few of which have been reproduced in nonprotein systems.⁴⁰ The knowledge of the metallic cores of enzymes has inspired coordination chemists to develop many biomimetic multimetallic complexes to study their subsequent reactivities.^{41, 42}

In the last two decades, a number of late transition-metal, multinuclear complexes containing silicon and germanium, in a variety of coordination modes, have been developed. In some cases, they have shown unusual bonding and reactivity patterns that are not commonly observed in monometallic complexes. For example, in 1988 Youngs and coworkers reported a number of silylene-bridged diplatinum systems that show silicon-silicon bonding interactions across the molecular square (Figure 1.10a).⁴³ The distance between the two silicon

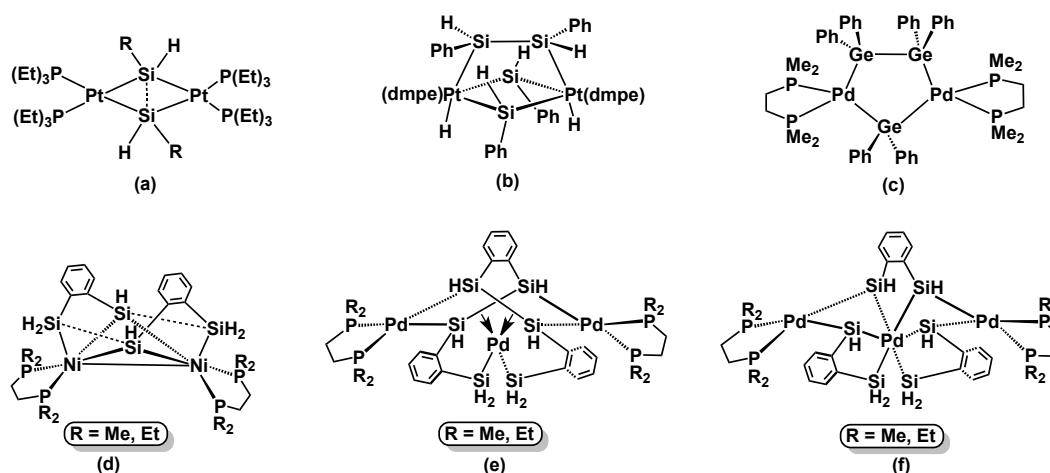


Figure 1.10: Examples of E–E interaction or E–E bond formation in multimetallic core.

atoms in these complexes was between 2.575(15) and 2.602(4) Å, this is well within the range observed for Si–Si single bonds (2.33–2.70 Å). Following this discovery, many other Pt₂ and Pd₂ systems were developed having similar Si–Si interactions.¹³ In 1993, Tilley and coworkers reported an unprecedented complex in which silicon–silicon bond formation was observed on a bimetallic (Pt₂) platform (Figure 1.10b).⁴⁴ In 2001, Tanaka and his group reported a

bis(silyl)/bis(μ -silylene) dinickel complex in which Si---Si bonding interactions between silicon atoms of the silyl and silylene units are implied, with distance of *ca.* 2.69 Å, which again compare quite well with the longest known Si–Si bonds (Figure 1.10d).⁴⁵ This structure can be viewed either as a stretched Si–Si σ -complex of a formal nickel(I) complex, or alternatively, as having an incipient Si–Si bond on a nickel (III) centre. This finding was followed by a fascinating synthesis of a tripalladium compound which can support the first true Si–Si σ -complex (Figure 1.10e).⁴⁶ The central core of this complex has six Si atoms in the coordination sphere of a central Pd(II) centre, which can be alternatively pictured as a Pd^{VI} complex (Figure 1.10f).⁴⁷ However, the average Si–Si bond separation in this complex (2.539(4) Å) together with a computational study suggest that this structure resembles Figure 1.10e instead of 1.10f. Germanium-germanium bond formation is also observed on a binuclear palladium platform. (Figure 1.10c).⁴⁸ In addition, recent investigations demonstrate the ability of bridging silylene and germylene ligands to stabilize an unusual planar multimetallic core (Figure 1.11), in which the three Si or Ge nuclei and the four Pd centres are coplanar.⁴⁹

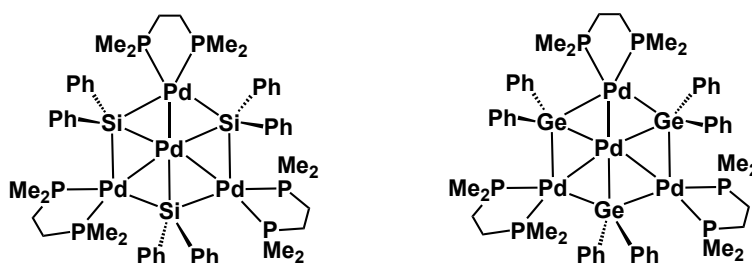
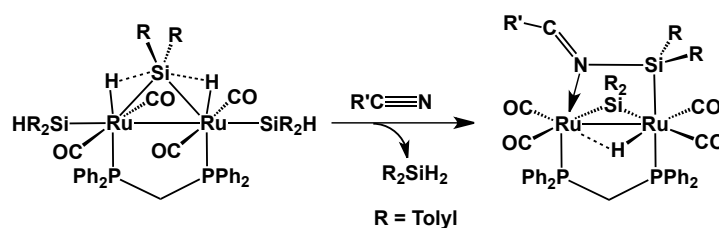


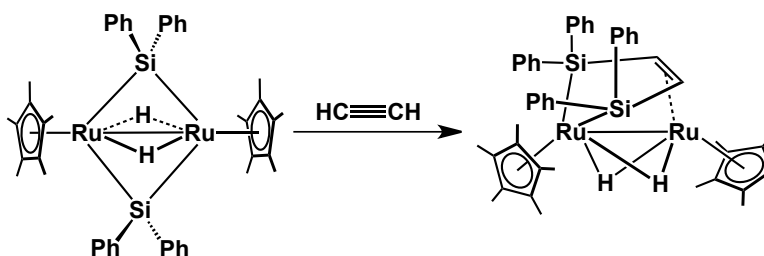
Figure 1.11: Planar multimetallic core stabilized by bridging-silylene and -germylene ligands

Not only can these bimetallic silylene or germylene-bridged complexes stabilize unusual bonding modes (as shown above) they can also act as catalysts in hydrosilylation and in the dehydrogenative polymerization of organosilanes. Kira and coworkers demonstrated stoichiometric hydrosilylation of nitriles (Scheme 1.8) and catalytic hydrosilylation of imines and ketones by a silyl-bridged diruthenium catalyst.⁵⁰ Suzuki and coworkers showed the insertion of alkynes into a M–Si bond in a bis(silylene)-bridged dinuclear ruthenium complex (Scheme 1.9).⁵¹ Later, Moïse and coworkers demonstrated the efficacy of an early-late

Scheme 1.8



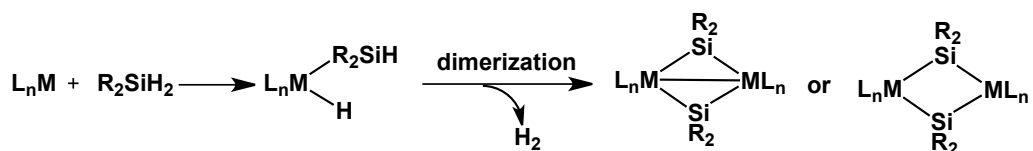
Scheme 1.9



heterobimetallic Rh/Ti complex (Figure 1.12) in catalyzing the hydrosilylation of acetophenone with diphenylsilane.⁵² A weak bonding interaction between rhodium and a titanium-bound Cl is thought to be responsible for the stabilization of a lower-valent intermediate such that the bimetallic complex delivers a much

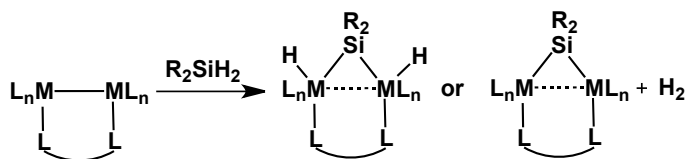
a Si–H or Ge–H bond of the organosilane or organogermane precursors can oxidatively add to a monometallic complex to produce a metal-silyl or metal-germyl intermediate followed by dimerization in which a second Si–H or Ge–H bond of the silyl or germyl group oxidatively adds to second metal fragment (Scheme 1.11); or 2) double oxidative addition of Si–H or Ge–H bonds to a

Scheme 1.11



preorganized bimetallic complex (Scheme 1.12). The bimetallic complexes generated from these reactions can either have an accompanying metal-metal bond or not. Less commonly used reactions to generate silylene- or germylene-

Scheme 1.12

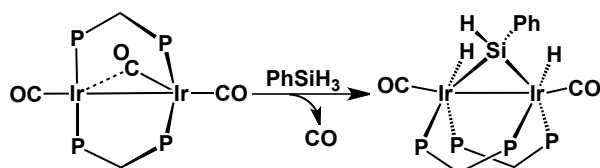


bridged complexes include, direct addition of stable silylenes or germynes to bimetallic complexes, oxidative addition of Si–X bonds ($X \neq H$) and the salt elimination method (reaction of metal halide species with silylmetallic reagents).³⁵

1.8 Motivations for this Research

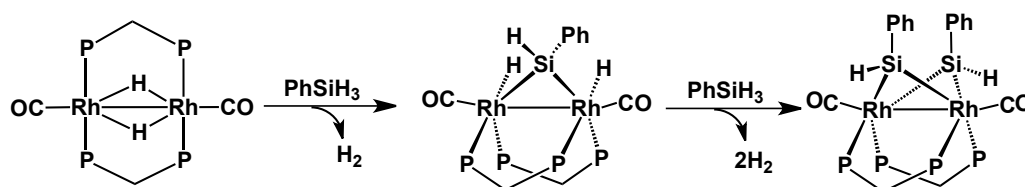
Homobinuclear late-metal complexes have played a dominant role in the chemistry of silylene- and germylene-bridged complexes, however, studies involving their heterobimetallic analogues are few.^{13,35} For example, our research group has investigated the reactivity of Si–H bonds of primary and secondary organosilanes with a dppm-bridged diiridium-tricarbonyl complex (dppm = Ph₂PCH₂PPh₂),⁵⁴ whereas Eisenberg and co-workers carried out similar reactivity studies with a related dirhodium-dihydride complex.⁵⁵ Although both studies showed some similarities they also pointed out some substantial differences in the reactivity patterns in these two homobimetallic complexes. For instance, the diiridium complex activates only one equivalent of primary silane to give a mono(silylene)-bridged diiridium dihydride complex (Scheme 1.13), even in the presence of excess silane under forcing conditions.⁵⁴ In contrast, the dirhodium

Scheme 1.13



system readily yields the exact analogue of the above silylene-bridged Ir₂ product in reaction with one equivalent of primary silanes but reacts further with additional silane to give a bis(silylene)-bridged complex (Scheme 1.14).⁵⁵ This difference in reactivity can be attributed to the greater Ir–ligand bond strengths which prevent the mono(silylene)-bridged, diiridium-dihydride complex from

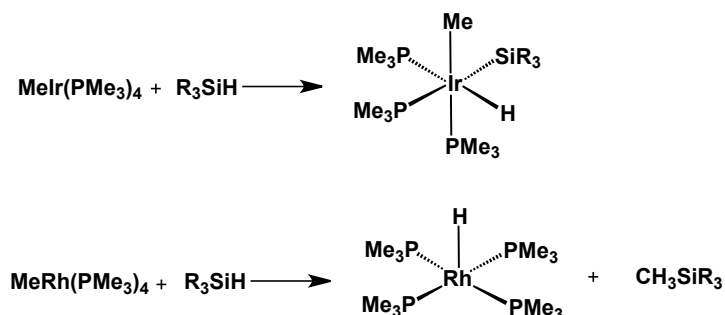
Scheme 1.14



attaining the necessary coordinative unsaturation to react with the second equivalent of silane. In contrast, the greater lability of Rh allows the Rh₂ analogue to achieve the necessary unsaturation.

Such differences in reactivity between Rh and Ir are also evident in monometallic examples. For instance Milstein demonstrated that the reaction of an Ir complex with a tertiary silane readily form a stable oxidative addition product whereas the analogous Rh complex forms a hydride complex due to the reductive elimination of this Si–C coupling product (Scheme 1.15).⁵⁶

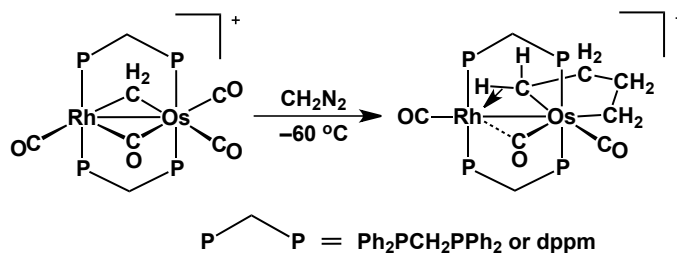
Scheme 1.15



Considering the role that Rh and Ir play during the Si–H bond activation processes and subsequent transformations in industrially important processes, it was of interest to us to determine how these two metals act together during such

processes in a bimetallic environment. Heterobimetallic complexes comprise an important subset of bimetallic complexes, the chemistry of which has been developed in anticipation that two different metals, when adjacent to each other, might act synergistically during substrate activation and subsequent transformations by their inherent differences in electronic and steric properties.⁵⁷ This phenomenon of mixed-metal synergism is obvious in many heterogeneous catalysts used in industry such as Ni/Mo or Ni/W in hydrocracking,⁵⁸ Co/Mo or Ni/Mo in hydrodesulfurization,⁵⁹ Pt/Re or Pt/Ir in gasoline reforming⁵⁹ and Ru/Rh in the formation of ethylene glycol from syn gas.⁶⁰ In these processes the roles of the different metals are not fully understood. Heterobimetallic synergism is also obvious in homogeneously catalyzed processes such as the Wacker process (in which a $[\text{PdCl}_4]^{2-}/\text{CuCl}$ combination is used for the oxidation of α -alkenes to aldehydes and ketones),⁶¹ the Cativa process (in which methanol and CO are converted to acetic acid catalyzed by a combination of Ir and Ru complexes)⁶² and many other chemical transformations involving the cleavage or formation of C–C and C–H bonds.^{40,57} Our research group has established an example of sequential C–C bond formation on a heterobimetallic Rh/Os complex by the coupling of methylene fragments (Scheme 1.16). In that study it was proposed that the greater lability of Rh facilitates insertion of the diazomethane-generated methylene fragment into the existing Rh–CH₂ bond while the greater strength of Os–hydrocarbyl bond plays a role in retaining the bridging fragments, allowing chain growth to occur.⁶³

Scheme 1.16



To properly study bimetallic synergism in homogeneous systems, it is imperative that the two metals always remain in close proximity during the processes of substrate binding, activation and transformation. Owing to the inherent lability of metal–metal bonds (usually more labile than most chemical bonds in organic substrates) many of these binuclear complexes undergo fragmentation into monometallic species during substrate binding or activation, removing any apparent advantage of having the metals initially bound together.

To circumvent this problem it is necessary to introduce bridging ligands that can stabilize the bimetallic core even in the case of metal–metal bond cleavage. Although several types of bridging ligands can be found in the literature, perhaps the most widely used has been *bis*(diphenylphosphino)methane or *dppm* (shown above in Scheme 1.17). Owing to its acute bite angle (67° to 74° , when bound to a single metal)⁶⁴ this ligand preferably binds to metal centres in a relatively unstrained bridging mode rather than the more strained chelating mode. A major advantage of this ligand is the presence of NMR active nuclei such as ^{31}P and ^1H which can provide valuable structural information about the solution species present. Moreover, the *dppm* ligand is a good σ donor, which increases the

electron density at the metals thereby rendering the metals more easily oxidizable. In addition, dppm complexes often have excellent solubility properties allowing solution NMR spectroscopy to be used for characterization while also generally having good crystalline characteristics in the solid state. Finally, it is inexpensive and readily available.

1.9 Objectives of this Thesis

Two mixed-metal complexes of rhodium and iridium, $[\text{RhIr}(\text{CO})_3(\text{dppm})_2]$ (**1**) and $[\text{RhIr}(\text{CH}_3)(\text{CO})_2(\text{dppm})_2][\text{CF}_3\text{SO}_3]$ (**2**), (Figure 1.13) have been synthesized and structurally characterized previously in this research group.⁶⁵ The Rh/Ir-tricarbonyl complex (**1**), is neutral and has only neutral ligands, suggesting the presence of both metals in the zero oxidation state. However, it appears more

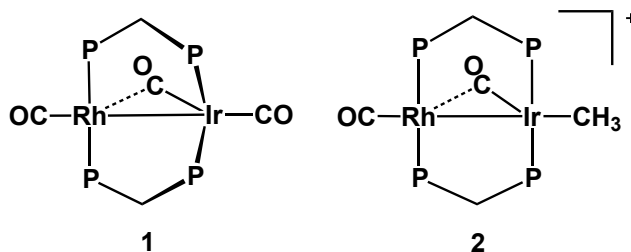


Figure 1.13: Complexes of interest for E–H bond activations

appropriate to view this complex as a mixed-valence, Rh(+I)/Ir(–I) complex, in which the pseudo-tetrahedral “Ir(CO)₂P₂” moiety donates a pair of electrons to the “Rh(CO)P₂⁺” centre, giving Rh a square-planar geometry. As such, only rhodium is coordinatively unsaturated. The second complex (**2**) is cationic and is related to **1** by formal replacement of CO by CH₃⁺, and as such has two fewer electrons, having both metals unsaturated. Both of these complexes undergo facile

activation of dihydrogen⁶⁵ and complex **2** undergoes insertion reactions of unsaturated species such as *tert*-butyl isocyanide (*t*BuNC) into the metal-carbon bond to yield the iminoacyl species $[\text{RhIr}(\text{CO})_2(\mu\text{-}^t\text{BuN}=\text{C}(\text{CH}_3))(\text{dppm})_2][\text{CF}_3\text{SO}_3]$.^{65b}

The first major goal of this thesis is to extend the reactivity study of different organosilanes to include that involving the neutral heterobimetallic complex, $[\text{RhIr}(\text{CO})_3(\text{dppm})_2]$ (**1**) and to compare its reactivity with those of the previously studied diiridium and dirhodium analogues. The main rationale is that bringing these two different metal centres together in the same core should give rise to subtly different reactivity patterns compared to the Rh₂ and Ir₂ analogues, possibly stabilizing analogues of unobserved intermediates in the previously studied dirhodium and diiridium systems and helping to establish a clearer picture of the mechanistic details. Furthermore, the presence of the NMR-active ¹⁰³Rh nucleus should allow reaction intermediates to be characterized at low temperature, enabling us to obtain a better understanding of the roles of the different adjacent metals.

The second goal is to compare the reactivities of silanes in the Rh/Ir cationic complex, $[\text{RhIr}(\text{CH}_3)(\text{CO})_2(\text{dppm})_2][\text{CF}_3\text{SO}_3]$ (**2**) with the neutral complex **1**. Many monometallic alkyl complexes are known to play an important role in Si-H bond activation,^{56,67} but to date no similar study have been carried out with a bimetallic alkyl complex. The third goal of this research is to study the reactivity of both neutral and cationic complexes towards Ge-H bond activation and compare the reactivity patterns of the Ge-H bond with those of its lighter

congener.

The final goal of this research project is to study the effect of using an electronically rich and less-sterically hindered bridging ligand in Si–H and Ge–H bond activation. Although, as noted earlier, complexes of *bis*(diphenylphosphino)methane have excellent solubility and crystallinity characteristics, a major disadvantage of this ligand is its steric bulk which can limit substrate access to the metals. Replacing the bulky phenyl substituents in dppm with the smaller ethyl groups to give *bis*(diethylphosphino)methane or depm (Figure 1.14) should give improved access to the metals. Furthermore, the replacement of phenyl by ethyl substituents increases the phosphine basicity, promoting oxidative addition reactions of the type noted earlier. This ligand can

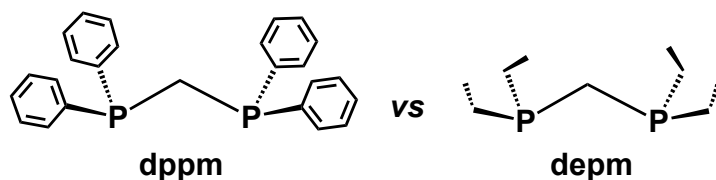


Figure 1.14: Steric difference between *dppm* and *dep*m

be readily prepared by the metathesis reaction of bis(dichlorophosphino)methane and EtMgBr in ether.⁶⁸ In the fifth Chapter of this thesis the reactivity of $[\text{RhIr}(\text{CO})_3(\text{dep}m)_2]$ ⁶⁹ with silanes will be described as a comparison with the *dppm* systems.

1.10 References

- 1) In *Metal-catalysis in Industrial Organic Processes*; Chiusoli, G. P.; Maitlis, P. M.; Eds.; The Royal Society of Chemistry: Cambridge, 2006.
- 2) Cornils, B.; Herrmann, W. A.; Rasch, M. *Angew. Chem. Int. Ed. Engl.* **1994**, *33*, 2144.
- 3) Britovsek, G. J. P.; Gibson, V. C.; Wass, D. F. *Angew. Chem. Int. Ed. Engl.* **1999**, *38*, 428 and references therein.
- 4) (a) Grubbs, R. H. *Tetrahedron. Lett.* **2004**, *60*, 7117. (b) Schrock, R. R.; Hoveyda, A. H. *Angew. Chem. Int. Ed. Engl.* **2003**, *42*, 4592.
- 5) (a) Heck, R. F. *J. Am. Chem. Soc.* **1986**, *90*, 5518. (b) King, A. O.; Okukado, N.; Negishi, E. *J. Chem. Soc. Chem. Commun.* **1977**, 683. (c) Miyaura, N.; Suzuki, A. *Chem. Rev.* **1995**, *95*, 2457.
- 6) Crabtree, R. H. In *The Organometallic Chemistry of the Transition Metals*; 4th ed.; John Wiley & Sons, Inc: Hoboken, 2005, p 241.
- 7) Marciniac, B.; Pawluc, P.; Pietraszuk, C. Inorganometallic Chemistry. In *Inorganic and Bioinorganic Chemistry*; Bertini, I., Ed.; In *Encyclopedia of Life Support Systems (EOLSS)*, developed under the Auspices of the UNESCO; EOLSS Publishing: Oxford, U.K., 2007 (<http://www.eolss.net>).
- 8) (a) Reichl, J. A.; Berry, D. H. *Adv. Organomet. Chem.* **1998**, *43*, 197. (b) Corey, J. Y. *Adv. Organomet. Chem.* **2004**, *51*, 1. (c) Tilley, T. D. *Acc. Chem. Res.* **1993**, *26*, 22.
- 9) (a) Marciniac, B. *Silicon Chem.* **2002**, *1*, 155. (b) Brook, M. A. *Silicon in Organic, Organometallic, and Polymer Chemistry*; Wiley: New York,

- 2000.** (c) Roy, A. K.; *Adv. Organomet. Chem.* **2007**, *55*, 1.
- 10) Chien, G. -P. C.; Kuo, J. -F.; Chen, C. -Y. *J. Polym. Sci. A Polym. Chem.* **1993**, *31*, 2423.
- 11) Piper, T. S.; Lemal, D.; Wilkinson, G. *Naturwissenschaften* **1956**, *43*, 129.
- 12) Chalk, A. J.; Harrod, J. F. *J. Am. Chem. Soc.* **1965**, *87*, 16.
- 13)(a) Corey, J. Y.; Braddock-Wilking, J. *Chem. Rev.* **1999**, *99*, 175. (b) Corey, J. Y. *Chem. Rev.* **2011**, *111*, 863.
- 14)(a) Matsuda, T.; Kadowaki, S.; Yamaguchi, Y.; Murakami, M. *Org. Lett.* **2010**, *12*, 1056 (b) Oda, H.; Morizawa, Y.; Oshima, K.; Nozaki, H. *Tetrahedron Lett.* **1984**, *25*, 3221.
- 15)(a) Lautens, M.; Klute, W. *Angew. Chem. Int. Ed. Engl.* **1996**, *35*, 442 (b) Miyake, H.; Yamamura, K. *Chem. Lett.* **1989**, *18*, 981. (c) Zhang, H. X.; Guilbé, F.; Balavoine, G. *J. Org. Chem.* **1990**, *55*, 981.
- 16)(a) Seitz, F.; Wrighton, M. S. *Angew. Chem. Int. Ed. Engl.* **1998**, *27*, 289. (b) Marciniak, B. *New. J. Chem.* **1997**, *21*, 815.
- 17)(a) Aitken, C. T.; Harrod, J. F.; Samuel, E. *J. Am. Chem. Soc.* **1986**, *108*, 4059. (b) Gauvin, F.; Harrod, J. F.; Woo, H. -G. *Adv. Organomet. Chem.* **1998**, *42*, 363. (c) Kim, B. -H.; Woo, H.-G. *Adv. Organomet. Chem.* **2004**, *52*, 143. (d) Miller, R. D. *Chem. Rev.* **1999**, *89*, 1359.
- 18)(a) West, R.; Fink, M.; Michl, J. *Science* **1981**, *214*, 1343. (b) Sekiguchi, A.; Kinjo, R.; Ichinohe, M. *Science* **2004**, *305*, 1755.
- 19)(a) Ojima, I.; Kogure, T.; Nagai, Y. *J. Organomet. Chem.* **1973**, *55*, C7. (b)

Chang, L. S.; Corey, J. *Organometallics* **1989**, *8*, 1885.

20)(a) Smith, E. E.; Du, G.; Fanwick, P. E.; Abu-Omar, M. M.; *Organometallics* **2010**, *29*, 6527. (b) Rosenberg, L.; Davis, C.; Yao, J. *J. Am. Chem. Soc.* **2001**, *123*, 5120. (c) Rosenberg, L.; Kobus, D. *J. Organomet. Chem.* **2003**, *685*, 107. (d) Fontaine, F. G.; Zargarian, D. *J. Am. Chem. Soc.* **2004**, *126*, 8786. (e) Itazaki, M.; Ueda, K.; Nakazawa, H. *Angew. Chem. Int. Ed. Engl.* **2009**, *48*, 3313.

21)(a) Luo, X. L.; Crabtree, R. H. *J. Am. Chem. Soc.* **1989**, *111*, 2527. (b) Biffis, A.; Basato, M.; Bricchese, M.; Ronconi, L.; Tubaro, C.; Zanella, A.; Graiff, A.; Tiripicchio, A. *Adv. Synth. Catal.* **2007**, 2485.

22)(a) Marciniec, B. *Comprehensive Handbook on Hydrosilylation*. Ed.; Pergamon: Oxford, **1992**. (b) Wiles, J. A.; Lee, C. E.; McDonald, R.; Bergens, S. H. *Organometallics* **1996**, *15*, 3782. (c) Berk, S. C.; Kreutzer, K. A.; Buchwald, S. L. *J. Am. Chem. Soc.* **1991**, *113*, 5093. (d) Mao, Z.; Gregg, B. T.; Cutlur, A. R. *J. Am. Chem. Soc.* **1995**, *117*, 10139. (e) Gutsulyak, D. V.; Vyboishchikov, S.F.; Nikonov, G. I. *J. Am. Chem. Soc.* **2010**, *132*, 5950.

23)(a) Chalk, A. J. *J. Organomet. Chem.* **1970**, *21*, 207. (b) Ojima, I.; Kumagai, M. *Tetrahedron. Lett.* **1974**, 4005. (c) Ojima, I.; Kumagai, M.; Nagai, Y. *J. Organomet. Chem.* **1976**, *111*, 43. (d) Gutsulyak, D. V.; Nikonov, G. I. *Angew. Chem. Int. Ed. Engl.* **2010**, *122*, 7715.

24) Becker, R.; Brunner, H.; Mahboobi, H.; Wiegrebe, W. *Angew. Chem. Int.*

Ed. Engl. **1985**, *24*, 995.

- 25) Xiong, Y.; Yao, S. L.; Driess, M. *J. Am. Chem. Soc.* **2009**, *131*, 7562.
- 26) Barron, A. *Comparison Between Silicon and Carbon*, Connexions Web site. <http://cnx.org/content/m32945/1.1/>, Nov 23, 2009.
- 27) (a) Kutzelnigg, W. *Angew. Chem. Int. Ed. Engl.* **1984**, *23*, 272. (b) Dewar, M. J. S.; Healy, E. *Organometallics* **1982**, *1*, 1705.
- 28) (a) Wang, Y.; Robinson, G. H. *Chem. Comm.* **2009**, 5201. (b) Li, L.; Fukawa, T.; Matsuo, T.; Hashizume, D.; Fueno, H.; Tanaka, K.; Tamao, K. *Nat. Chem.* **2012**, *4*, 361.
- 29) Kassaee, M. J.; Buazar, F.; Soleimani-Amiri, S. *J. Mol. Struct. (THEOCHEM)* **2008**, *866*, 52.
- 30) Belzner, J.; Ihmels, H. *Adv. Organomet. Chem.* **1998**, *43*, 1.
- 31) Waterman, R.; Hayes, P. G.; Tilley, T. D. *Acc. Chem. Res.* **2007**, *40*, 712.
- 32) Ogino, H. *Chem. Rec.* **2002**, *2*, 291.
- 33) (a) Grumbine, S. D.; Tilley, T. D.; Rheingold, A. L. *J. Am. Chem. Soc.* **1993**, *115*, 358. (b) Grumbine, S. D.; Tilley, T. D.; Arnold, F. P.; Rheingold, A. L. *J. Am. Chem. Soc.* **1993**, *115*, 7884. (c) Grumbine, S. D.; Tilley, T. D.; Arnold, F. P.; Rheingold, A. L. *J. Am. Chem. Soc.* **1994**, *116*, 5495.
- 34) Tokitoh, N.; Manmaru, K.; Okazaki, R. *Organometallics* **1994**, *13*, 167.

- 35) Ogino, H.; Tobita, H. *Adv. Organomet. Chem.* **1998**, *42*, 223.
- 36) Nikonov, G. I. *Adv. Organomet. Chem.* **2005**, *53*, 217.
- 37) Yang, J.; White, P. S.; Schauer, C. K.; Brookhart, M. *Angew. Chem. Int. Ed. Engl.* **2008**, *47*, 4141.
- 38) Schubert, U.; Ackermann, K.; Wörle, B. *J. Am. Chem. Soc.* **1982**, *104*, 7379.
- 39)(a) Dewar, M. *Bull. Soc. Chim. Fr.* **1951**, *18*, C79. (b) Chatt, J. Duncanson, L. A. *J. Chem. Soc.* **1953**, 2939.
- 40) Cowie, M. *Can. J. Chem.* **2005**, *83*, 1043.
- 41) Tolman, W. B. *Activation of Small Molecules: Organometallic and Bioinorganic Perspectives.* **2006**, Wiley-VCH Verlag GmbH & Co. KGaA.
- 42) Shibasaki, M.; Yamamoto, Y. *Multimetallic Catalysts in Organic Synthesis.* **2004**, Wiley-VCH Verlag GmbH & Co. KGaA.
- 43)(a) Zarate, E.A.; Tessier-Youngs, C. A.; Youngs, W. J. *J. Am. Chem. Soc.* **1988**, *110*, 4068. (b) Zarate, E.A.; Tessier-Youngs, C. A.; Youngs, W. J. *J. Chem. Soc., Chem. Commun.* **1989**, 577.
- 44) Heyn, R. H.; Tilley, T. D. *J. Am. Chem. Soc.* **1992**, *114*, 1917.
- 45) Shimada, S.; Rao, M. L. N.; Hayashi, T.; Tanaka, M. *Angew. Chem. Int. Ed. Engl.* **2001**, *40*, 213.

- 46) Chen, W. Z.; Shimada, S.; Tanaka, M. *Science* **2002**, *295*, 308.
- 47) Crabtree, R. H. *Science* **2002**, *295*, 288.
- 48) Tanabe, M.; Ishikawa, N.; Hanzawa, M.; Osakada, K. *Organometallics* **2008**, *27*, 5152.
- 49) (a) Tanabe, M.; Ishikawa, M.; Chiba, M.; Ide, T.; Osakada, K.; Tanase, T. *J. Am. Chem. Soc.* **2011**, *133*, 18598. (b) Shimada, S.; Li, Y.-H.; Choe, Y.-K.; Tanaka, M.; Bao, M.; Uchimaru, T. *Proc. Natl. Acad. Sci. U.S.A.* **2007**, *104*, 7758. (c) Aarii, H.; Takahashi, M.; Nanjo, M.; Mochida, K. *Organometallics* **2011**, *30*, 917. (d) Yamada, T.; Mawatari, A.; Tanabe, M.; Osakada, K.; Tanase, T. *Angew. Chem. Int. Ed. Engl.* **2009**, *48*, 568.
- 50) Hashimoto, H.; Aratani, I.; Kabuto, C.; Kira, M. *Organometallics* **2003**, *22*, 2199.
- 51) Takao, T.; Suzuki, H. *Organometallics* **1994**, *13*, 2554.
- 52) Comte, V.; Le Gendre, P.; Richard, P.; Moïse, C. *Organometallics* **2005**, *24*, 1439.
- 53) Tanabe, M.; Yomoto, R.; Osakada, K. *Chem. Comm.* **2012**, *48*, 2125.
- 54) McDonald, R.; Cowie, M. *Organometallics* **1990**, *9*, 2468.
- 55) (a) Wang, W. -D.; Eisenberg, R. *J. Am. Chem. Soc.* **1990**, *112*, 1833. (b) Wang, W. -D.; Hommeltoft, S. I.; Eisenberg, R. *Organometallics* **1988**, *7*, 2417. (c) Wang, W. -D.; Eisenberg, R. *Organometallics* **1991**, *10*, 2222.

- 56) (a) Aizenberg, M.; Milstein, D. *Angew. Chem. Int. Ed. Engl.* **1994**, *33*, 317. (b) Aizenberg, M.; Ott, J.; Elsevier, C. J. Milstein, D. *J. Organomet. Chem.* **1998**, *551*, 81.
- 57) Ritleng, V.; Chetcuti, M. J. *Chem. Rev.* **2007**, *107*, 797.
- 58) Robinson, P. R.; Dolbear, G. E. *Hydrotreating and Hydrocracking: Fundamentals.* **2006** In: Hsu, C. S.; Robinson, P. R., ed. Practical Advances in Petroleum Processing, Vol. 1. New York: Springer.
- 59) Guzzi, L.; Solymosi, F.; Tétényi, P.; *New Frontiers in Catalysis*; **1993**, *75(part c)*; Elsevier Science Publishers, Amsterdam.
- 60) Dombek, B. D.; *Adv. Catal.* **1983**, *32*, 325.
- 61) Henry, P. M. *Palladium Catalysed Oxidation of Hydrocarbons.* **1980**, Reidel, Dordrecht.
- 62) Jones, J. H. *Platinum Metals Rev.* **2004**, *44*, 94.
- 63) Trepanier, S. J.; Dennett, J. N. L.; Sterenberg, B. T.; McDonald, R.; Cowie, M. *J. Am. Chem. Soc.* **2004**, *126*, 8046.
- 64) Puddephatt, R. J. *Chem. Soc. Rev.* **1983**, *12*, 99.
- 65) (a) McDonald, R.; Cowie, M. *Inorg. Chem.* **1990**, *29*, 1564. (b) Oke, O.; McDonald, R.; Cowie, M. *Organometallics* **1999**, *18*, 1629.
- 66) Oke, O. Ph. D. Thesis, University of Alberta, **1999**, 24.

- 67)(a) Klei, S. R.; Tilley, T. D.; Bergman, R. G. *J. Am. Chem. Soc.* **2000**, *122*, 1816. (b) Taw, F. L.; Bergman, R. G.; Brookhart, M. *Organometallics* **2004**, *23*, 886.
- 68) Anderson, D. J. Ph. D. Thesis, University of Alberta. **2007**.
- 69) Slaney, M. E.; Anderson, D. J.; Ferguson, M. J.; McDonald, R.; Cowie, M. *Organometallics* **2012**, *31*, 2286.

Chapter 2

Multiple Silicon–Hydrogen Bond Activations at Adjacent Rhodium and Iridium Centres^{II}

2.1 Introduction

The chemistry of transition-metal complexes containing metal–silicon bonds occupies a prime position in a number of catalytic transformations including olefin and ketone hydrosilylation,¹ silane alcoholysis,² silane redistribution,³ silane reduction of haloarenes,⁴ and dehydrogenative silane oligomerization.⁵ One of the most versatile methods for generating Si-containing complexes is by oxidative addition of Si–H bonds in silanes. From the perspective of dehydrogenative silane oligomerization, the incorporation of two or more Si-containing fragments into metal complexes is of particular importance, potentially leading to the coupling of these fragments. Multinuclear complexes can play an important role in Si–Si coupling, since two or more metals have a greater capacity for silane oxidative addition and for the concomitant incorporation of multiple Si-containing fragments, than does a single metal. This has been amply demonstrated by the early work of Graham,^{6a} and more recently as described in reviews by Tobita and Ogino,^{6b} Corey and Braddock-Wilking,^{6c} and Tanaka and Shimada^{6d} in which a variety of complexes have been reported incorporating bis-silylene,⁷⁻¹⁸ silyl/silylene,¹⁹⁻²² bis-silyl,^{10-12,15,16,18,23} and silane/silyl¹⁵ combinations of groups.

Binuclear late-metal complexes have played a dominant role in the chemistry of Si-bridged species and within the group of bis-silylene-bridged

^{II} A version of this Chapter has been published. Mobarok, M. H.; Oke, O.; Ferguson, M. J.; McDonald, R.; Cowie, M. *Inorg. Chem.* **2010**, 49, 11556.

products, two structural classes have emerged in which the M_2Si_2 framework is either planar^{7, 11-14,16-19,23} or folded in a butterfly-type arrangement.^{7b,8,10,22} The strongest structural evidence for Si---Si interactions in these species has been found in the planar M_2Si_2 arrangement, in which the Si centres at opposite corners of a parallelepiped are in close contact.²⁴⁻²⁶ Si-Si bond formation should also be possible in the folded arrangement, having the Si atoms at the “wing-tips”, since such a geometry allows the Si centres to approach within bonding distance. Si-Si bond formation has also been reported between silyl and silylene-bridged moieties in a binuclear species.²²

In previous work on silane activation by pairs of adjacent metals, we had investigated a diiridium system in which, under the conditions investigated the incorporation of only a single silicon-containing group had been achieved.⁹ In contrast, Eisenberg and coworkers, investigating closely related Rh_2 systems, had observed the incorporation of up to two Si-containing fragments, to give folded Rh_2Si_2 cores.⁸ The difference in reactivity of these two systems can be rationalized by the greater lability of Rh, which more readily allows coordinative unsaturation to be achieved after double Si-H activation of the first silane. Although silane activation by a number of homodinuclear late metals (Pt,^{7,12,13,18,19,22b,27} Pd,^{14,17,28} Rh,^{8,11,20,21} Ir,⁹ Fe,²⁹ Ru,^{10,15,16,23,30} and Ni^{22a}) has been studied, only a few examples involving mixed-metal complexes have been reported.³¹ In order to learn more about the stepwise incorporation of silanes and the roles of the adjacent metals in the activation process by the Group 9 metals we have investigated the Rh/Ir combination of metals in the anticipation that the

greater tendency for Ir to undergo oxidative addition combined with the greater lability of Rh might lead to chemistry that differs from that observed with the homobinuclear analogues. These results are discussed in this chapter.

2.2 Experimental.

2.2.1 General Comments.

All solvents were dried (using appropriate drying agents), distilled before use, and stored under dinitrogen. Reactions were performed under an argon atmosphere using standard Schlenk techniques. Ph_2SiH_2 and PhSiH_3 were purchased from Aldrich and Alfa-Aesar, respectively; while MesSiH_3 ,^{32a} $\text{C}_6\text{H}_3\text{F}_2\text{SiH}_3$,^{32b} and Ph_2SiD_2 ^{32c} were prepared according to the literature methods. PhSiD_3 was prepared by a modified literature method (overnight reflux in ether instead of at room-temperature).³³ Silanes were dried over CaH_2 and distilled under Ar before use. ^{13}C -enriched CO (99.4%) and LiAlD_4 were purchased from Cambridge Isotope Laboratories, ^{13}C -enriched methyl-triflate and ^2H -enriched methyl triflate were purchased from Sigma-Aldrich. $[\text{RhIr}(\text{CO})_3(\text{dppm})_2]$ (**1**)³⁴ and $[\text{RhIr}(\text{CH}_3)(\text{CO})_2(\text{dppm})_2][\text{CF}_3\text{SO}_3]$ (**2**)³⁵ were prepared as previously reported. NMR spectra were recorded on Bruker AM-400, Varian Inova-400 or Varian Unity-500 spectrometers operating at 400.0, 399.8 or 499.8 MHz, respectively, for ^1H ; at 161.9, 161.8 or 202.3 MHz, respectively, for ^{31}P ; and at 100.6, 100.6 or 125.7 MHz, respectively, for ^{13}C nuclei. $^{29}\text{Si}\{^1\text{H}\}$ NMR spectra were acquired on the Varian Inova-400 spectrometer operating at 79.5 MHz by a combination of DEPT, 2D ^1H - ^{29}Si HSQC and 2D ^1H - ^{29}Si HMBC. The ^1H , $^{13}\text{C}\{^1\text{H}\}$ and $^{29}\text{Si}\{^1\text{H}\}$ NMR spectra were referenced internally to residual solvent proton signals relative

to tetramethylsilane whereas $^{31}\text{P}\{^1\text{H}\}$ and $^{19}\text{F}\{^1\text{H}\}$ NMR spectra were referenced relative to external standard 85 % H_3PO_4 and CCl_3F , respectively. In the ^1H NMR spectral results the aromatic protons in the range δ 8.50 – 6.20 are not reported. The ^{13}C NMR resonances of CO and CH_3 ligands were acquired using ^{13}CO and $^{13}\text{CH}_3$ -enriched samples. The ^{13}C NMR resonances for dppm methylene groups (which were not ^{13}C -enriched) are not reported for those complexes which are either in low NMR yield (**6** and **11**), were only observed at low temperature (**3**, **14** and **15**) or are unstable at room temperature (**16** and **17**) and therefore unsuitable for extended data acquisition. The ^{13}C NMR resonances for the aryl carbons (in the range of δ 125 to 135) are not reported since they appear in the typical region and give no structural information. The yields of all nonisolable complexes were determined by the integration of their resonances in ^{31}P NMR spectra, taking all the resonances present as 100% in a sealed NMR tube. Coupling constants tagged with an asterisk appeared as additional coupling when the respective ligands (either CO or CH_3) were ^{13}C -enriched and therefore were not included in the description of multiplicity. All spectra were recorded at 27 °C unless otherwise noted. Infrared spectra were obtained on a Nicolet Avatar 370 DTGS spectrometer. The elemental analyses were performed by the Microanalytical laboratory in the department.

2.2.2 Preparation of Compounds.

a. **[RhIr(H)(SiH₂Ph)(CO)₂(μ -CO)(dppm)₂] (3)**: In a septum-sealed NMR tube under an $\text{Ar}_{(\text{g})}$ atmosphere **[RhIr(CO)₃(dppm)₂] (1)** (30 mg 0.026 mmol) was dissolved in 0.7 mL of CD_2Cl_2 at ambient temperature producing a dark orange

solution, then cooled to $-80\text{ }^{\circ}\text{C}$. Addition of PhSiH_3 ($3.2\text{ }\mu\text{L}$, 0.026 mmol) by a microliter syringe resulted in a lightening of the solution colour. Compound **3** was formed quantitatively after 30 min as made evident by $^{31}\text{P}\{^1\text{H}\}$ NMR spectroscopy. $^{31}\text{P}\{^1\text{H}\}$ NMR ($-78\text{ }^{\circ}\text{C}$; CD_2Cl_2 , 161.9 MHz): δ 40.0 (Rh–P, 1P, ddd, $^1J_{\text{RhP(A)}} = 107\text{ Hz}$, $^2J_{\text{PP}} = 241\text{ Hz}$, $^2J_{\text{PP}} = 31\text{ Hz}$), 25.2 (Rh–P, 1P, ddd, $^1J_{\text{RhP}} = 89\text{ Hz}$, $^2J_{\text{PP}} = 152\text{ Hz}$, $^2J_{\text{PP}} = 31\text{ Hz}$), -3.3 (Ir–P, 1P, dd, $^2J_{\text{PP}} = 241\text{ Hz}$, $^2J_{\text{PP}} = 18\text{ Hz}$), -11.5 (Ir–P, 1P, dd, $^2J_{\text{PP}} = 152\text{ Hz}$, $^2J_{\text{PP}} = 18\text{ Hz}$); ^1H NMR ($-78\text{ }^{\circ}\text{C}$; CD_2Cl_2 , 399.8 MHz): δ 4.66 (CH_2 , m, 1H), 4.23 (Si–H, m, 1H), 4.14 (CH_2 , m, 1H), 4.07 (CH_2 , m, 1H), 4.05 (Si–H, m, 1H), 2.50 (CH_2 , m, 1H), -11.50 (ddd, 1H, $^2J_{\text{trans PH}} = 125.0\text{ Hz}$, $^2J_{\text{cis PH}} = 15.0\text{ Hz}$, $^4J_{\text{distal(trans)PH}} = 27.0\text{ Hz}$); $^{29}\text{Si}\{^1\text{H}\}$ NMR ($-78\text{ }^{\circ}\text{C}$; CD_2Cl_2 , 78.5 MHz , DEPT): δ -18.0 (dddd, $^1J_{\text{RhSi}} = 37\text{ Hz}$, $^2J_{\text{SiP}} = 137\text{ Hz}$, $^2J_{\text{SiP}} = 18.0\text{ Hz}$, $^4J_{\text{SiP}} = 18.0\text{ Hz}$); $^{13}\text{C}\{^1\text{H}\}$ NMR ($-78\text{ }^{\circ}\text{C}$; CD_2Cl_2 , 100.5 MHz): 229.0 (μ -CO, dm, 1C, $^2J_{\text{RhC}} = 34\text{ Hz}$), 199.0 (Rh–CO, dm, 1C, $J_{\text{RhC}} = 70.0\text{ Hz}$), 178.0 (Ir–CO, bt, 1C).

b. [RhIr(H)₂(CO)₂(μ -SiHPh)(dppm)₂] (4): In a 100 mL Schlenk tube, under anhydrous conditions and an Ar atmosphere, $[\text{RhIr}(\text{CO})_3(\text{dppm})_2]$ (**1**) (46 mg , 0.040 mmol) was dissolved in 5 mL of benzene at ambient temperature. Phenylsilane ($7.4\text{ }\mu\text{L}$, 0.060 mmol) was then added to the solution by syringe, resulting in an immediate colour change from dark orange to light yellow. The reaction was allowed to stir for 1 h, followed by the reduction of solvent volume to approximately 1 mL *in vacuo*. Subsequent slow addition of pentane gave a pale yellow powdery solid. The compound was recrystallized by layering the concentrated benzene solution of the compound with pentane at $-20\text{ }^{\circ}\text{C}$. Yield: 35 mg (71%). Anal. calcd. for $\text{C}_{58}\text{H}_{52}\text{IrO}_2\text{P}_4\text{RhSi}\cdot\text{C}_6\text{H}_6$: C, 58.79; H, 4.44. Found:

C, 58.53; H, 4.58. $^{31}\text{P}\{^1\text{H}\}$ NMR (27 °C; C_6D_6 , 161.9 MHz): δ 29.0 (Rh–P, 1P, bm), 15.9 (Rh–P, 1P, bm), –8.2 (Ir–P, 1P, bm), –14.0 (Ir–P, 1P, bm); ^1H NMR (27 °C; CDCl_2 , 499.8 MHz): δ 5.30 (CH_2 , m, 2H), 3.10 (CH_2 , m, 2H), –9.60 (Rh–H, bm, 1H), –10.90 (Ir–H, bm, 1H); $^{13}\text{C}\{^1\text{H}\}$ NMR (27 °C; CD_2Cl_2 , 100.5 MHz): 194.1 (Rh–CO, dt, 1C, $J_{\text{RhC}} = 70.0$ Hz), 181.1 (Ir–CO, t, 1C), δ 49.5 (CH_2 , 1C, m), 44.8 (CH_2 , 1C, m). $^{31}\text{P}\{^1\text{H}\}$ (–78 °C; CD_2Cl_2 , 161.9 MHz): δ 29.0 (Rh–P, 1P, ddd, $^1J_{\text{RhP}} = 101.1$ Hz, $^2J_{\text{PP}} = 131$ Hz, $^2J_{\text{PP}} = 11$ Hz), 15.9 (Rh–P, 1P, ddd, $^1J_{\text{RhP}} = 107.3$ Hz, $^2J_{\text{PP}} = 129$ Hz, $^2J_{\text{PP}} = 11$ Hz), –8.2 (Ir–P, 1P, dd, $^2J_{\text{PP}} = 131$ Hz, $^2J_{\text{PP}} = 9$ Hz), –14.0 (Ir–P, 1P, dd, $^2J_{\text{PP}} = 129$ Hz, $^2J_{\text{PP}} = 9$ Hz); ^1H NMR (–78 °C; CD_2Cl_2 , 399.8 MHz): δ 6.70 (Si–H, bs, 1H, $^1J_{\text{SiH}} = 190$), 5.50 (CH_2 , m, 1H), 5.25 (CH_2 , m, 1H), 3.10 (CH_2 , m, 1H), 2.80 (CH_2 , m, 1H), –9.50 (Rh–H, ddm, 1H, $^2J_{\text{trans PH}} = 145.0$, $J_{\text{RhH}} = 11.2$ Hz), –11.0 (Ir–H, dm, 1H, $^2J_{\text{trans PH}} = 123$); $^{29}\text{Si}\{^1\text{H}\}$ NMR (–78 °C; CD_2Cl_2 , 78.5 MHz, DEPT): δ 142.9 (dt, $^1J_{\text{SiRh}} = 30.1$ Hz, $^2J_{\text{PSi}} = 72.2$ Hz). IR: $\nu_{\text{SiH}} = 2045$ cm^{-1} , $\nu_{\text{CO}} = 1962$ cm^{-1} , 1942 cm^{-1} .

c. **[RhIr(H)₂(CO)₂(μ -SiHC₆H₂Me₃)(dppm)₂] (5)**: 52 mg (0.045 mmol) of [RhIr(CO)₃(dppm)₂] (**1**) in a Schlenk flask under Ar was dissolved in 5 mL of benzene. Addition of 30 μL (0.132 mmol) of mesitylsilane by syringe to the continuously stirring solution of complex **1** resulted in a slow colour change from orange to light yellow over the course of 3 h. After 6 h the solution volume was reduced to 2 mL under vacuum. Slow addition of 10 mL of pentane gave a pale yellow compound. Yield: 42 mg (73 %). Anal. calcd. for: C₆₁H₅₈IrO₂P₄RhSi: C, 57.64; H, 4.57. Found: C, 57.89; H, 4.89. $^{31}\text{P}\{^1\text{H}\}$ NMR (27 °C; CD_2Cl_2 , 161.9 MHz): δ 21.3 (bm), –12.1 (bm); ^1H (27 °C; CD_2Cl_2 , 399.8 MHz): δ 6.70 (Si–H, b,

1H), 5.30 (CH₂, m, 2H), 3.10 (CH₂, m, 2H), 2.97 (*o*-CH₃, s, 6H), 2.37 (*p*-CH₃, s, 3H), -9.30 (Rh-H, bm, 1H), -11.0 (Ir-H, bm, 1H); ³¹P{¹H} NMR (-78 °C; CD₂Cl₂, 161.9 MHz): δ 26.9 (Rh-P, 1P, m), 15.5 (Rh-P, 1P, m), -9.4 (Ir-P, 1P, m), -14.8 (Ir-P, 1P, m); ¹H NMR (-78 °C; CD₂Cl₂, 399.8 MHz): δ 6.70 (Si-H, bs, 1H), 5.40 (CH₂, m, 1H), 5.20 (CH₂, m, 1H), 3.10 (CH₂, m, 1H), 2.90 (CH₂, m, 1H), 2.97 (*o*-CH₃, s, 6H), 2.37 (*p*-CH₃, s, 3H), -9.30 (Rh-H, dm, 1H, ²J_{trans PH} = 140.0), -11.05 (Ir-H, dm, 1H, ²J_{trans PH} = 125.0); ¹³C{¹H} NMR (-78 °C; CD₂Cl₂, 100.5 MHz): δ 194.0 (Rh-CO, dm, 1C, ¹J_{RhC} = 68.0 Hz), 181.7 (Ir-CO, bs, 1C), 44.5 (CH₂, m, 1C), 48.3 (CH₂, m, 1C), 26.1 (*o*-CH₃, s, 2C), 20.1 (*p*-CH₃, s, 1C); ²⁹Si{¹H} NMR (-78 °C; CD₂Cl₂, 78.5 MHz, DEPT): δ 110.4 (m, ¹J_{SiRh} = 30.0 Hz, ²J_{SiP} = 67.0 Hz).

d. **[RhIr(CO)₂(μ-SiHPh)(μ-CO)(dppm)₂]** (**6**): In an NMR tube, [RhIr(H)₂(CO)₂(μ-SiHPh)(dppm)₂] (**4**) (30 mg, 0.024 mmol) was dissolved in 0.7 mL of C₆D₆ and the tube was pressurized to 1 atm with CO followed by heating the reaction tube at 60 °C for 2 h. The compound **6** appeared in approximately 10 % yield according to ³¹P{¹H} NMR spectroscopy. During the course of this reaction, some portion of **4** was also converted to [RhIr(CO)₃(μ-dppm)₂] (**1**) in approximately 5 % yield as confirmed by ³¹P{¹H} NMR while 85% of compound **4** was found to remain unconverted in the mixtures. Complex **6** also appeared in approximately the same quantity when the reaction was carried out for longer times (up to 24 h) at room temperature. An attempt to isolate complex **6**, by the addition of pentane to the concentrated benzene solution of above-mentioned mixture failed, presumably due its low concentration. ³¹P{¹H} NMR (27 °C;

C_6D_6 , 202.1 MHz): δ 45.1 (Rh–P, 1P, ddd, $^1J_{RhP} = 109$ Hz, $^2J_{PP} = 240$ Hz, $^2J_{PP} = 29$ Hz), 22.7 (Rh–P, 1P, ddd, $^1J_{RhP} = 109$ Hz, $^2J_{PP} = 142$ Hz, $^2J_{PP} = 29$ Hz), 9.4 (Ir–P, 1P, dd, $^2J_{PP} = 240$ Hz, $^2J_{PP} = 20$ Hz), – 8.9 (Ir–P, 1P, dd, $^2J_{PP} = 142$ Hz, $^2J_{PP} = 20$ Hz); 1H NMR (27 °C; C_6D_6 , 498.1 MHz): δ 4.36 (CH₂, m, 1H), 4.22 (CH₂, m, 1H), 3.50 (CH₂, m, 1H), 2.48 (CH₂, m, 1H); $^{13}C\{^1H\}$ NMR (27 °C; C_6D_6 , 100.5 MHz): 229.2 (μ -CO, 1C, $^1J_{RhC} = 31.9$ Hz), 199.9 (Rh–CO, d, 1C, $^1J_{RhC} = 78.8$ Hz), 183.4 (Ir–C), bs, 1C).

e. **[RhIr(CO)₃(κ^1 -dppm)(μ -SiHPh)₂(dppm)] (7)**: *Method 1*: In an NMR tube, under an Ar atmosphere, [RhIr(H)₂(CO)₂(μ -SiHPh)(dppm)₂] (**4**) (30 mg, 0.024 mmol) was dissolved in 0.7 mL of CD₂Cl₂. The tube was then evacuated and filled to a pressure of 1 atm with CO. 3.0 μ L (1 equivalent) of PhSiH₃ was added via a microlitre syringe to the NMR tube. After 18 h, complex **7** formed almost quantitatively (97 %) according to $^{31}P\{^1H\}$ NMR spectroscopy. During that time the colour of the solution changed from golden yellow to lemon-yellow. Transfer of Complex **7** from NMR tube to a 100 mL Schlenk tube and subsequent addition of 5 mL pentane resulted in a light yellow solid. However, the solvent could not be completely removed from **7** as some portion of it converted to [RhIr(CO)₂(μ -SiHPh)₂(dppm)₂](**8a**) under high vacuum or Ar flow. As a result microanalytical analysis could not be performed for this complex. Under the conditions noted above, the reaction of compound **4** with PhSiD₃ and CO resulted in deuterium scrambling in the product [RhIr(CO)₃(κ^1 -dppm)(μ -SiH(D)Ph)₂(dppm)] (**7a**). *Method 2*: Reaction of **1** with 2 equiv of PhSiH₃ at ambient temperature in a well-sealed NMR tube yielded **7** (NMR yield, 70 %) and **8a** (NMR yield, 30 %) after

24 h. $^{31}\text{P}\{^1\text{H}\}$ NMR (27 °C; CD_2Cl_2 , 202.1 MHz): δ 15.6 (Rh–P, 1P, ddd, $^1J_{\text{RhP}} = 105$ Hz, $^2J_{\text{PP}} = 108$ Hz, $^3J_{\text{RhP}} = 6$ Hz), 3.4 (Ir–P, 1P, dm, $^2J_{\text{PP}} = 41$ Hz), –10.5 (Ir–P, 1P, ddd, $^2J_{\text{PP}} = 41$ Hz, $^2J_{\text{PP}} = 13$ Hz, $^4J_{\text{PP}} = 4$ Hz), –24.5 (dangling–P, 1P, dd, $^2J_{\text{PP}} = 41$ Hz, $^4J_{\text{PP}} = 4$ Hz); ^1H NMR (27 °C; CD_2Cl_2 , 399.8 MHz): δ 6.20 (Si–H, dd, 1H, $^1J_{\text{SiH}} = 190.0$, $^3J_{\text{PH}} = 24.0$ Hz, $^3J_{\text{PH}} = 19.0$ Hz), 5.80 (Si–H, dd, 1H, $^1J_{\text{SiH}} = 190.0$ Hz), $^3J_{\text{PH}} = ^3J_{\text{PH}} = 5.3$ Hz), 4.21 (CH_2 , m, 1H), 3.73 (CH_2 , m, 1H), 3.10 (CH_2 , m, 1H), 2.80 (CH_2 , m, 1H); $^2\text{H}\{^1\text{H}\}$ NMR(27 °C; CD_2Cl_2 , 61.4 MHz): 6.24 (b, Si–D, 1D), 5.75 (b, Si–D, 1D); $^{13}\text{C}\{^1\text{H}\}$ NMR (27 °C; CD_2Cl_2 , 100.5 MHz): δ 198.0 (Rh–CO, dd, 1C, $^1J_{\text{RhC}} = 57.0$ Hz, $^2J_{\text{PC}} = 10.0$ Hz), 195.0 (Rh–CO, dd, 1C, $^1J_{\text{RhC}} = 75.0$ Hz, $^2J_{\text{PC}} = 22.0$ Hz), 186.0 (Ir–CO, bs, 1C), 37.6 (CH_2 , m, 1C), 34.2 (CH_2 , m, 1C); $^{29}\text{Si}\{^1\text{H}\}$ NMR (27 °C; CD_2Cl_2 , 78.5 MHz, DEPT, gHSQC): 101.8 (m), 136.6 (m).

f. **[RhIr(CO)₂(μ -SiHPh)₂(dppm)₂] (8a)**: A total of 50 mg (0.041mmol) of **[RhIr(H)₂(CO)₂(μ -SiHPh)(dppm)₂] (4)** in a Schlenk tube was dissolved in 5 mL of CH_2Cl_2 . A total of 5.5 μL (0.044mmol) of PhSiH_3 was dissolved in 1 mL CH_2Cl_2 in another flask and slowly transferred via cannula to the Schlenk flask containing the solution of **4**. Leaving the solution at ambient temperature for 24 h resulted in lightening of the yellow colour. Removal of the solvent under vacuum, redissolving in 2 mL of CH_2Cl_2 and subsequent slow addition of pentane yielded a pale yellow precipitate of **8a**. Yield 33 mg (56%). Anal. calcd. for $\text{C}_{64}\text{H}_{56}\text{IrO}_2\text{P}_4\text{RhSi}_2$: C, 57.66; H, 4.20. Found: C, 57.90; H, 4.35. Under the conditions noted above the reaction of compound **4** is reacted with PhSiD_3 resulted in deuterium scrambling in both silylene groups, yielding **[RhIr(CO)₂(μ -**

SiH(D)Ph)₂(dppm)₂] (**8a_d**) was produced. ³¹P{¹H} NMR (27 °C; CD₂Cl₂, 202.1 MHz): δ 29.3 (Rh–P, 1P, ddd, ¹J_{RhP} = 104 Hz, ²J_{PP} = 108 Hz, ²J_{PP} = 33 Hz), 21.5 (Rh–P, 1P, ddd, ¹J_{RhP} = 105 Hz, ²J_{PP} = 139 Hz, ²J_{PP} = 33 Hz), 2.6 (P_B, 1P, dd, ²J_{PP} = 108 Hz, ²J_{PP} = 25 Hz), – 7.8 (P_D, 1P, dd, ²J_{PP} = 139 Hz, ²J_{PP} = 25 Hz); ¹H NMR (27 °C; CD₂Cl₂, 399.8 MHz): δ 5.66 (Si–H, ddm, 1H, ¹J_{SiH} = 180.0 Hz, ³J_{PH} = 32.0 Hz, ³J_{HH} = 2.3 Hz), 5.52 (Si–H, m, 1H, ¹J_{Si-H} = 180 Hz), 5.27 (CH₂, m, 1H), 4.62 (CH₂, m, 1H), 3.10 (CH₂, m, 1H), 2.95 (CH₂, m, 1H); ¹³C{¹H} NMR (27 °C; CD₂Cl₂, 100.5 MHz): 198.9 (Rh–CO, dm, 1C, ¹J_{RhC} = 73.6 Hz), 186.6 (Ir–CO, bs, 1C), 39.3 (CH₂, dd, 1C, ¹J_{PC} = 34.7 and 23.2 Hz), 37.1 (CH₂, dd, 1C, ¹J_{PC} = 30.5 and 21.8 Hz); ²⁹Si{¹H} NMR (27 °C; CD₂Cl₂, 78.5 MHz, DEPT, gHSQC): 129.2 (m), 113.9 (m).

g. [RhIr(CO)₂(μ-SiHPh)₂(dppm)₂] (8b**):** *Method 1:* Under an atmosphere of Ar, 70 mg (0.061 mmol) of [RhIr(CO)₃(dppm)₂] (**1**) in a 100 mL Schlenk tube was dissolved in 10 mL of benzene. 30 μL (0.24 mmol, 4 equiv) of phenylsilane dissolved in 0.5 mL of benzene in a 10 mL Schlenk tube was slowly transferred to the 100 mL Schlenk tube. The reaction was set in an oil bath at 60 °C for 24 h. Within 3 h the solution became cloudy and the product began to precipitate. After 24 h, the yellow supernatant was removed through cannula, the white precipitate was washed with pentane and re-crystallized from CH₂Cl₂/pentane. Yield: 35 mg (43 %). Anal. calcd. for C₆₄H₅₆IrO₂P₄RhSi₂: C, 57.66; H, 4.20. Found: C, 57.81; H, 4.15. *Method 2:* Under the conditions noted above, **8b** can also be prepared by the reaction of **8a** (50 mg, 0.038 mmol) with PhSiH₃ (4.7 μL, 0.038). When **8a** (50 mg, 0.038 mmol) was reacted with PhSiD₃ under similar reaction conditions

deuterium was found to be scrambled over both silylene groups of **8b** to give **8b_d**. $^{31}\text{P}\{^1\text{H}\}$ NMR (27 °C; CD_2Cl_2 , 161.9 MHz): δ 28.6 (Rh–P, 2P, dm, $^1J_{\text{RhP}} = 105$ Hz), 0.3 (Rh–P, 2P, m); ^1H (CD_2Cl_2 , 399.8 MHz): δ 6.00 (Si–H, m, 2H, $^1J_{\text{SiH}} = 180.0$ Hz), 5.20 (CH_2 , m, 2H), 3.30 (CH_2 , m, 2H); $^2\text{H}\{^1\text{H}\}$ NMR (27 °C; CD_2Cl_2 , 61.4 MHz): 6.05 (b, Si–D); $^{13}\text{C}\{^1\text{H}\}$ NMR (27 °C; CD_2Cl_2 , 100.5 MHz): δ 200.0 (Rh–CO, dm, 1C, $^1J_{\text{RhC}} = 75.0$ Hz), 187.0 (Ir–CO, bs, 1C), 43.5 (CH_2 , m, 2C); $^{29}\text{Si}\{^1\text{H}\}$ (CD_2Cl_2 , 79.5 MHz, DEPT): δ 127.0 (m). IR: $\nu_{\text{SiH}} = 2197\text{ cm}^{-1}$, $\nu_{\text{CO}} = 1945\text{ cm}^{-1}$, 1928 cm^{-1} .

h. **[RhIr(CO)₂(μ -SiHC₆H₃F₂)₂(dppm)₂] (8c)**: Under Ar, 50 mg (0.044 mmol) of **[RhIr(CO)₃(dppm)₂] (1)** in a 50 mL Schlenk tube was dissolved in 5 mL of benzene. 29 μL (0.176 mmol, 4 equiv) of 3,5-difluorophenylsilane dissolved in 0.5 mL of benzene in a 10 mL Schlenk tube was slowly transferred to the 50 mL Schlenk tube. The reaction was set in an oil bath at 60 °C for 24 h. Colourless crystals were separated from the reaction mixture by removing solvent with a cannula and were re-crystallized from CH_2Cl_2 /ether. Yield: 29 mg (47 %). Anal. calcd. for $\text{C}_{64}\text{H}_{52}\text{F}_4\text{IrO}_2\text{P}_4\text{RhSi}_2$: C, 54.69; H, 3.70. Found: C, 54.85; H, 3.73. $^{31}\text{P}\{^1\text{H}\}$ NMR (27 °C; CD_2Cl_2 , 161.9 MHz): δ 28.0 (Rh–P, 2P, dm, $^1J_{\text{RhP}} = 108$ Hz), 0.3 (Ir–P, 2P, m); ^1H NMR (27 °C; CD_2Cl_2 , 399.8 MHz): δ 5.82 (Si–H, m, 2H, $^1J_{\text{SiH}} = 180$ Hz), 5.25 (CH_2 , m, 2H), 3.26 (CH_2 , m, 2H); $^{13}\text{C}\{^1\text{H}\}$ NMR (27 °C; CD_2Cl_2 , 100.5 MHz): δ 199.0 (Rh–CO, 1C, dm, $^1J_{\text{RhC}} = 70.0$ Hz), 187.0 (Ir–CO, 1C, bs), 43.8 (CH_2 , m, 2C); $^{29}\text{Si}\{^1\text{H}\}$ NMR (27 °C; CD_2Cl_2 , 79.5 MHz, DEPT): δ 125.0 (m); ^{19}F (CD_2Cl_2 , 376.1 MHz): -113.5 (m).

i. **[RhIr(CO)₂(μ-SiHPh)(μ-SiHC₆H₃F₂)(dppm)₂] (8d):** *Method 1:* Under an atmosphere of Ar, 50 mg (0.041 mmol) of [RhIr(H)₂(CO)₂(μ-SiHPh)(dppm)₂] (**4**) in a NMR tube was dissolved in 0.7 mL of C₆D₆. 13.0 μL (0.082 mmol, 2 equiv) of 3, 5-difluorophenylsilane was added to the NMR tube via microlitre syringe. The reaction was set in an oil bath at 60 °C for 24 h under dynamic Ar atmosphere during which time a white precipitate formed. The precipitated product (**8d**) was separated from the reaction mixture by removing solvent with a cannula and was re-crystallized from CH₂Cl₂/pentane. Yield: 25 mg (45 %). Anal. calcd. for C₆₄H₅₄F₂IrO₂P₄RhSi₂: C, 56.13; H, 3.95. Found: C, 56.37; H, 3.98. *Method 2:* Under the similar conditions, as mentioned above, 20 mg (0.022 mmol) of [RhIr(CO)₂(μ-SiHPh)₂(dppm)₂] (**8a**) was reacted with 7.8 μL (0.044 mmol, 2 equiv) of 3, 5-difluorophenylsilane. Multinuclear NMR analysis confirmed the complete conversion of **8a** to a mixture of **8b** (NMR yield, 50%), **8c** (NMR yield, 16.66%) and **8d** (NMR yield, 33.33%). ³¹P{¹H} NMR for **8d** (27 °C; CD₂Cl₂, 201.6 MHz): δ 27.6 (Rh–P, dm, 1P, ¹J_{RhP} = 107 Hz), 26.2 (Rh–P, dm, 1P, ¹J_{RhP} = 105 Hz), –1.1 (Ir–P, 1P, m), –1.6 (Ir–P, 1P, m); ¹H NMR for **8d** (27 °C; CD₂Cl₂, 498.1 MHz): δ 5.95 (Si–H, m, 1H, ¹J_{Si-H} = 180 Hz), 5.82 (Si–H, m, 1H, ¹J_{SiH} = 180 Hz), 5.26 (CH₂, m, 1H), 5.28 (CH₂, m, 1H), 3.25 (CH₂, m, 1H); ¹³C{¹H} NMR for **8d** (27 °C; CD₂Cl₂, 100.5 MHz): δ 199.5 (Rh–CO, dm, 1C, ¹J_{RhC} = 70.0 Hz), 187.0 (Ir–CO, bs, 1C), 43.5 (CH₂, m, 1C), 43.1 (CH₂, m, 1C); ²⁹Si{¹H} NMR for **8d** (27 °C; CD₂Cl₂, 79.5 MHz, DEPT): δ 126.3 (m), 125.2 (m); ¹⁹F NMR for **8d** (27 °C; CD₂Cl₂, 376.1 MHz): –111.9 (m).

j. **[RhIr(H)₂(CO)₂(μ-SiPh₂)(dppm)₂] (9)**: Under an Ar atmosphere, 50 mg of [RhIr(CO)₃(μ-dppm)₂] (**1**) (0.044 mmol) in a Schlenk tube was dissolved in 4 mL of benzene. 12.2 μL (1.5 equiv) of Ph₂SiH₂ was added by syringe to the vigorously stirred solution of **1** and the reaction was left for 6 h. During this time the colour of the solution lightened, accompanied by the formation of a pale yellow solid. The solvent was evaporated under vacuum and the residue was redissolved in 2 mL of C₆D₆. The slow addition of 6 mL of pentane resulted in the precipitation of complex **9** in 69% (40 mg) yield. Anal. calcd. for C₆₄H₅₆IrO₂P₄RhSi: C, 58.88; H, 4.29. Found: C, 59.19; H, 4.95. ³¹P{¹H} NMR (27 °C; CD₂Cl₂, 161.9 MHz): δ 21.5 (bm), -11.7 (bm); ¹H NMR (27 °C CD₂Cl₂, 399.8 MHz): δ 4.83 (CH₂, m, 2H), 3.14 (CH₂, m, 2H), -9.73 (bm), -11.50 (bm, 1H); ¹³C{¹H} NMR (27 °C; CD₂Cl₂, 100.5 MHz): δ 198.7 (Rh-CO, dt, 1C, ¹J_{RhC} = 69 Hz), 182.9 (Ir-CO, t, 1C), 50.2 (CH₂, m, 1C), 45.8 (CH₂, m, 1C); ³¹P{¹H} NMR (-78 °C; CD₂Cl₂, 161.9 MHz): δ 24.3 (Rh-P, 1P, m), 15.4 (Rh-P, 1P, m), -5.8 (Rh-P, 1P, m), -19.5 (Rh-P, 1P, m); ¹H NMR (-78 °C; CD₂Cl₂, 399.8 MHz): δ 5.35 (CH₂, m, 1H), 4.94 (CH₂, m, 1H), 3.13 (CH₂, bm, 1H), 2.94 (CH₂, m, 1H), -9.76 (Rh-H, ddd, 1H, ¹J_{RhH} = 15.0 Hz, ²J_{trans PH} = 120.0 Hz, ²J_{cis PH} = 14.0 Hz), -11.09 (Ir-H, dd, 1H, ²J_{trans PH} = 114.0, ²J_{cis PH} = 14 Hz). IR: ν_{CO} = 1980 cm⁻¹, 1937 cm⁻¹.

k. **[RhIr(CO)₄(κ¹-dppm)(μ-SiHPh)(dppm)](10) and [RhIr(CO)₂(μ-CO)(μ-SiHPh)(dppm)₂] (11)**: A total of 20 mg of [RhIr(H)₂(CO)₂(μ-SiPh₂)(dppm)₂] (**9**) was dissolved in 0.5 mL of CD₂Cl₂ in an NMR tube and pressurized with CO (1.0 atm). After 18 h, the ³¹P{¹H} NMR analysis showed the presence of tetracarbonyl

species, **10**, in about 75 % yield, together with $[\text{RhIr}(\text{CO})_3(\mu\text{-dppm})_2]$ (**1**) generated from **9** by the loss of silane. The reaction mixture was then transferred to a 10 mL Schlenk flask, and the solvent was removed under high vacuum. The deep orange residue was redissolved in 0.7 mL of CD_2Cl_2 , and the NMR analysis of this mixture indicated the formation of tricarbonyl silylene species, **11**, in approximately 10 % yield (according to NMR), leaving the solution as a mixture of **1**, **10** and **11** in a 2.5:1.6:6.5 ratio. Addition of CO to **11** generates **10**. Attempts to isolate analytically pure **10** and **11** failed.

$^{31}\text{P}\{^1\text{H}\}$ NMR for **10** (27 °C; CD_2Cl_2 , 161.9 MHz): δ 18.1 (Rh–P, 1P, ddd, $^1J_{\text{RhP}} = 101$ Hz, $^2J_{\text{PP}} = 125$ Hz, $^3J_{\text{PP}} = 5$ Hz), –10.3 (Ir–P, 1P, ddd, $^2J_{\text{PP}} = 40$ Hz, $^2J_{\text{PP}} = 5$ Hz), –10.4 (Ir–P, 1P, dd, $^2J_{\text{PP}} = 125$ Hz, $^4J_{\text{PP}} = 5$ Hz), –26.2 (Pendent–P, 1P, dd, $^2J_{\text{PP}} = 40$ Hz, $^4J_{\text{PP}} = 5$ Hz); ^1H NMR for **10** (27 °C; CD_2Cl_2 , 399.8 MHz): δ 3.17 (CH_2 , m, 2H) 2.84 (CH_2 , m, 2H); $^{13}\text{C}\{^1\text{H}\}$ NMR for **10** (27 °C; CD_2Cl_2 , 100.5 MHz): δ 212.4 (semi-bridging CO, dm, 1C, $^1J_{\text{RhC}} = 5.6$ Hz, 1C), 201.7 (Rh–CO, dm, 1C, $^1J_{\text{RhC}} = 71.8$ Hz), 201.6 (Rh–CO, dm, 1C, $^1J_{\text{RhC}} = 73.6$ Hz), 185.3 (Ir–CO, b, 1C), 60.3 (CH_2 , m, 1C), 37.9 (CH_2 , m, 1C).

$^{31}\text{P}\{^1\text{H}\}$ NMR for **11** (27 °C; CD_2Cl_2 , 161.9 MHz): δ 37.8 (Rh–P, 1P, ddd, $^1J_{\text{RhP}} = 107$ Hz, $^2J_{\text{PP}} = 255$ Hz, $^2J_{\text{PP}} = 30$ Hz), 27.5 (Rh–P, 1P, ddd, $^1J_{\text{RhP}} = 98$ Hz, $^2J_{\text{PP}} = 156$ Hz, $^2J_{\text{PP}} = 30$ Hz), 1.5 (Ir–P, 1P, dd, $^2J_{\text{PP}} = 255$ Hz, $^2J_{\text{PP}} = 22$ Hz), –5.3 (Ir–P, 1P, dd, $^2J_{\text{PP}} = 156$ Hz, $^2J_{\text{PP}} = 22$ Hz); ^1H NMR for **11** (27 °C; CD_2Cl_2 , 399.8 MHz): δ 4.37 (CH_2 , m, 1H), 3.98 (CH_2 , m, 1H), 2.66 (CH_2 , m, 1H), 2.32 (CH_2 , m, 1H); $^{13}\text{C}\{^1\text{H}\}$ NMR (27 °C; CD_2Cl_2 , 100.5 MHz) for **11**: 227.6 (Rh–CO, dm, 1C,

$^1J_{\text{RhC}} = 40.7$ Hz, 1C), 201.3 (Rh–CO, dm, 1C, $^1J_{\text{RhC}} = 70.0$ Hz), 186.0 (Ir–CO, bs, 1C).

1. **[RhIr(H)(SiPh₂H)(CO)₃(κ¹-dppm)(μ-SiPh₂)(dppm)] (12).** *Method 1:* A total of 30 mg of [RhIr(H)₂(CO)₂(μ-SiPh₂)(dppm)₂] (**9**) (0.023 mmol) in a Schlenk tube was dissolved in 4 mL of benzene and the tube was pressurized with 1 atm of CO followed by the addition of 4.25 μL (1 equiv) of Ph₂SiH₂. The reaction flask was sealed and left for 24 h after which the solvent was removed under high vacuum, and the solid redissolved in 1 mL of benzene. Slow addition of pentane resulted in the formation of lemon yellow precipitate, which was again recrystallized from the benzene/pentane to give analytically pure compound **12**.

Method 2: In a Schlenk tube 200 mg of [RhIr(CO)₃(dppm)₂] (0.174 mmol) was dissolved in 10 mL of benzene. Three freeze-pump-thaw cycles were applied to the solution, followed by the addition of 128 μL (4 equiv) of Ph₂SiH₂. The reaction was stirred for 48 h in the sealed Schlenk tube. The solution was concentrated to 2 mL and layered with pentane. After 24 h orange crystals were separated by the removal of solvent. Yield: 202 mg (76.8 %). Anal. calcd. for C₇₇H₆₆IrO₃P₄RhSi₂•1.5C₆H₆: C, 63.25; H, 4.59. Found: C, 63.16; H, 4.60. Under the conditions noted in method 1, the reaction of compound **9** with PhSiD₃ resulted in deuterium scrambling in silyle and hydride position of **12** to give **12_d**.

$^{31}\text{P}\{^1\text{H}\}$ NMR (27 °C; CD₂Cl₂, 161.9 MHz): δ 3.1 (Rh–P, 1P, ddd, $^1J_{\text{RhP}} = 94$ Hz, $^2J_{\text{PP}} = 103$ Hz, $^3J_{\text{PP}} = 6$ Hz), – 2.5 (Ir–P, 1P, dddd, $^2J_{\text{PP}} = 36$ Hz, $^2J_{\text{PP}} = 9$ Hz, $^3J_{\text{RhP}} = 5$ Hz, $^3J_{\text{PP}} = 6$ Hz), – 9.5 (Ir–P, 1P, ddd, $^2J_{\text{PP}} = 103$ Hz, $^2J_{\text{PP}} = 9$ Hz, $^4J_{\text{PP}} = 8$ Hz), – 27.9 (pendent–P, 1P, dd, $^2J_{\text{PP}} = 35$ Hz, $^4J_{\text{PP}} = 8$ Hz); ^1H NMR (27 °C; CD₂Cl₂,

399.8 MHz): δ 5.45 (CH₂, m, 1H), 5.30 (Si-H, d, 1H, $^1J_{\text{SiH}} = 180$ Hz $^3J_{\text{PH}} = 7$ Hz), 3.80 (CH₂, m, 1H), 3.20 (CH₂, m, 1H), 2.70 (CH₂, m, 1H), -10.50 (Ir-H, dd, 1H, $^2J_{\text{PH}} = 19$ Hz, $^2J_{\text{PH}} = 15$ Hz); $^2\text{H}\{^1\text{H}\}$ NMR (27 °C; CD₂Cl₂, 61.4 MHz): 5.29 (b, Si-D, 1D), -10.44 (b, Si-D, 1D), $^{13}\text{C}\{^1\text{H}\}$ NMR (27 °C; CD₂Cl₂, 100.5 MHz): δ 203.9 (Rh-CO, dddd, 1C, $^1J_{\text{RhC}} = 55.8$ Hz, $^2J_{\text{PC}} = 24.1$ Hz, $^3J_{\text{PC}} = 8.6$ Hz, $^2J_{\text{CC}} = 29.1$ Hz), 199.8 (Rh-CO, dm, 1C, $^1J_{\text{RhC}} = 55.6$ Hz, $^2J_{\text{PC}} = 22.3$ Hz, $^3J_{\text{PC}} = 9.4$ Hz), 186.1 (Ir-CO, bs, 1C), 59.2 (CH₂, m, 1C), 37.3 (CH₂, m, 1C); $^{29}\text{Si}\{^1\text{H}\}$ NMR (27 °C; CD₂Cl₂, 78.5 MHz, DEPT, gHSQC: δ -2.3 (dd, $^1J_{\text{RhSi}} = 18$, $^2J_{\text{PSi}} = 18$ Hz), 146.0. IR : $\nu_{\text{SiH}} = 2077$ cm⁻¹, $\nu_{\text{CO}} = 2032, 1943, 1972$ cm⁻¹.

m. **[RhIr(H)(SiMe₂H)(CO)₃(κ^1 -dppm)(μ -SiMe₂)(dppm)] (13):** A static atmosphere of dimethylsilane was placed over a solution of [RhIr(CO)₃(dppm)₂](1) (40 mg, 0.035 mmol in 3 mL of CH₂Cl₂) and the reaction mixture was stirred for 1 h. Addition of 10 mL of pentane caused the precipitation of a dull orange powdery solid which was washed twice with 5 mL portions of pentane and dried under Ar (44 mg, 88 %). Anal. calcd. for C₅₇H₅₈IrO₃P₄RhSi₂: C, 53.96; H, 4.57. Found C, 53.84; H, 4.24. $^{31}\text{P}\{^1\text{H}\}$ NMR (27 °C; CD₂Cl₂, 161.9 MHz): δ 6.6 (Rh-P, 1P, ddd, $^1J_{\text{RhP}} = 100$ Hz, $^2J_{\text{PP}} = 111$ Hz, $^3J_{\text{PP}} = 6$ Hz), 0.1 (Ir-P, 1P, dddd, $^2J_{\text{PP}} = 50$ Hz, $^2J_{\text{PP}} = 9$ Hz, $^3J_{\text{PP}} = 6$ Hz, $^3J_{\text{RhP}} = 5$ Hz), -9.9 (P_B, 1P, ddd, $^2J_{\text{PP}} = 111$ Hz, $^2J_{\text{PP}} = 9$ Hz $^4J_{\text{PP}} = 6$ Hz), -26.7 (pendent-P, 1P, dd, $^2J_{\text{PP}} = 50$ Hz, $^4J_{\text{PP}} = 6$ Hz); ^1H NMR (27 °C; CD₂Cl₂, 399.8 MHz): δ 4.84 (CH₂, m, 1H), 4.40 (CH₂, m, 1H), 4.20 (Si-H, m, 1H, $^3J_{\text{PH}} = 7.9$ Hz), 2.92 (CH₂, m, 2H), 0.84 (CH₃, m, 3H, $^4J_{\text{PH}} = 3.2$ Hz), 0.75 (CH₃, m, 3H, $^4J_{\text{PH}} = 3.2$ Hz), 0.24 (CH₃, d, 3H, $^3J_{\text{HH}} = 4.0$ Hz), 0.17 (CH₃, m, 3H, $^3J_{\text{HH}} = 4.0$ Hz), -11.20 (Ir-H, dd, 1H, $^2J_{\text{PH}} =$

15.0 Hz, $^2J_{\text{PH}} = 14.0$ Hz); $^{13}\text{C}\{^1\text{H}\}$ NMR (27 °C; CD_2Cl_2 , 100.5 MHz): δ 204.5 (Rh–CO, dddd, 1C, $^1J_{\text{RhC}} = 55.0$ Hz, $^2J_{\text{PC}} = 19.1$ Hz, $^3J_{\text{PC}} = 6.3$ Hz $^2J_{\text{CC}} = 21.8$ Hz), 203.4 (Rh–CO, dddd, 1C, $^1J_{\text{RhC}} = 55.0$ Hz, $^2J_{\text{PC}} = 19.0$ Hz, $^3J_{\text{PC}} = 8.9$ Hz $^2J_{\text{CC}} = 22.3$ Hz) 187.4 (Ir–CO, bs, 1C), IR : $\nu_{\text{CO}} = 1999, 1977$ cm^{-1} .

n. **[RhIr(CH₃)(SiHPh₂)(CO)(μ -H)(μ -CO)(dppm)₂][CF₃SO₃] (14)**: Under Ar, 28 mg (0.022 mmol) of [RhIr(CH₃)(CO)₂(dppm)₂][CF₃SO₃] (**2**) was taken into an NMR tube, dissolved in 0.7 mL of CD_2Cl_2 and cooled to -78 °C in an acetone-dry-ice bath. 4.1 μL (0.022 mmol) of diphenylsilane was added by a microliter syringe and the reaction was observed by low-temperature NMR. Immediately after addition of diphenylsilane the dark orange colour of the solution lightened. Between -80 °C to -60 °C, NMR analysis indicates the formation of [RhIr(CH₃)(SiHPh₂)(CO)(μ -H)(μ -CO)(μ -dppm)₂][CF₃SO₃] (**14**) as the major product (95 %) in the solution. No attempts were made to isolate this product at this temperature. ^{13}C -enriched compound **14** were prepared under the similar condition to those noted above, by reacting ^{13}C -enriched [RhIr($^{13}\text{CH}_3$)(^{13}CO)₂(dppm)₂][CF₃SO₃] (**2**) with Ph_2SiH_2 . $^{31}\text{P}\{^1\text{H}\}$ NMR (-78 °C; CD_2Cl_2 , 161.9 MHz): δ 29.0 (Rh–P, dm, 1P, $^1J_{\text{RhP}} = 140$ Hz), -6.1 (Ir–P, b, 1P), -8.6 (Ir–P, b, 1P); ^1H NMR (-78 °C; CD_2Cl_2 , 399.8 MHz): δ 5.50 (Si–H, dt, 1H, $^1J_{\text{SiH}} = 170.0$, $^3J_{\text{PH}} = 13.5$, $^3J_{\text{HH}} = 2.0$ Hz), 4.12 (CH₂, m, 2H), 3.59 (CH₂, m, 2H), 0.49 (CH₃, t, 3H, $^3J_{\text{PH}} = 6.9$ Hz), -8.44 (μ -H, dm, 1H, $^1J_{\text{RhH}} = 13.8$ Hz, $^3J_{\text{HH}} = 2.0$ Hz); $^{13}\text{C}\{^1\text{H}\}$ NMR (-78 °C; CD_2Cl_2 , 100.5 MHz): δ 216.6 (Rh–CO, dm, 1C, $^1J_{\text{RhC}} = 31$ Hz), 173.8 (Ir–CO, t, 1C, $^2J_{\text{PC}} = 9.8$ Hz, $^2J_{\text{CH(trans)}} = 24.0$ Hz), 14.8

(CH₃, td, 1C, ¹J_{RhC} = 29.0 Hz, ²J_{PC} = 6.0 Hz); ²⁹Si{¹H} NMR (−78 °C; CD₂Cl₂, 79.5MHz, DEPT, gHSQC): δ −25.7 (t, ²J_{SiP} = 10.0 Hz).

o. [RhIr(CH₃)(CO)₂(μ-H)(η¹:η²-SiHPh₂)(dppm)₂][CF₃SO₃] (**15**) : *Method 1:*

As the solution of **14**, as discussed above, warmed to −20 °C the colour of the solution turned yellow from light orange. ³¹P{¹H} NMR suggested that compound

15 was formed in 83 % yield, with 17 % of **14** still present in the solution. *Method*

2: 40 mg of [RhIr(CH₃)(CO)₂(dppm)₂][CF₃SO₃] (**2**) in a Schlenk tube was

dissolved in 2 mL of CH₂Cl₂ and the reaction was carried out as described above

at −15 °C (ethylene glycol/dry-ice bath). Addition of 5 mL of ether precipitated a

yellow solid. The solvent was removed by cannula and the solid was dried under

vacuum at 0 °C. The solid was again washed with 1 mL of CH₂Cl₂ at −15 °C,

which preferentially removed species **14** (which had precipitated with **15**), leaving

15 as a pure product. The compound was stable at room temperature in the solid

state; however, in solution it decomposed within 30 min. Yield 32 mg (70%).

Anal. calcd. for C₆₆H₅₉F₃IrO₅P₄RhSiS: C, 53.97; H, 4.02; S, 2.18. Found: C,

53.50; H, 3.91; S, 2.19. ¹³C-enriched compound **15** was prepared under the similar

condition as mentioned above, by reacting ¹³C-enriched

[RhIr(¹³CH₃)(¹³CO)₂(dppm)₂][CF₃SO₃] (**2**) with Ph₂SiH₂. ³¹P{¹H} NMR (−20 °C;

CD₂Cl₂, 161.9 MHz): δ 22.7 (Rh–P, 2P, dm, ¹J_{RhP} = 100 Hz), −13.4 (Ir–P, 2P, m);

¹H NMR (CD₂Cl₂, 399.8 MHz): δ 4.10 (CH₂, m, 2H), 3.25 (CH₂, m, 2H), 0.73 (t,

3H), −0.65 (μ-Si–H, ddm, 1H, ¹J_{RhH} = 24 Hz, ¹J_{SiH} = 84.0 Hz, ²J_{H–H} = 6 Hz), −9.2

(μ-H, 1H, ¹J_{RhH} = 19 Hz, ²J_{HH} = 6 Hz); ¹³C{¹H}NMR (−20 °C; CD₂Cl₂, 100.5

MHz): 193.2 (Rh–CO, dt, 1C, ¹J_{RhC} = 78 Hz, ²J_{PC} = 15 Hz), 178.0 (Ir–CO, bt, 1C,

$^2J_{\text{CH}(\text{trans})} = 24$ Hz), -22.6 (CH₃, bt, 1C, $^2J_{\text{PC}} = 7.0$ Hz); $^{29}\text{Si}\{\text{H}\}$ NMR (-20 °C; CD₂Cl₂, 79.5 MHz, dept, gHSQC): δ 6.31 (m).

p. **[RhIr(H)(COCH₃)(CO)(μ -H)(μ -SiPh₂)(dppm)₂][CF₃SO₃] (16) and [RhIr(CO)₂(μ -H)(μ -SiPh₂)(dppm)₂ (17) :** As the CD₂Cl₂ solution of **15**, as discussed above, was warmed to ambient temperature a mixture of two products, **16** and **17**, was formed in a 1:1 mixture. Both of these complexes slowly decomposed at ambient temperature to unidentified products over 12 h. So, attempts to isolate the analytically pure **16** and **17** failed. ^{13}C -enriched compound **16** and **17** were prepared under similar condition to those mentioned above, by reacting ^{13}C -enriched [RhIr($^{13}\text{CH}_3$)(^{13}CO)₂(dppm)₂][CF₃SO₃] (**2**) with Ph₂SiH₂. $^{31}\text{P}\{\text{H}\}$ NMR for **16** (27 °C; CD₂Cl₂, 161.9 MHz): δ 26.5 (Rh–P, 1P, dm, $^1J_{\text{RhP}} = 118$ Hz), 2.8 (Ir–P, 1P, m); ^1H NMR for **16** (27 °C; CD₂Cl₂, 400 MHz): δ 4.28 (CH₂, m, 2H), 3.49 (CH₂, m, 2H), 1.23 (CH₃CO, s, 3H), -8.86 (Ir–H, , 1H, $^1J_{\text{SiH}} = 32.0$, $^2J_{\text{PH}} = 13.2$ Hz), -14.98 (μ -H, m, 1H, $^1J_{\text{RhH}} = 22.0$ Hz, $^2J_{\text{P}(\text{Ir})\text{H}} = 13.2$ Hz, $^2J_{\text{P}(\text{Rh})\text{H}} = 10.9$ Hz); $^{13}\text{C}\{\text{H}\}$ NMR for **16** (27 °C; CD₂Cl₂, 100.5 MHz): δ 280.0 (CH₃CO, s, $^1J_{\text{CC}} = 26.0$ Hz), 193.7 (Rh–CO, dt, $^1J_{\text{Rh-C}} = 70$ Hz), 46 (CH₃CO, s, $^1J_{\text{CC}} = 26.0$ Hz); $^{29}\text{Si}\{\text{H}\}$ NMR for **16** (27 °C; CD₂Cl₂, 79.5MHz, gHSQC): δ 20.0. $^{31}\text{P}\{\text{H}\}$ NMR for **17** (27 °C; CD₂Cl₂, 161.9 MHz): δ 24.3 (Rh–P, 1P, dm, $^1J_{\text{RhP}} = 105$ Hz), 9.9 (Ir–P, 1P, m); ^1H NMR for **17** (27 °C; CD₂Cl₂, 399.8 MHz): δ 4.42 (CH₂, bm, 2H), 4.40 (CH₂, bm, 2H), -10.22 (μ -H, bm, 1H, $^1J_{\text{RhH}} = 15$ Hz); $^{13}\text{C}\{\text{H}\}$ for **17** (27 °C; CD₂Cl₂, 100.5 MHz): δ 187.6 (Rh–CO, dm, 1C, $^1J_{\text{RhC}} = 77.3$ Hz), 176.8 (Ir–CO, bt, 1C).

2.3 X-ray Data Collection and Structure Determination

2.3.1 General Considerations.

Single crystals suitable for X-ray diffraction were obtained either by the slow diffusion of ether into a CH₂Cl₂ solution of the compounds (**4**, **5**, **8a**, **8c**) or by the diffusion of *n*-pentane into benzene (**12**) or THF (**8b**). Data were collected on either a Bruker D8/APEX II CCD diffractometer³⁶ (**4**, **5**, **8a**, **8b**, **8c**) at -100 °C using Mo K α radiation or on a Siemens P4/RA diffractometer³⁶ (**12**) at -60 °C using graphite monochromated Cu K α radiation. Data were corrected for absorption through the use of Gaussian integration from indexing of the crystal faces. The structures were solved using the Patterson/structure expansion (*DIRDIF-2008*) program system^{37a} (**5**) or direct methods [*SIR97*^{37b} (**4**, **8a**, **8c**), *SHELXS-86*^{37c} (**12**), *SHELXS-97*^{37d} (**8b**)]. Refinement was completed using the program *SHELXL-97*^{37d} (**4**, **5**, **8a**, **8b**, **8c**) or *SHELXS-93*³⁸ (**12**). Hydrogen atoms were assigned positions based on the *sp*² or *sp*³ hybridization geometries of their attached carbon atoms. Metal hydrides for **4** and **5** and silicon-hydrogen for **4**, **5**, **8a**, **8b** and **8c** were located on a difference Fourier map and isotropically refined for **5** and **8c**, whereas for **8a** only their positional parameters were refined, while for **4** and **12** the metal hydrides and Si-hydrogens were idealized. All the hydrogen atoms for which thermal parameters were not refined were given thermal parameter 20 % greater than the parent atoms. See Appendix I for a listing of crystallographic experimental data and for selected bond lengths and angles for all structures.

2.3.2 Special refinement conditions.

i. **Compound 4:** Metal atoms were refined with a site occupancy of either $\text{Ir}_{0.60}\text{Rh}_{0.40}$ or $\text{Ir}_{0.40}\text{Rh}_{0.60}$. The hydrido ligands were refined with fixed Ir–H or Rh–H distances (1.55 Å) and with isotropic displacement parameters 120 % of U_{eq} for their attached metals. The silyl hydrogens were included with fixed Si–H distances (1.35 Å) and isotropic displacement parameters 120 % of U_{eq} for their attached silicons.

ii. **Compound 5:** Metal sites were refined with a site occupancy of either $\text{Ir}_{0.80}\text{Rh}_{0.20}$ or $\text{Ir}_{0.20}\text{Rh}_{0.80}$. (molecule A) or with a site occupancy of either $\text{Ir}_{0.75}\text{Rh}_{0.25}$ or $\text{Ir}_{0.25}\text{Rh}_{0.75}$. (molecule B). Cl atoms of dichloromethane solvent were refined with an occupancy factor of 0.5. Cl(1S) and C(1S) were refined with common anisotropic displacement parameters (due to these atoms occupying near-inversion-related positions as generated by the crystallographic inversion centre ($1/2, 0, 1/2$)). The positions and isotropic displacement parameters of the metal hydrides were freely refined. The position of silyl hydrogens (H(1SI) and H(2SI)) were freely refined, with these atoms assigned a common isotropic displacement parameter.

iii. **Compound 8a:** Metal atoms were refined with site occupancy of either $\text{Ir}_{0.55}\text{Rh}_{0.45}$ or as $\text{Ir}_{0.45}\text{Rh}_{0.55}$. The carbon atoms of one phenyl group of the silylene bridge were refined as two sets of positions, one set with an occupancy of 0.80 and with anisotropic displacement parameters, the other set with an occupancy of 0.20, fixed C–C bond lengths of 1.39 Å, and a common isotropic displacement parameter. The positions of the silyl hydrogens were refined, with these atoms

assigned isotropic displacement parameters 120 % of U_{eq} for their attached silicons.

iv. **Compound 8b**: Metal atoms were refined with site occupancy of either $\text{Ir}_{0.60}\text{Rh}_{0.40}$ or $\text{Ir}_{0.40}\text{Rh}_{0.60}$. Disordered phenyl rings were refined with occupancy of 0.50. The silyl hydrogens were included with fixed Si–H distances (1.40 Å) and isotropic displacement parameters 120 % of U_{eq} for their attached silicons. Attempts to refine peaks of residual electron density as disordered or partial-occupancy solvent tetrahydrofuran oxygen or carbon atoms were unsuccessful. The data were corrected for disordered solvent electron density through use of the SQUEEZE procedure^{39a} as implemented in *PLATON*.^{39b,c} A total solvent-accessible void volume of 1150 Å³ with a total electron count of 350 (consistent with 8 molecules of solvent tetrahydrofuran, or 2 molecules per formula unit of the $[\text{RhIr}(\text{CO})_2(\mu\text{-SiHPh})_2(\mu\text{-dppm})_2]$ molecule) was found in the unit cell.

v. **Compound 8c**: Metal atoms were refined with site occupancy of either $\text{Ir}_{0.52}\text{Rh}_{0.48}$ or as $\text{Ir}_{0.48}\text{Rh}_{0.52}$. Silyl hydrogens were refined isotropically. The positions and isotropic displacement parameters of the silyl hydrogens were freely refined.

vi. **Compound 12**: The hydrido ligand was refined with a fixed Ir–H(1) (1.65 Å) and with a fixed isotropic displacement parameter.

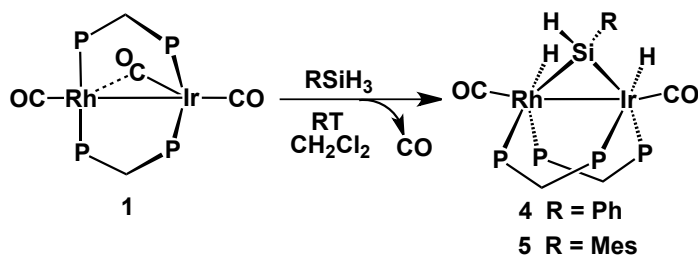
2.4 Results and Compound Characterization

2.4.1 Reactions of [RhIr(CO)₃(dppm)₂] with Primary Silanes

2.4.1.1 Monosilylene-bridged products

The reaction of [RhIr(CO)₃(dppm)₂] (**1**) with one equiv of the primary silanes, PhSiH₃ and MesSiH₃ (Mes = mesityl), proceeds as shown in Scheme 2.1, to give the silylene-bridged dihydride complexes, [RhIr(H)₂(CO)₂(μ-SiHR)(dppm)₂] (R = Ph (**4**) and R = Mes (**5**)), both of which were characterized by multinuclear NMR spectroscopy and X-ray crystallography. The NMR spectra of compounds **4** and **5** are closely comparable, so only those of **4** will be discussed.

Scheme 2.1



At ambient temperature, compound **4** displays four broad unresolved resonances in the ³¹P{¹H} NMR spectrum (Figure 2.1a) while at the same temperature the ¹H NMR spectrum displays the expected resonances for the dppm and silylene aryl groups. The dppm methylene protons of **4** appear as two multiplets at δ 5.30 and 3.10 while the broad silylene proton resonance (*ca.* δ 6.7) is buried beneath the aromatic protons as was confirmed by an HSQC experiment.

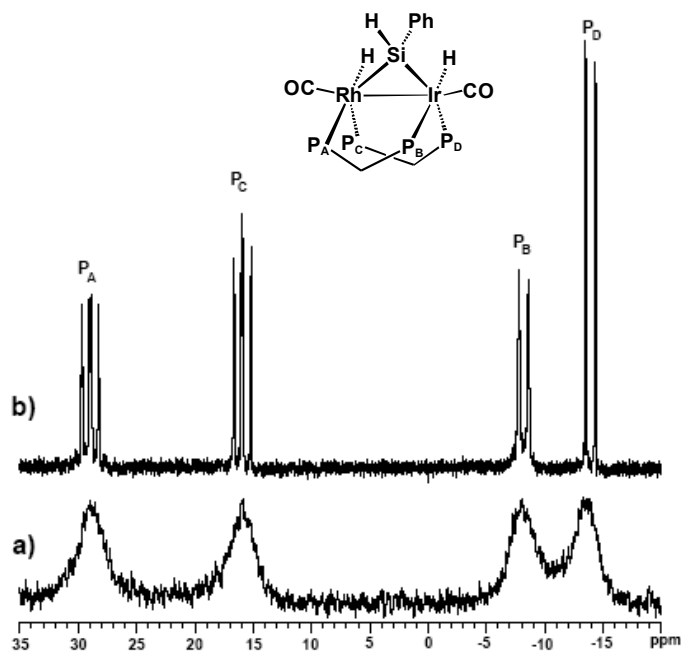


Figure 2.1: ^{31}P NMR spectra of complex **4** (a) at 20 °C and (b) at -40 °C

Both rhodium- and iridium-bound hydride ligands appear as very broad resonances, barely resolved above baseline, at *ca.* δ -9.6 and -10.9, respectively (Figure 2.2 a). The $^{31}\text{C}\{^1\text{H}\}$ NMR spectrum at this temperature shows a doublet of triplets at δ 194.1 ($^1J_{\text{RhC}} = 70$ Hz) and a triplet at δ 181.1, attributed to Rh- and Ir-bound carbonyls, respectively. Cooling both samples results in substantial sharpening in both the $^{31}\text{P}\{^1\text{H}\}$ NMR and ^1H NMR spectra demonstrating the fluxional nature of these species. Upon cooling to -40 °C, the $^{31}\text{P}\{^1\text{H}\}$ NMR resonances of **4** resolve into sharp multiplets at δ 29.0, 15.9, -8.2 and -14.0, consistent with an ABCDX spin system (Figure 2.1b). The assigned peaks for the phosphorus nuclei were established on the basis of the magnitude of the coupling

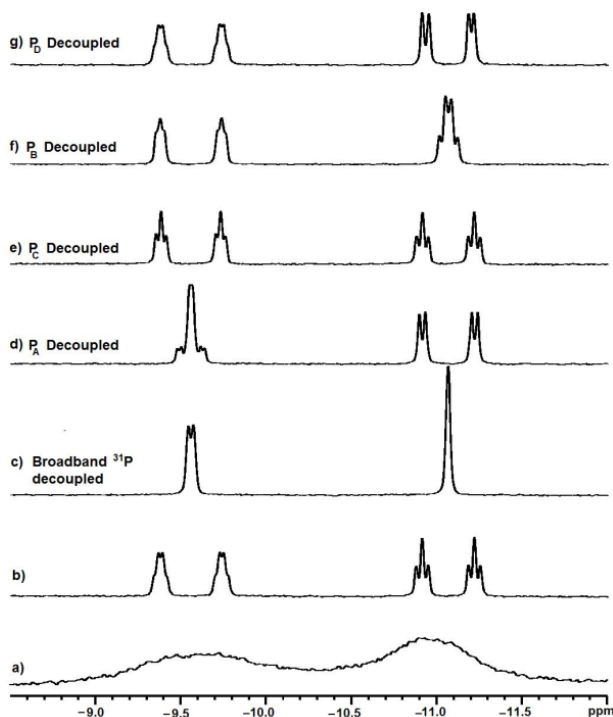


Figure 2.2: The metal-hydride region of ^1H -NMR spectrum of complex **4**: a) at 25 °C b) at -40 °C; spectra (c), (d), (e), (f) and (g) show different ^{31}P *P*-decoupling experiments at -40 °C.

to Rh and by ^{31}P homonuclear decoupling experiments. The down-field pair of resonances are assigned to the Rh-bound ^{31}P nuclei on the basis of their coupling (101.1 and 107.3 Hz) to ^{103}Rh .

In the ^1H -NMR spectrum at -40 °C four multiplets appear for the dppm-methylene protons, consistent with the structure shown for **4**, while the silicon- and metal-bound hydrogens all sharpen. The Si-bound proton appears as a broad singlet at δ 6.70 while the metal-hydride resonances appear at typically high field frequencies (see Fig. 2.2). Each of the hydride resonances displays strong coupling to the ^{31}P nucleus in the *trans* position ($^2J_{\text{HP(A)}} = 145$ Hz; $^2J_{\text{HP(B)}} = 123$ Hz, see Figure 2.1 for labeling) and additional, approximately equal coupling to

the distal ^{31}P nucleus at the other end of the diphosphine group that occupies the position *trans* to this hydride, and to the ^{31}P nucleus in the *cis* position (see Figure 2.2 for decoupling experiments). The Rh-bound hydride also displays 11.2 Hz coupling to this metal, as is obvious upon broadband ^{31}P decoupling (Figure 2.2 c).

The ^{29}Si NMR spectrum shows an approximate doublet of triplets at δ 142.9 with coupling to phosphorus and rhodium of 72 and 30 Hz, respectively. The P–Si coupling constant lies intermediate between the values reported for typically *trans* (*ca.* 183 Hz)⁴⁰ and *cis* (*ca.* 7.4 Hz)⁴¹ arrangements, in agreement with the intermediate arrangement obtained in the X-ray structure (*vide infra*).

Although the structures of both **4** and **5** were determined, only that of the latter is presented here owing to a disorder in the silylene phenyl ring of **4** and the overall similarities in both structures (see Appendix I for the structural information on compound **4**). Figure 2.3 shows the ORTEP diagram of one of the two crystallographically independent molecules of compound **5**. This structure very much resembles the homobinuclear analogs, $[\text{M}_2(\text{H})_2(\text{CO})_2(\mu\text{-SiRR}')(\text{dppm})_2]$ ($\text{M} = \text{Rh}, \text{Ir}$; $\text{R} = \text{Ph}, \text{Et}$; $\text{R}' = \text{H}, \text{Ph}$).⁹ In this species, as in all related dppm and silylene-bridged complexes, the metals are bridged by the silylene group while the diphosphines are bent back in a mutually *cis*, “cradle arrangement”. Both metals adopt distorted octahedral coordination geometries in which the hydride ligand on each metal is *trans* to one end of a diphosphine and *cis* to another, as suggested by the NMR spectral results. These hydrides do not

show any significant *trans*-influence as indicated by the closely comparable metal–phosphorus distances. Both hydride ligands and the silylene hydrogen were

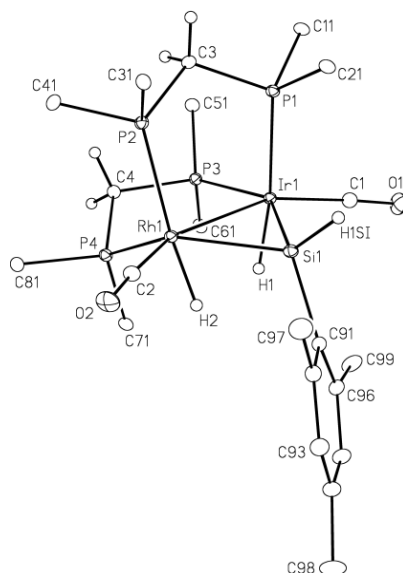


Figure 2.3: Perspective view of compound **5** showing the numbering scheme. Non-hydrogen atoms are represented by the Gaussian ellipsoids at the 20% probability level. Hydrogen atoms are shown arbitrarily small except for the mesityl protons which are not shown. For the *dppm* phenyl groups, only the ipso carbons are shown. Numbering for the aryl rings starts at the ipso carbon and works sequentially around the rings.

located and refined, yielding bond lengths (Ir–H(1) = 1.56(3) and 1.54(2) Å; Rh–H(2) = 1.48(3) and 1.52(3) and Si–H(SI) = 1.52(2) and 1.45(2) Å for the two independent molecules) that are typical for X-ray determinations.⁹ The silylene bridge is pseudo-*trans* at each metal to one end of the same diphosphine, with P(3)–Ir–Si angles of 145.08(2)° and 145.63(2)° and P(4)–Rh–Si angles of 129.52(2)° and 133.82(2)°.

As noted earlier, the Si–P coupling constant of 72 Hz, obtained in the ²⁹Si NMR spectrum, is consistent with the significant deviation from a rigorously

trans arrangement. This twist of the Rh coordination sphere with respect to that of Ir (P(1)–Ir–Rh–P(2) and P(3)–Ir–Rh–P(4) torsion angles ranging from 18.59(2)° to 21.40(2)°) is responsible for the greater deviation at Rh from a *trans* phosphine–silylene arrangement. This twisting of the coordination spheres at both metals forces the Rh-bound hydride into significantly closer contact with Si (2.19(3) and 2.24(3) Å) than that of Ir-bound hydride (2.60(3) and 2.63(3) Å). Whether these H---Si interactions corresponds to a significant degree of bonding between these two nuclei, is not clear. They lie beyond the 2.0 Å distances that Schubert has suggested as the upper limit of a Si–H agostic interaction^{6e} and consistent with this, we see no evidence of such an interaction in the NMR spectra. However, recent investigations indicate that a weak secondary interaction is possible between silicon and hydrogen when they lie within *ca.* 2.1 to 2.5 Å of each other.^{42, 43} If there is a weak Si–H interaction in the solid for the “Rh-bound” hydrides it is merely a solid-state effect, since there is a 3:2 disorder of the metals in the structure with the Rh position actually comprised of a 3:2 mix of Rh:Ir and the opposite being the case for the Ir position.

In order to gain a better understanding of the fluxionality in species **4**, saturation-transfer NMR experiments were carried out at lower temperature. When the Rh-bound hydride resonance was selectively saturated at –50 °C, resonances due to the Si-bound proton and the Ir-bound hydride collapse. A similar collapse was observed in the Si-bound proton and Rh-bound hydride resonances when Ir-bound proton was saturated, confirming the exchange among the three Si–H, Rh–H and Ir–H positions. However, accurately measuring the

intensity change in the silicon-bound proton resonance upon saturation of either metal-hydride resonance is not straightforward owing to overlap of this former signal with those of the phenyl groups. Alternatively, information about the differing exchange rates at Rh and Ir (which are expected to differ owing to the inherently different labilities of the metals) can, in principle, be obtained by saturation of the Si-bound proton resonance and observation of relative intensities resulting from different rates of saturation transfer to the pair of hydride resonances, which are well resolved. However, saturation of the Si-H resonance is not possible without simultaneous saturation of at least some of the phenyl proton resonances (due to their close proximity to Si-H in the ^1H NMR spectrum), and we were concerned that saturation transfer via NOE effects between these phenyl protons and the metal-hydrides could bias the exchange results. We therefore, carried out saturation transfer difference (STD) experiments, in which the difference between a normal ^1H NMR spectrum minus the spectrum resulting from the saturation transfer experiment is obtained, allowing the influence of saturating the metal-hydride resonances on the Si-bound hydrogen to be more readily determined. At $-50\text{ }^\circ\text{C}$, STD experiments suggest that the exchange process is approximately twice as fast at Rh than at Ir, as indicated by the intensity of the Si-bound proton peak which is twice as intense when the Rh-H resonance is irradiated (indicating more saturation transfer) compared to the intensity when the Ir-hydride resonance saturated. (See Figure A.3 in Appendix I). The metal-hydride signals also display saturation transfer in much the same way as each one of the the Rh-H or Ir-H resonances is saturated.

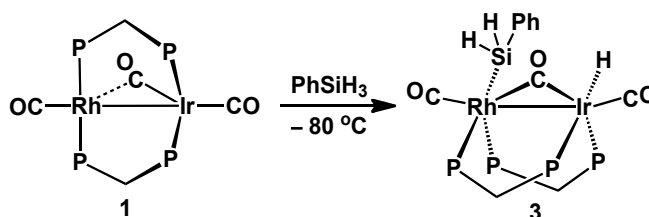
In the dirhodium analogue, $[\text{Rh}_2(\text{CO})_2(\text{H})_2(\mu\text{-SiHPh})(\text{dppm})_2]$,⁸ fluxionality similar to that noted above, was attributed to rapid oxidative addition and reductive elimination of the Si–H bonds at both metal centres, while no such fluxionality was observed in analogous diiridium species, $[\text{Ir}_2(\text{CO})_2(\text{H})_2(\mu\text{-SiHPh})(\text{dppm})_2]$,⁹ indicating the importance of at least one labile Rh centre to facilitate the exchange process.

We suggest at least two mechanisms that would explain the differing exchange rates involving the Rh- and Ir-bound hydrides with the silylene hydrogen. First, sequential oxidative addition/ reductive elimination (OA/RE) of a Rh and Ir-bound silyl group at the adjacent metal could be occurring, as proposed for the Rh_2 analogue. Faster exchange at the more labile Rh centre would rationalize the observed difference in exchange rate at lower temperatures. Alternatively, OA/RE could be occurring only at the more labile Rh centre accompanied by migration of the hydrides between the metals. Unfortunately, not enough data are available to establish whether either or both exchange mechanisms are involved.

If the addition of one equiv of PhSiH_3 to a CD_2Cl_2 solution of **1** is carried out at $-78\text{ }^\circ\text{C}$, almost quantitative formation of the first Si–H activation product, a silyl/hydride complex, $[\text{RhIr}(\text{H})(\text{SiH}_2\text{Ph})(\text{CO})_2(\mu\text{-CO})(\text{dppm})_2]$ (**3**), occurs (Scheme 2.2). This species was fully characterized by multi-nuclear NMR spectroscopy (see Figure A.4 in Appendix I for selected NMR spectra). At this temperature, the $^{31}\text{P}\{^1\text{H}\}$ NMR spectrum shows four multiplets, at δ 40.0, 25.2, –3.3 and –11.5, and again the two downfield resonances are assigned to Rh-bound

^{31}P nuclei on the basis of their large Rh–P couplings. The ^1H -NMR spectrum shows a doublet of doublets of doublets for the hydride at high field with one

Scheme 2.2

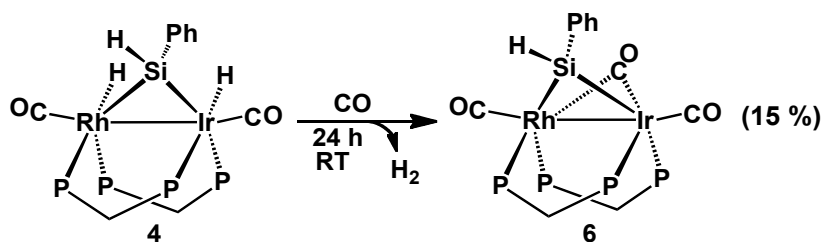


large *trans* P–H coupling (125 Hz) and two smaller couplings due to two other ^{31}P nuclei as described earlier for complex 4. This signal collapses to a singlet upon broadband ^{31}P -decoupling, with no resolvable coupling to Rh, confirming that it is Ir-bound. Selectively decoupling the ^{31}P signal at $\delta -3.3$ results in loss of the large *trans* $^2J_{\text{PH}}$ coupling. The two diastereotopic Si-bound hydrogens show two multiplet resonances at $\delta 4.23$ and 4.05 in the ^1H -NMR spectrum. SST NMR spectroscopy shows no sign of exchange between Si- and Ir-bound hydrogens at this temperature. $^{29}\text{Si}\{^1\text{H}\}$ NMR spectroscopy shows a well resolved multiplet (dddd) at $\delta -18.0$ having a large *trans* Si–P coupling constant (137 Hz), indicating a *trans*-disposition of the silyl group to one of the Rh-bound ^{31}P nuclei. The other couplings are due to Rh, the *cis*- ^{31}P and the distal- ^{31}P nucleus at the other end of diphosphine that is bound *trans* to the silyl group. It is also worth noting that due to the strong *trans*-influence of the the silyl ligand, the ^{31}P -nucleus *trans* to this group exhibits a reduced $^1J_{\text{Rh-P}}$ value (89 Hz) compared to the coupling of the ^{31}P -nuclei *cis* to the silyl group (107 Hz).¹¹ The position of the silyl group on Rh was also confirmed by a ^{13}C - ^1H HMBC NMR experiment in which the Si-bound protons show a three-bond correlation to both the Rh-bound and the bridging

carbonyls whereas the Ir-bound CO displays a two-bond correlation to the Ir-bound hydride. Three resonances at δ 178.0 (t), 199.0 (dt, $^1J_{\text{RhC}} = 70$ Hz) and 229.0 (m, $^1J_{\text{RhC}} = 34$ Hz), in the $^{13}\text{C}\{^1\text{H}\}$ NMR spectrum can be assigned to the Ir-bound, Rh-bound and bridging CO ligands, respectively. When a solution of **3** is warmed to -40 °C this species begins to disappear, being replaced by compound **4**, resulting from the oxidative addition of the second Si–H bond, and at -20 °C compound **4** is the sole species remaining, as indicated by NMR spectroscopy.

The reaction of species **4** with 1.0 atm of CO either at 60 °C over 30 min or at ambient temperature for 24 h results in the formation of the silylene and carbonyl-bridged species $[\text{RhIr}(\text{CO})_2(\mu\text{-SiPhH})(\mu\text{-CO})(\text{dppm})_2]$ (**6**) in approximately 10% yield (by $^{31}\text{P}\{^1\text{H}\}$ -NMR spectroscopy) by the reductive elimination of H_2 and CO addition (Scheme 2.3). Some of the tricarbonyl

Scheme 2.3



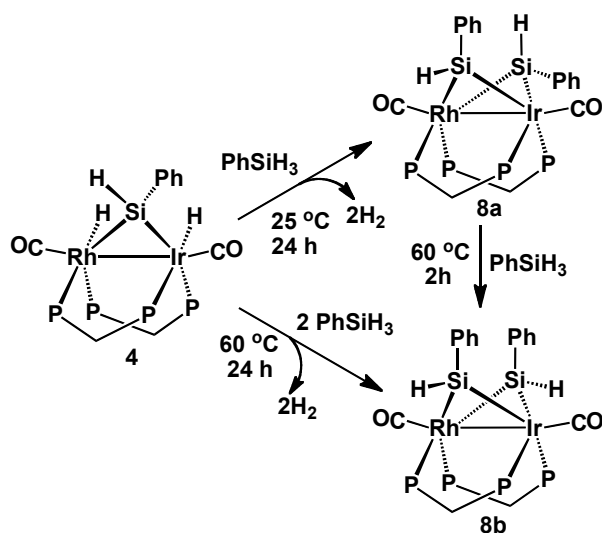
$[\text{RhIr}(\text{CO})_3(\text{dppm})_2]$ (**1**) (5%) also forms during the course of this reaction, indicating some silane loss from **4** in the presence of excess CO. The low yield of **6** is in contrast to the Rh_2 analogue, $[\text{Rh}_2(\text{CO})_2(\mu\text{-SiPhH})(\mu\text{-CO})(\text{dppm})_2]$, which forms quantitatively under similar conditions⁸ and also contrasts with the analogous Ir_2 dihydrides⁹ which are unreactive to CO. The $^{31}\text{P}\{^1\text{H}\}$ NMR and ^1H

NMR spectra of **6** display the typical resonances expected for an ABCDX system. The bridging CO appears as a downfield multiplet in the $^{13}\text{C}\{^1\text{H}\}$ NMR spectrum at δ 229.2 ($^1J_{\text{RhC}} = 31.9$ Hz) along with two other resonances at δ 199.9 ($^1J_{\text{RhC}} = 78.8$ Hz) and 183.4, assignable to Rh- and Ir-bound carbonyls, respectively. The formation of **6** in the presence of CO by the elimination of H_2 from **4** implies the possibility of incorporating other substrates, such as additional silane into this silylene-bridged core.

2.4.1.2 Bis-silylene-bridged products.

Further reaction of **4** with 1 equiv of phenylsilane or the reaction of **1** with two equiv of phenylsilane at ambient temperature yields the bis(silylene)-bridged complex, $[\text{RhIr}(\text{CO})_2(\mu\text{-SiPhH})_2(\text{dppm})_2]$ (**8a**), in which one silylene phenyl substituent is axial while the other is equatorial as shown in Scheme 2.4. At ambient temperature, in the presence of excess silane compound **8a** slowly converts, over a period of several days, to isomer **8b** in which both silylene

Scheme 2.4



phenyl groups are axial (see Figure A.5 in Appendix I for ^{31}P NMR spectrum for the isomeric conversion from **8a** to **8b**). This conversion takes only 2 h if heated to 60 °C. In the absence of excess silane complex **8a** is stable even at elevated temperature (60 °C), with no isomerization to **8b** observed.

The identities of isomers **8a** and **8b** were unambiguously established by their X-ray structure determinations, which are shown in Figure 2.4, with a

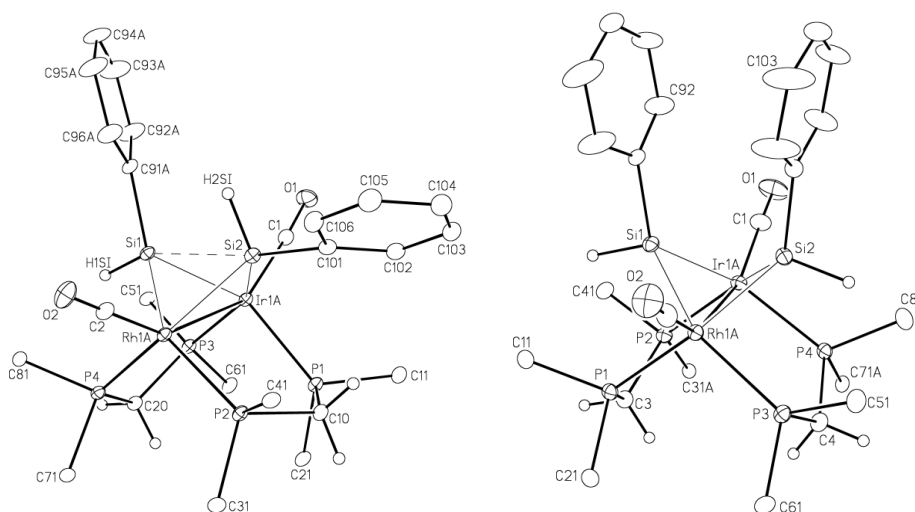


Figure 2.4: Perspective view of **8a** (left) and **8b** (right) showing the numbering scheme. Silylene-hydrogen positions of **8a** have been refined but these atoms were assigned thermal parameters 20% greater than those of their attached atoms. All hydrogens are shown artificially small in the figure. Other thermal parameters are shown as described in Figure 2.3. Only the ipso carbons of the dppm phenyl groups are shown.

summary of metrical parameters given in Table 2.1. Although superficially very similar, the significant difference in these two structures is, as noted above, the orientation of the silylene substituents. In **8b**, the phenyl ring on each silylene

group is axial such that the pair has an almost parallel π -stacking type of arrangement in which the distance between the *ipso* carbons is 3.291(5) Å, while the distance between the centroid of both groups is 3.736 Å and can be compared

Table 2.1: Selected bond distances (Å) and angles (deg) for **8a** and **8b**

Bond distances	8a	8b	Bond angles	8a	8b
Ir–Rh	2.796(3)	2.821(3)	Rh–Ir–Si(1)	53.88(3)	53.19(3)
Ir–Si(1)	2.364(1)	2.367(1)	Rh–Ir–Si(2)	54.44(3)	53.23(3)
Ir–Si(2)	2.366(1)	2.369(1)	Ir–Rh–Si(1)	53.70(2)	53.49(3)
Rh–Si(1)	2.369(1)	2.358(1)	Ir–Rh–Si(2)	53.60(3)	53.52(3)
Rh–Si(2)	2.392(1)	2.360(1)	Si(1)–Ir–Si(2)	71.51(4)	74.37(4)
Si(1)---Si(2)	2.764(1)	2.862(1)	Si(1)–Rh–Si(2)	70.97(4)	74.71(4)
Si(1)–H2SI	2.81(4)		Rh–Si(1)–Ir	72.42(3)	73.31(3)
			Rh–Si(2)–Ir	71.96(3)	73.24(3)

to the sum of the van der Waals radii for such groups (*ca.* 3.70 Å). Surprisingly perhaps, isomer **8b**, in which both bulky phenyl groups are adjacent, is favoured. However, in this axial/axial arrangement both groups avoid more serious repulsive interactions with the dpmm phenyl groups, while adopting the relatively favourable π -stacking arrangement noted above. Nevertheless, the mutual repulsion of these groups is obvious in the Si(1)–Ir–Si(2) and Si(1)–Rh–Si(2) angles in the two species (71.51(4)° and 70.97(4)°, respectively in **8a**, 74.37(4) and 74.71(4)° respectively in **8b**) demonstrating an opening up of the Rh(μ -SiHR)₂Ir “wing-tip” arrangement of the pair of μ -silylene groups, for the diaxial arrangement. This repulsion is more clearly demonstrated by the increase in Si---Si separation from 2.764(1) Å in **8a** to 2.862(1) Å in **8b**. Although it is tempting to attribute this difference to a weakly attractive interaction between two Si atoms

in the former (in which the Si---Si separation is close to the longest known Si–Si bond distance *ca.* 2.70 Å),^{44a} it is difficult to rule out a purely steric origin to these differences.

As a further indication that Si---Si contacts display little direct bonding interaction, the analogous species, $[\text{RhIr}(\text{CO})_2(\mu\text{-SiHC}_6\text{H}_3\text{F}_2)_2(\text{dppm})_2]$ (**8c**), having fluoro substituents in the meta position of the phenyl groups, was synthesized. As anticipated⁴⁵ the aryl rings in **8c**, having the electron-withdrawing fluorines attached, (Figure 2.5) have a closer approach than in **8b**, and display a separation between the *ipso* carbons of 3.233 Å and between the aryl-group centroids of 3.551 Å, yet the Si---Si separation (2.873(1) Å) is larger in this fluoro-substituted case, indicating that closer approach of Si atoms in **8c** is not inhibited by aryl-group repulsion.

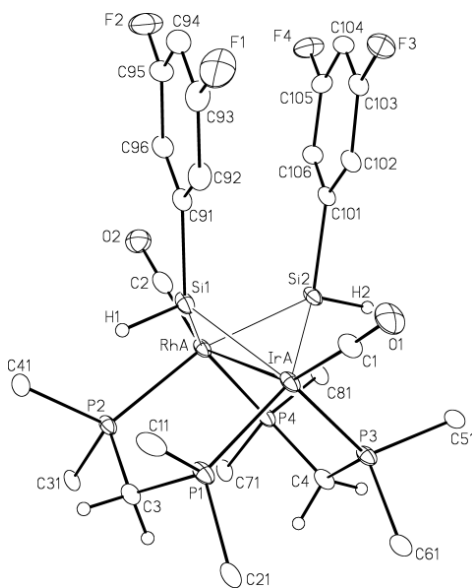


Figure 2.5: Perspective view of $[\text{RhIr}(\text{CO})_2(\mu\text{-SiHC}_6\text{H}_3\text{F}_2)_2(\text{dppm})_2]$ (**8c**) showing the numbering scheme. Thermal parameters are shown as described in Figure 2.3. Only the *ipso* carbons of the *dppm* phenyl groups are shown.

Consistent with the X-ray structures, in which all phosphorus environments are chemically inequivalent, the $^{31}\text{P}\{^1\text{H}\}$ NMR spectrum of **8a** shows four resonances at δ 29.3, 21.5, 2.6 and -7.8 (see Figure A.5 in Appendix I). The absence of symmetry in **8a** is also obvious in the ^1H NMR spectrum in which four multiplets appear for the inequivalent methylene protons and two resonances, a doublet of doublet of multiplets at δ 5.66 ($^3J_{\text{PH}} = 32$ Hz) and a broad multiplet δ 5.52 (with no observable $^3J_{\text{PH}}$ coupling), for two chemically inequivalent silicon-bound protons are observed. $^{29}\text{Si}\{^1\text{H}\}$ NMR shows two multiplets at δ 129.2 and δ 113.9 for **8a** indicating two different environments for the Si atoms. Interestingly, the two Si-bound protons show mutual coupling of 2.3 Hz, which is clearly demonstrated by 2D COSY and homonuclear $^1\text{H}\{^1\text{H}\}$ NMR experiments. Although coupling of this magnitude could arise from four-bond coupling through the dimetal-bis-silylene framework, it is significant that comparable 3-bond H–Si–Si–H coupling values between 2.2 and 2.5 Hz have been reported in a number of disilanes.^{44b} This coupling together with the relatively short Si---Si contact is suggestive of significant Si---Si interaction in this species, suggesting that the origin of the short contact may not arise exclusively from steric influences. Another explanation for the observed coupling between these silylene protons is the presence of a secondary Si–H interaction^{42, 43} involving the axial Si–H bond and the adjacent silylene group (see Figure 2.4). This possibility had previously been suggested for an analogous Rh_2 species on the basis of NMR studies,⁸ and now the structure determination of **8a** demonstrates the orientation of the axial

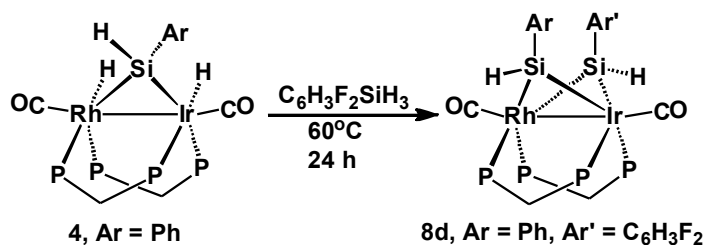
hydrogen towards the adjacent Si atom, although the contact (2.81(4) Å) appears to be long for such an interaction.^{43a}

The higher symmetry of **8b** is manifested in an AA'BB'X-type pattern in the $^{31}\text{P}\{^1\text{H}\}$ NMR spectrum in which only two multiplets at δ 28.6 (dm) ($^1J_{\text{RhP}} = 105$ Hz) and 0.3 (m) appear (see Figure A.5 in Appendix I). Also consistent with the higher symmetry, the ^1H NMR spectrum of **8b** shows two peaks for two types of dppm methylene protons (aimed towards or away from the μ -SiHPh groups) and one peak representing the Si-bound protons, all integrating equally as 2:2:2. In the $^{29}\text{Si}\{^1\text{H}\}$ -NMR spectrum, a multiplet at δ 127.0 is observed, having unresolved P–Si and Rh–Si coupling; this resonance lies slightly upfield compared to the monosilylene-bridged species **4** (δ 142.9). In both isomers (**8a** and **8b**) two $^{13}\text{C}\{^1\text{H}\}$ NMR resonance are observed for the carbonyls at *ca.* 187 and 200, with the latter displaying 74 Hz coupling to Rh in both compounds, confirming that for each species one carbonyl resides on each metal. The NMR spectra for **8c** very much resemble those of **8b**.

The reaction of complex **4** with two equivalent of 3,5-difluorophenylsilane produced mixed silylene-bridged complex $[\text{RhIr}(\text{CO})_2(\mu\text{-SiHPh})(\mu\text{-SiHC}_6\text{H}_3\text{F}_2)(\text{dppm})_2]$ (**8d**) in a moderate yield (45%), (Scheme 2.5), displaying two doublets of multiplets at δ 27.6 and 26.2 for Rh-bound phosphorus nuclei and two multiplets at δ –1.1 and –1.6 for Ir-bound ones in the $^{31}\text{P}\{^1\text{H}\}$ NMR spectrum. The Si-bound hydrogens appear as two multiplets at δ 5.95 and 5.82 in the ^1H NMR, and two multiplets appear at δ 126.3 and 125.2 in the $^{29}\text{Si}\{^1\text{H}\}$ NMR. The ^{19}F NMR spectrum displays a multiplet at δ –111.9, which is different from the

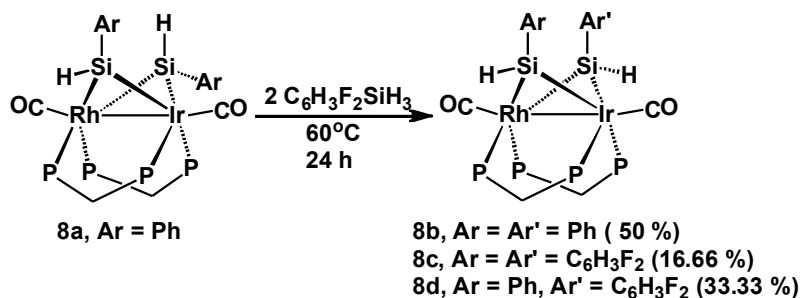
^{19}F chemical shift of **8c** ($\delta -113.5$, measured in the same temperature, solvent and frequency) and eliminates the possibility that the above-mentioned reaction is producing a fifty-fifty mixture of **8b** and **8c**.

Scheme 2.5



As noted earlier, the isomerization of **8a** to **8b** requires excess silane, implying the reversible incorporation of a third Si-containing fragment at the same stage of the isomerization. To test this possibility, compound **8a** was reacted with 3,5-difluorophenylsilane (Scheme 2.6). This reaction with 2 equiv of with 3,5-difluorophenylsilane produces a mixture of **8b** (50 %), **8c** (16.66 %) and **8d** (33.33 %) (the yields were calculated by the integration of Si–H resonances of **8b**,

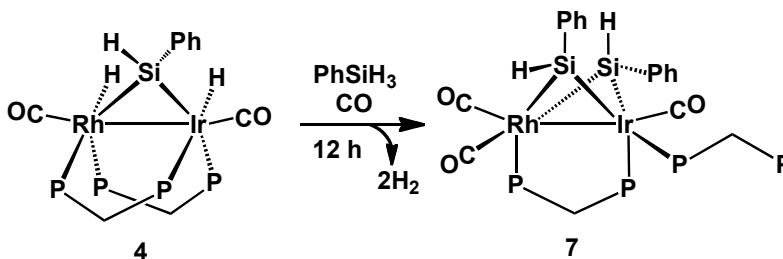
Scheme 2.6



8c and **8d** with respect to the residual solvent peak). The formation of products **8c** and **8d**, containing 3,5-difluorophenylsilylene moiety, confirms that the added silane has been incorporated, and the presence of **8b** indicates that this occurs before the elimination of one of the original SiHPh groups.

The reaction of **4** with 1 equiv of PhSiH₃ in the presence of CO results in almost quantitative formation of a *bis*(silylene)-bridged tricarbonyl complex [RhIr(CO)₃(κ¹-dppm)(μ-SiHPh)₂(dppm)] (**7**), in which one end of a diphosphine ligand is pendent, having been displaced from Rh by a carbonyl ligand (Scheme 2.7). The ³¹P{¹H} NMR spectrum of **7** displays four resonances at *ca.* δ 15.6, 3.4,

Scheme 2.7



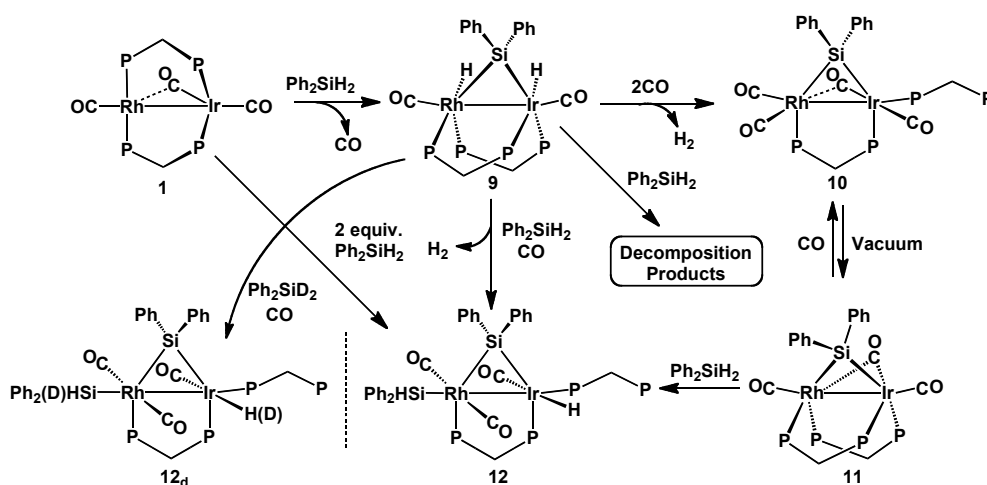
–10.5 and –24.5, of which only one at low-field displays coupling to Rh (105 Hz). The high-field resonance is close to the value for free dppm (δ –23.0), consistent with the presence of the pendent group. The ¹H-NMR spectrum displays two peaks for the two Si-hydrogens at δ 5.80 (dd) and 6.20 (dd), indicating chemically inequivalent environments, presumably a result of their axial/equatorial orientation as shown in **8a**. In this case, these inequivalent protons do not show mutual coupling. In the ²⁹Si{¹H} NMR spectrum, two resonances

appear at δ 101.8 (m) and 136.6 (m) for the two inequivalent silylene groups. The downfield NMR shifts for these groups indicate that both of them are in bridging positions.^{6b} Under high vacuum conditions or at elevated temperature, complex **7** converts exclusively to **8a** (in variable amounts, up to 20 %) by the loss of one CO from Rh and subsequent recoordination of the pendent end of the diphosphine. Neither isomer **8a** nor **8b** reacts with H₂ to release disilane as was the case in a previously reported dirhodium complex.¹¹

2.4.2 Reactions of [RhIr(CO)₃(dppm)₂] with Secondary Silanes.

The reaction of diphenylsilane with complex **1** yields the diphenylsilylene-bridged complex, [RhIr(H)₂(CO)₂(μ -SiPh₂)(dppm)₂] (**9**) (Scheme 2.8), analogous to the phenylsilylene-bridged species **4**. The formation of **9** is slower than that of **4**, requiring 6 h at ambient temperature, presumably due to the larger steric bulk

Scheme 2.8



of the more substituted silane. Like **4**, compound **9** is fluxional at 27 °C. The $^{31}\text{P}\{^1\text{H}\}$ NMR spectrum at this temperature appears as two broad peaks at *ca.* δ 21.5 and -11.7 , and cooling to -40 °C causes each broad signal to split into two sets of peaks (with unresolved P–M–P coupling), indicating the different environments of all phosphorus nuclei. The ^1H NMR spectrum behaves similarly, with two sets of broad, unresolved resonances each for the hydrides (δ -9.73 and -11.50) and for the dppm methylene protons (δ 4.83 and 3.14) at ambient temperature, which resolve upon cooling to -40 °C with the hydride resonances each displaying similar *trans* and *cis* coupling as was shown in complex **4** and with dppm methylene resonances appearing as four signals (δ 5.35, 4.94, 3.13, 2.94). Again, a saturation transfer NMR experiment at -20 °C indicates that the fluxionality of this species involves exchange of the metal-bound hydrides.

Upon further addition of diphenylsilane to **9**, incorporation of a second silylene group, as observed with primary silanes, was not observed; instead only decomposition products resulted. However, the addition of 1 equiv of diphenylsilane in the presence of 1 atm of CO quantitatively yields an unusual silyl(μ -silylene) complex, $[\text{RhIr}(\text{H})(\text{SiPh}_2\text{H})(\text{CO})_3(\kappa^1\text{-dppm})(\mu\text{-SiPh}_2)(\text{dppm})]$ (**12**), by the loss of 1 equiv of H_2 , dissociation of the Rh-end of one dppm group to give a pendent Ir-bound diphosphine and addition of the second equiv of silane. This compound also resulted from the reaction of compound **1** with 2 equiv of Ph_2SiH_2 in a sealed tube (Scheme 2.8). Clearly, the presence of CO is necessary to stabilize this silyl(silylene) complex, which is too crowded to allow the pendent dppm to coordinate to alleviate the unsaturation.

The $^{31}\text{P}\{^1\text{H}\}$ NMR spectrum for compound **12** displays an ABCDX spin pattern with peaks at δ 3.1, -2.5, -9.5 and -27.9 in which the resonance at δ 3.1 displays strong Rh–P coupling (94 Hz) while the upfield doublet of doublets is close to that of free dppm (δ -23.0), suggesting that this latter ^{31}P resonance corresponds to the pendent end of the dppm group. This high-field resonance is also close to that reported earlier for compound **7**, the related dirhodium species $[\text{Rh}_2(\text{CO})_3(\kappa^1\text{-dppm})(\mu\text{-CO})(\mu\text{-SiEt}_2)(\text{dppm})]^{8}$ and for other metal complexes having $\kappa^1\text{-dppm}$ ligands.⁴⁶ The Ir-bound ^{31}P nucleus of the pendent-dppm ligand exhibits weak coupling of 5 Hz to Rh. Since this coupling is far less than expected for direct bonding to Rh, this weak coupling presumably occurs via the Rh–Ir bond as the pendent phosphine is almost trans to the Rh–Ir axis (see the X-ray structure in Figure 2.6). A satisfactory simulation of the ^{31}P NMR spectrum of **12** was obtained by employing the values $J_{\text{RhP(A)}} = 94.4$ Hz, $J_{\text{RhP(D)}} = 5.1$ Hz, $J_{\text{P(A)P(B)}} = 103$ Hz, $J_{\text{P(A)P(D)}} = 5.6$ Hz, $J_{\text{P(B)P(C)}} = 8.3$ Hz, $J_{\text{P(B)P(D)}} = 6.5$ Hz, $J_{\text{P(C)P(D)}} = 35.6$ Hz (see Figure 2.7 for labeling).

The $^{13}\text{C}\{^1\text{H}\}$ NMR spectrum for **12** shows the presence of two carbonyl groups on Rh (δ 203.9 ($^1J_{\text{RhC}} = 55.8$ Hz) and δ 199.8 Hz ($^1J_{\text{RhC}} = 55.6$ Hz)) and one on Ir (δ 186.1), and the magnitude of the C–C couplings ($^2J_{\text{CC}} = 29.1$ Hz, determined by enriching the sample with ^{13}CO) between the pair of Rh-bound carbonyls is consistent with a mutually *trans* arrangement of these groups.⁴⁸ In the ^1H NMR spectrum the silyl hydrogen appears as doublet at δ 5.30 ($^3J_{\text{PH}} = 7.1$ Hz) with no resolvable coupling to Rh and collapses to a singlet only upon irradiation of the Rh-bound ^{31}P resonance, indicating that the silyl group is bound

to Rh. The hydride ligand appears as doublet of doublets at $\delta -10.5$ with approximately 15 and 19 Hz *cis*-coupling to both Ir-bound ^{31}P nuclei as established by selective $^{31}\text{P}\{^1\text{H}\}$ decoupling experiments. The absence of Rh–H coupling further indicates that the hydride is terminally bound to Ir. The terminally bound silyl group appears at $\delta -2.3$, as a pseudo-triplet in the $^{29}\text{Si}\{^1\text{H}\}$ NMR spectrum with coincidentally equal coupling to both ^{103}Rh and the Rh-bound ^{31}P nucleus, whereas the bridging silylene group appears at $\delta 146.0$. These chemical shifts are characteristic of a silyl and silylene groups, respectively (*vide supra*).

An X-ray structure determination of **12**, shown in Figure 2.6, confirms the proposed structure. To a first approximation, the geometry at each metal is

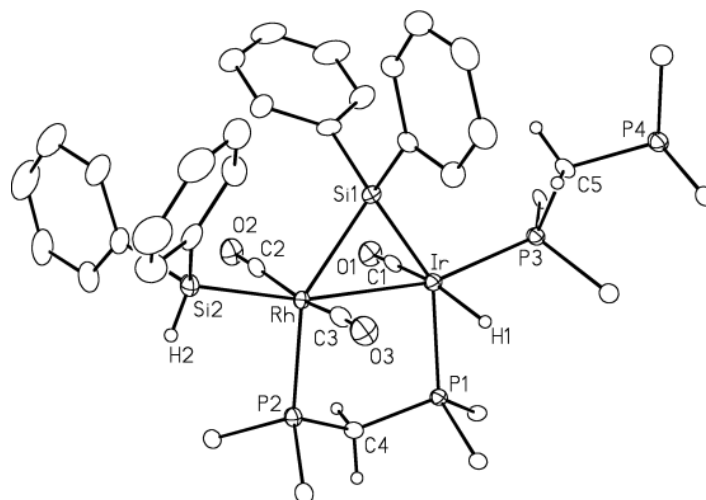


Figure 2.6: ORTEP drawing of **12** showing the atom labelling scheme. Thermal parameters are as described in Figure 2.3. Only the ipso carbons are shown for the dppm phenyl groups.

distorted octahedral in which the major distortions result from the strain imposed by the bridging SiPh₂ group which lies almost opposite the bridging dppm group. This silylene-bridged complex also has an accompanying Rh-bound diphenylsilyl group. The Rh–Si(1) and Ir–Si(1) bond lengths of 2.427(2) Å and 2.338(2) Å, respectively for the μ-silylene group are essentially equal to the Rh–Si(2) distance (2.398(2) Å) for the terminal silyl group, and all are comparable to previous determinations of related species.^{19-22, 49} As deduced from the NMR spectral data above, one dppm group is pendent and bound to Ir almost opposite the Rh–Ir bond, and opposite the silyl group on the adjacent metal. The mutually *trans* disposition of the two carbonyl groups on Rh as seen in the solution ¹³C{¹H} NMR spectrum is also present in the solid state. The closely comparable solution NMR and X-ray results indicate that there is no significant difference in the solution and solid-state structures of **12**.

The reaction of 2 equiv of Me₂SiH₂ with complex **1**, in the presence of CO yields the analogous species, [RhIr(H)(SiMe₂H)(CO)₃(η¹-dppm)(μ-SiMe₂)(dppm)] (**13**), having similar spectral parameters. In keeping with the much lower steric bulk of dimethylsilane, this reaction is much faster than that of diphenylsilane taking 1 h as opposed to 24 h for the latter, although the lower steric bulk is not enough to allow the formation of a pair of silylene bridges as seen for the primary silanes.

When the diphenylsilylene-bridged dihydride complex **9** is pressurized with CO in a sealed NMR tube at room temperature, the tetracarbonyl species,

$[\text{RhIr}(\text{CO})_4(\kappa^1\text{-dppm})(\mu\text{-SiPh}_2)(\text{dppm})]$ (**10**) results, in 75 % yield (according to ^{31}P NMR spectroscopy) accompanied by the evolution of H_2 (see Scheme 2.8). Also present in the reaction mixture is $[\text{RhIr}(\text{CO})_3(\text{dppm})_2]$ (**1**) resulting from the displacement of diphenylsilane by CO. The analogous tetracarbonyl complex was not observed during the reaction of **4** with CO, which gave only 10% of a tricarbonyl species (**6**) under similar conditions. The $^{13}\text{C}\{^1\text{H}\}$ NMR spectrum of this new species displays resonances at δ 212.4 ($^1J_{\text{RhC}} = 5.6$ Hz), 201.7 ($^1J_{\text{RhC}} = 71.8$ Hz), 201.6 ($^1J_{\text{RhC}} = 73.6$ Hz) and 185.3, which are assignable to one weakly bridging and three terminally bonded carbonyl groups, respectively. The absence of hydride signals in the ^1H NMR spectrum, together with the $^{31}\text{P}\{^1\text{H}\}$ NMR spectrum, which is characteristic of an ABCDX spin system and the chemical shift for the free end of the pendent diphosphine group, which appears up-field at δ -26.2 in the ^{31}P NMR spectrum, is consistent with the formulation shown in Scheme 8, much like that described above for **7** and **12** and related dirhodium species.⁸ Compound **10** loses CO reversibly to form the tricarbonyl species, $[\text{RhIr}(\text{CO})_2(\mu\text{-CO})(\mu\text{-SiPh}_2)(\text{dppm})_2]$ (**11**), in which the pendent dppm has re-coordinated to Rh to form a cradle-like tricarbonyl species, similar to compound **6** and the related species $[\text{Rh}_2(\text{CO})_2(\mu\text{-CO})(\mu\text{-SiPh}_2)(\text{dppm})_2]$.⁸ However, as with **6**, the formation of **11** is not complete, appearing as only approximately 10 % of the mixture of **1** and **10**. The spectral parameters from the ^{31}P spectral simulations for compounds **10** and **11** are summarized in Figure 2.7:

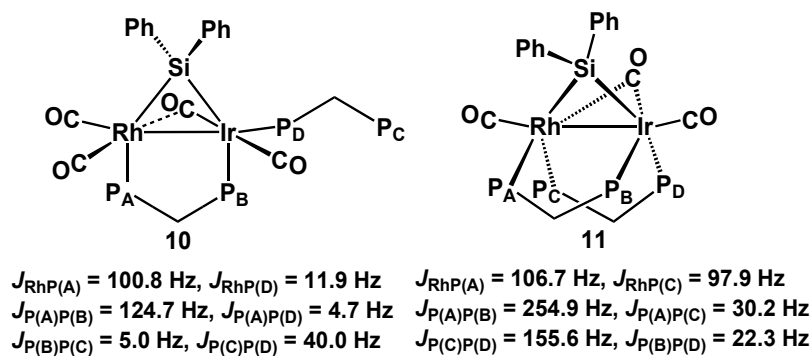


Figure 2.7: Coupling constants of **10** and **11** obtained from spectral simulation of the $^{31}\text{P}\{^1\text{H}\}$ spectra.

Not surprisingly, in the presence of excess diphenylsilane the mixture of compounds **1**, **10** and **11** yields **12** after 1 day. The reaction of **9** with Ph_2SiD_2 under 1 atm pressure of CO gives rise to the deuterium scrambled product (**12_d**), having a D:H ratio of 4:1, as confirmed by the ^2H NMR in which two peaks at δ 5.29 and -10.44 appear for the silyl deuterium and Ir-bound deuteride, respectively. In the ^1H NMR spectrum these two resonances appear at approximately 20 % intensity compared to the dppm-methylene protons and with the same resonances in a non-deuterated sample. The scrambling of H/D indicates that H_2 loss does not precede silane activation.

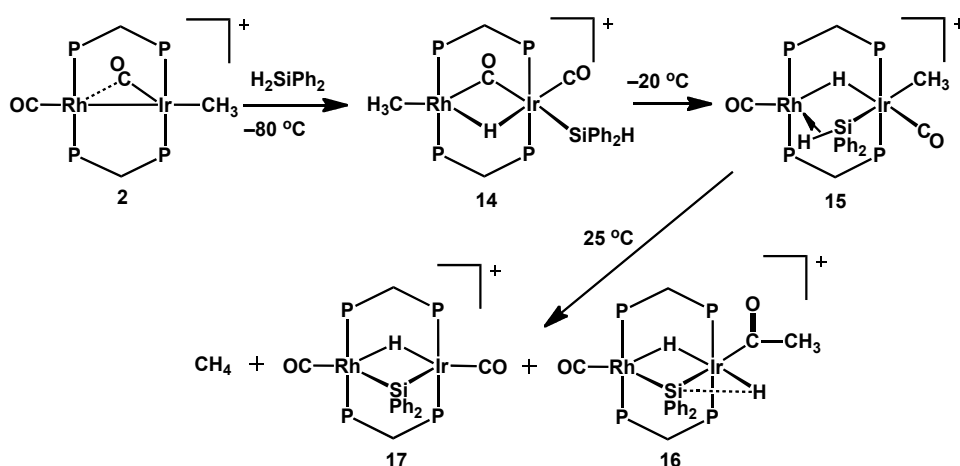
Bimetallic silyl(μ -silylene) complexes are not common in the literature, with only a few having been reported.^{19-22, 49} Silyl(silylene) complexes are of interest as many transition-metal-mediated reactions of organosilicon compounds, such as Si-Si bond formation, isomerisation and redistribution of organosilicon compounds, are thought to proceed via such species.^{49,50} More recently, a monometallic silyl(silylene) complex was shown to promote Si-Si bond formation by a 1,2-silyl migration from the metal to the silylene ligand in the

presence of a strong donor.⁵¹ Formation of the silyl(μ -silylene) compounds (**12** and **13**) noted above, is also in contrast to the reaction of secondary silanes with the dirhodium analogue of **1**, in which a P–C bond of a dppm ligand was cleaved followed by the formation of a P–Si bond to give $[\text{Rh}_2(\mu\text{-H})(\text{CO})_2(\text{dppm})(\mu\text{-Ph}_2\text{PCH}_2\text{PPhSiEt}_2)]$.⁸ Attempts to promote Si–Si bond formation in **12** and **13** by heating and/or reaction with Lewis bases were not successful.

2.4.3 Reactions of $[\text{RhIr}(\text{CH}_3)(\text{CO})_2(\text{dppm})_2][\text{CF}_3\text{SO}_3]$ with Secondary Silanes.

The addition of 1 equiv of Ph_2SiH_2 to a CD_2Cl_2 solution of the cationic complex, $[\text{RhIr}(\text{CH}_3)(\text{CO})_2(\text{dppm})_2][\text{CF}_3\text{SO}_3]$ (**2**), at -78°C , yields the silyl/hydride complex, $[\text{RhIr}(\text{CH}_3)-(\text{SiPh}_2\text{H})(\text{CO})(\mu\text{-CO})(\mu\text{-H})(\text{dppm})_2][\text{CF}_3\text{SO}_3]$ (**14**) (Scheme 2.9). Multinuclear NMR spectroscopy suggests that in this case Si–H bond activation has been initiated at Ir, in contrast to the reactivity of silanes with the neutral complex (**1**), described above, in which Si–H bond activation is presumed to be initiated at Rh. The formation of **14** is also accompanied by methyl migration from Ir to Rh. The ^1H NMR spectrum of **14** shows the silyl hydrogen as a triplet of doublets at δ 5.50 ($^3J_{\text{PH}} = 13.5$ Hz, $^3J_{\text{HH}} = 2.0$ Hz) in which the ^{29}Si satellites indicate $^1J_{\text{SiH}} = 170$ Hz, consistent with a classical Si–H bond, and a hydride signal at δ -8.44 as a doublet of doublets of multiplets ($^1J_{\text{RhH}} = 13.8$ Hz, $^3J_{\text{HH}} = 2.0$ Hz). Resonances for the dppm methylene groups and all phenyl groups are as expected. Selective decoupling of the Ir-bound ^{31}P nuclei results in a collapse of the signal for the silyl hydrogen to a doublet, while decoupling of the the Rh-bound ^{31}P nuclei has no affect on this resonance,

Scheme 2.9



establishing that the silyl group is bound to Ir. Broadband ^{31}P -decoupling transforms the multiplet resonance for the hydride, described above, to a doublet of doublets, showing coupling to Rh and the silyl proton. The three-bond coupling of the bridging hydride to the silyl proton was confirmed by the homonuclear ($^1\text{H}\{^1\text{H}\}$) NMR decoupling experiments. In addition, the selective decoupling of both the Rh- and Ir-bound ^{31}P nuclei results in sharpening of the multiplets confirming that the hydride is bridging the metals. The methyl protons appear as a triplet at δ 0.49 ($^3J_{\text{PH}} = 6.9$ Hz) which collapses to a broad singlet upon irradiation of the Rh-bound ^{31}P nuclei, indicating that this group has migrated from Ir to Rh. The absence of 2-bond coupling between Rh and the methyl protons is not unusual.⁴⁷ In the $^{29}\text{Si}\{^1\text{H}\}$ NMR spectrum a triplet is observed at δ -25.7 , consistent with a terminally bound silyl group. Moreover, the small $^2J_{\text{SiP}}$ coupling (10 Hz) implies a mutually *cis* disposition of Si and the adjacent ^{31}P nuclei. The $^{13}\text{C}\{^1\text{H}\}$ NMR spectrum exhibits resonances at δ 216.6 ($^1J_{\text{RhC}} = 31.2$ Hz) due to a bridging carbonyl and at δ 173.8 for the terminally bound carbonyl on Ir. If

$^{13}\text{CH}_3$ -enriched compound **2** is used as precursor, an additional doublet of triplets ($^1J_{\text{RhC}} = 29$ Hz) appears in the $^{13}\text{C}\{^1\text{H}\}$ NMR at δ 14.8, due to the Rh-bound methyl group. The *trans* disposition of the Ir-bound CO and the bridging hydride was confirmed in the ^{13}C NMR spectrum by ^{13}CO enrichment of **14**, which shows *trans* $^2J_{\text{CH}}$ coupling of 24 Hz. Compound **14** is fluxional in solution as revealed by the $^{31}\text{P}\{^1\text{H}\}$ NMR spectra. At -80 °C the Ir-bound ^{31}P nuclei appear as two broad peaks at δ -6.1 and -8.6 while the Rh-bound phosphines appear as a single sharp and well-resolved resonance at δ 29.0. At -60 °C the former peaks coalesce to a broad unresolved peak centred at δ -7.3 and finally at -40 °C, this resonance resolves into a multiplet consistent with the BB' part of an AA'BB'X spin system. The signals due to the Rh-bound ^{31}P nuclei, silyl hydrogen and the bridging hydride ligand remain sharp and unaffected throughout the temperature range from -80 °C and -40 °C, indicating that these groups are not significantly affected by fluxional processes. The origin of this fluxionality is not clearly understood, although it might result from an asymmetry in the environments of the silyl phenyls which renders both Ir-bound ^{31}P nuclei inequivalent in the static low-temperature structure.

Upon warming above -40 °C, a new species $[\text{RhIr}(\text{CH}_3)(\text{CO})_2(\mu\text{-H})(\mu\text{-}\eta^1\text{-}\eta^2\text{-SiPh}_2\text{H})(\text{dppm})_2][\text{CF}_3\text{SO}_3]$ (**15**) begins to appear together with complex **14** and at -20 °C compound **15** is the major product (83%, according to ^{31}P NMR spectroscopy) with 17% unconverted **14** (Scheme 2.9). This species, like **14**, at this temperature, displays a pattern typical of AA'BB'X spin system in the $^{31}\text{P}\{^1\text{H}\}$ NMR spectrum and the ^1H NMR spectrum suggests migration of the

methyl group back to Ir, as evidenced by its triplet resonance at δ 0.73 in the ^1H NMR which upon irradiation of the Ir-bound ^{31}P nuclei collapses to a singlet. The resonance for this ligand in the $^{13}\text{C}\{^1\text{H}\}$ NMR spectrum appears as a triplet at δ – 22.6 ($^2J_{\text{PC}} = 7.0$ Hz) showing no Rh coupling. The high-field chemical shift of this signal is consistent with an Ir-bound methyl ligand in this system, in contrast to the Rh-bound methyl groups, which tend to resonate significantly downfield as observed for **14**. The silicon–hydrogen moiety is bound to Rh in a non-classical, agostic fashion as shown by its ^1H NMR resonance which appears as a multiplet (dddd) at δ – 0.65 ($^1J_{\text{RhH}} = 24$ Hz, $^2J_{\text{HH}} = 6$ Hz, $^3J_{\text{P(Ir)-H(Si)}} = 9$ Hz, $^3J_{\text{P(Rh)-H(Si)}} = 8$ Hz) (Figure 2.8). The additional coupling shown by this hydrogen to the Ir-bound

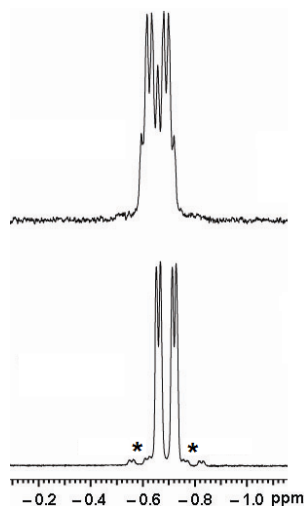


Figure 2.8: ^1H -NMR resonance of the Si–H moiety (above) and with broadband ^{31}P -decoupling (below) for **15** at – 20 °C. ^{29}Si satellites marked by the asterisks.

^{31}P nuclei, as established by selective ^{31}P decoupling experiments, indicates that the silyl group is σ -bound to Ir. The chemical shift of this agostic proton is significantly upfield compared to the silyl hydrogen of **14**, which appears at δ

5.50, but still lies downfield from a classical metal hydride resonance in this system. Similar high-field signals for M–H–Si protons have been reported for $[\text{Ir}_2(\text{H})(\text{CO})_2(\mu\text{-}\eta^1\text{:}\eta^2\text{-SiPh}_2\text{H})(\text{dppm})_2]$,⁹ $[\text{Cp}_2\text{Ti}(\mu\text{-H})(\mu\text{-}\eta^1\text{:}\eta^2\text{-HSiPhH})\text{TiCp}_2]$ ^{52a} and $[\text{Mn}_2(\text{CO})_6(\mu\text{-}\eta^3\text{-H}_2\text{SiPh}_2)(\text{dppm})_2]$.^{52b} Furthermore, the small coupling constant (*ca.* 8 Hz.) between this hydrogen and the Rh-bound ³¹P nuclei, compared to typical values for a terminal hydride on Rh (*ca.* 20 Hz) argues in support of a three-centre Rh–H–Si interaction in **15**, consistent with an inherently weaker Rh–H interaction.

However, the most compelling evidence for the agostic nature of this Si–H bond is given by the observed Si satellites (Figure 2.8) in the ¹H-NMR spectrum demonstrating Si–H coupling of 84 Hz, typical of agostic or η^2 -silane complexes,^{8b} which is significantly lower than the coupling constant for a classical Si–H bond as was shown in complex **14** (¹J_{Si-H} = 170 Hz). The ²⁹Si NMR spectrum of **15** also shows a significant downfield shift to δ 6.31 compared with the chemical shift (δ –25.7) for the terminally bonded Si in compound **14**.

The terminal nature of the two carbonyl ligands was confirmed by the ¹³C{¹H} NMR spectrum, showing signals at δ 193.2 (dt, ¹J_{RhC} = 78.4 Hz, ²J_{PC} = 15 Hz) and 178.0. Once again the *trans* disposition of the Ir-bound CO and the hydride was established by the *trans* C–H coupling constant of 24 Hz, observed in the proton-coupled ¹³C NMR spectrum. In a doubly-enriched (¹³CH₃/¹³CO) sample of compound **15** the mutually *cis* arrangement of the Ir-bound CO and CH₃ groups was established by their low mutual coupling of 2 Hz in the ¹³C NMR spectrum. Compound **15** appears to be static in solution at –20 °C, displaying no

observable exchange between the silyl hydrogen and the bridging hydride as was confirmed by SST NMR experiments, which is in contrast to the report of such exchange for the related $[(\text{dippe})_2(\text{Rh})_2(\mu\text{-H})(\mu\text{-}\eta^1\text{:}\eta^2\text{-SiPh}_2\text{H})]$.¹¹ Compound **15** is unstable at ambient temperature in solution but was isolated analytically pure at $-20\text{ }^\circ\text{C}$ and found to be stable at ambient temperature in the solid state as confirmed by redissolving the solid compound at $-20\text{ }^\circ\text{C}$ and subsequent NMR studies. The conversion of **14** to **15** was found to be irreversible as cooling **15** to $-80\text{ }^\circ\text{C}$ did not produce **14**. Unfortunately, attempts to obtain single X-ray quality crystals of **15** were unsuccessful.

When allowed to warm to ambient temperature, compound **15** transforms into two new species in an approximate 1:1 ratio (Scheme 2.9). One of these products, the silylene-bridged acetyl dihydride complex, $[\text{RhIr}(\text{H})(\text{COCH}_3)(\text{CO})(\mu\text{-H})(\mu\text{-SiPh}_2)(\text{dppm})_2][\text{CF}_3\text{SO}_3]$ (**16**), is the result of oxidative addition of the second Si–H bond, concomitant with migratory insertion of the methyl group and a carbonyl. The other product, identified as a silylene-bridged monohydride complex, $[\text{RhIr}(\text{CO})_2(\mu\text{-H})(\mu\text{-SiPh}_2)(\text{dppm})_2][\text{CF}_3\text{SO}_3]$ (**17**), has resulted from oxidative addition of the second Si–H bond and accompanying reductive elimination of methane, identified by a singlet at $\delta\ 0.21$ in the ^1H NMR spectrum. The $^{13}\text{C}\{^1\text{H}\}$ NMR spectrum of the crude product mixture also shows $^{13}\text{CH}_4$ as a singlet at $\delta\ -4.3$, which disappears upon work-up as the gas is lost.

The acetyl carbonyl of compound **16** appears as a singlet at $\delta\ 280.0$ in the $^{13}\text{C}\{^1\text{H}\}$ NMR spectrum and the methyl group gives rise to a singlet at $\delta\ 46.0$,

indicating that this group is not directly bonded to either metal. In addition, these signals appear as doublets in the doubly-enriched ($^{13}\text{CH}_3/^{13}\text{CO}$) compounds, showing a mutual coupling of 26 Hz. The other carbonyl is shown to be Rh-bound (δ 193.7; $^1J_{\text{RhC}} = 70$ Hz). The acetyl protons appear in ^1H NMR spectrum as a singlet at δ 1.23. This spectrum also shows signals at -8.86 (triplet, $^2J_{\text{PH}} = 13.2$ Hz) and -14.98 (doublet of doublet of doublets, $^1J_{\text{RhH}} = 22$ Hz, $^2J_{\text{P(Ir)H}} = 13.2$ Hz, $^2J_{\text{P(Rh)H}} = 10.9$ Hz) assigned to terminal (Ir) and bridging hydride ligands, respectively. When the Ir-bound ^{31}P nuclei were decoupled the terminal hydride signal collapses to a singlet, showing ^{29}Si satellites with coupling of only 32 Hz, indicating a weak interaction of the hydrido group with Si. This interaction is further confirmed by an HSQC NMR experiment, which shows a peak for ^{29}Si at δ 20.0 (consistent with the bridging nature of the SiPh_2 group) displaying a correlation with the Ir-bound hydride.

The $^{13}\text{C}\{^1\text{H}\}$ -NMR spectrum for compound **17** shows a doublet of multiplets at δ 187.6 with Rh coupling of *ca.* 77 Hz and a broad triplet at 176.8, assigned to terminal carbonyls on Rh and Ir, respectively. The ^1H NMR spectrum for this compound displays broad multiplet at δ 4.42 and 4.40 for the dppm methylenes and a broad multiplets with unresolved P–H coupling at δ -10.22 for the hydride which integrates to approximately half with those of the dppm methylenes groups. Cooling the sample to -40 °C does not result in simplification of the hydride resonance; however, the broadband-decoupled $^1\text{H}\{^{31}\text{P}\}$ NMR spectrum gives a doublet with Rh coupling ($^1J_{\text{RhH}} = 15$ Hz). Compound **17** can also be generated from the reaction of the diphenylsilylene-bridged complex,

[RhIr(H)₂(CO)₂(μ-SiPh₂)(dppm)₂] (**9**) with 1 equiv of trifluoromethane sulfonic acid, accompanied by H₂ evolution, further confirming its formulation.

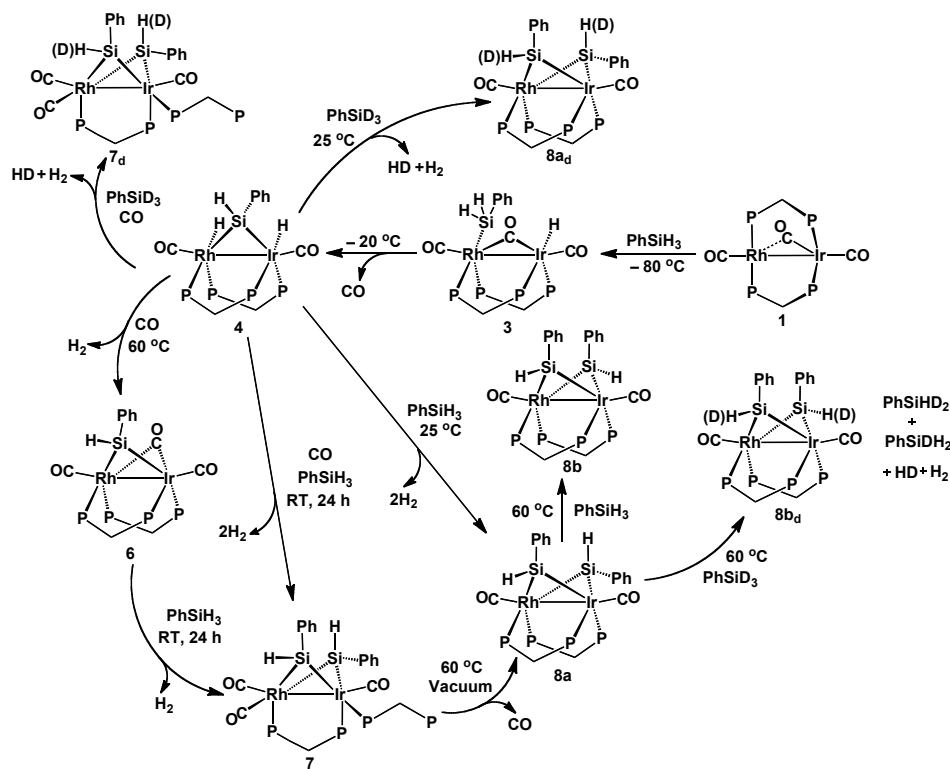
2.5 Discussion

In the major part of this chapter the reactivity of the neutral species [RhIr(CO)₃(dppm)₂] (**1**) with a limited number of primary and secondary silanes was studied. Not surprisingly, the difference in steric bulk of these classes of silanes resulted in significant differences in their reactivities, with the smaller phenylsilanes readily forming products in which two silylene groups bridged the metals. Based upon the reactions carried out under various conditions, involving **1** and phenylsilane, a stepwise sequence of transformations leading to the final *bis*(silylene)-bridged product (**8b**) is proposed and shown (for phenylsilane) in Scheme 2.10.

At -80 °C the reaction of PhSiH₃ with **1** (shown at the upper right of Scheme 2.10) initially proceeds by activation of one Si-H bond to form the silyl/hydride complex **3** having the silyl group on Rh and the hydride on Ir. Although this low-temperature intermediate does not conclusively establish at which metal centre Si-H bond-activation is initiated, two possibilities can be proposed; either the Si-H bond oxidatively adds at Rh followed by hydride migration to Ir or it adds at Ir followed by silyl migration to Rh. We feel that the much higher mobility of a hydride ligand favours addition at Rh followed by migration of hydride. Although hydride migration at low temperatures is well precedented,⁵³ there are a few examples of silyl migration reported in bimetallic complexes, even at ambient temperature^{31c, e, k, l} and the migration of an aryl-silyl

group in the presence of bulky dppm ligands would appear not to be facile. Furthermore, oxidative addition at Rh is consistent with the coordinative unsaturation at this metal, and the saturation at Ir. Upon warming the solution of **3**

Scheme 2.10



to $-20\text{ }^{\circ}\text{C}$ conversion to the silylene-bridged dihydride species (**4**) occurs by the oxidative addition of the second Si–H bond. No intermediate was observed during this transformation; however, it is presumed to take place through a silyl-bridged agostic intermediate in which one Si–H bond of the Rh-bound silyl group interacts with Ir to form a σ -complex. The unsaturation at Ir required for the agostic Si–H interaction and subsequent oxidative addition of the Si–H bond can occur by transfer of the bridging carbonyl to Rh concomitant with Rh–Ir bond

cleavage. The loss of one of the Rh-bound carbonyls following the second Si–H bond cleavage is then accompanied by hydride migration from Ir to Rh to give **4**.

The reaction of **4** with another equiv of PhSiH₃ at ambient temperature yields the *bis*(silylene)-bridged product **8a**. As was the case for compound **3**, complex **4** is again coordinatively saturated, necessitating ligand loss in order to accommodate a second silane. The reaction of **4** with PhSiD₃ in the presence of and in the absence of CO (yielding deuterium scrambled **7_d** or **8a_d**, respectively) eliminates the possibility that H₂ loss from **4** precedes activation of the second silane, since H₂ and HD are produced equally, accompanied by incorporation of both H and D into both silylene ligands. Unsaturation can also result from dissociation of one end of a diphosphine unit (probably from the more labile Rh centre) or by reductive elimination of a hydride and one end of the μ -silylene bridge (again, probably from the Rh centre) to yield a transient Ir-bound silyl group. The observation of the pendent-dppm species **7** and of the silyl/silylene product **12** supports phosphine dissociation. Furthermore, the recoordination of the pendent-dppm group at Rh upon carbonyl removal from **7** to give **8a** offers additional support for phosphine dissociation/reassociation steps.

A necessary intermediate in the transformation of **4** to **8a** is one containing the original bridging silylene group together with a terminal silyl group, resulting from the first Si–H activation of the added silane. Although no such species was observed in the reaction with primary silanes, a model species (stabilized by CO addition) was observed with diphenylsilane. This model silyl/silylene-bridged compound (**12**) (see Scheme 2.8) confirms phosphine dissociation from Rh and

concomitant silane addition at this metal. In the absence of the additional carbonyl ligand, oxidative addition of one of the remaining Si–H bonds of the phenylsilyl group in the putative silyl/silylene intermediate occurs with H₂ elimination promoted by recoordination of the pendent phosphine at Rh.

In the case of the monosubstituted bis(silylene)-bridged products, the kinetic product (**8a**) in which the aryl substituent on one μ -silylene group is axial while the other is equatorial minimizes unfavourable interactions between these groups, while having unfavourable interactions between the equatorial substituent and the dppm phenyls (see Scheme 2.4). In the axial/axial isomer (**8b**) the unfavourable interactions between both axial substituents can be alleviated by an increase in the separation of these groups, which is permitted by the lower steric interactions with the dppm groups (having hydrogens in both equatorial sites on the Si atoms). This is not possible with doubly substituted silylene groups, for which repulsive interactions with each other and with dppm phenyl groups simultaneously result.

Although Scheme 2.10, offers a credible rationalization for the multiple Si–H activation processes leading to the bis(silylene)-bridged products, the observation that the axial/equatorial isomer of the bis(silylene)-bridged **8a** requires additional silane for isomerisation to the axial/axial isomer (**8b**) to occur and the deuterium/hydrogen scrambling that occurs, points to additional complexities that are not fully understood. It appears that an unobserved transient, containing three Si-containing units are involved at some stage. Such M₂Si₃ species have been reported.⁵⁴ This proposal is supported by the observation of a mixed phenylsilylene/difluorophenylsilylene product (**8d**) together with bis-

phenylsilylene (**8b**) and bis-difluorophenylsilylene (**8c**) product in the reaction of the bis-phenylsilylene precursor (**8a**) with difluorophenylsilane.

In the second, minor part of this study, we investigated the reactivity of the related cationic precursor, $[\text{RhIr}(\text{CH}_3)(\text{CO})_2(\text{dppm})_2][\text{CF}_3\text{SO}_3]$ (**2**) with diphenylsilane. This species has two fewer electrons than the neutral tricarbonyl compound **1**, which leads to unsaturation at both metals in **2**, instead of only at Rh in **1**. This additional unsaturation is manifested in silane oxidative addition at Ir (see Scheme 2.9) instead of at Rh as was proposed in the reaction of **1**.

In this cationic system the agostic interaction of a silyl Si–H bond with the adjacent metal is observed. Although such species were presumably involved in the double Si–H activation by the neutral tricarbonyl precursor **1**, these intermediates were never observed in these neutral species. Presumably the positive charge on **2** inhibits the second Si–H activation step, allowing the bridged agostic species, in which the silyl group is σ -bound to Ir while involved in an agostic interaction with Rh, to be observed. Warming slightly leads to a subtle rearrangement, which brings about further weakening of this remaining Si–H bond. This transformation can be viewed as resulting from migration of the diphenylsilyl group from Ir to Rh and of the agostic interaction to Ir. The greater tendency of Ir to cleave the Si–H bond is evident in the ^1H NMR spectrum, which displays a very weak one-bond Si–H coupling of only 32 Hz, indicative of a weak Si–H interaction, lying close to the silylene-bridged hydride extreme.

2.6 Conclusions

In this Rh/Ir system we were able to observe species not observed in the Rh₂ and Ir₂ systems giving us a clearer picture of the roles of the adjacent metals in the different steps leading to the eventual activation of up to four Si–H bonds and the incorporation of two Si-containing fragments. Evidence has been obtained for interactions between pairs of adjacent bridging silylene groups, although the nature of these interactions is not clear. This and the observation of a silyl/silylene unit in the Rh/Ir core suggest the possibility of Si–Si coupling at these centres.

2.7 References

- 1) (a) Marciniak, B. *Silicon Chem.* **2002**, *1*, 155. (b) Brook, M. A. *Silicon in Organic, Organometallic, and Polymer Chemistry*; Wiley: New York, 2000. (c) Calimano, E.; Tilley T. D. *J. Am. Chem. Soc.* **2009**, *131*, 11161. (d) Ojima, I.; Kogure, T.; Nihonyanagi, M.; Nagai, Y. *J. Chem. Soc., Chem. Commun.* **1972**, 938. (e) Ojima, I.; Nihonyanagi, M.; Nagai, Y. *Bull. Chem. Soc. Jpn.* **1972**, *45*, 3506. (f) Jiménez M.V.; Pérez-Torrente J. J.; Bartolomé M. I.; Gierz, V.; Lahoz, F. J.; and Oro, L. A. *Organometallics*, **2008**, *27*, 224.
- 2) (a) Luo; X. L.; Crabtree, R. H. *J. Am. Chem. Soc.* **1989**, *111*, 2527. (b) Biffis, A.; Basato, M.; Briccese, M.; Ronconi, L.; Tubaro, C.; Zanella, A.; Graiff, A.; Tiripicchio, A. *Adv. Synth. Catal.* **2007**, 2485.
- 3) (a) Hashimoto, H.; Tobita, H.; Ogino, H. *J. Organomet. Chem.* **1995**, *499*, 205. (b) Radu, N. S.; Hollander, F. J.; Tilley, T. D.; Rheingold, A. L. *Chem. Commun.* **1996**, *21*, 2459. (c) Gavenonis, J.; Tilley, T. D. *Organometallics* **2004**, *23*, 31.

- 4) (a) Boukherroub, R.; Chatgiliaoglu, C.; Manuel, G. *Organometallics* **1996**, *15*, 1508. (b) Esteruelas, M. A.; Herrero, J.; Lopez, F. M.; Martin, M.; Oro, L. A. *Organometallics* **1999**, *18*, 1110. (c) Diaz, J.; Esteruelas, M. A.; Herrero, J.; Moralejo, L.; Olivan, M. *J. Catal.* **2000**, *195*, 187.
- 5) (a) Aitken, C. T.; Harrod, J. F.; Samuel, E. *J. Am. Chem. Soc.* **1986**, *108*, 4059. (b) Tilley, T. D. *Acc. Chem. Res.* **1993**, *26*, 22. (c) Rosenberg, L.; Davis, C. W.; Yao, J. Z. *J. Am. Chem. Soc.* **2001**, *123*, 5120. (d) Fontaine, F.-G.; Zargarian, D. *J. Am. Chem. Soc.* **2004**, *126*, 8786. (e) Corey, J. Y. *Adv. Organomet. Chem.* **2004**, *51*, 1.
- 6) (a) Graham, W. A. G. *J. Organomet. Chem.* **1986**, *300*, 81 and references therein. (b) Ogino, H.; Tobita, H. *Adv. Organomet. Chem.* **1998**, *42*, 223 and references therein. (c) Corey, J. Y.; Braddock-Wilking, J. *Chem. Rev.* **1999**, *99*, 175 and reference therein. d) Shimada, S.; Tanaka, M. *Coord. Chem. Rev.* **2006**, *250*, 991. e) Schubert, U. *Adv. Organomet. Chem.* **1990**, *30*, 151.
- 7) (a) Zarate, E.A.; Tessier-Youngs, C. A.; Youngs, W. J. *J. Am. Chem. Soc.* **1988**, *110*, 4068. (b) Zarate, E.A.; Tessier-Youngs, C. A.; Youngs, W. J. *J. Chem. Soc., Chem. Commun.* **1989**, 577.
- 8) a) Wang, W. -D.; Hommeltoft, S. I.; Eisenberg, R. *Organometallics* **1988**, *7*, 2417. (b) Wang, W. -D.; Eisenberg, R. *J. Am. Chem. Soc.* **1990**, *112*, 1833. (c) Wang, W. -D.; Eisenberg, R. *Organometallics* **1992**, *11*, 908.
- 9) McDonald, R.; Cowie, M. *Organometallics* **1990**, *9*, 2468.
- 10) Suzuki, H.; Takao, T.; Tanaka, M.; Morooka, Y. *J. Chem. Soc., Chem. Commun.* **1992**, 476.

- 11) Fryzuk, M. D.; Rosenberg, L.; Rettig, S. J. *Organometallics* **1999**, *18*, 958.
- 12) Sanow, L. M.; Chai, M.; McConnville, D. B.; Galat, K. J.; Simons, R. S.; Rinaldi, P. L.; Youngs, W. J.; Tessier, C. A. *Organometallics* **2000**, *19*, 192.
- 13) Braddock-Wilking, J.; Levchinsky, Y.; Rath, N. P. *Organometallics* **2001**, *20*, 474.
- 14) Fürstner, A.; Krause, H.; Lehmann, C. W. *Chem. Commun.* **2001**, 2372.
- 15) Hashimoto, H.; Hayashi, Y.; Aratani, I.; Kabuto, C.; Kira, M. *Organometallics* **2002**, *21*, 1534.
- 16) Takao, T.; Amako, M. A.; Suzuki, H. *Organometallics* **2003**, *22*, 3855.
- 17) Tanabe, M.; Mawatari, A.; Osakada, K. *Organometallics* **2007**, *26*, 2937.
- 18) Tanabe, M.; Ito, D.; Osakada, K. *Organometallics*, **2008**, *27*, 2258.
- 19) Shimada, S.; Tanaka, M.; Honda, K. *J. Am. Chem. Soc.* **1995**, *117*, 8289.
- 20) Osakada, K.; Koizumi, T.; Yamamoto, T. *Angew. Chem. Int. Ed. Engl.* **1998**, *37*, 349.
- 21) Koizumi, T.A.; Osakada, K.; Yamamoto, T. *Organometallics* **1998**, *19*, 5721.
- 22) (a) Shimada, S.; Rao, M. L. N.; Hayashi, T.; Tanaka, M. *Angew. Chem. Int. Ed. Engl.* **2001**, *40*, 213. (b) Shimada, S.; Li, Y.-H.; Rao, M. L. N.; Tanaka, M. *Organometallics* **2006**, *25*, 3796.
- 23) Takao, T.; Yoshida, S.; Suzuki, H. *Organometallics* **1995**, *14*, 3855.
- 24) (a) Anderson, A. B.; Shiller, P.; Zaratén, E. A.; Tessier-Youngs, C. A.; Youngs, W. J. *Organometallics* **1989**, *8*, 2320. (b) Aullón, G.; Alemany, P.; Alvarez, S. *J. Organomet. Chem.* **1994**, *478*, 75.

- 25) Sakaki, S.; Yamaguchi, S.; Musashi, Y.; Sugimoto, M. *J. Organomet. Chem.* **2001**, *635*, 17.
- 26) Nakajima, S.; Yokogawa, D.; Nakao, Y.; Sato, H.; Sakaki, S. *Organometallics* **2004**, *23*, 4672.
- 27) (a) Brittingham, K. A.; Gallaher, T. N.; Schreiner, S. *Organometallics* **1995**, *14*, 1070 (b) Heyn, R. H.; Tilley, T. D. *J. Am. Chem. Soc.* **1992**, *114*, 1917.
- 28) (a) Yamada, T.; Mawatari, A.; Tanabe, M.; Osakada, K.; Tanase, T. *Angew. Chem. Int. Ed. Engl.* **2009**, *48*, 568. (b) Herrmann, W. A.; Härter, P.; Gstötmayr, C. W. K.; Bielert, F.; Seeboth, N.; Sirsch, P. *J. Organomet. Chem.* **2002**, *649*, 141.
- 29) (a) Tobita, H.; Kawano, Y.; Ogino, H. *Chem. Lett.* **1989**, 2155. (b) Kawano, Y.; Tobita, H.; Ogino, H. *Angew. Chem. Int. Ed. Engl.* **1991**, *30*, 843. (c) Kawano, Y.; Tobita, H.; Shimoi, M.; Ogino, H. *J. Am. Chem. Soc.* **1994**, *116*, 8575. (d) Ohki, Y.; Kojima, T.; Oshima, M.; Suzuki, H. *Organometallics* **2001**, *20*, 2654.
- 30) (a) Campion, B. K.; Heyn, R. H.; Tilley, T. D. *Organometallics* **1992**, *11*, 3918. (b) Takao, T.; Suzuki, H.; Tanaka, T. *Organometallics* **1994**, *13*, 2554. (c) Takao, T.; Amako, M. A.; Suzuki, H. *Organometallics* **2001**, *20*, 3406. (d) Takao, T.; Yoshida, S.; Suzuki, H. *Chem. Lett.* **2001**, *11*, 1100. (e) Takao, T.; Yoshida, S.; Suzuki, H. *Organometallics* **2005**, *24*, 521.
- 31) (a) Powell, J.; Sawyer, J. F.; Shiralian, M. *Organometallics* **1989**, *8*, 557. (b) Sakaba, H.; Ishida, K.; Horino, H. *Chem. Lett.* **1998**, 149. (c) Bodensieck, U.; Braunstein, P.; Deck, W.; Faure, T.; Knorr, M.; Stern, C. *Angew. Chem. Int. Ed. Engl.* **1994**, *33*, 2440. (d) Knorr, M.; Strohmam, C.; Braunstein, P.

Organometallics **1996**, *15*, 5653. (e) Braunstein, P.; Morise, X.; *Organometallics* **1998**, *17*, 540. (f) Braunstein, P.; Durand, J.; Morise, X.; Tiripicchio, A.; Ugozzoli, F. *Organometallics* **2000**, *19*, 444. (g) Braunstein, P.; Durand, J.; Knorr, M.; Strohmann, C. *Chem. Commun.* **2001**, 211. (h) Braunstein, P.; Clerc, G.; Morise, X.; *Organometallics* **2001**, *20*, 5036. (i) Tanabe, M.; Osakada, K. *Inorg. Chim. Acta* **2003**, *350*, 201 (j) Yamada, T.; Tanabe, M.; Osakada, K.; Kim, Y-J. *Organometallics* **2004**, *23*, 4771. (k) Braunstein, P.; Faure, T.; Knorr, M. *Organometallics* **1999**, *18*, 1791. (l) Shelby, Q. D.; Lin, W.; Girolami, G. S. *Organometallics* **1999**, *18*, 1791.

32) (a) Minge, O.; Nogai, S.; Schmidbaur, H. *Z. Naturforsch. B* **2004**, *59*, 153. (b) Molander, G. A.; Corrette, C. P. *Organometallics* **1998**, *17*, 5504. (c) Prince, P. D.; Bearpark, M. J.; McGrady, G. S.; Steed, G. W. *Dalton. Trans.* **2008**, 271.

33) Benkeser, R. A.; Landesman, H.; Foster, D. J. *J. Am. Chem. Soc.* **1952**, *648*, 74.

34) McDonald, R.; Cowie, M. *Inorg. Chem.* **1990**, *29*, 1564.

35) Oke, O. Ph.D. Thesis, University of Alberta. **1999**, 24.

36) Programs for diffractometer operation, data collection, data reduction, and absorption correction were those supplied by (a) Bruker (b) Siemens.

37) (a) Beurskens, P. T.; Beurskens, G.; de Gelder, R.; Smits, J. M. M.; Garcia-Granda, S.; Gould, R. O. (2008). The *DIRDIF-2008* program system. Crystallography Laboratory, Radboud University Nijmegen, The Netherlands. (b) Altomare, A.; Burla, M. C.; Camalli, M.; Cascarano, G. L.; Giacovazzo, C.; Guagliardi, A.; Moliterni, A. G. G.; Polidori, G.; Spagna, R. *J. Appl. Cryst.* **1999**,

- 32, 115. (c) Sheldrick, G. M. *Acta Crystallogr.* **1990**, *A46*, 467. (d) Sheldrick, G. M. *Acta Crystallogr.* **2008**, *A64*, 112.
- 38) Sheldrick, G. M. *SHELXL-93*. Program for crystal structure determination. University of Göttingen, Germany, 1993.
- 39) (a) Sluis, P. van der; Spek, A. L. *Acta Crystallogr.* **1990**, *A46*, 194 (b) Spek, A. L. *Acta Crystallogr.* **1990**, *A46*, C34; Spek, A. L. *J. Appl. Cryst.* **2003**, *36*, 7. *PLATON* - a multipurpose crystallographic tool. Utrecht University, Utrecht, The Netherlands.
- 40) Aizenberg, M.; Ott, J.; Elsevier, C. J.; Milstein, D. *J. Organomet. Chem.* **1998**, *551*, 81.
- 41) Nishihara, Y.; Takemura, M.; Osakada, K. *Organometallics* **2002**, *21*, 825.
- 42) (a) Nikonov, G. I.; Kuzmina, L. G.; Vyboishchikov, S. F.; Lemenovskii, D. A.; Howard, J. A. K. *Chem. Eur. J.* **1999**, *5*, 2947. (b) Nikonov, G. I. *J. Organomet. Chem.* **2001**, *635*, 24.
- 43) (a) Lachaize, S.; Sabo-Etienne, S. *Eur. J. Inorg. Chem.* **2006**, 2115. (b) Perutz, R. N.; Sabo-Etienne, S. *Angew. Chem. Int. Ed. Engl.* **2007**, *46*, 2578.
- 44) (a) Wiberg, N.; Schuster, H.; Simon, A.; Peter, K. *Angew. Chem. Int. Ed. Engl.* **1986**, *25*, 79. (b) Corey, J. Y.; Kraichely D. M.; Huhmann, J. L.; Braddock-Wilking, J.; Lindeberg, A. *Organometallics* **1995**, *14*, 2704.
- 45) Cozzi, F.; Ponzini, F.; Annunziata, R.; Cinquini, M.; Siegel, J. S. *Angew. Chem., Int. Ed. Engl.* **1995**, *34*, 1019.
- 46) (a) Bruce, M. I; Cifuentes, M. P.; Grundy, K. R.; Liddell, M. J.; Snow, M. R.; Tiekink, E. R. T. *Aust. J. Chem.* **1988**, *41*, 603. (b) Brown, M. P.; Yavari, A.; Hill,

- R. H.; Puddephatt, R. J. *J. Chem. Soc. Dalton Trans*, **1985**, 2421. (c) Azam, K. A.; Brown, M. P.; Hill, R. H.; Puddephatt, R.J.; Yavari, A. *Organometallics* **1984**, *3*, 697. (d) Car, S. W.; Shaw, B. L.; Thornton-Pett, M. *J. Chem. Soc. Dalton Trans*. **1987**, 1763.
- 47) Trepanier, S. J.; Dennett, J. N. L.; Sterenberg, B. T.; McDonald, R.; Cowie, M. *J. Am. Chem. Soc.* **2004**, *126*, 8046.
- 48) (a) Antonelli, D. M.; Cowie, M. *Inorg. Chem.* **1990**, *29*, 3342. (b) Vaartstra, B. A.; Xiao, J.; Jenkins, J. A.; Verhagen, R.; Cowie, M. *Organometallics* **1991**, *10*, 2708. (c) Mague, J. T.; De Vries, S. H. *Inorg. Chem.* **1982**, *21*, 1632.
- 49) Pannell, K. H.; Sharma, H. K.; Kapoor, R. N.; Cervantes-Lee, F. *J. Am. Chem. Soc.* **1997**, *119*, 9315.
- 50) (a) Ogino, H. *Chem. Rec.* **2002**, *2*, 291. (b) Sharma H. K.; Pannell, K. H. *Chem. Rev.* **1995**, *95*, 1351.
- 51) Tobita, H.; Matsuda, A.; Hashimoto, H.; Ueno, K.; Ogino, H. *Angew. Chem. Int. Ed. Engl.* **2004**, *43*, 221.
- 52) (a) Aitken, C. T.; Harrod, J. F.; Samuel, E. *J. Am. Chem. Soc.* **1986**, *108*, 4059. (b) Carreno, R.; Riera, V.; Ruiz, M. A; Jeannin, Y.; Philiche-Levisalles, M. *J. Chem. Soc. Dalton Trans.* **1990**, 15.
- 53) Vaarstra, B. A.; O'Brien, K. N.; Eisenberg, R.; Cowie, M. *Inorg. Chem.* **1988**, *27*, 3668.
- 54) Fryzuk, M. D.; Rosenberg, L.; Rettig S. J. *Inorg. Chim. Acta.* **1994**, *222*, 345.

Chapter 3

Germyl and Germylene-Bridged Complexes of Rh/Ir and Subsequent Chemistry of a Bridging Germylene Group.^{III}

3.1 Introduction

There has been significant recent interest in the chemistry of transition-metal complexes containing germanium, in large part owing to the expanding role of this metal in transition-metal catalyzed reactions.^{1,2} For example, germanium has been shown to function as a modifier in the Pd- and Rh-mediated hydrogenation of citral and other unsaturated hydrocarbons,³ and can also give rise to improved selectivity in Ir/Pt-mediated hydrocracking.⁴ However, little is understood about the roles of germanium in these processes, or indeed about the potential roles that germanium may play in organotransition-metal chemistry in general. Some recent investigations have focused on the synthesis of germanium-containing polynuclear complexes as models for the above-noted heterogeneous catalysts,⁵ although the reactivities of these model systems with H₂ have not yet been reported. Transition-metal complexes containing a terminal germylene group have also demonstrated interesting insertion reactions with small molecules such as CO₂,⁶ nitrosobenzene⁷ and oxygen⁸, not unlike 2+2 cycloaddition reactions involving metal carbenes, and monometallic germyl complexes have given rise to Ge–Ge bond formation,⁹ a necessary step in the generation of Ge-containing oligomers.

^{III} A version of this Chapter has been published. Mobarok, M. H.; Ferguson, M. J.; McDonald, R.; Cowie, M. *Inorg. Chem.* **2012**, *51*, 4020.

In contrast to the relatively underdeveloped chemistry of germanium, the neighboring congener, Si, has a well established chemistry with transition metals, in which silyl-¹⁰ and silylene-containing complexes¹¹ have been shown to be involved in a range of homogeneously catalyzed processes such as olefin and ketone hydrosilylation,¹² dehydrogenative polymerization of silanes¹³ and silane alcoholysis.¹⁴ On the basis of the close similarity of these two congeners, it can be anticipated that Ge should display related reactivity. Nevertheless, owing to their subtle differences, one can imagine that studies on one of these congeners can yield valuable information about the other, through the observation of species with one element that can model unobserved intermediates in the chemistry of the other, leading to a more complete understanding of both. For example, Tanabe *et al.* reported the stepwise generation of a (GePh₂)₄-containing metallacycle which served as a model for unobserved, early steps in silylene oligomerization.⁹

In a previous Chapter, we discussed the activation of Si–H bonds in a series of primary and secondary silanes by heterobinuclear, dppm-bridged (dppm = Ph₂PCH₂PPh₂) complexes of Rh/Ir, which yielded silyl- and silylene-containing products.¹⁵ Investigations of Si–H bond activation by closely related Rh₂¹⁶ and Ir₂¹⁷ complexes have also been studied. In this Chapter, we continue our investigation of the Rh/Ir system to include the reactivity with germanes, as a comparison with the related silane chemistry and to develop some of the chemistry of bridging-germylene groups. As indicated in the previously, the Rh/Ir combination of metals exploits the strong tendency for low-valent Ir to undergo oxidative addition and the greater resulting bond strengths involving this metal,

combined with the greater lability at Rh. This combination also takes advantage of the useful NMR characteristics of Rh as an aid in characterization of labile intermediates, which we anticipate will assist in determining the roles of the different metals in the stepwise activation of Ge–H bonds.

3.2 Experimental.

3.2.1 General Comments.

All solvents were dried (using appropriate drying agents), distilled before use, and stored under dinitrogen. Reactions were performed under an argon atmosphere using standard Schlenk techniques. ^tBuGeH₃ was purchased from Gelest Inc., while Ph₂GeH₂ and PhGeH₃ were prepared by the reaction of the corresponding chlorides (which were purchased from Alfa Inorganics and Gelest Inc., respectively) with LiAlH₄. PhGeD₃ was prepared analogously using LiAlD₄. Germanes were dried and distilled over CaH₂ under Ar and kept under subdued light. ¹³C-enriched CO (99.4%) was purchased from Cambridge Isotope Laboratories, while ¹³C-enriched methyl-triflate was purchased from Sigma-Aldrich. The compounds [RhIr(CO)₃(dppm)₂] (**1**)¹⁸ and [RhIr(CH₃)(CO)₂(dppm)₂][CF₃SO₃] (**2**),¹⁹ were prepared as previously reported. The tetraphenylborate and tetrakis(3,5-bis(trifluoromethyl)phenyl)borate (BAR^F₄[−]) salts of compound **2** (**2**[BPh₄] and **2**[BAR^F₄]) were synthesized by an anion exchange reaction of **2** using NaBPh₄ and NaBAR^F₄, respectively, in THF (1:1 stoichiometry; 30 min reaction time) followed by the evaporation of THF and extraction of the synthesized complex with dichloromethane. NMR spectra were recorded on Varian Inova-400 or Varian Unity-500 spectrometers operating at

399.8 or 499.8 MHz, respectively, for ^1H ; at 161.9 or 201.6 MHz, respectively, for ^{31}P ; and at 100.5 or 125.7 MHz, respectively, for ^{13}C nuclei. ^1H and $^{13}\text{C}\{^1\text{H}\}$ spectra were referenced internally to residual solvent proton signals relative to tetramethylsilane whereas $^{31}\text{P}\{^1\text{H}\}$ and ^{19}F NMR spectra were referenced relative to the external standards, 85 % H_3PO_4 and CCl_3F , respectively. In the ^1H NMR spectral results the aromatic protons in the range δ 8.50–6.20 are not reported. The yields of all nonisolable complexes were determined by the integration of their resonances in the ^{31}P NMR spectra, taking all resonances present as 100 %. All spectra were recorded at 27 °C unless otherwise noted. Elemental analyses were performed by the Microanalytical Laboratory in the Department.

3.2.2 Preparation of Compounds.

a. **[RhIr(H)(GeH₂Ph)(CO)₂(μ -CO)(dppm)₂] (18)**: In a septum-sealed NMR tube under an Ar atmosphere, **[RhIr(CO)₃(dppm)₂] (1)** (30 mg, 0.026 mmol) was dissolved in 0.7 mL of CD_2Cl_2 at ambient temperature producing a dark orange solution, then cooled to -78 °C. Addition of PhGeH_3 (3.2 μL , 0.026 mmol) by a microliter syringe resulted in a lightening of the solution colour. Compound **18** was formed quantitatively after 30 min as confirmed by $^{31}\text{P}\{^1\text{H}\}$ NMR spectroscopy. No attempt was made to isolate this compound at this temperature. Further warming resulted in a subsequent transformation as described below. $^{31}\text{P}\{^1\text{H}\}$ NMR (-80 °C; CD_2Cl_2 , 161.9 MHz): δ 37.5 (Rh–P, ddd, 1P, $^2J_{\text{PP}} = 240$ Hz, $^1J_{\text{RhP}} = 133$ Hz, $^2J_{\text{PP}} = 28$ Hz), 28.8 (Rh–P, ddd, 1P, $^2J_{\text{PP}} = 142$ Hz, $^1J_{\text{RhP}} = 126$ Hz, $^2J_{\text{PP}} = 28$ Hz), -5.5 (Ir–P, dd, 1P, $^2J_{\text{PP}} = 240$ Hz, $^2J_{\text{PP}} = 18$ Hz), -12.4 (Ir–P, dd, 1P, $^2J_{\text{PP}} = 142$ Hz, $^2J_{\text{PP}} = 18$ Hz); ^1H NMR (-80 °C; CD_2Cl_2 , 399.8 MHz): δ

4.60 (CH₂, m, 1H), 4.23 (Ge–H, m, 1H), 4.14 (CH₂, m, 1H), 3.93 (CH₂, m, 1H), 3.87 (Ge–H, m, 1H), 2.59 (CH₂, m, 1H), –11.50 (Ir–H, ddd, 1H, ²J_{trans PH} = 125.0 Hz, ⁴J_{distal(trans) PH} = 27.0 Hz, ²J_{cis PH} = 13.0 Hz); ¹³C{¹H} NMR (–80 °C; CD₂Cl₂, 100.5 MHz): δ 229.9 (μ-CO, dm, 1C, ²J_{RhC} = 34 Hz), 198.2 (Rh–CO, dm, 1C, ¹J_{RhC} = 78 Hz), 178.0 (Ir–CO, bt, 1C, ²J_{PC} = 12 Hz).

b. [RhIr(H)(GeH₂^tBu)(CO)₂(μ-CO)(dppm)₂] (19): In a septum-sealed NMR tube under an Ar atmosphere, [RhIr(CO)₃(dppm)₂] (**1**) (32 mg, 0.028 mmol) was dissolved in 0.7 mL of CD₂Cl₂ at ambient temperature producing a dark orange solution, then cooled to –78 °C. 3.8 μL (0.028 mmol) of ^tBuGeH₃ was then added via a microliter syringe. No immediate colour change was observed at this temperature, however, warming to –40 °C initiated a reaction, and after 30 min at this temperature complex **19** was formed in approximately 40 % yield along with 60 % of unreacted complex **1**. Again no attempt was made to isolate this compound at this temperature. Further warming resulted in a subsequent transformation as described below. ³¹P{¹H} NMR (–40 °C; CD₂Cl₂, 161.9 MHz): δ 39.4 (Rh–P, ddd, 1P, ²J_{PP} = 245 Hz, ¹J_{RhP} = 107.5 Hz, ²J_{PP} = 28 Hz), 29.8 (Rh–P, ddd, 1P, ²J_{PP} = 152 Hz, ¹J_{RhP} = 96 Hz, ²J_{PP} = 28 Hz), –5.5 (Ir–P, dd, 1P, ²J_{PP} = 245 Hz, ²J_{PP} = 18 Hz), –12.4 (Ir–P, 1P, dd, ²J_{PP} = 152 Hz, ²J_{PP} = 18 Hz); ¹H NMR (–40 °C; CD₂Cl₂, 399.8 MHz): δ 4.83 (CH₂, m, 1H), 3.98 (CH₂, m, 1H), 3.40 (Ge–H, m, 1H), 3.32 (CH₂, m, 1H), 3.29 (Ge–H, m, 1H), 2.56 (CH₂, m, 1H), 1.22 (^tBu, s, 9H), –11.39 (Ir–H, ddd, 1H, ²J_{trans PH} = 125.5 Hz, ⁴J_{distal(trans) PH} = 30.3 Hz, ²J_{cis PH} = 12.5 Hz); ¹³C{¹H} NMR (–40 °C; CD₂Cl₂, 100.5 MHz): δ 229.8 (μ-CO, dm, 1C,

$^2J_{\text{RhC}} = 33$ Hz), 198.5 (Rh–CO, dm, 1C, $^1J_{\text{RhC}} = 77$ Hz), 178.0 (Ir–CO, bt, 1C, $^2J_{\text{PC}} = 12$ Hz).

c. [RhIr(H)₂(CO)₂(μ-GeHPh)(dppm)₂] (20): In a 100 mL Schlenk tube, under anhydrous conditions and an Ar atmosphere, compound **1** (70 mg, 0.061 mmol) was dissolved in 5 mL of CH₂Cl₂ and cooled to 0 °C in an ice-water bath. Phenylgermane (7.5 μL, 0.061 mmol) was then added to the solution by a microliter syringe, resulting in an immediate colour change from dark orange to light yellow. The reaction was allowed to stir for 10 min, followed by the reduction of solvent volume at the same temperature to approximately 1 mL *in vacuo*. Subsequent slow addition of 5 mL of pentane gave a pale yellow powder. The solid was further washed twice with 10 mL of pentane to give analytically pure compound in 73 % isolated yield (56.6 mg). Anal. calcd. for C₅₈H₅₂IrO₂P₄RhGe·C₆H₆ : C, 56.86 ; H, 4.29. Found: C, 56.97; H, 4.44. $^{31}\text{P}\{^1\text{H}\}$ NMR (27 °C; CD₂Cl₂, 161.9 MHz): δ 27.8 (bm), 16.3 (bm), –8.3 (bm), –13.9 (bm); ^1H NMR (27 °C; CD₂Cl₂, 399.8 MHz): δ 5.42 (CH₂, m, 2H), 3.25 (CH₂, m, 1H), 2.92 (CH₂, m, 1H), –10.45 (Rh–H, bm, 1H), –11.65 (Ir–H, bm, 1H); $^{31}\text{P}\{^1\text{H}\}$ NMR (–40 °C; CD₂Cl₂, 161.9 MHz): δ 27.1 (Rh–P, dm, 1P, $^1J_{\text{RhP}} = 98$ Hz), 16.9 (Rh–P, dm, 1P, $^1J_{\text{RhP}} = 125$ Hz), –10.0 (Ir–P, m, 1P), –14.0 (Ir–P, m, 1P); ^1H NMR (–40 °C; CD₂Cl₂, 399.8 MHz): δ 5.40 (CH₂, m, 2H), 3.24 (CH₂, m, 1H), 2.85 (CH₂, m, 1H), –10.30 (Rh–H, ddm, 1H, $^2J_{\text{trans PH}} = 150.0$ Hz, $^1J_{\text{RhH}} = 12.0$ Hz), –11.78 (Ir–H, dm, 1H, $^2J_{\text{trans PH}} = 127.1$ Hz); $^{13}\text{C}\{^1\text{H}\}$ NMR (–40 °C, CD₂Cl₂, 100.5 MHz): δ 193.8 (Rh–CO, dm, 1C, $^1J_{\text{RhC}} = 62.8$ Hz), 180.3 (Ir–CO, s, 1C), 49.8 (CH₂, m, 1C), 43.7 (CH₂, m, 1C). IR (CH₂Cl₂): ν(CO) = 1964 (s), 1946 (s)

cm^{-1} , $\nu(\text{M-H}) = 2091$ (w, br) cm^{-1} . Compound **20** was also produced upon warming the solution of **18** to 0 °C. $[\text{RhIr}(\text{D})_2(\text{CO})_2(\mu\text{-GeDPh})(\text{dppm})_2]$ (**20-D₃**) was prepared as described for **20**, by reaction of **1** with PhGeD_3 . ^2H NMR (−80 °C, CH_2Cl_2 , 61.4 MHz): δ 6.92 (Ge–D, s, 1D), −10.47 (Rh–D, s, 1D), −11.86 (Ir–D, s, 1D).

d. $[\text{RhIr}(\text{H})_2(\text{CO})_2(\mu\text{-GeH}^t\text{Bu})(\text{dppm})_2]$ (**21**): In a 100 mL Schlenk tube, under anhydrous conditions and an Ar atmosphere, compound **1** (65 mg, 0.057 mmol) was dissolved in 5 mL of benzene at ambient temperature. *t*-Butylgermane (9.0 μL , 0.065 mmol) was then added to the solution by syringe, resulting in an immediate colour change from dark orange to light yellow. The reaction was allowed to stir for 30 min, followed by the reduction of solvent volume to approximately 1 mL *in vacuo*. Subsequent slow addition of pentane gave a pale yellow powder in 92 % isolated yield (65.3 mg). X-ray quality crystals were grown by the slow diffusion of diethylether into the concentrated CH_2Cl_2 solution of **21**. Anal. calcd. for $\text{C}_{56}\text{H}_{58}\text{GeIrO}_2\text{P}_4\text{Rh}$: C, 53.61; H, 4.66. Found: C, 53.69; H, 4.70. $^{31}\text{P}\{^1\text{H}\}$ NMR (27 °C, CD_2Cl_2 , 201.6 MHz): δ 28.4 (Rh–P, dm, 1P, $^1J_{\text{RhP}} = 112$ Hz), 15.3 (Rh–P, dm, 1P, $^1J_{\text{RhP}} = 117$ Hz), −8.3 (Ir–P, m, 1P), −14.6 (Ir–P, m, 1P); ^1H NMR (27 °C, CDCl_2 , 498.1 MHz): δ 6.70 (Ge–H, bs, 1H), 5.45 (CH_2 , m, 2H), 3.22 (CH_2 , m, 1H), 2.91 (CH_2 , m, 1H), 1.59 (^tBu , m, 9H), −10.65 (Rh–H, ddm, 1H, $^2J_{\text{trans PH}} = 149.9$ Hz, $^1J_{\text{RhH}} = 12.0$ Hz), −11.78 (Ir–H, dm, 1H, $^2J_{\text{trans PH}} = 126.5$ Hz); $^{13}\text{C}\{^1\text{H}\}$ NMR (27 °C, CD_2Cl_2 , 100.5 MHz): δ 195.2 (Rh–CO, dm, 1C, $^1J_{\text{RhC}} = 66.5$ Hz), 181.3 (Ir–CO, s, 1C), 51.8 (CH_2 , m, 1C), 45.6 (CH_2 , m, 1C), 30.9 (^tBu , s, 1C), 30.6 (^tBu , s, 3C). IR (CH_2Cl_2): $\nu(\text{CO}) = 1944, 1896$ (s) cm^{-1} ,

$\nu(\text{Ge-H}) = 2097 \text{ (w) cm}^{-1}$. Compound **21** was also produced upon warming solutions of **19** to ambient temperature.

e. **[RhIr(GeH₂Ph)(H)₂(CO)₂(κ¹-dppm)(μ-GePhH)(μ-H)(dppm)] (22)**: In a septum-sealed NMR tube under an Ar atmosphere, **[RhIr(H)₂(CO)₂(μ-GeHPh)(dppm)₂] (20)** (30 mg 0.023 mmol) was dissolved in 0.7 mL of CD₂Cl₂ and then cooled to -78 °C. 3.2 μL (1.1 equiv) of PhGeH₃ was added to the NMR tube via a microliter syringe. No reaction was observed by NMR at this temperature. Upon warming to -40 °C, the intermediate **22** was observed in the ³¹P{¹H} NMR spectrum in approximately 30 % yield after 1 h reaction time. Further warming to -20 °C led to several unidentified products. ³¹P{¹H} NMR (-40 °C, CD₂Cl₂, 161.9 MHz): δ 21.8 (Rh-P, dm, 1P, ¹J_{RhP} = 102 Hz), -10.5 (Ir-P, m, 1P), -18.3 (Ir-P, m, 1P), -28.4 (Pendent-P, m, 1P); ¹H NMR (-40 °C; CD₂Cl₂, 399.8 MHz): δ 5.22 (CH₂, m, 1H), 4.92 (CH₂, m, 1H), 3.67 (Ge-H, m, 1H), 3.58 (Ge-H, m, 1H), 3.31 (CH₂, m, 1H), 2.56 (CH₂, m, 1H), -12.10 (Rh-H, ddm, 1H, ²J_{trans PH} = 159 Hz, ¹J_{RhH} = 12.0 Hz), -12.58 (μ-H, b, 1H, ¹J_{RhH} = 14.0 Hz), -12.75 (Ir-H, dm, 1H, ²J_{trans PH} = 129 Hz).

f. **[RhIr(CO)₂(μ-GeHPh)(μ-GePh₂)(dppm)₂] (23)**: 74 mg (0.058 mmol) of **[RhIr(H)₂(CO)₂(μ-GeHPh)(dppm)₂] (20)** in a Schlenk flask was dissolved in 10 mL of CH₂Cl₂ followed by the addition of 11 μL (0.058 mmol) of Ph₂GeH₂. The reaction mixture was stirred gently for 24 h during which time the yellow solution of **20** turned orange. The solvent volume was reduced to approximately 1 mL under high vacuum, and the solution layered with 3 mL of pentane yielding light yellow crystals (suitable for X-ray analysis) of compound **23** after 48 h in 77 %

yield. Anal. calcd. for $C_{70}H_{60}Ge_2IrO_2P_4Rh$: C, 56.17; H, 4.01. Found: C, 55.91; H, 4.16. $^{31}P\{^1H\}$ NMR (27 °C; CD_2Cl_2 , 201.6 MHz) δ 35.8 (Rh–P, ddd, 1P, $^1J_{RhP}$ = 112 Hz, $^2J_{PP}$ = 116 Hz, $^2J_{PP}$ = 28 Hz), 24.4 (Rh–P, ddd, 1P, $^1J_{RhP}$ = 115 Hz, $^2J_{PP}$ = 140 Hz, $^2J_{PP}$ = 28 Hz), 7.8 (Ir–P, dd, 1P, $^2J_{PP}$ = 116 Hz, $^2J_{PP}$ = 20 Hz), –7.9 (Ir–P, dd, 1P, $^2J_{PP}$ = 140 Hz, $^2J_{PP}$ = 20 Hz); 1H NMR (27 °C; CD_2Cl_2 , 498.1 MHz): δ 6.14 (Ge–H, m, 1H), 5.13 (CH_2 , m, 1H), 4.49 (CH_2 , m, 1H), 3.02 (CH_2 , m, 1H), 2.94 (CH_2 , m, 1H); $^{13}C\{^1H\}$ (CD_2Cl_2 , 100.5 MHz): δ 200.5 (Rh–CO, dm, 1C, $^1J_{RhC}$ = 76 Hz), 187.0 (Ir–CO, bs, 1C), 37.5 (CH_2 , m, 1C), 34.1 (CH_2 , m, 1C)

g. $[RhIr(H)_2(CO)_2(\mu-GePh_2)(dppm)_2]$ (24): Under an Ar atmosphere, 100 mg of compound **1** (0.087 mmol) in a Schlenk tube was dissolved in 20 mL of CH_2Cl_2 . The solution was then cooled to 0 °C in an ice-water-bath, 17.8 μ L (1.1 equiv) of Ph_2GeH_2 was added by syringe to the vigorously stirred solution of **1** and the reaction was left for 6 h at this temperature under a dynamic Ar flow (which is important for effective removal of released CO, otherwise the reaction mainly gave a mixture of complexes **24** and **25**). During this time the colour of the solution lightened. The solvent was reduced to 1 mL *in vacuo* and the remaining solution was layered with 3 mL of pentane. Colourless crystals were separated after 24 h. Isolated yield 40 % (47.0 mg). Anal. calcd. for $C_{64}H_{56}GeIrO_2P_4Rh$: C, 56.95; H, 4.15. Found: C, 56.72; H, 4.29. $^{31}P\{^1H\}$ NMR (27 °C; CD_2Cl_2 , 161.9 MHz): δ 27.5 (Rh–P, m, 1P), 18.1 (Rh–P, m, 1P); –0.2 (Ir–P, m, 1P), –8.3 (Ir–P, m, 1P). 1H NMR (27 °C; CD_2Cl_2 , 399.8 MHz): δ 4.01 (CH_2 , bm, 1H), 3.82 (CH_2 , bm, 1H), 2.95 (CH_2 , bm, 1H), 2.55 (CH_2 , bm, 1H), –10.78 (bm), –11.09 (bm, 1H); $^{31}P\{^1H\}$ NMR (–80 °C; CD_2Cl_2 , 161.9 MHz): δ 27.1(Rh–P, m, 1P), 17.8 (Rh–P,

m, 1P), -0.8 (Ir-P, m, 1P), -8.6 (Ir-P, m, 1P); ^1H NMR (-80 °C; CD_2Cl_2 , 399.8 MHz): δ 4.12 (CH_2 , m, 1H), 3.95 (CH_2 , m, 1H), 3.00 (CH_2 , bm, 1H), 2.63 (CH_2 , m, 1H), -10.76 (Rh-H, ddm, 1H, $^2J_{\text{trans PH}} = 129.0$ Hz, $^1J_{\text{RhH}} = 13.0$ Hz), -11.09 (Ir-H, dm, 1H, $^2J_{\text{trans PH}} = 115.0$ Hz). $^{13}\text{C}\{^1\text{H}\}$ NMR (27 °C; CD_2Cl_2 , 100.5 MHz): δ 197.9 (Rh-CO, dt, 1C, $^1J_{\text{RhC}} = 69$ Hz, $^2J_{\text{PC}} = 10$ Hz), 182.9 (Ir-CO, t, 1C, $^2J_{\text{PC}} = 13$ Hz).

h. **[RhIr(H)(GePh₂H)(CO)₃(κ^1 -dppm)(μ -GePh₂)(dppm)] (25):** In a Schlenk tube 100 mg (0.087 mmol) of compound **1** was dissolved in 5 mL of benzene at ambient temperature. Three freeze-pump-thaw cycles were applied to the solution, followed by the addition of 64 μL (4 equiv) of Ph_2GeH_2 . After stirring the solution overnight in the sealed Schlenk tube, the solvent volume was reduced *in vacuo* to 2 mL. Subsequent addition of 10 mL of pentane gave rise to a yellow powder. Orange crystals were obtained by the diffusion of pentane into a concentrated fluorobenzene solution of the compound. Isolated yield 68 % (95.0 mg). Anal. calcd. for. $\text{C}_{77}\text{H}_{66}\text{Ge}_2\text{IrO}_3\text{P}_4\text{Rh}\cdot 1.5\text{C}_6\text{H}_5\text{F}$: C 59.05; H, 4.21. Found: C, 59.32; H, 4.41. $^{31}\text{P}\{^1\text{H}\}$ NMR (27 °C; C_6D_6 , 161.9 MHz): δ 4.2 (Rh-P, ddd, 1P, $^1J_{\text{RhP}} = 108$ Hz, $^2J_{\text{PP}} = 108$ Hz, $^3J_{\text{PP}} = 5$ Hz), -2.3 (Ir-P, dd, 1P, $^2J_{\text{PP}} = 45$ Hz, $^3J_{\text{PP}} = 5$ Hz), -8.3 (Ir-P, ddd, 1P, $^2J_{\text{PP}} = 108$ Hz, $^2J_{\text{RhP}} = 8$ Hz, $^4J_{\text{PP}} = 8$ Hz), -28.5 (pendent-P, dd, 1P, $^2J_{\text{PP}} = 45$ Hz, $^4J_{\text{PP}} = 8$ Hz); ^1H NMR (27 °C; C_6D_6 , 498.1 MHz): δ 5.65 (Ge-H, d, 1H, $^3J_{\text{PH}} = 6.1$ Hz), 5.16 (CH_2 , m, 1H), 3.88 (CH_2 , m, 1H), 3.54 (CH_2 , m, 1H), 3.26 (CH_2 , m, 1H), -10.82 (Ir-H, dd, 1H, $^2J_{\text{PH}} = 19.6$ Hz, $^2J_{\text{PH}} = 14.6$ Hz); $^{13}\text{C}\{^1\text{H}\}$ NMR (27 °C; CD_2Cl_2 , 100.5 MHz): δ 202.4 (Rh-CO, dm, 1C, $^1J_{\text{RhC}} =$

43.8 Hz), 200.5 (Rh–CO, dm, 1C, $^1J_{\text{RhC}} = 43.8$ Hz), 184.8 (Ir–CO, bs, 1C), 58.3 (CH₂, m, 1C), 38.5 (CH₂, m, 1C).

i. **[RhIr(CH₃)(GeHPh₂)(CO)(μ-H)(μ-CO)(dppm)₂][CF₃SO₃] (26):** Under Ar, 30 mg (0.023 mmol) of [RhIr(CH₃)(CO)₂(dppm)₂][CF₃SO₃] (**2**) was taken into an NMR tube, dissolved in 0.7 mL of CD₂Cl₂ and cooled to –78 °C in an acetone-dry-ice bath. 4.3 μL (0.023 mmol) of diphenylgermane was added by a microliter syringe and the reaction was monitored by low-temperature NMR spectroscopy. Immediately after addition of diphenylgermane the dark orange colour of the solution lightened. Between –80 °C to –60 °C, NMR analysis indicated the quantitative formation of [RhIr(CH₃)(GeHPh₂)(CO)(μ-H)(μ-CO)(μ-dppm)₂][CF₃SO₃] (**26**) in solution. No attempt was made to isolate this compound at this temperature. ¹³C-enriched compound **26** was prepared as discussed above, by reacting ¹³C-enriched [RhIr(¹³CH₃)(¹³CO)₂(dppm)₂][CF₃SO₃] (**2**) with Ph₂GeH₂. ³¹P{¹H} NMR (–80 °C; CD₂Cl₂, 161.9 MHz): δ 28.3 (Rh–P, dm, 2P, $^1J_{\text{RhP}} = 140$ Hz), –9.1 (Ir–P, m, 2P); ¹H NMR (–80 °C; CD₂Cl₂, 399.8 MHz): δ 5.09 (Ge–H, t, 1H, $^3J_{\text{PH}} = 13.0$ Hz), 4.10 (CH₂, m, 2H), 3.40 (CH₂, m, 2H), 0.49 (CH₃, t, 3H, $^3J_{\text{PH}} = 6.8$ Hz), –8.94 (μ-H, dm, 1H, $^1J_{\text{RhH}} = 13.6$ Hz); ¹³C{¹H} (–80 °C; CD₂Cl₂, 100.5 MHz): δ 214.8 (μ-CO, dm, 1C, $^1J_{\text{RhC}} = 29$ Hz), 173.3 (Ir–CO, t, 1C, $^2J_{\text{PC}} = 9.0$ Hz), 32.7 (CH₂, m, 2C) 15.1 (CH₃, dt, 1C, $^1J_{\text{RhC}} = 28.0$ Hz, $^2J_{\text{PC}} = 6.0$ Hz); ¹⁹F NMR (–80 °C; CD₂Cl₂, 376.3 MHz): δ 79.3 (CF₃SO₃, s, 3F).

j. **[RhIr(CH₃)(CO)₂(μ-GeHPh₂)(μ-H)(dppm)₂][CF₃SO₃] (27) :** *Method 1:* Warming the solution of compound **26** to –20 °C resulted in a colour change of the solution to light green from light orange. ³¹P{¹H} NMR suggested the

quantitative formation of compound **27**. *Method 2*: 70 mg (0.055 mmol) of compound **2** in a Schlenk tube was dissolved in 3 mL of THF followed by three freeze-pump-thaw cycles. The reaction flask was then cooled to $-15\text{ }^{\circ}\text{C}$ in a salt-ice-water bath. 10.2 μL (0.055 mmol) of Ph_2GeH_2 was dissolved in another Schlenk tube and the solution was cannula transferred to the first flask. The reaction was stirred for 30 min at this temperature during which time a greenish-yellow precipitate settled at the bottom of the flask. After removal of THF via cannula, the solids were washed with ether to give analytically pure complex. Isolated yield 67 % (55.2 mg). The complex was stable at ambient temperature in the solid state under an inert atmosphere, however, was unstable above $20\text{ }^{\circ}\text{C}$ in a solution of CH_2Cl_2 . Anal. calcd. for $\text{C}_{66}\text{H}_{59}\text{F}_3\text{IrO}_5\text{P}_4\text{RhGeS}$: C, 52.42; H, 3.91. Found: C, 52.79; H, 4.23. ^{13}C -enriched compound **27** was prepared under the similar conditions as mentioned above, by reacting $[\text{RhIr}(^{13}\text{CH}_3)(^{13}\text{CO})_2(\text{dppm})_2][\text{CF}_3\text{SO}_3]$ (**2**) with Ph_2GeH_2 . $^{31}\text{P}\{^1\text{H}\}$ NMR ($-20\text{ }^{\circ}\text{C}$; CD_2Cl_2 , 161.9 MHz): δ 21.4 (Rh-P, dm, 2P, $^1J_{\text{RhP}} = 99\text{ Hz}$), -15.6 (Ir-P, m, 2P); ^1H NMR ($-20\text{ }^{\circ}\text{C}$; CD_2Cl_2 , 399.8 MHz): δ 4.08 (CH_2 , m, 2H), 3.36 (CH_2 , m, 2H), 0.89 (CH_3 , t, 3H, $^3J_{\text{PH}} = 6.4\text{ Hz}$), -1.92 ($\mu\text{-Ge-H}$, ddm, 1H, $^1J_{\text{RhH}} = 25.2\text{ Hz}$, $^2J_{\text{HH}} = 7.0\text{ Hz}$), -9.23 (ddm, $\mu\text{-H}$, 1H, $^1J_{\text{RhH}} = 16.8\text{ Hz}$, $^2J_{\text{HH}} = 7.0\text{ Hz}$); $^{13}\text{C}\{^1\text{H}\}$ NMR ($-20\text{ }^{\circ}\text{C}$, CD_2Cl_2 , 100.5 MHz): δ 192.4 (Rh-CO, dt, 1C, $^1J_{\text{RhC}} = 78.5\text{ Hz}$, $^2J_{\text{PC}} = 14.2\text{ Hz}$), 177.5 (Ir-CO, t, 1C, $^2J_{\text{PC}} = 7.8\text{ Hz}$), 36.9 (CH_2 , m), -25.1 (CH_3 , bt, 1C, $^2J_{\text{PC}} = 7.0\text{ Hz}$). ^{19}F NMR ($-20\text{ }^{\circ}\text{C}$; CD_2Cl_2 , 376.3 MHz): δ 79.3 (CF_3SO_3 , s, 3F).

k. **$[\text{RhIr}(\text{CO})_2(\mu\text{-H})(\mu\text{-GePh}_2)(\text{dppm})_2][\text{CF}_3\text{SO}_3]$ (**28**)** : *Method 1*: As the solution of compound **27** was warmed to ambient temperature the colour turned

dark green from light green within a period of 2 h. $^{31}\text{P}\{^1\text{H}\}$ NMR suggested the quantitative formation of compound **28**. *Method 2*: 70 mg (0.055 mmol) of compound **2** in a Schlenk tube was dissolved in 3 mL of dry CH_2Cl_2 followed by three freeze-pump-thaw cycles. 10.2 μL (0.055 mmol) of Ph_2GeH_2 was dissolved in the same solvent in another Schlenk tube and the solution was cannula transferred to the former flask at ambient temperature. The reaction was left stirring gently for 4 h during which time the dark orange reaction mixture turned to light yellow then to dark green. Addition of 10 mL of pentane resulted in a bright green powder in 90 % isolated yield (73.3 mg). Anal. calcd. for $\text{C}_{65}\text{H}_{55}\text{F}_3\text{IrO}_5\text{P}_4\text{RhGeS}$: C, 51.97; H, 3.78. Found: C, 52.16; H, 3.70. The same complexes having the $[\text{BPh}_4]^-$ and $[\text{BAr}^{\text{F}}_4]^-$ anions, (**28** $[\text{BPh}_4]$ and **28** $[\text{BAr}^{\text{F}}_4]$) were synthesized by the following procedure: Under an atmosphere of Ar, 53 mg (0.036 mmol) of **2** $[\text{BPh}_4]$ or 72 mg of **2** $[\text{BAr}^{\text{F}}_4]$ (0.036 mmol) was dissolved in 1 mL of THF or diethyl ether, respectively, in a 10 mL Schlenk tube, followed by the addition of 6.8 μL (0.036 mmol) of Ph_2GeH_2 by a microliter syringe at ambient temperature. After 4 h the dark green solution was layered with pentane in both cases. Dark-yellow crystals (suitable for X-ray analysis) of both compounds were separated after 24 h in 80 % (48.5 mg) and 83 % (64 mg) isolated yield, respectively. ^{13}C -enriched compound **28** was prepared as noted above, by reacting ^{13}C -enriched $[\text{RhIr}(^{13}\text{CH}_3)(^{13}\text{CO})_2(\text{dppm})_2][\text{CF}_3\text{SO}_3]$ (**2**) with Ph_2GeH_2 . $^{31}\text{P}\{^1\text{H}\}$ NMR (27 °C; CD_2Cl_2 , 201.6 MHz): δ 24.3 (Rh–P, dm, 2P, $^1J_{\text{RhP}} = 100$ Hz), 0.5 (Ir–P, m, 2P); ^1H NMR (27 °C; CD_2Cl_2 , 498.1 MHz): δ 4.83 (CH_2 , m, 2H), 3.69 (CH_2 , m, 2H), –9.91 (dm, μ -H, 1H, $^1J_{\text{RhH}} = 18.9$ Hz); $^{13}\text{C}\{^1\text{H}\}$

NMR (27 °C, CD₂Cl₂, 125.7 MHz): 196.4 (Rh–CO, dt, 1C, ¹J_{RhC} = 67.9 Hz, ²J_{PC} = 14.0 Hz), 185.5 (Ir–CO, t, 1C, ²J_{PC} = 8.0 Hz), 37.9 (CH₂, m, 2C). ¹⁹F NMR (27 °C; CD₂Cl₂, 376.3 MHz): δ 79.1 (CF₃SO₃, s, 3F).

l. **[RhIr(H)(CO)₂(μ-GeHPh₂)(μ-H)(dppm)₂][CF₃SO₃] (29):** *Method 1:* Under an Ar atmosphere 50 mg of [RhIr(CO)₂(μ-H)(μ-GePh₂)(dppm)₂][CF₃SO₃] (**28**) (0.033 mmol) was dissolved in a septum-sealed Schlenk tube with 1 mL of CH₂Cl₂. 6.1 μL (0.033 mmol) of Ph₂GeH₂ was then introduced to the solution via microliter syringe. The dark green solution turned orange within 3 h. Addition of 2 mL of pentane gave rise to a pale yellow powder in 76 % isolated yield (38 mg). *Method 2:* A septum-sealed NMR tube containing 50 mg (0.033 mmol) of [RhIr(CO)₂(μ-H)(μ-GePh₂)(dppm)₂][CF₃SO₃] (**28**) in 0.7 mL of CD₂Cl₂, was pressurized with 1 atm of H₂. Within 5 min the dark green solution turned orange. Multinuclear NMR suggested quantitative conversion of **28** to **29**. Addition of 2 mL of pentane yielded a pale yellow powder as before in 85 % isolated yield (42.5 mg). The deuterium isotopologue of **29**, [RhIr(D)(CO)₂(μ-GeDPh₂)(μ-H)(dppm)₂][CF₃SO₃] (**29-D₂**) was synthesized by the reaction of **28** with 1 atm pressure of D₂ under the similar conditions. *Method 3:* To a septum-sealed NMR tube containing a solution of 50 mg (0.033 mmol) of compound **28** in 0.7 mL of CD₂Cl₂, was added 6.1 μL (0.033) of Ph₂SiH₂ via microliter syringe. The dark green solution slowly turned orange over the period of 6h. Addition of 2 mL of pentane yielded a pale yellow powder. The same complex with the [BPh₄][−] and [BAr^F₄][−] anions, **29[BPh₄]** and **29[BAr^F₄]**, was synthesized by the following procedure: Under an atmosphere of Ar, 70 mg of **28[BPh₄]** or 90 mg of

28[**BAr**^F₄] was dissolved in 1 mL of CH₂Cl₂ in a 10 mL Schlenk tube, followed by the pressurization of the flask with 1 atm of H₂. Within 5 min the dark green solution turned orange in both cases and no significant reaction rate difference was observed with these reactions compared to that of described in *method 2* with OTf⁻ as counteranion. The solvent in the solution of **29**[**BPh**₄] was removed under high vacuum and the pale yellow solid was redissolved in 0.5 mL of THF. Layering with 1 mL of ether in an NMR tube gave rise to light-yellow X-ray quality crystals (suitable for X-ray analysis) of **29**[**BPh**₄] after 6 h in 75 % isolated yield. Anal. calcd. for C₈₈H₇₇BGeIrO₂P₄Rh: C, 63.28; H, 4.61. Found: C, 63.49; H, 4.72. ¹³C-enriched compound **29** was prepared as noted above, by reacting ¹³C-enriched [RhIr(¹³CH₃)(¹³CO)₂(dppm)₂][CF₃SO₃] (**2**) with Ph₂GeH₂. ³¹P{¹H} NMR (27 °C; CD₂Cl₂, 161.9 MHz): δ 22.9 (Rh–P, m, 1P), –11.5 (Ir–P, bm); ¹H NMR (27 °C; CD₂Cl₂, 498.1 MHz): δ 4.33 (CH₂, m, 2H), 3.47 (CH₂, bm, 2H), –2.00 (μ–Ge–H, b, 1H); –9.62 (Ir–H, b, 1H), –10.30 (μ–H, b, 1H); ³¹P{¹H} NMR (–80 °C; CD₂Cl₂, 161.9 MHz): δ 22.5 (Rh–P, dm, 1P, ¹J_{RhP} = 102 Hz), –12.6 (Ir–P, m); ¹H NMR (–80 °C; CD₂Cl₂, 399.9 MHz): δ 4.15 (CH₂, m, 2H), 3.05 (CH₂, bm, 2H), –2.77 (μ–Ge–H, d, 1H, ¹J_{RhH} = 27.6 Hz); –9.24 (Ir–H, s, 1H), –9.81 (μ–H, dm, 1H, ¹J_{RhH} = 18.8 Hz); ¹³C{¹H} NMR (–40 °C; CD₂Cl₂, 125.7 MHz): δ 193.1 (Rh–CO, dt, 1C, ¹J_{RhC} = 80.7 Hz, ²J_{PC} = 15.0 Hz), 185.5 (Ir–CO, s, 1C), 35.4 (CH₂, m, 2C). ¹⁹F NMR (–80 °C; CD₂Cl₂, 376.3 MHz): δ 79.2 (CF₃SO₃, s, 3F).

m. [**RhIr**(CO)₂(Ge(OH)Ph₂)(μ–H)₂(dppm)₂][CF₃SO₃] (**30**): To a septum-sealed Schlenk tube containing 70 mg (0.047 mmol) of compound **28** in 2 mL of CH₂Cl₂

under argon, was added 0.9 μL (0.050 mmol) of deoxygenated water. The dark green solution changed to orange within 5 to 10 min. After 30 min, the addition of 5 mL of ether resulted in a dark orange solid in 83 % isolated yield (58.9 mg). Anal. calcd. for $\text{C}_{65}\text{H}_{57}\text{F}_3\text{GeIrO}_6\text{P}_4\text{RhS}$: C, 51.55; H, 3.76. Found: C, 51.61; H, 3.83. X-ray quality crystals were obtained by layering diethylether over a concentrated CH_2Cl_2 solution of **30**. The deuterium isotopologue of **30**, $[\text{RhIr}(\text{CO})_2(\text{Ge}(\text{OD})\text{Ph}_2)(\mu\text{-D})(\mu\text{-H})(\text{dppm})_2][\text{CF}_3\text{SO}_3]$ (**30-D₂**) was synthesized by the reaction of **28** with 1 equiv of D_2O under similar conditions. $^{31}\text{P}\{^1\text{H}\}$ NMR (27 $^\circ\text{C}$; CD_2Cl_2 , 161.9 MHz): δ 24.4 (Rh–P, dm, 2P, $^1J_{\text{RhP}} = 105$ Hz), –5.7 (Ir–P, m, 2P); ^1H NMR (27 $^\circ\text{C}$; CD_2Cl_2 , 498.1 MHz): δ 3.47 (CH_2 , bm, 4H), 1.41 (O–H, b, 1H); –9.81 ($\mu\text{-H}$, b, 1H), –12.05 ($\mu\text{-H}$, b, 1H); $^{13}\text{C}\{^1\text{H}\}$ NMR (27 $^\circ\text{C}$; CD_2Cl_2 , 125.7 MHz): δ 186.2 (Rh–CO, dt, 1C, $^1J_{\text{RhC}} = 77.3$ Hz, $^2J_{\text{PC}} = 17.0$ Hz), 176.4 (Ir–CO, t, 1C, $^2J_{\text{PC}} = 11.6$ Hz), 36.8 (CH_2 , m, 2C). ^{19}F NMR (27 $^\circ\text{C}$; CD_2Cl_2 , 376.3 MHz): δ 79.1 (CF_3SO_3 , s, 3F). $^2\text{H}\{^1\text{H}\}$ NMR (27 $^\circ\text{C}$, CH_2Cl_2 , 61.4 MHz): δ 1.59 (OD, bs, 1D), –9.76 ($\mu\text{-D}$, s, 1D); $^{31}\text{P}\{^1\text{H}\}$ NMR (–80 $^\circ\text{C}$; CD_2Cl_2 , 161.9 MHz): δ 26.4 (Rh–P, ddm, 1P, $^2J_{\text{trans-PP}} = 312$ Hz, $^1J_{\text{RhP}} = 105$ Hz), 22.8 (Rh–P, ddm, 1P, $^2J_{\text{trans-PP}} = 312$ Hz, $^1J_{\text{RhP}} = 105$ Hz), –4.0 (Ir–P, dm, 1P, $^2J_{\text{trans-PP}} = 312$ Hz), –6.9 (Ir–P, dm, 1P, $^2J_{\text{trans-PP}} = 312$ Hz); ^1H NMR (–80 $^\circ\text{C}$; CD_2Cl_2 , 399.9 MHz): δ 6.10 (CH_2 , m, 1H), 4.47 (CH_2 , m, 1H), 4.01 (CH_2 , m, 1H), 2.84 (CH_2 , m, 1H), –9.93 ($\mu\text{-H}$, ddm, 1H, $^1J_{\text{RhH}} = 17.6$ Hz, $^2J_{\text{HH}} = 7.6$ Hz); –12.27 ($\mu\text{-H}$, ddm, 1H, $^1J_{\text{RhH}} = 20.6$ Hz, $^2J_{\text{HH}} = 7.6$ Hz).

n. $[\text{RhIr}(\text{CO})_2(\text{Ge}(\text{OMe})\text{Ph}_2)(\mu\text{-H})_2(\text{dppm})_2][\text{CF}_3\text{SO}_3]$ (**31**): To a septum-sealed Schlenk tube containing a solution of 70 mg (0.047 mmol) of $[\text{RhIr}(\text{CO})_2(\mu\text{-H})(\mu\text{-H})_2(\text{dppm})_2][\text{CF}_3\text{SO}_3]$ (**31**)

$\text{GePh}_2(\text{dppm})_2[\text{CF}_3\text{SO}_3]$ (**28**) in 2 mL of CH_2Cl_2 under argon, was added 1.9 μL (0.047 mmol) of deoxygenated methanol. The dark green colour of the solution changed to reddish orange within 5 min. After 30 min, the addition of 5 mL of ether yielded an orange solid in 80 % isolated yield. X-ray quality crystals were obtained by layering ether on a concentrated CH_2Cl_2 solution of **31** in an NMR tube. Anal. calcd. for $\text{C}_{66}\text{H}_{59}\text{F}_3\text{GeIrO}_6\text{P}_4\text{RhS}$: C, 51.87; H, 3.86. Found: C, 51.97; H, 3.93. The deuterium isotopologue of **31**, $[\text{RhIr}(\text{CO})_2(\text{Ge}(\text{OCD}_3)\text{Ph}_2)(\mu\text{-D})(\mu\text{-H})(\text{dppm})_2][\text{CF}_3\text{SO}_3]$ (**31-D₄**) was synthesized by the reaction of **28** with 1 equiv of CD_3OD under the similar conditions. $^{31}\text{P}\{\text{H}\}$ NMR (27 °C; CD_2Cl_2 , 161.9 MHz): δ 24.5 (Rh–P, dm, 2P, $^1J_{\text{RhP}} = 104$ Hz), –6.1 (Ir–P, m, 2P); ^1H NMR (27 °C; CD_2Cl_2 , 498.1 MHz): δ 4.49 (CH_2 , bm, 4H), 3.42 (OCH_3 , s, 3H); –9.78 ($\mu\text{-H}$, b, 1H), –12.16 ($\mu\text{-H}$, b, 1H); ^{19}F NMR (27 °C; CD_2Cl_2 , 376.3 MHz): δ 79.1 (CF_3SO_3 , s, 3F). $^{31}\text{P}\{\text{H}\}$ NMR (–80 °C; CD_2Cl_2 , 161.9 MHz): δ 24.9 (Rh–P, ddm, 1P, $^2J_{\text{trans-PP}} = 308$ Hz, $^1J_{\text{RhP}} = 104$ Hz), 22.8 (Rh–P, ddm, 1P, $^2J_{\text{trans-PP}} = 308$ Hz, $^1J_{\text{RhP}} = 104$ Hz), –5.8 (Ir–P, m, 2P); ^1H NMR (–80 °C; CD_2Cl_2 , 399.9 MHz): δ 6.02 (CH_2 , m, 1H), 4.57 (CH_2 , m, 1H), 4.13 (CH_2 , m, 1H), 2.47 (CH_2 , m, 1H), –9.80 ($\mu\text{-H}$, ddm, 1H, $^1J_{\text{RHH}} = 17.6$ Hz, $^2J_{\text{HH}} = 7.1$ Hz); –12.40 ($\mu\text{-H}$, ddm, 1H, $^1J_{\text{RHH}} = 17.1$ Hz, $^2J_{\text{HH}} = 7.6$ Hz). $^{13}\text{C}\{\text{H}\}$ NMR (–80 °C, CD_2Cl_2 , 125.7 MHz): δ 185.5 (Rh–CO, dt, 1C, $^1J_{\text{RhC}} = 77.0$ Hz, $^2J_{\text{PC}} = 17.0$ Hz), 175.7 (Ir–CO, t, 1C, $^2J_{\text{PC}} = 11.3$ Hz), 36.3 (CH_2 , m, 1C), 34.9 (CH_2 , m, 1C).

o. **$[\text{RhIr}(\text{CO})_2(\text{GeClPh}_2)(\mu\text{-H})_2(\text{dppm})_2][\text{CF}_3\text{SO}_3]$ (**32**):** To a septum-sealed Schlenk tube containing a solution of 85 mg (0.047 mmol) of $[\text{RhIr}(\text{CO})_2(\mu\text{-H})(\mu\text{-GePh}_2)(\text{dppm})_2][\text{CF}_3\text{SO}_3]$ (**28**) in 2 mL of CH_2Cl_2 under argon, was added 220 μL

(0.26 mmol, 5 equiv) of 2 M ether solution of HCl via a microliter syringe. The dark green solution immediately changed to reddish orange. Addition of 5 mL of ether resulted in a brick-red powder in 67 % isolated yield. $^{31}\text{P}\{^1\text{H}\}$ NMR (27 °C; CD_2Cl_2 , 161.9 MHz): δ 23.8 (Rh–P, dm, 1P, $^1J_{\text{RhP}} = 110$ Hz), –7.3 (Ir–P, m); ^1H NMR (27 °C; CD_2Cl_2 , 498.1 MHz): δ 4.48 (CH_2 , bm, 2H), 4.26 (CH_2 , bm, 2H); –10.27 ($\mu\text{-H}$, b, 1H), –11.68 ($\mu\text{-H}$, b, 1H); δ 183.8 (Rh–CO, dt, 1C, $^1J_{\text{RhC}} = 75.0$ Hz, $^2J_{\text{PC}} = 17.0$ Hz), 174.6 (Ir–CO, t, 1C, $^2J_{\text{PC}} = 12.0$ Hz). ^{19}F NMR (27 °C; CD_2Cl_2 , 376.3 MHz): δ 79.1 (CF_3SO_3 , s, 3F).

3.3 X-ray Data Collection and Structure Determination.

3.3.1 General Considerations.

Single crystals suitable for X-ray diffraction were obtained by slow diffusion of pentane into CH_2Cl_2 (**20**, **23**, **24**, **30**), benzene (**21**), fluorobenzene (**25**) or THF (**28**) solutions of the compounds, or by the diffusion of ether into THF (**29**) or dichloromethane (**31**) solutions of the compounds. Data were collected on either a Bruker D8/APEX II CCD diffractometer (**20**, **21**, **23**, **24**, **25**, **29**, **30**), Bruker PLATFORM/SMART 1000 CCD diffractometer (**28**), or Bruker PLATFORM/APEX II CCD (**31**) diffractometer at –100 °C using Mo $K\alpha$ radiation.²⁰ Data were corrected for absorption through the use of Gaussian integration from indexing of the crystal faces. The structures were solved using the Patterson location of heavy atoms followed by structure expansion (*DIRDIF-2008*)²¹ (**20**, **21**, **23**, **25**, **28** and **30**) or direct methods (*SHELXS-97*²² (**24**, **31**), *SIR97*²³ (**29**)). Refinement was carried out using the program *SHELXL-97*.²² Hydrogen atoms attached to carbons were assigned positions on the basis of the

sp^2 or sp^3 hybridization geometries of their parent atoms and were given isotropic displacement parameters 20 % than the U_{eq} 's of their parent carbons. The hydroxyl hydrogen in **30** was generated in an idealized position (assuming sp^3 hybridization of the oxygen) with a displacement parameter 150 % of that of the attached oxygen); the O–H bond vector was allowed to freely rotate with respect to the Ge–O bond during refinement. Metal hydrides for compound **20**, **21**, **23**, **28**, **29**, **30** and **31** and Ge-bound hydrogens for **20**, **21**, **24**, and **29** were located from difference Fourier maps and treated as detailed below. A listing of crystallographic experimental data is provided for all structures in Appendix II.

3.3.2 Special refinement conditions.

i. Compound 20. One metal atom position was refined with a site occupancy of 60 % Ir/40 % Rh (Ir(A)/Rh(B)); the other was refined as 60 % Rh/40 % Ir (Rh(A)/Ir(B)). The GeHPh and hydrido ligands were split into two sets of positions with relative occupancies of 80 % (H(1A), H(2A), Ge(A), H(1GE), and the phenyl carbons C(91A) through C(96A)) and 20 % (H(1B), H(2B), Ge(B), H(2GE), and the phenyl carbons C(91B) through C(96B)). Both metal-hydride (1.55 Å) and germyl-hydrogen (1.45 Å) distances were fixed during refinement.

ii. Compound 21. One metal atom position was refined with a site occupancy of 60 % Ir/40 % Rh (Ir(A)/Rh(B)); the other was refined as 60 % Rh/40 % Ir (Rh(A)/Ir(B)). Both metal-hydride (1.55 Å) and germyl-hydrogen (1.45 Å) distances were fixed during refinement. Adjacent atomic positions for the

disordered solvent dichloromethane molecule were refined with common isotropic displacement parameters.

iii. Compound 23. Metal atom positions (designated Ir(A)/Rh(B) and Rh(A)/Ir(B)) were refined with a 50 % site occupancy each of Ir and Rh. The coordinates and thermal parameter for the Ge-bound hydrogen (H1(GE)) were allowed to freely refine.

iv. Compound 24. Metal atom positions (designated Ir(A)/Rh(B) and Rh(A)/Ir(B)) were refined with a 50 % site occupancy each of Ir and Rh. The Ir(A)–H(1) and Rh(A)–H(2) distances were restrained to be 1.60(1) Å. Attempts to refine peaks of residual electron density as disordered or partial-occupancy solvent dichloromethane chlorine or carbon atoms were unsuccessful. The data were corrected for disordered solvent electron density through use of the SQUEEZE procedure as implemented in *PLATON*.²⁴ A total solvent-accessible void volume of 807 Å³ with a total electron count of 282 (consistent with 6 molecules of solvent dichloromethane, or 2 molecules per formula unit of the RhIr molecule) was found in the unit cell. The value of the Flack parameter observed herein (0.085(11)) was indicative of a minor degree of racemic twinning, and was accommodated during the refinement (using the *SHELXL-97* TWIN instruction).

v. Compound 25. The coordinates and thermal parameter for the hydrido ligand (H(1)) were allowed to freely refine, whereas the Ge(2)–H(2GE) distance (1.45 Å) was fixed during refinement. The F–C_{ipso} (1.35(1) Å) and F···C_{ortho} (2.37(1) Å) distances within the disordered solvent fluorobenzene molecules were

restrained during refinement. One PhF molecule was split into two sets of positions with a 70 %/30 % distribution of occupancy factors; the aromatic rings of these molecules were modelled as idealized hexagons with a C–C bond distance of 1.39 Å and 120° bond angles.

vi. Compound 28. One metal atom position was refined with a site occupancy of 55 % Ir/45 % Rh (Ir(A)/Rh(B)); the other was refined as 55 % Rh/45 % Ir (Rh(A)/Ir(B)). The coordinates and thermal parameter for the bridging hydrido ligand (H(1)) were allowed to freely refine. The O–C (1.45(1) Å) and C–C (1.50(1) Å) distances within the disordered solvent tetrahydrofuran molecules were restrained to idealized values during refinement.

vii. Compound 29. The coordinates and thermal parameters for the hydrido ligands (H(1), H(2), H(3)) were allowed to freely refine. The O–C (1.45(1) Å) and C–C (1.50(1) Å) distances within the disordered solvent tetrahydrofuran molecule were restrained to idealized values during refinement. Attempts to refine peaks of residual electron density as additional disordered or partial-occupancy solvent tetrahydrofuran oxygen or carbon atoms were unsuccessful. The data were corrected for disordered solvent electron density through use of the SQUEEZE procedure as implemented in *PLATON*.²⁴ A total solvent-accessible void volume of 674 Å³ with a total electron count of 167 (consistent with 4 molecules of solvent tetrahydrofuran, or 2 molecules per formula unit of the Rh/Ir complex) was found in the unit cell.

viii. Compound 30. The coordinates and thermal parameters for the bridging hydrido ligands (H(1), H(2)) were allowed to freely refine. Attempts to refine

peaks of residual electron density as disordered or partial-occupancy solvent dichloromethane chlorine or carbon atoms were unsuccessful. The data were corrected for disordered solvent electron density through use of the SQUEEZE procedure as implemented in *PLATON*.²⁴ A total solvent-accessible void volume of 876.2 Å³ with a total electron count of 264 (consistent with 6 molecules of solvent CH₂Cl₂, or 1.5 molecules of CH₂Cl₂ per formula unit of the Rh/Ir complex ion) was found in the unit cell.

ix. Compound 31. The coordinates and thermal parameters for the bridging hydrido ligands (H(1), H(2)) were allowed to freely refine. The following distance restraints were applied to the partially occupied/disordered dichloromethane and diethyl ether molecules: C–Cl, 1.80(1) Å; C–C, 1.53(1) Å; C–O, 1.43(1) Å; C···C, 2.34(1) Å; C···O, 2.42(1) Å.

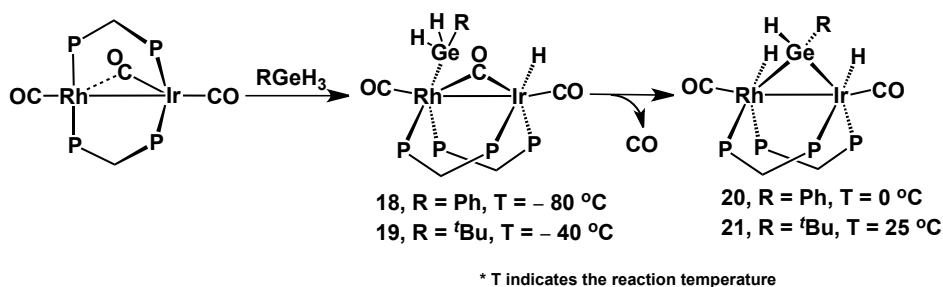
3.4 Results and Characterization of Compounds.

3.4.1 Reactions of [RhIr(CO)₃(dppm)₂] with Primary and Secondary Germanes.

The reaction of [RhIr(CO)₃(dppm)₂] (**1**) with one equiv of phenylgermane at –80 °C in CD₂Cl₂ results in the quantitative formation of the germyl/hydride complex [RhIr(H)(GeH₂Ph)(CO)₂(μ-CO)(dppm)₂] (**18**) by the single Ge–H bond activation as shown in Scheme 3.1. The analogous complex, [RhIr(H)(GeH₂^tBu)(CO)₂(μ-CO)(dppm)₂] (**19**), is also formed in the reaction of **1** with ^tBuGeH₃, although for this reaction a slightly elevated temperature (–40 °C) is required. The spectroscopic features of both compounds **18** and **19** are closely comparable (see Experimental data), hence only the NMR data for compound **18**

will be discussed. In these compounds, oxidative addition of the germane can occur at either Rh or Ir, with migration of one of the fragments (either germyl or hydride) to the adjacent metal. Although Ir should have the greater tendency for

Scheme 3.1



oxidative addition, we view **1** as having a Rh(+1)/Ir(-1) formulation in which the saturated, pseudo-tetrahedral “Ir(CO)₂P₂” fragment functions as a 2-electron donor to Rh, giving the latter a square-planar 16e⁻ configuration.¹⁸ As a consequence of the unsaturation at Rh, we suggest that oxidative addition of the Ge-H bond occurs at this metal with hydride migration to Ir. This suggestion is also consistent with the presumed greater migratory tendency of the much smaller hydride than of the germyl ligand, since addition at Ir would necessitate migration of the germyl unit to Rh, in order to give the product observed (*vide infra*). The ³¹P{¹H} NMR spectrum of **18** shows four well resolved peaks at δ 37.5, 28.8, -5.5 and -12.4 indicating the chemical inequivalence of all ³¹P nuclei; the two downfield resonances are attributed to the Rh-bound phosphorus nuclei, as indicated by the observed Rh-P coupling of 133 and 126 Hz. Of note, the ¹J_{Rh-P} value for the ³¹P nuclei trans to the germyl ligand (126 Hz) is not much different from the value cis to the same ligand (133 Hz), suggesting that the germyl ligand

does not exert a substantial trans-influence. This is in contrast to the analogous silyl complex (see previous chapter), in which the strong trans influence of the silyl ligand results in a substantially reduced $^1J_{\text{RhP}}$ value for the ^{31}P nucleus opposite this group.¹⁵ In the ^1H NMR spectrum of **18** a doublet of doublet of doublets for the hydride resonance is observed at $\delta -11.50$, displaying a large coupling of 125 Hz to the trans ^{31}P nucleus; the other couplings result from two other ^{31}P nuclei, as explained for the analogous silyl complexes in the previous chapter.¹⁵ The two diastereotopic Ge-bound hydrogens appear as two multiplets at $\delta 4.23$ and 3.87 . The positions of both germyl and hydride ligands, as shown in Scheme 3.1, were confirmed by selective ^{31}P -decoupling and ^{13}C - ^1H HMBC NMR experiments as previously described in the characterization of $[\text{RhIr}(\text{H})(\text{SiH}_2\text{Ph})(\text{CO})_2(\mu\text{-CO})(\text{dppm})_2]$.¹⁵ Three resonances at $\delta 178.0$ (t), 198.2 (dt, $^1J_{\text{RhC}} = 78$ Hz) and 229.9 ($^1J_{\text{RhC}} = 34$ Hz), in the $^{13}\text{C}\{^1\text{H}\}$ NMR spectrum can be assigned to the Ir-bound, Rh-bound and bridging CO ligands, respectively.

Warming the solution of **18** to 0°C or reacting $[\text{RhIr}(\text{CO})_3(\text{dppm})_2]$ (**1**) with one equiv of phenylgermane at this temperature in CH_2Cl_2 leads to the formation of the phenylgermylene-bridged dihydride, $[\text{RhIr}(\text{H})_2(\text{CO})_2(\mu\text{-GeHPh})(\text{dppm})_2]$ (**20**) (Scheme 2.1) – the result of oxidative addition of two Ge–H bonds – one at each metal. The related *tert*-butylgermylene-bridged dihydride, $[\text{RhIr}(\text{H})_2(\text{CO})_2(\mu\text{-GeH}^t\text{Bu})(\text{dppm})_2]$ (**21**) is obtained analogously. Both **20** and **21** exhibit very similar NMR spectra, except that complex **20** appears to be fluxional (see Figure A.7 in Appendix II) at room temperature (*vide infra*) while complex **21** shows no sign of fluxionality, having ^{31}P resonances that are sharp and well-resolved

between $-80\text{ }^{\circ}\text{C}$ and ambient temperature (see Figure A.8 in Appendix II). At ambient temperature, compound **20** displays four broad unresolved resonances in the $^{31}\text{P}\{^1\text{H}\}$ NMR spectrum and at the same temperature the ^1H NMR spectrum shows three broad peaks at δ 5.42, 3.25 and 2.92 for the methylene protons (integrating as 2:1:1; the first resulting from coincidental overlap of two resonances) and two very broad peaks in the upfield region (δ -10.45 for Rh–H and -11.65 for Ir–H) for the metal-bound hydrides. Although the Ge-bound proton for **20** could not be located in the ^1H NMR spectrum, being obscured by the aromatic protons, the Ge–D resonance for $[\text{RhIr}(\text{D})_2(\text{CO})_2(\mu\text{-GeDPh})(\text{dppm})_2]$ (**20-D₃**) was observed at δ 6.92 in the ^2H NMR spectrum (see Figure A.7 in Appendix II). For **21** the Ge–H resonance appears as a broad singlet at δ 6.70. Unfortunately, the IR data are of little use in further characterizing these species; in addition to the strong stretches for the terminal carbonyls in **20** and **21**, the only metal–hydride stretch for each compound is weak and broad at ca. 2090 cm^{-1} (as confirmed by deuterium labeling). However the similarity of the NMR spectra with those of a silylene-bridged analogue¹⁵ and the X-ray structures of **20** and **21** (*vide infra*) leave little doubt about their formulation. Upon cooling to $-40\text{ }^{\circ}\text{C}$ the $^{31}\text{P}\{^1\text{H}\}$ NMR resonances of **20** resolve into sharp multiplets at δ 27.1, 16.9, -10.0 and -14.0 . The down-field pair of resonances are again assigned to the Rh-bound ^{31}P nuclei on the basis of their couplings (98 and 125 Hz) to ^{103}Rh . The substantially reduced Rh–P coupling of one of the Rh-bound ^{31}P nuclei is presumably a consequence of the greater trans-influence of the hydride ligand than the bridging-germylene unit which is pseudo-trans to the other Rh-bound ^{31}P

nucleus (*vide infra*). The methylene protons and metal hydride peaks also become sharp and well resolved at this temperature, the latter of which display distinct coupling to the ^{31}P nucleus in the trans positions at each metal ($^2J_{\text{HP}} = 150$ Hz; $^2J_{\text{HP}} = 127$ Hz). A broadband ^{31}P decoupling experiment also allows the resolution of Rh coupling ($^1J_{\text{RhH}} = 12$ Hz) in the former signal. The $^{13}\text{C}\{^1\text{H}\}$ NMR spectrum shows a doublet of multiplets at δ 193.8 ($^1J_{\text{RhC}} = 63$ Hz) and a broad singlet at δ 180.3, attributed to Rh- and Ir-bound carbonyls, respectively.

Like its silylene-bridged counterpart, $[\text{RhIr}(\text{H})_2(\text{CO})_2(\mu\text{-SiHPh})(\text{dppm})_2]$ (**4**),¹⁵ the fluxionality of **20** appears to arise due to exchange between the three metal-bound hydrides. This exchange phenomenon was confirmed by saturation transfer NMR experiments at 0 °C, in which selective saturation of the Rh-bound hydride leads to collapse of the Ir-bound hydride and *vice versa*. We were unable to observe the effect of selective saturation on the Ge-bound hydrogen due to our inability to locate it in the NMR spectrum. This exchange process presumably occurs through rapid, reversible oxidative addition/reductive elimination involving the Ge–H bonds, as explained in our previous study on Si–H bond activation¹⁵ and in related studies by Eisenberg and coworkers.¹⁶ As noted earlier, complex **21** shows no sign of exchange at ambient temperature. In this case, the static nature of compound **21** can be attributed to the greater steric bulk of the *tert*-butyl group, which inhibits its fluxionality.

The structures of both complexes **20** and **21**, shown in Figure 3.1, highlight their similarities to each other and to their silylene analogues^{15, 17} in which the bridging-germylene ligand is pseudo- trans to one diphosphine unit and the metal-

bound hydrides are approximately trans to the other diphosphine unit (see Appendix II). The distance between the two Group 9 metals (2.8691(2) Å for **20** and 2.8736(2) Å for **21**) suggests the presence of a formal metal–metal bond in each complex while the Ir–Ge (Ir(A)–Ge(A) = 2.4234(1) Å for **20** and Ir–Ge = 2.4303(3) Å for **21**) and Rh–Ge distances (Rh(A)–Ge(A) = 2.4000(4) Å for **20**

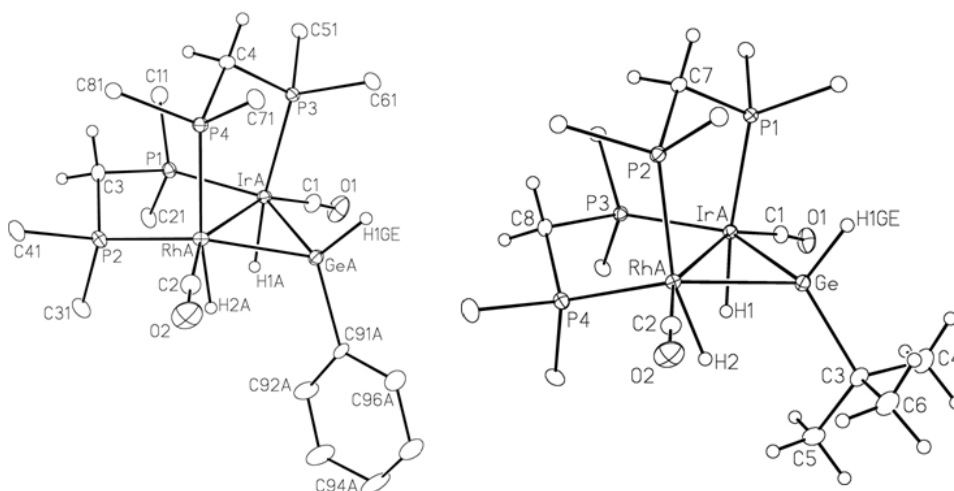


Figure 3.1: Perspective views of the major disordered form of compound **20** (left) and of **21** (right) showing the numbering scheme. Non-hydrogen atoms are represented by Gaussian ellipsoids at the 20% probability level. Hydrogen atoms are shown arbitrarily small. For the dppm phenyl groups, only the ipso carbons are shown. For **20**, Rh(A) and Ir(A) were refined at 60% occupancy, while H(1A), H(2A), Ge(A), H(1GE), and the phenyl carbons C(91A) through C(96A) were refined at 80% occupancy. For **21**, Rh(A) and Ir(A) were refined at 60% occupancy.

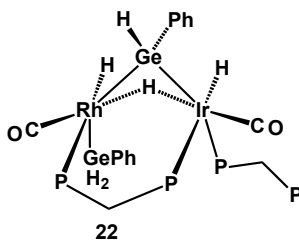
and Rh–Ge = 2.4294(3) for **21**) are symmetrical and slightly shorter than the previously reported homobimetallic Rh₂^{5a} and Ir₂^{5b} complexes. The Ir–Ge–Rh angles (73.00(1)° for **20** and 72.50(1)° for **21**) are also comparable to the values in the above homobimetallic systems⁵ but larger than in one germylene-bridged

diiridium complex for which the angle was more acute ($\text{Ir-Ge-Ir} = 66.96(2)^\circ$).^{2g} Surprisingly, the metal-bound hydrides do not show a significant trans-influence in the solid state as indicated by the closely comparable metal-phosphorus distances (ca. 2.34 Å for both structures; see Appendix II) even though a substantially reduced Rh–P coupling constant was observed by $^{31}\text{P}\{^1\text{H}\}$ NMR spectroscopy for the Rh-bound ^{31}P nuclei which is trans to the hydride. Owing to the crystallographic disorder between the Rh and Ir positions in these and some other compounds in this report, the X-Ray studies cannot rule out the possibility of additional disorder involving Rh_2 and Ir_2 species. However, this possibility is unambiguously ruled out by the NMR studies, which show coupling of one end of the dppm ligands to ^{103}Rh while the other end is Ir-bound and displays no metal coupling.

Further reaction of **20** with one equiv of phenylgermane at room temperature leads to several unidentified products accompanied by H_2 evolution (as observed in the ^1H NMR). This is in contrast to the related silicon chemistry in which further reaction with phenylsilane, either in the presence or absence of CO, gave stable bis(silylene) complexes.¹⁵ Even under an atmosphere of CO, reaction of **20** with another equiv of phenylgermane again leads to a mixture of unidentified products.

However, reaction of **20** with phenylgermane at low temperature does give a single product. Addition of 1 equiv of PhGeH_3 to **20** at -80°C results in no reaction but upon warming to -40°C a product is observed in the $^{31}\text{P}\{^1\text{H}\}$ NMR spectrum in about 30% yield after approximately 1 h reaction time (along with 70

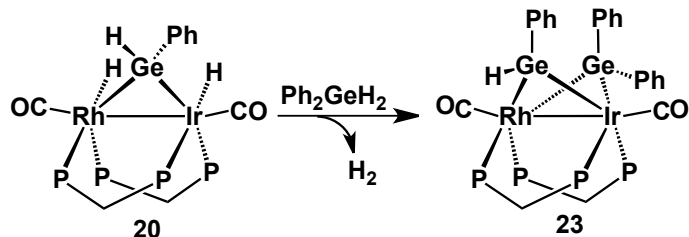
% unreacted **20**). This new species (**22**) displays four multiplets at δ 21.8, -10.5 , -18.3 and -28.4 in the $^{31}\text{P}\{^1\text{H}\}$ NMR spectrum, the high-field resonance of which is close to that of free dppm (δ -23.0), suggesting that one arm of a diphosphine has dissociated and remains pendent. Only one resonance displays coupling to Rh ($^1J_{\text{RhP}} = 102$ Hz) indicating that phosphine dissociation has taken place from the Rh end of one dppm group. Pendent dppm species have previously been observed in related silylene-bridged complexes of RhIr¹⁵ and Rh₂,¹⁶ but interestingly were not observed in the less labile Ir₂¹⁷ system. In the ^1H NMR spectrum two doublets of multiplets (at δ -12.10 for Rh-H ($^1J_{\text{RhH}} = 12$ Hz) and -12.75 for Ir-H) and a broad resonance (at δ -12.58) are observed in a 1:1:1 ratio. The first two show distinct trans P-H coupling ($^2J_{\text{PH}} = 159$ and 129 Hz), indicating that one diphosphine unit maintains a trans disposition with respect to the metal-hydrides. The last peak sharpens upon selective decoupling of each of the Ir- and Rh-bound ^{31}P nuclei, identifying it as bridging, and appears as a doublet ($^1J_{\text{RhH}} = 14$ Hz) upon broadband ^{31}P decoupling. The two diastereotopic Ge-bound hydrogens of the germyl group appear at δ 3.67 and 3.58 in the proton NMR spectrum. On the basis of these spectral data the product, $[\text{RhIr}(\text{H})_2(\text{GeH}_2\text{Ph})(\text{CO})_2(\kappa^1\text{-dppm})(\mu\text{-H})(\mu\text{-GeHPh})(\text{dppm})]$ (**22**) is assigned the structure shown below. This species is unstable and warming the reaction mixture to -20 °C leads to its transformation



to several other unidentified products; nevertheless it is clear that the incorporation of a second germane into the original RhIrGe core is possible.

Although we were unable to generate a *bis*(phenylgermylene)-bridged species by reaction of **20** with phenylgermane, the reaction of **20** with 1 equiv of diphenylgermane leads to an unprecedented *mixed bis*(germylene) complex, [RhIr(CO)₂(μ-GeHPh)(μ-GePh₂)(dppm)₂] (**23**) in which both mono- and disubstituted germylene fragments are incorporated (Scheme 3.2). The ³¹P{¹H}

Scheme 3.2



NMR spectrum of this complex shows four sharp, well-resolved resonances at δ 35.8, 24.4, 7.8 and -7.9 (again, the down-field pair of resonances show distinct Rh–P coupling), confirming the chemical inequivalence of all ³¹P nuclei created by two different metals and different germylene bridges. Consistent with this formulation, the ¹H NMR spectrum displays four multiplets for the dppm methylene protons at δ 5.13, 4.49, 3.02 and 2.94 while the Ge-bound proton in the phenylgermylene unit appears as multiplet at δ 6.14. The ¹³C{¹H} NMR displays two resonances for Rh- and Ir-bound carbonyls at δ 200.5 and 187.0, respectively.

The solid-state structure of the bis(germylene) compound **23** is depicted in Figure 3.2 confirming the incorporation of a second germylene unit. The Rh–Ir

bond distance (2.8070(3) Å) is shorter than for the mono-germylene-bridged complexes (**20**, **21** and **24** (*vide infra*)) where distances between 2.8691(2) Å and

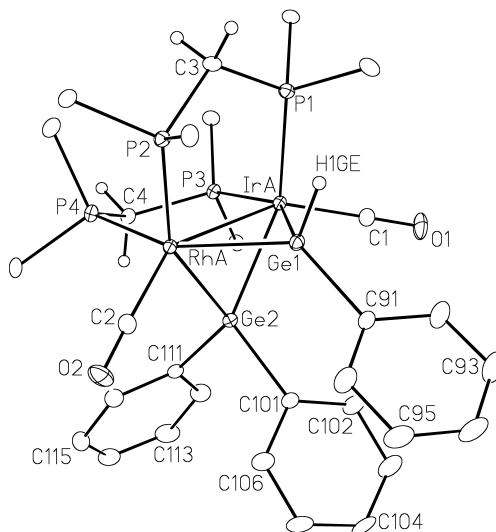


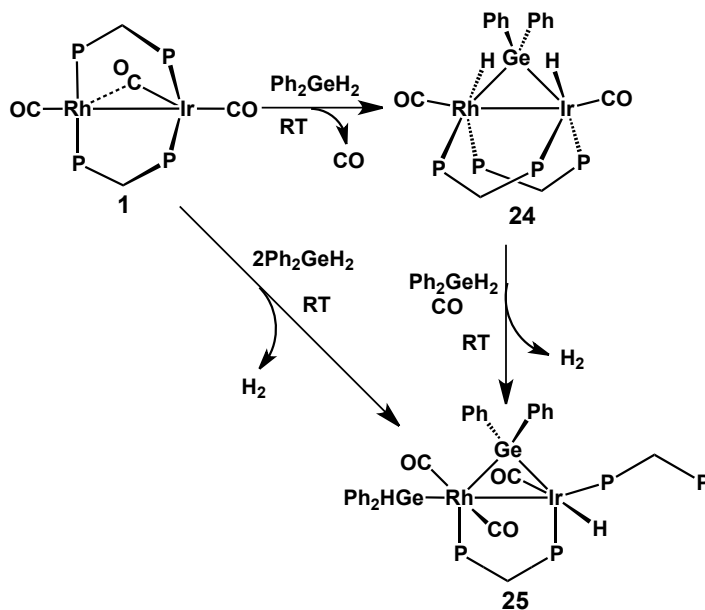
Figure 3.2: Perspective view of **23** showing the numbering scheme. Atom labeling scheme and thermal parameters are as described in Figure 3.1. Rh(A) and Ir(A) were refined at 50% occupancy. For the *dppm* phenyl groups only the *ipso* carbons are shown.

2.8970(6) Å were observed, presumably resulting from incorporation of the second acutely bridging germylene unit. The Ir–Ge and Rh–Ge distances are comparable with those of the mono-germylene bridged complexes (see Appendix II); however, the Rh–Ge–Ir angles (Ir(A)–Ge(1)–Rh(A) = 70.17(1)° and Ir(A)–Ge(2)–Rh(A) = 69.42(1)°) are more acute than the corresponding angles of compounds **20** (72.00(1)°), **21** (72.50(1)°) and **24** (72.42(3)°) (*vide infra*), consistent with the shorter Rh–Ir distance in **23**. The separation between the two bridging Ge atoms (Ge(1)–Ge(2) = 2.9921(6) Å) is significantly longer than a normal Ge–Ge bond (ca. 2.44 Å)^{9a,9b} but is also substantially shorter than the sum

of their van der Waals radii (4.22 Å).²⁵ As a consequence, it is not clear whether this intermediate distance is a result of the steric demands within the complex or a weak interaction between these two metals.

The reaction of **1** with one equiv of diphenylgermane gives rise to the monogermylene-bridged complex, $[\text{RhIr}(\text{H})_2(\text{CO})_2(\mu\text{-GePh}_2)(\text{dppm})_2]$ (**24**) in relatively low yield (40%), by double Ge–H bond activation (Scheme 3.3), much

Scheme 3.3



as observed for the primary germanes. This species has very similar NMR features to complexes **20** and **21** and shows fluxional behaviour at ambient temperature (as confirmed by variable temperature NMR spectroscopy). Its structure is shown in Figure 3.3. Unlike the structures of **20** and **21**, which have the pair of hydride ligands on the same face of the Ir–Rh–Ge plane, the metal-

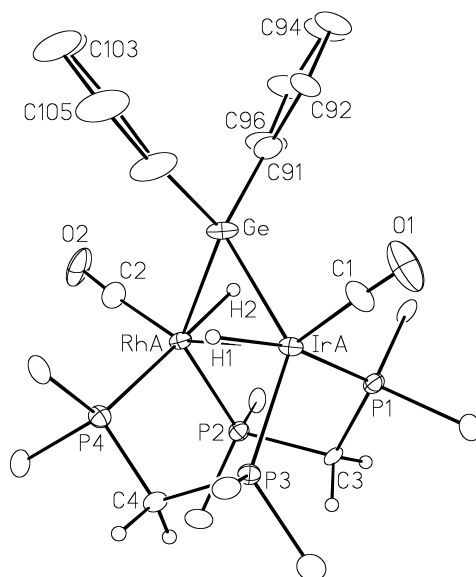


Figure 3.3: Perspective view of **24** showing the numbering scheme. Atom labeling scheme and thermal parameters are as described in Figure 3.1. Rh(A) and Ir(A) were refined at 50% occupancy. For the dppm phenyl groups only the ipso carbons are shown.

bound hydrides in **24** occupy opposite faces of this plane. With the mono-substituted germylene groups (**20** and **21**) both small hydrides ligands are directed towards the bulkier germylene substituent (Ph or ^tBu) allowing the bulky diphosphines to avoid these groups. However, in this disubstituted germylene group the symmetric environment on each side of the Ir–Rh–Ge plane favours one hydride on each side. As a consequence there is significant twisting about the Rh–Ir bond (torsion angles: P(1)–Ir–Rh–P(2) = 30.05(8)° and P(3)–Ir–Rh–P(4) = 29.92(8)°) allowing the dppm groups to minimize repulsions with the μ-GePh₂ group (for **20** these torsion angles are much smaller: P(1)–Ir–Rh–P(2) = 15.26(3)° and P(3)–Ir–Rh–P(4) = 13.86(3)°). The Rh–Ir distance (2.8790(6) Å) is again consistent with a formal metal–metal bond, while the Rh–Ge (2.437(1) Å) and Ir–Ge (2.437(1) Å) distances are closely comparable with those of complexes **20** and

21 (*vide supra*). The slight elongation of the Rh–P and Ir–P distances opposite the respective hydrides (2.346(2), 2.335(2) Å) compared to those opposite the germylene unit (2.317(2), 2.325(2) Å) may reflect the higher trans influence of the hydrides.

The reaction of **1** with two equiv of diphenylgermane in a sealed container or the reaction of **24** with 1 equiv of diphenylgermane in the presence of 1 atm of CO leads to the formation of the unusual germyl(germylene) complex, [RhIr(H)(GeHPh₂)(CO)₃(κ¹-dppm)(μ-GePh₂)(dppm)] (**25**) accompanied by H₂ loss (see Scheme 3.3). Although the product yield under a CO atmosphere is quantitative, reaction of **1** without the addition of CO is accompanied by decomposition leading to low yields of **25** (according to ³¹P{¹H} NMR). The reaction of **24** with diphenylgermane in the absence of CO leads only to decomposition. This behaviour very much resembles that of the silylene-bridged analogue, [RhIr(H)₂(CO)₂(μ-SiPh₂)(dppm)₂]¹⁵ and is in contrast to the reactivity of **1** with excess phenylgermane, which leads to decomposition at ambient temperature with or without CO.

The ³¹P{¹H} NMR spectrum for compound **25** displays four resonances in a similar spin pattern as was observed for **22** with the upfield resonance (δ –28.5) representing the pendent end of one diphosphine. In the ¹H NMR spectrum of **25** the germyl hydrogen appears as a doublet at δ 5.65 (³J_{PH} = 6.9 Hz) and collapses to a singlet upon irradiation of the Rh-bound ³¹P resonance, indicating that the germyl group is bound to Rh, although no resolvable coupling to Rh is observed. The Ir-bound hydride ligand appears as a doublet of doublets at δ –10.82 with

approximately 15 and 20 Hz cis-coupling to both Ir-bound ^{31}P nuclei as established by selective $^{31}\text{P}\{^1\text{H}\}$ decoupling experiments; the absence of Rh-H coupling, indicates that this hydride is terminally bound to Ir. In the $^{13}\text{C}\{^1\text{H}\}$ NMR spectrum for **25** two Rh-bound carbonyl groups (δ 202.4 and δ 200.5, both displaying 43.8 Hz coupling to Rh) and one on Ir (δ 184.8) are observed.

An ORTEP drawing of **25** is shown in Figure 3.4, clearly confirming the germyl/germylene formulation and the pendent dppm arrangement. The Rh–Ge

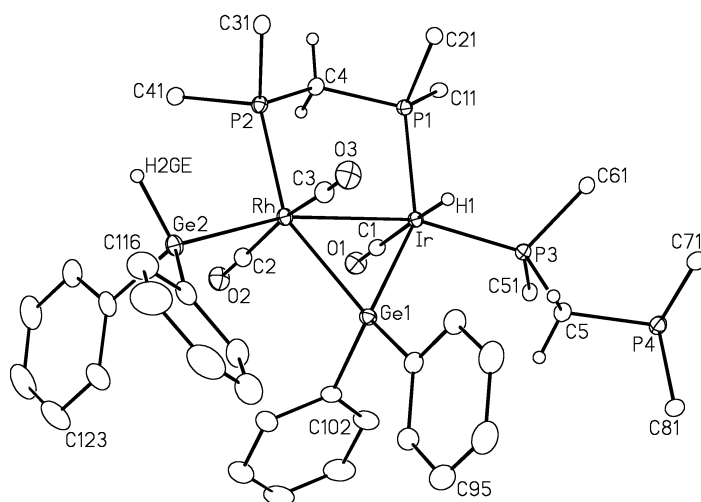


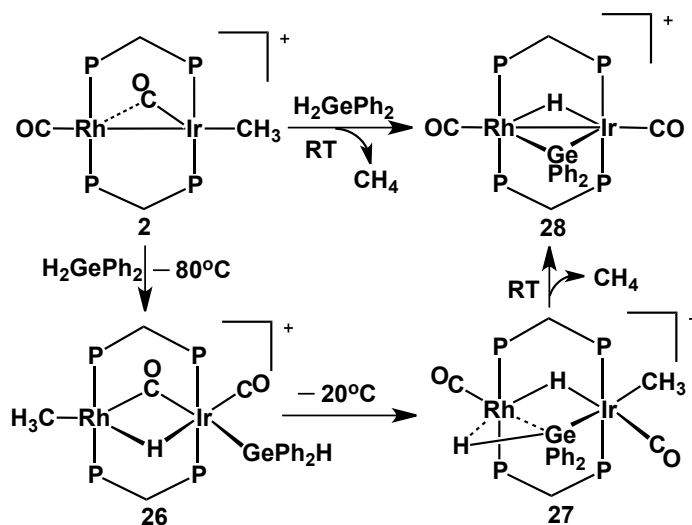
Figure 3.4: Perspective view of **25** showing the numbering scheme. Atom labeling scheme and thermal parameters are as described in Figure 3.1. For the dppm phenyl groups only the ipso carbons are shown.

bond distances (Rh–Ge(1) = 2.4923(3) Å and Rh–Ge(2) = 2.4665(3) Å) are comparable to previously reported dirhodium germylene complexes;^{8a} however, the Ir–Ge(1) distance (2.4103(2) Å) is slightly shorter than those previously reported.^{2g, 8b} The Ir-bound hydride was located and refined, lying trans to the Ir-bound CO with a typical Ir–H distance of 1.55(3) Å.

3.4.2 Reactions of $[\text{RhIr}(\text{CH}_3)(\text{CO})_2(\text{dppm})_2][\text{CF}_3\text{SO}_3]$ with Primary & Secondary Germanes.

The reaction of cationic $[\text{RhIr}(\text{CH}_3)(\text{CO})_2(\text{dppm})_2][\text{CF}_3\text{SO}_3]$ (**2**) with 1 equiv of diphenylgermane at ambient temperature leads to a dark green, highly air- and moisture- sensitive, germylene- and hydride-bridged complex, $[\text{RhIr}(\text{CO})_2(\mu\text{-GePh}_2)(\mu\text{-H})(\text{dppm})_2][\text{CF}_3\text{SO}_3]$ (**28**) in high yield together with one equiv of methane (Scheme 3.4). The complex has been characterized by multinuclear NMR spectroscopy and an X-ray structure determination.

Scheme 3.4



Two resonances at δ 24.3 and 0.5 are observed in the $^{31}\text{P}\{^1\text{H}\}$ NMR spectrum of **28**, corresponding to the Rh- and Ir-bound ends of the diphosphines, and as is commonly observed, the downfield peak corresponds to that bound to Rh as confirmed by the large Rh-P coupling of 100 Hz. In the ^1H NMR spectrum a multiplet, corresponding to the bridging hydride ligand, appears at δ -9.91. Selective decoupling of each of the resonances for the Ir- and Rh-bound ^{31}P nuclei results in a collapse of the hydride resonance to a doublet of triplets while ^{31}P

broadband decoupling gives a doublet ($^1J_{\text{RhH}} = 18.9$ Hz). The $^{13}\text{C}\{^1\text{H}\}$ NMR spectrum displays a doublet of triplets for the Rh-bound CO ($^1J_{\text{RhC}} = 67.9$ Hz, $^2J_{\text{PC}} = 14.0$ Hz) and a triplet for the Ir-bound CO ($^2J_{\text{PC}} = 8.0$ Hz). The complex shows no sign of fluxionality at room temperature, as both the $^{31}\text{P}\{^1\text{H}\}$ and ^1H NMR spectra remain unchanged as the temperature is lowered to -80 °C.

The X-ray structure determination of **28** (Figure 3.5) shows that unlike its neutral analogues (complexes **20**, **21** and **24**), in which the incorporation of a bridging germylene unit is accompanied by bending back of the dppm units into a cradle-shape geometry, the A-frame core of **28** is maintained, having an almost

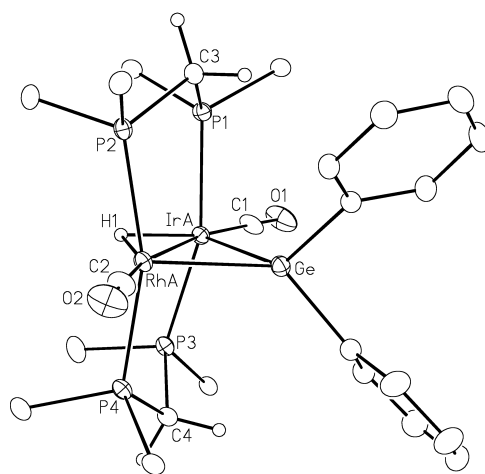


Figure 3.5: *Perspective view of the complex cation of **28** showing the numbering scheme. Atom labeling scheme and thermal parameters are as described in Figure 3.1. Rh(A) and Ir(A) were refined at 55% occupancy. For the dppm phenyl groups only the ipso carbons are shown.*

trans arrangement of diphosphines at each metal (P(1)–Ir(A)–P(3) = $160.90(4)^\circ$ and P(2)–Rh(A)–P(4) = $162.19(3)^\circ$) with the bridging germylene unit on the face of the complex opposite the hydride ligand. The bending of the phosphines away

from the μ -GePh₂ group and towards the much smaller hydride ligand allows the phenyl groups to minimize unfavourable contacts. The Rh–Ir bond length (2.8337(3) Å) of **28** is close to that of the starting complex **2** (2.8290(7) Å)¹⁹ in spite of a bridging hydride ligand, which generally results in an increase in the associated metal–metal separation,²⁶ while the Ir–Ge and Rh–Ge distances in this cationic complex are found to be slightly elongated and the Ir–Ge–Rh angle is more acute (69.11(1)°) than in the neutral analogue (*vide supra*). The disorder in the positions of the Rh and Ir atoms (a result of the symmetry of the complex) does not allow a differentiation of the bonds involving the Group 9 metals, as a result, the bridging germylene and hydride groups appear to be symmetrically bridged (Rh(A)–Ge = 2.4875(5) Å, Ir(A)–Ge = 2.5088(5) Å and Rh(A)–H(1) = 1.77(4) Å, Ir(A)–H(1) = 1.75(4) Å).

When the reaction is monitored at low temperature two intermediates in the formation of **28** are observed by NMR spectroscopy (Scheme 3.4). Addition of one equiv of diphenylgermane to **2** at –80 °C gives rise to the first intermediate, a germyl/hydride complex, $[\text{RhIr}(\text{CH}_3)(\text{GeHPh}_2)(\text{CO})(\mu\text{-H})(\mu\text{-CO})(\text{dppm})_2][\text{CF}_3\text{SO}_3]$ (**26**), resulting from Ge–H bond activation at Ir accompanied by methyl migration from Ir to Rh. In complex **2** both metals are unsaturated so the greater tendency for oxidative addition at the heavier congener favours addition to Ir. In the ³¹P{¹H} NMR spectrum a doublet of multiplets appears at δ 28.3 (¹J_{RhP} = 140 Hz) for the Rh-bound ³¹P nuclei while a multiplet at higher field (δ –9.1) appears for the Ir-bound ³¹P nuclei. This pattern, characteristic of an AA'BB'X spin system, suggests an A-frame geometry for this

intermediate. In the ^1H NMR spectrum, the germyl proton appears as a triplet at δ 5.09, and collapses to a singlet upon selective irradiation of the Ir-bound ^{31}P nuclei, while the bridging hydride appears as a doublet of multiplets at δ -8.94 and simplifies upon selective and broadband ^{31}P decoupling (see Figure 3.6). The

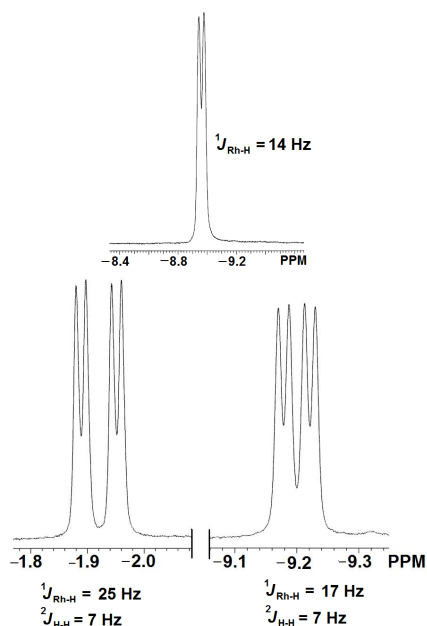


Figure 3.6: $^1\text{H}\{^{31}\text{P}\}$ NMR spectrum (broadband ^{31}P decoupled) of high-field regions for complex **26** (above) and **27** (below).

methyl protons appear as a triplet at δ 0.49 showing no apparent coupling to Rh; however, this resonance collapses to a singlet upon irradiation of the Rh-bound ^{31}P nuclei. The absence of resolvable two-bond Rh–H coupling in hydrocarbyl groups is common.^{15,27} When $^{13}\text{CH}_3$ -enriched complex **2** is used as starting material a doublet of triplets at δ 15.1 ($^1J_{\text{RhC}} = 28.0$ Hz, $^2J_{\text{PC}} = 6.0$ Hz) is observed in the $^{13}\text{C}\{^1\text{H}\}$ NMR spectrum for this methyl group, in which the magnitude of the coupling to Rh confirms its binding to this metal. The $^{13}\text{C}\{^1\text{H}\}$ NMR spectrum

also displays two resonances at δ 214.8 and 173.3 assigned to the bridging and the Ir-bound carbonyls, respectively. Upon broadband phosphorus-decoupling the terminally bound Ir–CO appears in the proton-coupled ^{13}C NMR spectrum as a doublet, displaying a trans C–H coupling of 26 Hz.

Upon warming to $-20\text{ }^\circ\text{C}$ the resonances in the $^{31}\text{P}\{^1\text{H}\}$ NMR spectrum due to **26** disappear completely, accompanied by the appearance of a new set corresponding to a second intermediate at δ 21.4 ($^1J_{\text{RhP}} = 99\text{ Hz}$) and -15.6 . This intermediate (Scheme 3.4) is formulated as $[\text{RhIr}(\text{CH}_3)(\text{CO})_2(\mu\text{-H})(\mu\text{-GeHPh}_2)(\text{dppm})_2][\text{CF}_3\text{SO}_3]$ (**27**), in which the Ge–H bond of the Ir-bound germyl ligand now interacts with Rh in an agostic fashion. In the ^1H NMR spectrum this agostic hydride appears as a doublet of doublets of multiplets at δ -1.92 ($^1J_{\text{RhH}} = 25\text{ Hz}$, $^2J_{\text{HH}} = 7\text{ Hz}$) showing coupling to Rh and two-bond coupling to the bridging hydride ligand (Figure 3.6). The upfield shift of this germyl-bridged proton compared to the terminal germyl protons in **18**, **19**, **22**, **25** and **26** supports its agostic interaction. The bridging hydride at δ -9.23 displays coupling to Rh and to the agostic hydride ($^1J_{\text{RhH}} = 17\text{ Hz}$, $^2J_{\text{HH}} = 7\text{ Hz}$), both of which are clear upon broadband ^{31}P decoupling, shown in Figure 6, and both resonances sharpen upon selective decoupling of both Ir- and Rh-bound ^{31}P resonances indicating the involvement of these ligands with both metals. The ^1H NMR spectrum suggests migration of the methyl group back to Ir, as evidenced by its triplet resonance at δ 0.89 in the ^1H NMR spectrum which upon irradiation of the Ir-bound ^{31}P nuclei collapses to a singlet and by the triplet at *ca.* δ -25.1 ($^2J_{\text{PC}} = 7.0\text{ Hz}$) in the $^{13}\text{C}\{^1\text{H}\}$ NMR spectrum showing no Rh coupling. The high-field chemical shift

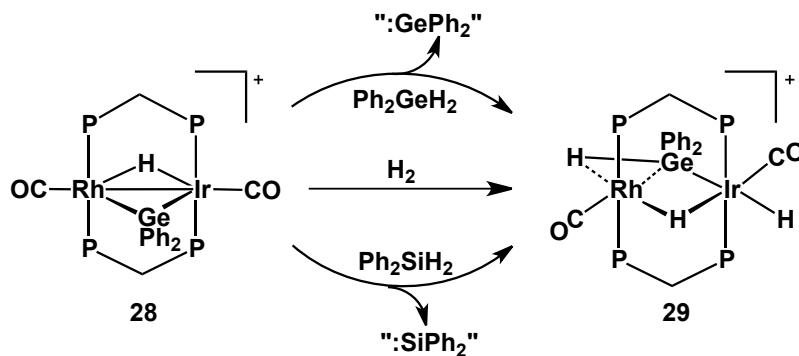
of this signal is also consistent with an Ir-bound methyl ligand, in contrast to the Rh-bound methyl groups which tend to resonate significantly down-field as observed for **26**. The Rh-bound CO appears as a doublet of triplets at δ 192.4 ($^1J_{\text{RhC}} = 78.5$ Hz) and the Ir-bound CO appears as a triplet at δ 177.5. In the proton-coupled ^{13}C NMR spectrum the latter resonance shows additional coupling ($^2J_{\text{CH}} = 26$ Hz) due to the trans disposition of the bridging hydride. Upon warming to room temperature, reductive elimination of methane from Ir leads to the exclusive formation of the hydride- and germylene-bridged complex **28**. We find it curious that methane elimination results at this stage and not earlier (from **26**) when the hydrides and methyl groups are adjacent on the more labile Rh centre, although the failure for reductive elimination to occur from the lower oxidation state Rh is consistent with our Rh(I)/Ir(III) formulation for these species.

Reactions of complex **2** with 1 equiv of primary germanes (R = Ph or t Bu), under a variety of conditions do not occur cleanly but instead yield several unidentified complexes (according to NMR), so the reactions were not pursued further.

3.4.3 Reactivity of the Cationic Germylene-Bridged Complex (**28**)

Attempts to synthesize a cationic germyl/germylene complex by reaction of $[\text{RhIr}(\text{CO})_2(\mu\text{-GePh}_2)(\mu\text{-H})(\text{dppm})_2][\text{CF}_3\text{SO}_3]$ (**28**) with an additional equiv of diphenylgermane instead yields the germyl-bridged dihydride complex $[\text{RhIr}(\text{H})(\text{CO})_2(\mu\text{-GeHPh}_2)(\mu\text{-H})(\text{dppm})_2][\text{CF}_3\text{SO}_3]$ (**29**) (Scheme 3.5) as characterized by multinuclear NMR and X-ray diffraction analysis. Compound **29**

Scheme 3.5



is a rare example of a cationic germyl-bridged complex,²⁸ which is presumably formed by the activation of pair of Ge–H bonds in the added germane, followed by the elimination of a “GePh₂” fragment, presumably as oligomers. An analogous silylene elimination was proposed to explain the conversion of a monometallic Pt-silylene complex to a Pt-dihydride product.²⁹ Compound **29** can be viewed as the product of H₂ addition to **28**, and consistent with this interpretation, the reaction of **28** with 1 atm of dihydrogen yields **29** within minutes (Scheme 3.5). Compound **29** can also be prepared from the reaction of **28** with 1 equiv of diphenylsilane over a 6 h period, with concomitant loss of a “SiPh₂” fragment. The fates of the germylene and silylene fragments produced in these reactions were not established.

The ¹H NMR spectrum of **29** at 27 °C displays three broad peaks (barely above the baseline) at δ –2.00, –9.62 and –10.30, which upon cooling to –78 °C sharpen while shifting to δ –2.77, –9.24 and –9.81 (see Figure A.15 in Appendix II). The down-field peak is assigned to the agostic Ge–H unit on the basis of its chemical shift compared to classical metal-hydrides. Upon ³¹P broadband

decoupling, this peak and the peak at $\delta -9.81$ display coupling to Rh of 27.6 Hz and 18.8 Hz, respectively. Selective ^{31}P decoupling of the Rh-bound ^{31}P resonance confirms that these two hydride signals also couple to these ^{31}P nuclei while the resonance at $\delta -9.24$ remains unchanged. However, upon selective ^{31}P decoupling of the Ir-bound ^{31}P nuclei, both high-field resonances sharpen, confirming the formulation in Scheme 3.5.

At intermediate temperatures a minor isomer of **29** (labeled as **29a**) is observed, so at $-20\text{ }^\circ\text{C}$ two new resonances are observed in the ^1H NMR spectrum at $\delta -10.6$ and -11.3 in a 2:1 ratio and having approximately 10 % of the total intensity of those due to **29**. This is accompanied by new broad $^{31}\text{P}\{^1\text{H}\}$ resonances at *ca.* $\delta 23.0$ (almost buried under the corresponding resonance for **29**) and -6.8 (see Figure A.15 in Appendix II). Clearly, the breadth of the ambient-temperature resonances for **29** is a result of exchange between these isomers, which is confirmed by saturation-transfer experiments at $-20\text{ }^\circ\text{C}$. Based on the 2:1 integration ratio of hydride resonances of **29a**, we contemplated the possibility of dihydrogen/hydride species. However, this possibility was ruled out by the T_1 relaxation time measurements for the hydrides of both **14** and **29a** at $-20\text{ }^\circ\text{C}$, in which all hydrides of both isomers have very similar relaxation times (*ca.* 0.4 s at 400 MHz). At lower temperatures the equilibrium between these isomers shifts in favour of **29** such that at $-80\text{ }^\circ\text{C}$ this is the only species visible in NMR spectra. The breadth of the NMR resonances for **29a** and its low abundance over a relatively narrow temperature range did not allow us to further characterize this species.

The X-ray structure of the cation of complex **29** is shown in Figure 3.7. Again the A-frame shape of the complex is maintained in the solid state, in which Rh adopts a trigonal bipyramidal arrangement (with the Ge–H bond occupying one site) while Ir is octahedral. The Rh–Ir distance is now elongated to 3.0273(2)

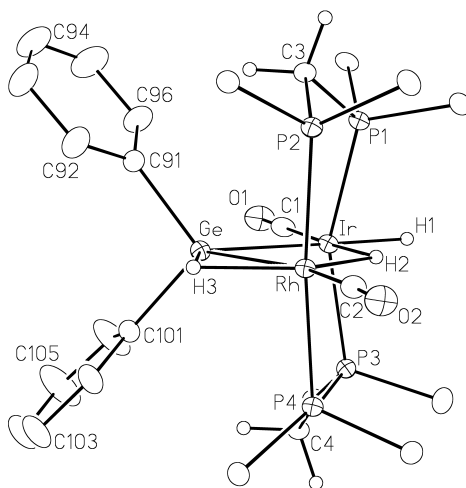


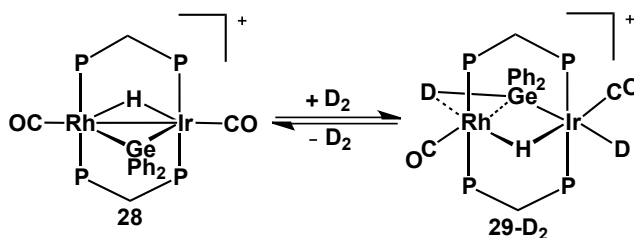
Figure 3.7: Perspective view of the complex cation of **29** showing the numbering scheme. Thermal parameters are as described in Figure 3.1. For the *dppm* phenyl groups only the ipso carbons are shown.

Å from 2.8337(3) Å in the precursor (**28**), accompanied by a widening of the Rh–Ge–Ir angle, from 69.11(1)° to 72.253(8)°. This significant elongation of the Rh–Ir distance suggests the absence of a formal metal-metal bond in complex **29**. The Rh–Ge distance (2.6106(3) Å) is significantly longer than Ir–Ge (2.5228(3) Å), as expected for the agostic interaction involving Rh. This is supported by the Rh–H(3) bond distance of 1.85(3) Å, which is somewhat longer than expected for a classical hydride, but clearly within bonding distance. The bridging hydride (Rh–H(2) = 1.96(3) Å and Ir–H(2) = 1.67(3) Å) is found to be significantly more

strongly bonded to Ir than to Rh possibly a result of the trans-influence of the agostic Ge–H interaction. Surprisingly, this Rh-hydride interaction is even weaker than that of the agostic Ge–H interaction, consistent with the NMR results that showed a larger Rh coupling for the agostic hydride (*vide supra*). Both dpmm groups are bent away from the bulky GeHPh₂ group towards the much smaller hydride ligand.

H₂ addition to **28** is reversible, so refluxing **29** in CH₂Cl₂ under an Ar flow regenerates the monohydride **28**. The reaction of **28** with D₂ initially yields the product (**29-D₂**) in which deuterium incorporation occurs as shown in Scheme 3.6. At 30 min after D₂ addition, ²H NMR spectroscopy displays three high-field

Scheme 3.6

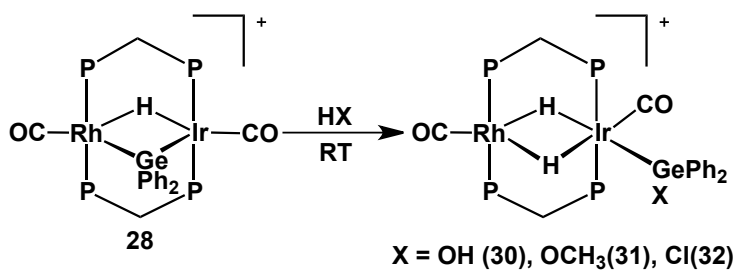


resonances at –78 °C analogous to the hydride resonances for **29** except that the highest-field signal for the bridging group appears with very low intensity as a shoulder on the adjacent resonance. At the same time, the ¹H resonance for **29-D₂** at –9.81 has changed little, integrating at approximately 0.8:2:2 with the pair of methylene proton resonances while the two other resonances (at δ –2.77 and –9.24) appear with approximately one tenth of the intensity (see Figure A.16 in Appendix II), indicating that initial deuterium incorporation is primarily on the germyl group and the Ir-bound hydride. Slight incorporation of deuterium in the

bridging position suggests slow exchange involving all hydrides, and leaving the reaction mixture for 48 h leads to equal deuterium/hydrogen scrambling over all hydride positions, with all three of the hydride resonances at 1/3 of the intensity of a single hydrogen. A saturation transfer NMR experiment at $-20\text{ }^{\circ}\text{C}$ also indicates exchange between all the hydrides in which the selective saturation of any hydride signal leads to the significantly decreased intensity of the other two. In an attempt to understand how deuterium incorporation initially occurs in the two positions on *opposite sides* of the “RhIrP₄” plane, the reaction was monitored at low temperature but no intermediate was observed.

Compound **28** does not react with CO₂ in contrast to a monometallic platinum-germylene complex in which CO₂ reversibly couples to the metal-germylene unit.⁶ However, this species reacts stoichiometrically with water, methanol and HCl as shown in Scheme 3.7, leading to the coordination of the corresponding nucleophile at Ge and cleavage of the Rh–Ge bond yielding the germanol dihydride, [RhIr(CO)₂(Ge(OH)Ph₂)(μ-H)₂(dppm)₂][CF₃SO₃] (**30**), the

Scheme 3.7



germamethoxy dihydride, [RhIr(CO)₂(Ge(OCH₃)Ph₂)(μ-H)₂(dppm)₂][CF₃SO₃](**31**) and the germethylchloride dihydride

[RhIr(CO)₂(GeClPh₂)(μ-H)₂(dppm)₂][CF₃SO₃](**32**), respectively. All have very comparable spectroscopic features. To our knowledge the reactivity of water or methanol with bridging germylene complexes has not previously been reported, although reaction of monometallic silylene and stannylene complexes with water is well documented.^{29,30} Interestingly, the neutral germylene-bridged analogues (**30**, **31** and **32**) do not react with water or methanol.

At ambient temperature the ³¹P{¹H} NMR spectrum of **30** displays somewhat broad resonances: a doublet of multiplets at δ 24.4 for the Rh-bound ³¹P nuclei and a multiplet at δ -5.7 for the Ir-bound ³¹P nuclei. In the ¹H NMR spectrum a broad peak at δ 3.47 is observed for four methylene protons, a broad singlet at δ 1.41 corresponds to the hydroxyl group and two broad multiplets at δ -9.81 and -12.05 appear for the bridging hydrides. The breadth of these resonances suggests fluxionality and cooling a CD₂Cl₂ solution of **30** to -80 °C leads to four resonances in the ³¹P{¹H} NMR spectrum at δ 26.4 (ddm, ¹J_{RhP} = 105 Hz, ²J_{trans-PP} = 312 Hz), 22.8 (ddm), -4.0 (dm, ²J_{trans-PP} = 312 Hz) and -6.9(dm). At this temperature the hydride resonances are sharper, showing coupling to Rh of 17.6 and 20.6 Hz, and upon broadband decoupling of the ³¹P nuclei, mutual coupling of 7.6 Hz between the hydrides is resolved. The ¹³C{¹H} NMR displays a typical doublet of triplets and a triplet for Rh- and Ir-bound carbonyls. We assume that this fluxionality is result a of restricted rotation about the Ir-Ge bond, giving rise to top/bottom asymmetry in the static structure.

When the reaction of **28** is carried out with 1 equiv of D₂O, two resonances are observed at δ 1.59 and -9.76 in the ²H NMR spectrum for the OD and

bridging deuteride groups, respectively. However, unlike the observation for a monometallic Pd stannylene complex, water addition to **28** is not reversible;²⁹ surprisingly, no H/D exchange is observed when complex **30** is exposed to D₂O. Similarly, CH₃OH addition to **28** is not reversible as confirmed by CD₃OD addition to **31**.

The structures of both **30** and **31** have been confirmed by X-ray crystallography and the ORTEP diagram of complex **31** is shown in Figure 3.8 (the structure of **30** is provided in Appendix II). The Rh–Ir distance in **31** (2.8605(3) Å) (2.8605(3) Å) indicates a strong mutual attraction of the metals via

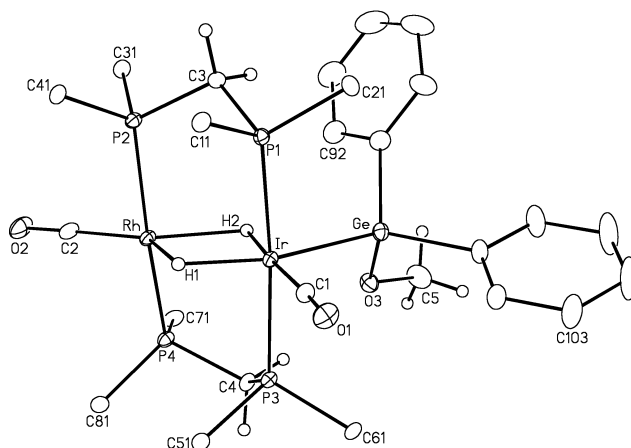


Figure 3.8: *Perspective view of the complex cation of 31 showing the numbering scheme. The atom labeling scheme and thermal parameters are as described in Figure 3.1. For the dppm phenyl groups only the ipso carbons are shown.*

the pair of bridging hydrides. These hydride ligands are significantly closer to Ir than to Rh (Rh–H(1) = 2.04(5) Å, Rh–H(2) = 1.89(4) Å, Ir–H(1) = 1.67(5) Å, Ir–H(2) = 1.68(4) Å); nevertheless, the magnitude of the Rh–H coupling in the ¹H NMR spectrum is substantial for both (¹J_{RhH} = 17.1 and 17.6 Hz).

3.5 Discussion

In this Chapter we investigated the formation of mixed-metal germyl and germylene complexes by Ge–H bond activation of primary and secondary germanes promoted by either of two complexes that involve the Rh/Ir metal combination. We had a number of goals in this study: (1) to discover what roles the two different metals might play in these activations; (2) to determine some mechanistic details about the stepwise activations; (3) to determine the differences in reactivity of the two complexes (one neutral and other cationic); (4) to investigate the reactivity of bridging germylene groups; and (5) to compare the reactivities of silanes and less studied germane analogues. As will be explained, we have had some success in each of these goals.

The two complexes studied, $[\text{RhIr}(\text{CO})_3(\text{dppm})_2]$ (**1**) and $[\text{RhIr}(\text{CH}_3)(\text{CO})_2(\text{dppm})_2][\text{CF}_3\text{SO}_3]$ (**2**), although superficially similar, have some significant differences. Although compound **1**, being neutral and having only neutral ligands, appears to involve two metals in their zero oxidation state, we instead consider this species to be a mixed-valence, Rh(+I)/Ir(–I) complex,¹⁸ in which the pseudo-tetrahedral “Ir(CO)₂P₂[–]” moiety donates a pair of electrons to the “Rh(CO)P₂⁺” centre, giving Rh a square-planar geometry. As such only Rh is coordinatively unsaturated. Compound **2** is related to **1** by formal replacement of CO by CH₃⁺, and as such has two fewer electrons, having both metals unsaturated.

The above differences are initially seen in their low-temperature reactions with germanes during the first Ge–H bond activation step. Reaction with **1** occurs at the coordinatively unsaturated Rh centre to yield a Rh-bound germyl ligand;

even at $-80\text{ }^{\circ}\text{C}$ hydride migration to Ir has occurred. In contrast, the first step in the reaction of **2** with germanes occurs at Ir yielding an Ir-bound germyl group, consistent with the greater tendency of this metal to undergo oxidative addition. Although the Ge–H bond activation steps presumably proceed through a σ -complex involving the Ge–H bond being activated, such an intermediate is never seen. For the second Ge–H activation step, the germyl-bridged agostic intermediate is again not detected for reactions involving the neutral species **1**. However, agostically bridged germyl groups are observed in reactions involving the cationic species **2**; presumably the positive charge of **2** is enough to lower the tendency for activation of the second Ge–H bond, allowing such an intermediate to be observed.

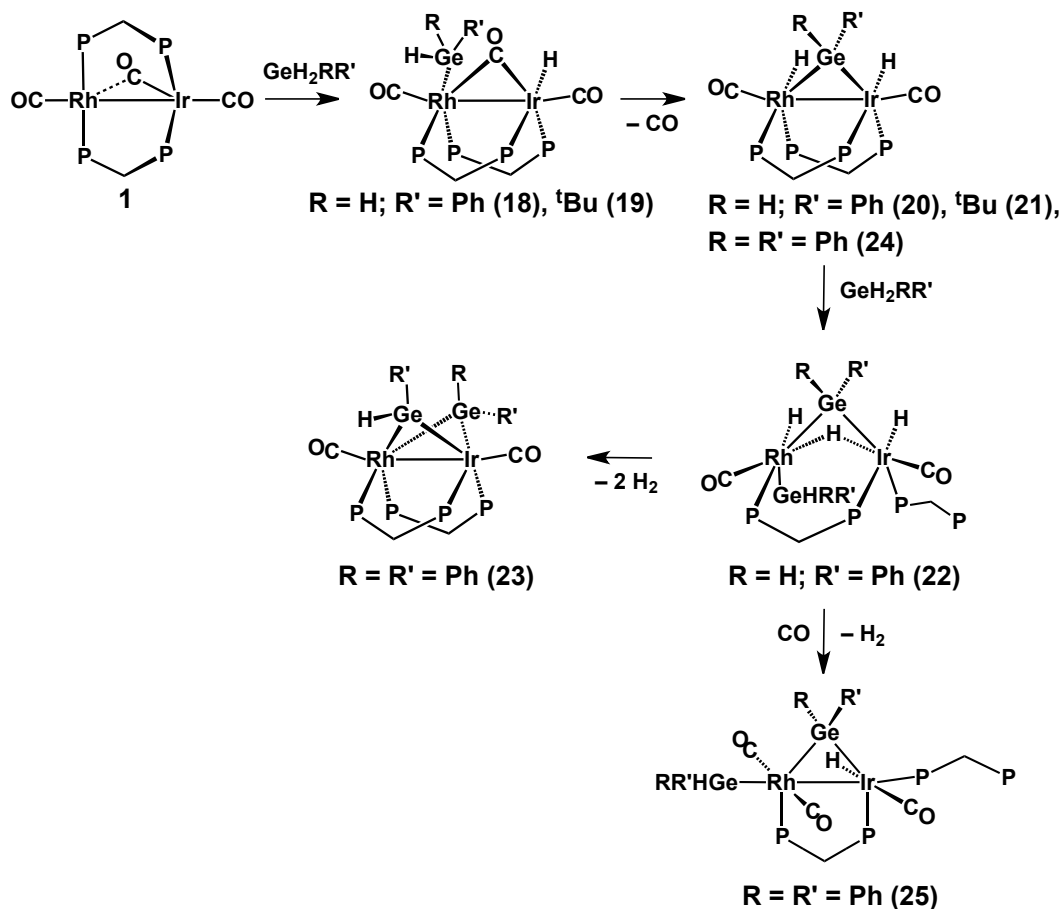
In much of the chemistry investigated low temperature studies allowed us to establish details about the stepwise activation processes involved, and to determine the natures of some intermediates. To our knowledge this is the only study to report such details about Ge–H bond activation. In the incorporation of up to two germanium-containing fragments by complex **1**, a number of intermediates were characterized at low temperature. As noted above, the first products of Ge–H bond activation, involving phenyl and *t*-butylgermane, namely $[\text{RhIr}(\text{H})(\text{GeH}_2\text{R})(\text{CO})_2(\mu\text{-CO})(\text{dppm})_2]$ (R = Ph (**18**), *t*Bu (**19**)) were observed and characterized at $-80\text{ }^{\circ}\text{C}$.

Incorporation of a second germanium-containing fragment in the germylene-bridged products has also been observed, although depending on the bridging germylene unit and the germane added, several different (but related)

outcomes are observed. Surprisingly, the incorporation of a second equivalent of phenylgermane into the phenylgermylene-bridged product, $[\text{RhIr}(\text{H})_2(\text{CO})_2(\mu\text{-GeHPh})(\text{dppm})_2]$ (**20**) is only observed at low temperature with decomposition occurring when this product is warmed above $-40\text{ }^\circ\text{C}$. This low-temperature intermediate, $[\text{RhIr}(\text{H})_2(\text{GeH}_2\text{Ph})(\text{CO})_2(\kappa^1\text{-dppm})(\mu\text{-H})(\mu\text{-GeHPh})(\text{dppm})]$ (**22**), is the result of dissociation of the Rh-end of one bridging dppm group accompanied by oxidative addition of phenylgermane at the unsaturated Rh centre.

In contrast, reaction of **20** with diphenylgermane (Scheme 3.2) yields the mixed digermylene-bridged product, $[\text{RhIr}(\text{CO})_2(\mu\text{-GeHPh})(\mu\text{-GePh}_2)(\text{dppm})_2]$ (**23**) with the elimination of 2 equiv of H_2 . Although these are dramatically different results, they are in fact closely related as proposed in Scheme 3.8, which depicts the different species observed in the reactivity of **1** with different germanes, and the possible relationships between them. We assume that the reaction of **20** with diphenylgermane proceeds via an intermediate analogous to **22** and that the subsequent transformation to **23** occurs by a sequence of steps involving H_2 elimination, oxidative addition of the remaining Ge–H bond of the germyl group, elimination of the second equiv of H_2 , and recoordination of the pendent end of the κ^1 -diphosphine at Rh. It is not clear why an analogous species containing two bridging phenylgermylene groups was not obtained in the reaction of **20** with phenylgermane, but presumably the additional germanium-bound hydrogen, which would be prone to oxidative addition, and the smaller size of the

Scheme 3.8



monosubstituted germyl ligand in **22**, which allows more facile approach to the adjacent metal, play a role.

The third variation in reactivity with a second germane is seen in the reaction of $[\text{RhIr}(\text{H})_2(\text{CO})_2(\mu\text{-GePh}_2)(\text{dppm})_2]$ (**24**) with diphenylgermane (Schemes 3.3 and 3.8) which results in decomposition in the absence of CO, but yields $[\text{RhIr}(\text{H})(\text{GeHPh}_2)(\text{CO})_3(\kappa^1\text{-dppm})(\mu\text{-GePh}_2)(\text{dppm})]$ (**25**) under a CO atmosphere. This product is closely related to **22** (apart from the different substituents on Ge), in which two hydride ligands have been replaced by CO. We

assume that when the initial trihydride diphenylgermyl intermediate, analogous to **22**, loses H₂, oxidative addition of the germyl–H bond, to give a *bis*-diphenylgermylene-bridged product analogous to **23** is inhibited, owing to the greater bulk of the disubstituted germyl and germylene groups. Since the pendent dppm is also too bulky to re-coordinate, decomposition occurs in the absence of an additional ligand required to alleviate the unsaturation. However, under CO the stable tricarbonyl species **25** is formed, having both metals coordinatively saturated. The coordinative unsaturation required for reaction of the saturated species [RhIr(H)₂(CO)₂(μ-GeRR')(dppm)₂] with a second equiv of germane presumably results from dissociation of the Rh-end of a diphosphine, and two examples of compounds containing a pendent dppm group were characterized. However, we cannot rule out that the unsaturation necessary for subsequent reaction with a germane results from the reductive elimination of a hydride and germylene fragment from one metal to give an unsaturated germyl compound, since exchange of the germylene hydrogen with the Rh- and Ir-bound hydrides is proposed to occur by such a process.

In spite of the current interest in late transition metal catalysts containing germanium in hydrogenation reactions, surprisingly little has been published on the reactivity of mixed transition metal/germanium-containing complexes with H₂; in fact, the reactivity of germyl and germylene-bridged complexes has to-date received very little attention. In this paper we report the addition of H₂ and HX (X = OH, OMe, Cl) to a cationic germylene-bridged Rh/Ir complex. Although mechanistically these two reaction types (with H₂ or HX) presumably differ, the

final products have some similarities. In both cases the transfer of one hydrogen to the transition metals occurs while either H or X binds to Ge, converting the μ -germylene to a germyl ligand. In the H_2 reaction the diphenylgermyl ligand produced is bridging, interacting with Rh in an agostic manner via a Ge–H bond, while the polar substrates all yield terminal germyl groups. The extremely facile migration of a hydrogen from one face of the “RhIrP₄” plane to the other upon reaction of **28** with H_2 (even at $-40\text{ }^\circ\text{C}$) suggests a deprotonation/reprotonation step rather than the concerted rearrangement of ligands, although the counteranion used (BPh_4^- , $BAr^F_4^-$ or OTf^-) plays no obvious role in such a transfer, with no rate difference being observed with these counteranions.

Finally, as suggested in the Introduction and as alluded to throughout this paper, the chemistry of compounds **1** and **2** with germanes displays many similarities to that involving the analogous silanes studied in the previous chapter. However, some subtle differences are observed. Our inability to generate complexes containing two bridging monosubstituted germylene groups is in contrast to the related silylene species, which are readily obtained, and suggests a more facile oxidative addition of the remaining Ge–H bond of the targeted μ -GeHR unit compared to Si–H, consistent with the weaker Ge–H than Si–H bonds. The exclusive formation of the germylene- and hydride-bridged complex, $[RhIr(CO)_2(\mu\text{-GePh}_2)(\mu\text{-H})(dppm)_2][CF_3SO_3]$ (**28**) from the reaction of **2** with diphenylgermane, is another subtle difference from the silane chemistry in which the reaction of **2** with 1 equiv of diphenylsilane led to the two different products – a silylene/hydride-bridged complex, $[RhIr(CO)_2(\mu\text{-SiPh}_2)(\mu\text{-H})(dppm)_2][CF_3SO_3]$

(17) and a silylene-bridged, acetyl complex, $[\text{RhIr}(\text{CO})_2(\text{H})(\text{C}(\text{CH}_3)\text{O})(\mu\text{-H})(\mu\text{-SiPh}_2)(\text{dppm})_2][\text{CF}_3\text{SO}_3]$ (16).¹⁵ This latter result demonstrates the greater trans labilizing effect of the silyl group,³¹ which promotes migration of the methyl ligand in an intermediate such as 15 (see previous chapter) to the adjacent carbonyl.

3.6 References

- 1) (a) Shinohara, A.; McBee, J.; Tilley, T. D. *Inorg. Chem.* **2009**, *48*, 8081. (b) Hayes, P. G.; Waterman, R.; Glaser, P. B.; Tilley, T. D. *Organometallics* **2009**, *28*, 5082. (c) Takaoka, A. Mendiratta, A.; Peters, J. C. *Organometallics* **2009**, *28*, 3744. (d) Feldman, J. D.; Peters, J. C.; Tilley, T. D. *Organometallics* **2002**, *21*, 4065
- 2) (a) Tanabe, M.; Ishikawa, N.; Osakada, K. *Organometallics* **2006**, *25*, 796. (b) Usui, Y.; Hosotani, S.; Ogawa, A.; Nanjo, M.; Mochida, K. *Organometallics* **2005**, *24*, 4337. (d) White, C. P.; Braddock-Wilking, J.; Corey, J. Y.; Xu, H.; Redekop, E.; Sedinkin, S.; Rath, N. P. *Organometallics* **2007**, *26*, 1996. (e) Arii, H.; Nanjo, M.; Mochida, K. *Organometallics* **2008**, *27*, 4147. (f) Mohamed, B. A. S.; Kikuchi, M.; Ueno, K.; Tobita, H.; Ogino, H. *Chem. Lett.*, **2004**, *33*, 112. (g) Hawkins, S. M.; Hitchcock, P. B.; Lappert, M. F.; Rai, A. K; *J. Chem. Soc., Chem. Comm.* **1986**, *18*, 1689.
- 3) (a) Bodnar, Z.; Mallat, T.; Bakos, I.; Szabo, S.; Zsoldos, Z.; Schay, Z. *Appl. Catal. A* **1993**, *102*, 105. (b) Lafaye, G.; Micheaud-Especel, C.; Montassier, C.; Marcot, P. *Appl. Catal. A Gen.* **2004**, *257*, 107. (c) Lafaye, G.; Micheaud-Especel, C.; Montassier, C.; Marcot, P. *Appl. Catal. A Gen.*

- 2002**, 230, 19 (d) Ekou. T.; Vicente, A.; Lafaye, G.; Especel, C.; Marcot, P. *Appl. Catal. A Gen.* **2006**, 314, 73.
- 4) (a) Macleod, N.; Freyer, J. R.; Stirling, G.; Webb, G. *Catal. Today* **1998**, 46, 37.
- 5) (a) Adams, R. D.; Trufan, E. *Inorg. Chem.* **2010**, 49, 3029. (b) Adams, R. D.; Trufan, E. *Organometallics* **2010**, 29, 4346. (c) Adams, R. D.; Trufan, E. *Inorg. Chem.* **2009**, 48, 6124. (d) Adams, R. D.; Captain, B. Trufan, E. *J. Cluster. Sci.* **2007**, 18, 642.
- 6) Litz, K. E.; Henderson, K.; Gourley, R. W.; Holl, M. M. B. *Organometallics*, **1995**, 14, 5008.
- 7) Litz, K. E.; Kempf, J. W.; Holl, M. M. B. *J. Am. Chem. Soc.* **1998**, 120, 7484.
- 8) (a) Cygan, Z. T.; Bender IV, J. E.; Litz, K. E.; Kempf, J. W.; Holl, M. M. B. *Organometallics*, **2002**, 21, 5373. (b) York, J. T.; Young Jr, V. G. Tolman, W. B. *Inorg. Chem.* **2006**, 45, 4191.
- 9) (a) Tanabe, M.; Ishikawa, N.; Hanzawa, M.; Osakada, K. *Organometallics*, **2008**, 27, 5152. (b) Tanabe, M.; Hanzawa, M.; Ishikawa, N.; Osakada, K. *Organometallics*, **2009**, 28, 6014. (c) Tanabe, M.; Osakada, K. *Organometallics*, **2010**, 29, 4702.
- 10) (a) Corey, J. Y.; Braddock-Wilking, J. *Chem. Rev.* **1999**, 99, 175; and references therein.
- (b) Corey, J. Y. *Chem. Rev.* **2011**, 111, 863 and references therein.

- 11)(a) Waterman, R.; Hayes, P. G.; Tilley, T. D. *Acc. Chem. Res.* **2007**, *40*, 712. (b) Okazaki, M.; Tobita, H.; Ogino, H. *Dalton. Trans.* **2003**, 493.
- 12)(a) Marciniak, B. *Silicon Chem.* **2002**, *1*, 155. (b) Brook, M. A. *Silicon in Organic, Organometallic, and Polymer Chemistry*; Wiley: New York, 2000. (c) Calimano, E.; Tilley T. D. *J. Am. Chem. Soc.* **2009**, *131*, 11161. (d) Ojima, I.; Kogure, T.; Nihonyanagi, M.; Nagai, Y. *J. Chem. Soc., Chem. Commun.* **1972**, 938. (e) Ojima, I.; Nihonyanagi, M.; Nagai, Y. *Bull. Chem. Soc. Jpn.* **1972**, *45*, 3506. (f) Jiménez M.V.; Pérez-Torrente J. J.; Bartolomé M. I.; Gierz, V.; Lahoz, F. J.; and Oro, L. A. *Organometallics*, **2008**, *27*, 224.
- 13)(a) Aitken, C. T.; Harrod, J. F.; Samuel, E. *J. Am. Chem. Soc.* **1986**, *108*, 4059. (b) Tilley, T. D. *Acc. Chem. Res.* **1993**, *26*, 22. (c) Rosenberg, L.; Davis, C. W.; Yao, J. Z. *J. Am. Chem. Soc.* **2001**, *123*, 5120. (d) Fontaine, F.-G.; Zargarian, D. *J. Am. Chem. Soc.* **2004**, *126*, 8786.
- 14)(a) Luo; X. L.; Crabtree, R. H. *J. Am. Chem. Soc.* **1989**, *111*, 2527. (b) Biffis, A.; Basato, M.; Briccese, M.; Ronconi, L.; Tubaro, C.; Zanella, A.; Graiff, A.; Tiripicchio, A. *Adv. Synth. Catal.* **2007**, 2485.
- 15) Mobarok, M. H.; Oke, O.; Ferguson, M. J.; McDonald, R.; Cowie, M. *Inorg. Chem.* **2010**, *49*, 11556.
- 16)(a) Wang, W. -D.; Hommeltoft, S. I.; Eisenberg, R. *Organometallics* **1988**, *7*, 2417. (b) Wang, W. -D.; Eisenberg, R. *J. Am. Chem. Soc.* **1990**, *112*, 1833. (c) Wang, W. -D.; Eisenberg, R. *Organometallics* **1991**, *10*, 2222. (d) Wang, W.-D.; Eisenberg, R. *Organometallics* **1992**, *11*, 908.

- 17) McDonald, R.; Cowie, M. *Organometallics* **1990**, *9*, 2468.
- 18) McDonald, R.; Cowie, M. *Inorg. Chem.* **1990**, *29*, 1564.
- 19) Oke, O.; McDonald, R.; Cowie, M. *Organometallics* **1999**, *18*, 1629.
- 20) Programs for diffractometer operation, data collection, data reduction, and absorption correction were those supplied by Bruker
- 21) Beurskens, P. T.; Beurskens, G.; de Gelder, R.; Smits, J. M. M.; Garcia-Granda, S.; Gould, R. O. (2008). The *DIRDIF-2008* program system. Crystallography Laboratory, Radboud University Nijmegen, The Netherlands.
- 22) Sheldrick, G. M. *Acta Crystallogr.* **2008**, *A64*, 112–122.
- 23) Altomare, A.; Burla, M. C.; Camalli, M.; Cascarano, G. L.; Giacovazzo, C.; Guagliardi, A.; Moliterni, A. G. G.; Polidori, G.; Spagna, R. *J. Appl. Cryst.* **1999**, *32*, 115–119.
- 24) (a) Sluis, P. van der; Spek, A. L. *Acta Crystallogr.* **1990**, *A46*, 194–201.
(b) Spek, A. L. *Acta Crystallogr.* **1990**, *A46*, C34. (c) Spek, A. L. *J. Appl. Cryst.* **2003**, *36*, 7–13.
- 25) Mantina, M.; Chamberlin, A. C.; Valero, R.; Cramer, C. J.; Truhlar, D. G. *J. Phys. Chem. A* **2009**, *113*, 5806.
- 26) Bau, R.; Drabnis, M. H. *Inorg. Chim. Acta* **1997**, *259*, 27.
- 27) Trepanier, S. J.; Dennett, J. N. L.; Sterenberg, B. T.; McDonald, R.; Cowie, M. *J. Am. Chem. Soc.* **2004**, *126*, 8046.
- 28) Ogino, H.; Tobita, H. *Adv. Organomet. Chem.* **1998**, *42*, 223.

- 29) Feldman, J. D.; Mitchell, G. P.; Nolte, J.-O.; Tilley, T. D. *J. Am. Chem. Soc.* **1998**, *120*, 11184.
- 30) (a) Hayes, P. G.; Gribble, C. W.; Waterman, R. Tilley, T. D. *J. Am. Chem. Soc.* **2009**, *131*, 4606. (b) Schager, F.; Seevogel, K.; Pörschke, K. R.; Kessler, M.; Krüger, C. *J. Am. Chem. Soc.* **1996**, *118*, 13075.
- 31) (a) Minato, M.; Zhou, D.-Y.; Sumiura, K.; Hirabayashi, R.; Yamaguchi, Y.; Ito, T. *Chem. Comm.* **2001**, 2654 (b) Minato, M.; Nishiuchi, J.-Y.; Kakeya, M.; Matsumoto, T.; Yamaguchi, Y.; Ito, T. *Dalton. Trans.* **2003**, 483.

Chapter 4

Mixed Bis(μ -Silylene) and (μ -Silylene)/(μ -Germylene) Complexes at a Rh/Ir Core: Nature of the Si---Si Interactions in the Bis(μ -Silylene) Species.^{IV}

4.1 Introduction

Bimetallic complexes containing bridging silicon- or germanium-containing units comprise an important class of compounds in organotransition-metal chemistry,¹ being implicated in E–E (E = Si, Ge)² and E–C bond formation.^{2h,3} In addition, recent investigations have demonstrated the use of bridging silylene and germylene groups in generating unique Si- and Ge-containing clusters,⁴ including unusual examples containing planar arrays of mutually bonded late transition metals.^{4b,d} From the perspective of Si–Si bond formation, there has been significant interest in the incorporation of more than one bridging SiR₂ unit (both R groups can be the same or different) in multimetallic complexes,^{2b,2e-g,5} involving both early and late transition metals, although those involving late transition metals are in the majority.¹ For complexes having the M₂(SiR₂)₂ framework, two major structural classes have emerged in which this M₂Si₂ core is either planar and diamond-shaped^{2b-e,6} or folded in a butterfly-type arrangement, having the Si atoms in the wing-tips with respect to the M–M bond.^{2c,2f,3a,7-9} Within the planar “M₂(SiR₂)₂” class a number of examples have been characterized in which the Si---Si separation is short,^{2b,2c,3e,6c,6d,6f} approaching that of a normal Si–Si covalent bond, suggesting a significant degree of bonding between these atoms,¹⁰ while in the butterfly-type structures^{2c,2f,3a,7,9a,9c}

^{IV} A version of this Chapter has been accepted for publication. Mobarok, M. H.; Ferguson, M. J.; McDonald, R.; Cowie, M. (*Inorg. Chem.*)

these interactions, although significantly shorter than normal van der Waals contacts, are generally significantly longer than expected for a Si–Si bond, leading to ambiguity regarding the exact nature of these interactions.

In the butterfly-type $M_2(\text{SiR}_2)_2$ structures in which the pair of SiR_2 groups are folded towards each other about the M–M bond, it is tempting to suggest some degree of nascent Si---Si bonding which could, under appropriate conditions, lead to coupling of the SiR_2 fragments. Although related studies involving two or more bridging GeR_2 units are much less common, the many similarities in the chemistry of Si and Ge^{1a} suggest that related $M_2(\text{GeR}_2)_2$ complexes may also be capable of coupling pairs of GeR_2 units. Our studies have demonstrated many parallels in the formation of analogous butterfly-type “ $\text{RhIr}(\mu\text{-EHR})_2$ ” complexes (E = Si, Ge) in reactions of $[\text{RhIr}(\text{CO})_3(\text{dppm})_2]$ (dppm = $\text{Ph}_2\text{PCH}_2\text{PPh}_2$) with primary silanes^{9a} and germanes,^{9b} while, like silanes, catalytic dehydrogenative coupling of germanes has been observed using both early¹¹ and late¹² transition metals, although it has not been established whether germylene groups play a role in these coupling reactions.

With the above ideas in mind we set out to expand the scope of $M_2(\mu\text{-ER}_2)_2$ butterfly-type complexes by generating a series of such species containing pairs of different $\mu\text{-ER}_2$ groups – either having different substituents on each silylene unit or having mixed silylene and germylene units. The former group may have potential for the generation of silicon-containing oligomers and polymers having differing sequences of substituents, while the latter could be capable of generating Si/Ge-containing oligomers and polymers. Silicon- and germanium-based

polymers are of interest owing to their optical and electronic properties,¹³ and for related reasons there has also been significant interest in mixed SiGe-containing oligomers and polymers.¹⁴ Polysilane copolymers, containing different SiR₂ units, are of interest since they can display substantially different physical properties from those of related homopolymers,^{13b} allowing flexibility in the modification of polymer properties.

To date, most of the silylene- or germylene-bridged complexes within the butterfly M₂E₂ class are bridged by the same ER₂ unit (E = Si or Ge). Although a few complexes having [M₂(μ-ER₂)(μ-E'R₂)] or [M₂(μ-ER₂)(μ-ER'₂)] frameworks have been reported, their syntheses are not selective and they are generally produced as a mixture of products from which the desired species must be isolated.^{2b,6g} Two examples of monometallic mixed (silylene)/(germylene) complexes have been reported,¹⁵ but to the best of our knowledge there are no reports describing the *selective* incorporation of two different bridging units into a bimetallic core.

In general, two synthetic approaches have been adopted for the incorporation of pairs of bridging ER₂ units at a bimetallic core: (1) oxidative addition of E-H bonds of primary or secondary silanes or germanes to monometallic precursors, with subsequent dimer formation;^{2d,6df6g,16,17} and (2) oxidative addition of these silanes or germanes at a pre-organized bimetallic complex.^{3a,6a,7,9,18} The former approach does not appear to be a viable option for the selective incorporation of two different bridging ER₂ groups, being likely to generate mixtures of M₂(ER₂)₂, M₂(E'R'₂)₂ and M₂(ER₂)(E'R'₂) products.

However, the second approach appears to be more promising, through the stepwise incorporation of the first ER_2 unit followed by the incorporation of the second such unit, containing either different substituents on each E or different elements (E = Si, Ge), assuming that the first " $M_2(ER_2)$ " complex is stable in the absence of excess reagent.

In a previous study on silane activation by a diphosphine-bridged diiridium complex, our group demonstrated that one bridging SiR_2 unit could be incorporated through reactions of an Ir_2 precursor with primary and secondary silanes, to yield $[Ir_2(H)_2(CO)_2(\mu-SiRR')(dppm)_2]$ (R = R' = Me, Et, Ph or R = Ph, R' = H).⁸ However, incorporation of a second Si-containing unit did not occur owing to the inert nature of these coordinatively saturated mono(silylene)-bridged dihydride products. In contrast, a related dirhodium system, studied by Eisenberg and coworkers, readily incorporates two bridging Si units in reactions involving primary silanes to produce bis(silylene) complexes^{3a,7} – a result of the greater lability of the first silylene-bridged product, $[Rh_2(H)_2(CO)_2(\mu-SiHR)(dppm)_2]$, which is able to generate the coordinative unsaturation necessary for reaction with the second silane.^{3a,7} Although in this case the reaction could be halted at a mono(silylene)-bridged dirhodium species, subsequent reaction with one equivalent of a different primary or secondary silane did not lead to the incorporation of the pair of different bridging silylene units, and instead resulted in exchange of the Si-containing units, generating a new mono(silylene)-bridged product.¹⁹ Interestingly, the displacement of bridging silylene groups by germylene groups at a Pt_2 core has also been reported.^{17b,20}

Recently we reported a variety of mono- and bis-silylene-bridged and bis-germylene-bridged complexes via the oxidative addition of the appropriate silanes and germanes at a Rh/Ir core.⁹ This mixed-metal combination combines the two characteristics of the above homobinuclear compounds, having a labile Rh and a more inert Ir center. This combination appears to give us the “intermediate” reactivity that allows the isolation of mono-silylene- or mono-germylene-bridged species, which can subsequently react with a second equivalent of the silane or germane precursor, without displacement of the first unit. Although most of the work reported for the silane and germane activation centered on the stepwise addition of the same silane or germane substrates, we reported one example in which two *different* germylene groups were incorporated, using the stepwise activation of the two different germanes.^{9b} In the present report we extend this study to the preparation of mixed-bis(silylene)-bridged and (silylene)/(germylene)-bridged species.

An additional goal of this study was to determine the nature of the Si---Si interactions in the butterfly-type $M_2(SiR_2)_2$ compounds, which as noted above have Si---Si separations that are intermediate between bonding and non-bonding. Most of the “ $MM'(\mu-ERR')_2(dppm)_2$ ” complexes within the butterfly-type class contain at least one aryl group in each bridging ERR' unit, stacked in a parallel arrangement,^{3a,7,9} presumably to minimize unfavorable interactions between these aryl groups and the dppm phenyl rings, while maintaining a relatively favorable parallel arrangement of these aryl groups.²¹ It is well established that substituents on such aryl groups can have a significant influence on the separation between π -

stacked groups, with electron-withdrawing substituents resulting in shorter aryl-aryl separations.^{21,22} We were curious about how substituents either directly on Si or Ge or on the aryl groups, could influence the E---E separations, and wondered whether such influences could shed light on the nature of the E---E interactions. For this part of the study we limit the compounds studied to a series of bis(silylene)-bridged complexes of the type $[\text{RhIr}(\text{CO})_2(\mu\text{-SiArR})(\mu\text{-SiAr'R'})\text{(dppm)}_2]$.

4.2 Experimental

4.2.1 General Comments.

All solvents were dried (using appropriate drying agents), distilled before use, and stored under dinitrogen. Reactions were performed under an argon atmosphere using standard Schlenk techniques. Ph_2SiH_2 and PhSiH_3 were purchased from Aldrich and Alfa-Aesar, respectively, while Ph_2SiD_2 and MesSiH_3 (Mes = mesityl) were prepared according to the literature methods.^{23a,23b} Silanes were dried over CaH_2 and distilled under Ar before use. PhGeH_3 and Ph_2GeH_2 were synthesized by the reduction of the corresponding chlorides (obtained from Gelest Inc. and Alfa Inorganics, respectively) with LiAlH_4 and kept under argon and subdued light. ^{13}C -enriched CO (99.4%) and LiAlD_4 were purchased from Cambridge Isotope Laboratories. The compounds, $[\text{RhIr}(\text{CO})_3(\text{dppm})_2]$,²⁴ $[\text{RhIr}(\text{H})_2(\text{CO})_2(\mu\text{-SiHPh})(\text{dppm})_2]$ (**1**)^{9a} and $[\text{RhIr}(\text{H})_2(\text{CO})_2(\mu\text{-GeHPh})(\text{dppm})_2]$ (**3**)^{9b} were prepared as previously reported. NMR spectra were recorded on Varian Inova-400 or Varian Unity-500 spectrometers operating at the resonance frequencies for the NMR nuclei as given

in the spectral information. The ^1H , $^{13}\text{C}\{^1\text{H}\}$ and $^{29}\text{Si}\{^1\text{H}\}$ NMR spectra were referenced internally to residual solvent proton signals relative to tetramethylsilane whereas $^{31}\text{P}\{^1\text{H}\}$ and $^{19}\text{F}\{^1\text{H}\}$ NMR spectra were referenced relative to external 85 % H_3PO_4 and CCl_3F standards, respectively. In the ^1H -NMR spectral results the aromatic protons in the range δ 8.50 – 6.20 are not reported. The ^{13}C NMR resonances for the aryl carbons (in the range of δ 125 to 135) are also not included. In the spectral data below, the following NMR abbreviations are used: m = multiplet, s = singlet, d = doublet, t = triplet, b = broad; combinations of these abbreviations are also used. The term “multiplet” is applied to resonances for which the coupling constants cannot be resolved and imply nothing about the order of the spectrum. The elemental analyses were performed by the Microanalytical Laboratory in the Department.

4.2.2 Preparation of Compounds

a. **[RhIr(H)₂(CO)₂(μ -SiHC₆H₃F₂)(dppm)₂] (33)**: To a slurry of 80 mg (0.069 mmol) of **[RhIr(CO)₃(dppm)₂] (1)** in 1 mL of toluene under an atmosphere of Ar in a septum-sealed NMR tube, was added 11.5 μL (0.069 mmol) of 3,5-C₆H₃F₂SiH₃ via a microliter syringe followed by an Ar flow through NMR tube by a needle-inlet and needle-outlet. Rapid evolution of CO was observed, accompanied by dissolution of the starting complex followed by the precipitation of compound **33** as yellow solid within 20 min. The toluene was removed via cannula and the precipitate was washed with 3 mL of pentane followed by the removal of residual solvents under high vacuum to give analytically pure compound in 72 % (59 mg) isolated yield. Anal. calcd. for C₅₈H₅₀ F₂IrO₂P₄RhSi :

C, 55.13 ; H, 3.96. Found: C, 55.43; H, 4.18. $^{31}\text{P}\{^1\text{H}\}$ NMR (27 °C; CD_2Cl_2 , 161.8 MHz): δ 27.5 (Rh–P, bm, 1P), 14.8 (Rh–P, bm, 1P), –9.7 (Ir–P, bm, 1P), –14.9 (Ir–P, bm, 1P); ^1H NMR (27 °C; CD_2Cl_2 , 399.8 MHz): δ 5.43 (CH_2 , m, 2H), 3.08 (CH_2 , m, 2H), –9.75 (Rh–H, bm, 1H), –11.20 (Ir–H, bm, 1H); $^{31}\text{P}\{^1\text{H}\}$ NMR (–40 °C; CD_2Cl_2 , 161.8 MHz): δ 27.6 (Rh–P, dm, 1P, $^1J_{\text{RhP}} = 97$ Hz), 15.2 (Rh–P, dm, 1P, $^1J_{\text{RhP}} = 110$ Hz), –9.7 (Ir–P, m, 1P), –15.2 (Ir–P, m, 1P); ^1H NMR (–40 °C; CD_2Cl_2 , 161.8 MHz): δ 6.48 (Si–H, bs, 1H, $^1J_{\text{SiH}} = 178$ Hz), 5.48 (CH_2 , m, 1H), 5.30 (CH_2 , m, 1H), 3.13 (CH_2 , m, 1H), 2.84 (CH_2 , m, 1H), –9.65 (Rh–H, ddm, 1H, $^2J_{\text{trans PH}} = 143.9$, $^1J_{\text{RhH}} = 12$ Hz), –11.25 (Ir–H, dm, 1H, $^2J_{\text{trans PH}} = 122$ Hz); $^{13}\text{C}\{^1\text{H}\}$ NMR (–40 °C; CD_2Cl_2 , 100.5 MHz): δ 193.3 (Rh–CO, dm, 1C, $J_{\text{Rh-C}} = 76$ Hz), 180.5 (Ir–CO, m, 1C), δ 48.7 (CH_2 , m, 1C), 43.9 (CH_2 , m, 1C); $^{29}\text{Si}\{^1\text{H}\}$ NMR (–40 °C; CD_2Cl_2 , 78.5 MHz, DEPT): δ 141.2 (m). ^{19}F NMR (–40 °C; CD_2Cl_2 , 376.1 MHz): δ –112.4 (m).

b. [RhIr(CO)₂(μ -SiHPh)(μ -SiPh₂)(dppm)₂] (34): 70 mg (0.057 mmol) of [RhIr(H)₂(CO)₂(μ -SiHPh)(dppm)₂] (**4**) was dissolved in 15 mL of CH_2Cl_2 in a Schlenk flask followed by the addition of 15.9 μL (0.086 mmol) of Ph_2SiH_2 . The reaction mixture was stirred gently for 48 h during which time the yellow solution lightened. NMR spectroscopy of the crude mixture suggested quantitative conversion of complex **4** to **34**. The solvent volume was reduced to approximately 0.5 mL under high vacuum. Layering the solution with 2 mL of pentane in an NMR tube yielded light yellow crystals (suitable for X-ray analysis) of compound **34** after 72 h in 56 % (45 mg) isolated yield. Anal. calcd. for $\text{C}_{70}\text{H}_{60}\text{IrO}_2\text{P}_4\text{RhSi}_2$: C, 59.71; H, 4.26. Found: C, 59.41; H, 4.42. $^{31}\text{P}\{^1\text{H}\}$ NMR (27 °C; CD_2Cl_2 , 201.6

MHz): δ 32.4 (Rh–P, ddd, 1P, $^1J_{\text{RhP}} = 100$ Hz, $^2J_{\text{PP}} = 106$ Hz, $^2J_{\text{PP}} = 32$ Hz), 22.6 (Rh–P, ddd, 1P, $^1J_{\text{RhP}} = 105$ Hz, $^2J_{\text{PP}} = 142$ Hz, $^2J_{\text{PP}} = 32$ Hz), 7.8 (Ir–P, dd, 1P, $^2J_{\text{PP}} = 106$ Hz, $^2J_{\text{PP}} = 25$ Hz), –7.9 (Ir–P, dd, 1P, $^2J_{\text{PP}} = 142$ Hz, $^2J_{\text{PP}} = 25$ Hz); ^1H NMR (27 °C; CD_2Cl_2 , 498.1 MHz): δ 5.77 (Si–H, m, 1H, $^1J_{\text{SiH}} = 168$ Hz), 5.00 (CH_2 , m, 1H), 4.45 (CH_2 , m, 1H), 2.92 (CH_2 , m, 2H); $^{13}\text{C}\{^1\text{H}\}$ NMR (27 °C; CD_2Cl_2 , 100.5 MHz): δ 200.5 (Rh–CO, dm, 1C, $^1J_{\text{RhC}} = 76$ Hz), 187.0 (Ir–CO, bs, 1C), 37.5 (CH_2 , m, 1C), 34.1 (CH_2 , m, 1C); $^{29}\text{Si}\{^1\text{H}\}$ NMR (27 °C; CD_2Cl_2 , 78.5 MHz, DEPT): δ 125.6 (μ -SiPhH, tm, $^2J_{\text{SiP}} = 70$ Hz), 141.5 (μ -SiPh₂, m).

c. $[\text{RhIr}(\text{CO})_2(\mu\text{-SiHPh})(\mu\text{-SiClPh})(\text{dppm})_2]$ (35**):** Under an atmosphere of Ar, 11.4 μL (0.057 mmol) of PhClSiH_2 was added to a slurry of 70 mg (0.057 mmol) of **4** in 0.7 mL of toluene in an NMR tube. The mixture was left under a dynamic Ar atmosphere overnight at 50 °C. Light yellow crystals accumulated on the surface of the tube, and were collected and washed with 3 mL of pentane. Evaporation of the residual solvent resulted in analytically pure compound **35** in 40 % (31 mg) isolated yield. Redissolving the solid in a minimum volume of toluene and subsequent layering of the toluene solution with pentane in an NMR tube yielded light yellow crystals (suitable for X-ray analysis) of compound **35** after 72 h. Anal. calcd. for $\text{C}_{64}\text{H}_{55}\text{ClIrO}_2\text{P}_4\text{RhSi}_2$: C, 56.26; H, 4.02. Found: C, 56.39; H, 4.16. $^{31}\text{P}\{^1\text{H}\}$ NMR (27 °C; CD_2Cl_2 , 201.6 MHz): δ 35.3 (Rh–P, m, 1P), 33.3 (Rh–P, m, 1P), 4.0 (Ir–P, m, 1P), 3.4 (Ir–P, m, 1P); ^1H NMR (27 °C; CD_2Cl_2 , 498.1 MHz): δ 5.50 (Si–H, m, 1H, $^1J_{\text{SiH}} = 180$ Hz), 5.11 (CH_2 , m, 1H), 4.42 (CH_2 , m, 1H), 4.21 (CH_2 , m, 1H), 2.85 (CH_2 , m, 1H); $^{13}\text{C}\{^1\text{H}\}$ NMR (27 °C; CD_2Cl_2 , 100.5 MHz): δ 200.4 (Rh–CO, dm, 1C, $^1J_{\text{RhC}} = 74$ Hz), 186.3 (Ir–CO, bs, 1C),

43.5 (CH₂, m, 1C), 35.2 (CH₂, m, 1C); ²⁹Si{¹H} NMR (27 °C; CD₂Cl₂, 78.5 MHz, DEPT): δ 123.8 (μ-SiPhH, m); the μ-SiClPh group was not observed.

d. **[RhIr(CO)₂(μ-SiHPh)(μ-SiMePh)(dppm)₂] (36)**: 100 mg (0.081 mmol) of [RhIr(H)₂(CO)₂(μ-SiHPh)(dppm)₂] (**4**) in a Schlenk flask was dissolved in 5 mL of toluene followed by the addition of 16.8 μL (0.122 mmol) of MePhSiH₂. The reaction mixture was stirred under a dynamic Ar atmosphere overnight at 50 °C during which time a white precipitate settled at the bottom of the flask. The supernatant was removed by cannula and the precipitate was washed with 5 × 3 mL of pentane. Evaporation of the residual solvent resulted in analytically pure compound **36** in 59 % (65 mg) isolated yield. Redissolving the solid in a minimum volume of benzene and subsequent layering of the solution with pentane in an NMR tube yielded light yellow crystals (suitable for X-ray analysis) of compound **36** after 48 h. Anal. calcd. for C₆₅H₅₈IrO₂P₄Rh Si₂: C, 57.93; H, 4.31. Found: C, 58.01; H, 4.31. ³¹P{¹H} NMR (27 °C; CD₂Cl₂, 201.6 MHz): δ 31.4 (Rh–P, m, 1P), 30.2 (Rh–P, m, 1P), 2.4 (Ir–P, m, 1P), –1.3 (Ir–P, m, 1P); ¹H NMR (27 °C; CD₂Cl₂, 498.1 MHz): δ 5.89 (Si–H, m, 1H, ¹J_{SiH} = 169 Hz), 5.16 (CH₂, m, 1H), 4.41 (CH₂, m, 1H), 4.09 (CH₂, m, 1H), 2.89 (CH₂, m, 1H), –0.42 (CH₃, m, 3H); ¹³C{¹H} NMR (27 °C; CD₂Cl₂, 100.5 MHz): δ 200.4 (Rh–CO, d, 1C, ¹J_{RhC} = 75 Hz), 187.5 (Ir–CO, bs, 1C), 47.3 (CH₂, m, 1C), 36.8 (CH₂, m, 1C); ²⁹Si{¹H} NMR (27 °C; CD₂Cl₂, 78.5 MHz, DEPT, gHSQC): δ 130.7 (μ-SiPhH, tm, ²J_{SiP} = 66 Hz); 139.2 (μ-SiPhMe).

e. **[RhIr(CO)₂(μ-SiHC₆H₃F₂)(μ-SiMePh)(dppm)₂] (37)**: To a slurry of 60 mg (0.047 mmol) of [RhIr(H)₂(CO)₂(μ-SiHC₆H₃F₂)(dppm)₂] (**33**) in 0.6 mL of

CD₂Cl₂ under an atmosphere of Ar in a septum-sealed NMR tube was added excess PhMeSiH₂ (26.0 μL; 0.188 mmol) followed by the gentle heating of the septum-sealed NMR tube at 40 °C for 12 h in an oil-bath. NMR spectroscopy of the reaction mixture suggested quantitative conversion of **33** to compound **37**. Addition of 1 mL of pentane yielded a white precipitate. After removing the solvent via cannula, the white powder was dried under high vacuum to give analytically pure compound in 60 % isolated yield. ³¹P{¹H} NMR (27 °C; CD₂Cl₂, 201.6 MHz): δ 31.4 (Rh–P, ddd, 1P, ¹J_{RhP} = 106 Hz, ²J_{PP} = 149 Hz, ²J_{PP} = 31 Hz), 29.6 (Rh–P, ddm, 1P, ¹J_{RhP} = 100 Hz, ²J_{PP} = 115 Hz, ²J_{PP} = 31 Hz) 1.4 (Ir–P, dd, 1P, ²J_{PP} = 115 Hz, ²J_{PP} = 24 Hz), –1.2 (Ir–P, dd, 1P, ²J_{PP} = 149 Hz, ²J_{PP} = 24 Hz); ¹H NMR (27 °C; CD₂Cl₂, 498.1 MHz): δ 5.74 (Si–H, m, 1H, ¹J_{SiH} = 173 Hz), 5.14 (CH₂, m, 1H), 4.41 (CH₂, m, 1H), 4.09 (CH₂, m, 1H), 2.84 (CH₂, m, 1H), –0.42 (CH₃, m, 3H); ¹³C{¹H} NMR (27 °C; CD₂Cl₂, 100.5 MHz): δ 200.7 (Rh–CO, d, 1C, ¹J_{RhC} = 72 Hz), 187.0 (Ir–CO, bs, 1C), 47.1 (CH₂, m, 1C), 36.8 (CH₂, m, 1C); 19.3 (CH₃, m, 1C); ²⁹Si{¹H} NMR (27 °C; CD₂Cl₂, 78.5 MHz, DEPT): δ 129.6 (Si–H, m), 139.5 (Si–CH₃, m); ¹⁹F NMR (27 °C; CD₂Cl₂, 376.1 MHz): δ –114.0 (m).

f. **[RhIr(CO)₂(μ-SiHC₆H₃F₂)(μ-SiHC₆H₂Me₃)(dppm)₂] (38)**: To a slurry of 50 mg (0.040 mmol) of **[RhIr(H)₂(CO)₂(μ-SiHC₆H₃F₂)(dppm)₂] (33)** in 0.6 mL of CD₂Cl₂ under an atmosphere of Ar in a septum-sealed NMR tube was added 13.0 μL of C₆H₂Me₃SiH₃ (0.080 mmol) followed by gentle heating at 40 °C for 12 h in an oil-bath. Addition of 1 mL of pentane yielded a white precipitate. After removing the solvent via cannula, the white powder was dried under high vacuum

to give analytically pure compound in 54 % (30 mg) isolated yield. Anal. calcd. for $C_{67}H_{60}F_2IrO_2P_4RhSi_2$: C, 57.08; H, 4.25. Found: C, 57.17; H, 4.33. $^{31}P\{^1H\}$ NMR (27 °C; CD_2Cl_2 , 201.6 MHz): δ 29.2 (Rh–P, ddd, 1P, $^1J_{RhP} = 103$ Hz, $^2J_{PP} = 130$ Hz, $^2J_{PP} = 30$ Hz), 24.8 (Rh–P, ddm, 1P, $^1J_{RhP} = 100$ Hz, $^2J_{PP} = 130$ Hz, $^2J_{PP} = 30$ Hz), –1.4 (Ir–P, dd, 1P, $^2J_{PP} = 130$ Hz, $^2J_{PP} = 22$ Hz), –3.8 (Ir–P, m, 1P, $^2J_{PP} = 130$ Hz, $^2J_{PP} = 22$ Hz); 1H NMR (27 °C; CD_2Cl_2 , 498.1 MHz): δ 5.89 (Si–H, m, 1H, $^1J_{SiH} = 169$ Hz), 5.84 (Si–H, m, 1H, $^1J_{SiH} = 190$ Hz), 5.11 (CH₂, m, 1H), 4.68 (CH₂, m, 1H), 3.92 (CH₂, m, 1H), 3.10 (CH₂, m, 1H), 2.50 (*o*-CH₃, s, 3H), 2.25 (*o*-CH₃, s, 3H), 2.12 (*p*-CH₃, s, 3H); $^{13}C\{^1H\}$ NMR (27 °C; CD_2Cl_2 , 100.5 MHz): δ 199.4 (Rh–CO, dm, 1C, $^1J_{RhC} = 74$ Hz), 185.9 (Ir–CO, s, 1C), 40.1 (CH₂, m, 1C), 38.5 (CH₂, m, 1C); 25.6 (*o*-CH₃, m, 1C), 25.4 (*o*-CH₃, m, 1C), 22.3 (*p*-CH₃, m, 1C); $^{29}Si\{^1H\}$ NMR (27 °C; CD_2Cl_2 , 78.5 MHz, DEPT): δ 119.6 (Si–H, m), 96.0 (Si–H, m); ^{19}F NMR (27 °C; CD_2Cl_2 , 376.1 MHz): δ –114.1 (m).

g. **[RhIr(CO)₂(μ -SiHPh)(μ -GePh₂)(dppm)₂] (39)**: 70 mg (0.057 mmol) of [RhIr(H)₂(CO)₂(μ -SiHPh)(dppm)₂] (**4**) in a Schlenk flask was dissolved in 10 mL of CH₂Cl₂ followed by the addition of 11 μ L (0.057 mmol) of Ph₂GeH₂. The reaction mixture was stirred gently for 12 h during which time the yellow solution turned orange. NMR spectroscopy of the crude mixture showed formation of **39** in approximately 90 % yield together with a previously reported product [RhIr(CO)₂(μ -GeHPh)(μ -GePh₂)(dppm)₂] (**23**)^{9b} in 10 % yield. (When the compound **4** was reacted with excess (approximately 4 equiv) germane the portion of minor product **23** increased to as high as 25 %). The solvent volume of a 9:1 mixture of these products was reduced to approximately 0.7 mL under high

vacuum. Layering the solution with 2 mL of pentane in an NMR tube yielded light yellow co-crystals (suitable for X-ray analysis) of compounds **39** and **23** after 72 h in 3:1 ratio. $^{31}\text{P}\{^1\text{H}\}$ NMR (27 °C; CD_2Cl_2 , 201.6 MHz): δ 35.8 (Rh–P, ddd, 1P, $^1J_{\text{RhP}} = 112$ Hz, $^2J_{\text{PP}} = 142$ Hz, $^2J_{\text{PP}} = 30$ Hz), 24.4 (Rh–P, ddd, 1P, $^1J_{\text{RhP}} = 104$ Hz, $^2J_{\text{PP}} = 138$ Hz, $^2J_{\text{PP}} = 30$ Hz), 7.8 (Ir–P, dd, 1P, $^2J_{\text{PP}} = 112$ Hz, $^2J_{\text{PP}} = 23$ Hz), -7.9 (Ir–P, dd, 1P, $^2J_{\text{PP}} = 138$ Hz, $^2J_{\text{PP}} = 23$ Hz); ^1H NMR (27 °C; CD_2Cl_2 , 498.1 MHz): δ 5.72 (Si–H, m, 1H, $^1J_{\text{SiH}} = 168$ Hz), 5.12 (CH₂, m, 1H), 4.42 (CH₂, m, 1H), 2.98 (CH₂, m, 1H), 2.94 (CH₂, m, 1H); $^{13}\text{C}\{^1\text{H}\}$ NMR (27 °C; CD_2Cl_2 , 100.5 MHz): δ 199.8 (Rh–CO, dm, 1C, $^1J_{\text{RhC}} = 73$ Hz), 186.2 (Ir–CO, bs, 1C), 36.8 (CH₂, m, 1C), 34.5 (CH₂, m, 1C); $^{29}\text{Si}\{^1\text{H}\}$ NMR (27 °C; CD_2Cl_2 , 78.5 MHz, DEPT): δ 128.7 (Si–H, tm, $^2J_{\text{SiP}} = 70$ Hz).

h. **[RhIr(CO)₂(μ -SiHPh)(μ -GeHPh)(dppm)₂] (40)**: In a sealed NMR tube, 70 mg (0.055 mmol) of **[RhIr(H)₂(CO)₂(μ -GeHPh)(dppm)₂] (20)** was dissolved in 0.7 mL of CH_2Cl_2 under an atmosphere of Ar, followed by the addition of 6.8 μL (0.055 mmol) of PhSiH_3 . The reaction mixture slowly changed colour from yellow to orange over a period of 12 h. After this period, the solution was transferred to a Schlenk flask via cannula. NMR spectroscopy of the crude products showed 70 % formation of complex **40** along with 30 % of other unidentified products. Unfortunately, repeated attempts to isolate this complex from the crude mixture did not succeed. $^{31}\text{P}\{^1\text{H}\}$ NMR (27 °C; CD_2Cl_2 , 201.6 MHz): δ 27.3 (Rh–P, ddd, 1P, $^1J_{\text{RhP}} = 104$ Hz, $^2J_{\text{PP}} = 112$ Hz, $^2J_{\text{PP}} = 30$ Hz), 23.0 (Rh–P, ddd, 1P, $^1J_{\text{RhP}} = 118$ Hz, $^2J_{\text{PP}} = 139$ Hz, $^2J_{\text{PP}} = 30$ Hz), 0.7 (Ir–P, dd, 1P, $^2J_{\text{PP}} = 112$ Hz, $^2J_{\text{PP}} = 22$ Hz), -7.2 (Ir–P, dd, 1P, $^2J_{\text{PP}} = 138$ Hz, $^2J_{\text{PP}} = 22$ Hz); ^1H

NMR (27 °C; CD₂Cl₂, 498.1 MHz): δ 6.20 (Si–H, m, 1H, ¹J_{SiH} = 168 Hz), 5.91 (Ge–H, m, 1H), 5.25 (CH₂, m, 1H), 4.65 (CH₂, m, 1H), 3.12 (CH₂, m, 1H), 2.91 (CH₂, m, 1H); ¹³C{¹H} NMR (27 °C; CD₂Cl₂, 100.5 MHz): δ 200.3 (Rh–CO, dm, 1C, ¹J_{RhC} = 73 Hz), 186.9 (Ir–CO, bs, 1C), 35.7 (CH₂, m, 1C), 343 (CH₂, m, 1C); ²⁹Si{¹H} NMR (27 °C; CD₂Cl₂, 78.5 MHz, DEPT): δ 129.7 (Si–H, tm, ²J_{SiP} = 68 Hz).

i. **[RhIr(CO)₂(μ-SiPh₂)(μ-GeHPh)(dppm)₂] (41)**: 70 mg (0.055 mmol) of **[RhIr(H)₂(CO)₂(μ-GeHPh)(dppm)₂] (20)** in a Schlenk flask was dissolved in 10 mL of CH₂Cl₂ followed by the addition of 15.3 μL (0.083 mmol) of Ph₂SiH₂. The reaction mixture was stirred gently for 48 h during which time the yellow solution lightened slightly. NMR spectroscopy of the crude mixture showed approximately 90 % conversion to complex **41** along with 10 % unreacted compound **20**. Reduction of the solvent volume to approximately 1 mL under high vacuum, followed by layering the solution with 3 mL of pentane yielded light yellow crystals (suitable for X-ray analysis) of compound **41** after 72 h in 49 % (39 mg) isolated yield. Under refluxing condition in dichloromethane, this reaction required approximately 8 to 10 h to reach completion. Anal. calcd. for C₇₀H₆₀GeIrO₂P₄RhSi: C, 57.88; H, 4.13. Found: C, 58.19; H, 4.19. ³¹P{¹H} NMR (27 °C; CD₂Cl₂, 201.6 MHz): δ 32.4 (Rh–P, ddd, 1P, ¹J_{RhP} = 98 Hz, ²J_{PP} = 111 Hz, ²J_{PP} = 31 Hz), 24.4 (Rh–P, ddd, 1P, ¹J_{RhP} = 115 Hz, ²J_{PP} = 145 Hz, ²J_{PP} = 31 Hz), 7.8 (Ir–P, dd, 1P, ²J_{PP} = 111 Hz, ²J_{PP} = 23 Hz), –7.9 (Ir–P, dd, 1P, ²J_{PP} = 145 Hz, ²J_{PP} = 23 Hz); ¹H NMR (27 °C; CD₂Cl₂, 498.1 MHz): δ 6.19 (Ge–H, m, 1H), 5.00 (CH₂, m, 1H), 4.50 (CH₂, m, 1H), 2.98 (CH₂, m, 1H), 2.91 (CH₂, m, 1H); ¹³C{¹H}

(27 °C; CD₂Cl₂, 100.5 MHz): δ 200.2 (Rh–CO, dm, 1C, ¹J_{RhC} = 73 Hz), 187.5 (Ir–CO, bs, 1C), 37.5 (CH₂, m, 1C), 33.4 (CH₂, m, 1C).

j. [RhIr(CO)₂](μ-SiPhMe)(μ-GeHPh)(dppm)₂ (**42**): 70 mg (0.055 mmol) of [RhIr(H)₂(CO)₂(μ-GeHPh)(dppm)₂] (**20**) in a Schlenk flask was dissolved in 10 mL of CH₂Cl₂ followed by the addition of 15.1 μL (0.11 mmol) of MePhSiH₂. The reaction mixture was stirred gently for 72 h during which time the yellow solution became orange. NMR spectroscopy of the crude mixture showed approximately 90 % conversion to complex **42** along with 10 % unreacted compound **20**. Reduction of the solvent volume to approximately 1 mL under high vacuum followed by the slow addition of pentane to a stirring solution of **42** yielded a yellow powder in 53 % (41 mg) isolated yield. In refluxing dichloromethane, the reaction was complete in 12 h but it also produced approximately 20% unidentified products. Anal. calcd. for C₆₅H₅₈GeIrO₂P₄Rh Si: C, 56.15; H, 4.17. Found: C, 56.38; H, 4.31. ³¹P{¹H} NMR (27 °C; CD₂Cl₂, 201.6 MHz): δ 34.0 (Rh–P, ddd, 1P, ¹J_{RhP} = 117 Hz, ²J_{PP} = 153 Hz, ²J_{PP} = 30 Hz), 30.1 (Rh–P, ddd, 1P, ¹J_{RhP} = 105 Hz, ²J_{PP} = 142 Hz, ²J_{PP} = 30 Hz), 2.5 (Ir–P, dd, 1P, ²J_{PP} = 142 Hz, ²J_{PP} = 20 Hz), 1.0 (Ir–P, dd, 1P, ²J_{PP} = 153 Hz, ²J_{PP} = 20 Hz); ¹H NMR (27 °C; CD₂Cl₂, 498.1 MHz): δ 6.40 (Ge–H, m, 1H), 5.17 (CH₂, m, 1H), 4.43 (CH₂, m, 1H), 4.18 (CH₂, m, 1H); 2.94 (CH₂, m, 1H); ¹³C{¹H} NMR (27 °C; CD₂Cl₂, 100.5 MHz): δ 200.9 (Rh–CO, dm, 1C, ¹J_{RhC} = 74 Hz), 187.1 (Ir–CO, bs, 1C), 46.9 (CH₂, m, 1C), 37.1 (CH₂, m, 1C), –7.9 (CH₃, s, 1C); ²⁹Si{¹H} (27 °C; CD₂Cl₂, 78.5 MHz, DEPT): δ 139.7 (Si–H, tm, ²J_{SiP} = 73 Hz).

k. **[RhIr(CO)₂(μ-SiClPh)(μ-GeHPh)(dppm)₂] (43)**: Under an atmosphere of Ar, 7.4 μL (0.055 mmol) of PhClSiH₂ was added to a solution of 70 mg (0.055 mmol) of **20** in 10 mL of CH₂Cl₂ in a Schlenk tube and was left stirring under a dynamic Ar atmosphere overnight at ambient temperature. The solvent was removed under reduced pressure and the residue was redissolved in minimum amount of toluene. Slow addition of 5 mL of pentane to the stirring toluene solution yielded a light yellow powder in 42 % (33 mg) isolated yield. ³¹P{¹H} NMR (27 °C; CD₂Cl₂, 201.6 MHz) δ 38.0 (Rh–P, ddd, 1P, ¹J_{RhP} = 114 Hz, ²J_{PP} = 158 Hz, ²J_{PP} = 30 Hz), 32.8 (Rh–P, ddd, 1P, ¹J_{RhP} = 98 Hz, ²J_{PP} = 125 Hz, ²J_{PP} = 30 Hz), 5.6 (Ir–P, dd, 1P, ²J_{PP} = 158 Hz, ²J_{PP} = 21 Hz), 3.7 (Ir–P, dd, 1P, ²J_{PP} = 125 Hz, ²J_{PP} = 21 Hz); ¹H NMR (27 °C; CD₂Cl₂, 498.1 MHz): δ 5.89 (Ge–H, m), 5.13 (CH₂, m, 1H), 4.47 (CH₂, m, 1H), 4.23 (CH₂, m, 1H), 2.84 (CH₂, m, 1H); ¹³C{¹H} NMR (27 °C; CD₂Cl₂, 100.5 MHz): δ 200.1 (Rh–CO, dm, 1C, ¹J_{RhC} = 76 Hz), 185.8 (Ir–CO, bs, 1C), 43.0 (CH₂, m, 1C), 35.6 (CH₂, m, 1C).

4.3 X-ray Data Collection and Structure Determination.

4.3.1 General considerations.

Single crystals suitable for X-ray diffraction were obtained by the slow diffusion of pentane into CH₂Cl₂ (**34**, **37**, **39**, **41**), benzene (**36**, **42**) or toluene (**35**) solutions of the compounds. Data were collected on either a Bruker D8/APEX II CCD diffractometer (**34**, **35**, **36**, **42**) or Bruker PLATFORM/APEX II CCD (**39**, **41**) diffractometer at –100 °C using Mo Kα radiation.²⁵ Data were corrected for absorption through the use of Gaussian integration from indexing of the crystal faces. The structures were solved using Patterson location of heavy atoms

followed by structure expansion (*DIRDIF-2008*)²⁶ (**34, 41**) or by direct methods (*SHELXL-97*)²⁷ (**35, 36, 39, 42**). Refinement was carried out using the program *SHELXL-97*.²⁷ For each complex, the metal atom sites were found to be disordered, thus were treated as a combination of 50% Ir and 50% Rh sharing the same site. Hydrogen atoms attached to carbons were assigned positions based on the *sp*² or *sp*³ hybridization geometries of their parent atoms, and were given isotropic displacement parameters 20 % greater than the *U*_{eq}'s of their parent carbons. The hydrogen atoms attached to silicon or germanium atoms were located from difference Fourier maps, and their atomic coordinates and thermal parameters were allowed to freely refine. A listing of crystallographic experimental data is provided for all structures in Appendix III.

4.3.2 Special refinement conditions.

i. Compound 35: The two solvent toluene molecules were found to be disordered, and were each split into two sets of atom positions, each having an occupancy factor of 0.5. Distances involving the methyl carbons of these molecules were restrained during refinement: $d(\text{C}(10\text{S})-\text{C}(11\text{S})) = d(\text{C}(20\text{S})-\text{C}(21\text{S})) = d(\text{C}(30\text{S})-\text{C}(31\text{S})) = d(\text{C}(40\text{S})-\text{C}(41\text{S})) = 1.50(1) \text{ \AA}$; $d(\text{C}(10\text{S})\cdots\text{C}(12\text{S})) = d(\text{C}(10\text{S})\cdots\text{C}(16\text{S})) = d(\text{C}(20\text{S})\cdots\text{C}(22\text{S})) = d(\text{C}(20\text{S})\cdots\text{C}(26\text{S})) = d(\text{C}(30\text{S})\cdots\text{C}(32\text{S})) = d(\text{C}(30\text{S})\cdots\text{C}(36\text{S})) = d(\text{C}(40\text{S})\cdots\text{C}(42\text{S})) = d(\text{C}(40\text{S})\cdots\text{C}(46\text{S})) = 2.52(1) \text{ \AA}$. The phenyl rings of these solvent toluene molecules were modelled as idealized regular hexagons with C–C bond lengths of exactly 1.39 Å and C–C–C ring bond angles of exactly 120°.

ii. Compound 37: One of the two solvent dichloromethane molecules was found to be disordered. One chlorine and one carbon atom of this molecule were split into two positions each, with relative occupancy factors of 0.667 and 0.333. The C–Cl distances within this molecule were restrained to be the same (within 0.03 Å) during refinement.

iii. Compound 39: The atomic position labelled ‘Si’ was refined as a combination of 75% Si and 25% Ge sharing the same site.

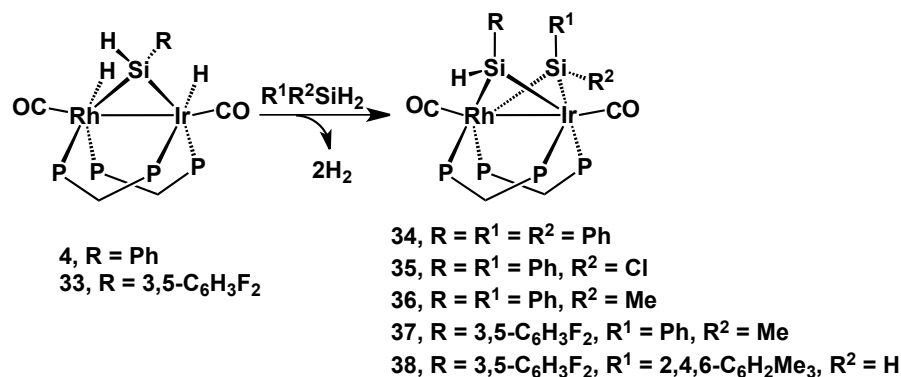
iv. Compound 41: One chlorine atom of the solvent dichloromethane molecule was disordered over two positions, which were refined with relative occupancy factors of 0.8 and 0.2, and with common anisotropic displacement parameters.

4.4 Results and Characterization of Compounds.

4.4.1 Mixed *bis*(μ -silylene) Complexes

Reaction of the silylene-bridged dihydride complexes, $[\text{RhIr}(\text{H})_2(\text{CO})_2(\mu\text{-SiHR})(\text{dppm})_2]$ (**4**, R = Ph; **33**, R = C₆H₃F₂) with one equiv of either secondary or primary silanes (Ph₂SiH₂, PhClSiH₂, PhMeSiH₂, C₆H₂Me₃SiH₃) yields a series of mixed bis(silylene)-bridged complexes, $[\text{RhIr}(\text{CO})_2(\mu\text{-SiHR})(\mu\text{-SiR}_1\text{R}_2)(\text{dppm})_2]$ (R = R¹ = R² = Ph (**34**); R = R¹ = Ph, R² = Cl (**35**); R = R¹ = Ph, R² = Me (**36**); R = 3,5-C₆H₃F₂, R¹ = Ph, R² = Me (**37**); R = 3,5-C₆H₃F₂, R¹ = 2,4,6-C₆H₂Me₃, R² = H (**38**)) (Scheme 4.1), by double Si–H bond activation and concomitant reductive elimination of 2 equiv of hydrogen either at ambient temperature (**34** and **35**) or at 40 to 50 °C (**36**, **37**, **38**). All complexes were characterized by multinuclear NMR spectroscopy and X-ray crystallography (except for complex **38**, the structure of which could not be refined due to unresolved disorder in the crystals).

Scheme 4.1



The NMR spectra of these complexes are all closely comparable, showing four multiplets in the $^{31}\text{P}\{^1\text{H}\}$ NMR spectra owing to the chemical inequivalence of all ^{31}P nuclei. The two downfield resonances are assigned to Rh-bound ^{31}P nuclei on the basis of their coupling to ^{103}Rh (between 98 to 118 Hz). Although for compounds **34**, **37** and **38** the coupling to Rh (*ca.* 100 Hz) is clearly resolved from the other couplings, it is not resolved for **35** and **36**, but is nevertheless obvious from the greater complexity of these signals owing to the additional Rh coupling. A multiplet is observed for the Si-bound proton of each complex in the ^1H NMR spectrum at between δ 5.5 and 5.9, displaying ^{29}Si satellites ($^1J_{\text{SiH}} \approx 168$ to 180 Hz), and each resonance collapses to a singlet upon broadband ^{31}P decoupling. In the $^{29}\text{Si}\{^1\text{H}\}$ NMR spectra two distinct multiplets are observed (with the exception of compound **35** for which the μ -SiPhCl group was not detected) at between δ 96 to δ 142 as is usually observed for bridging silylene units; these chemical shifts lie intermediate between typical values for silyl groups and terminal silylene units.¹ Incorporation of the different substituents was confirmed by using NMR spectroscopy. For instance, complex **38** displays a

multiplet at $\delta -114.1$ in the ^{19}F NMR spectrum corresponding to the fluoroaryl group while in the ^1H NMR spectrum three singlets in a 1:1:1 ratio appear at δ 2.50, 2.25 and 2.12 for the three mesityl methyl groups. The $^{13}\text{C}\{^1\text{H}\}$ NMR spectra display a doublet of multiplets (at *ca.* δ 200) and a broad singlet (at *ca.* δ 187), for the Rh- and Ir-bound carbonyls, respectively. Comparison of the ^1H and $^{31}\text{P}\{^1\text{H}\}$ NMR spectra of these complexes with those of the previously reported bis(silylene)-bridged complexes, $[\text{RhIr}(\text{CO})_2(\mu\text{-SiHR})_2(\text{dppm})_2]$ ($\text{R} = \text{Ph}$ or $\text{C}_6\text{H}_3\text{F}_2$),^{9a} eliminates the possibility that the reactions shown in Scheme 4.1 produce a mixture of *homo*-bis(silylene)-bridged products, ($[\text{RhIr}(\text{CO})_2(\mu\text{-SiHR})_2(\text{dppm})_2]$ and $[\text{RhIr}(\text{CO})_2(\mu\text{-SiR}^1\text{R}^2)_2(\text{dppm})_2]$), instead of the single *mixed* bis(silylene)-bridged products. In addition, our previous studies^{9a} established that bis(silylene)-bridged complexes, in which both silylene fragments are disubstituted, such as $[\text{RhIr}(\text{CO})_2(\mu\text{-SiR}_2)_2(\text{dppm})_2]$ ($\text{R} = \text{Ph}$, or Me), could not be obtained due to the steric demands of the pair of bulky bridging units. Selected spectra for the above species are given in Appendix III.

The X-ray structures of compounds **34**, **35**, **36** and **37**, shown in Figure 4.1, confirm the mixed bis(silylene) formulations for these species. Selected structural parameters for these compounds are given in Appendix III. All complexes adopt a “cradle-shape” diphosphine arrangement in which these groups are *cis* at both metals. Each metal has a distorted octahedral geometry, similar to the previously reported dppm-bridged bis(μ -silylene),^{3a,7,9a} and bis(μ -germylene) complexes.^{9b} The metal-metal distances in these complexes (approximately 2.80 Å) are consistent with the presence of a formal metal-metal bond while the non-bonded

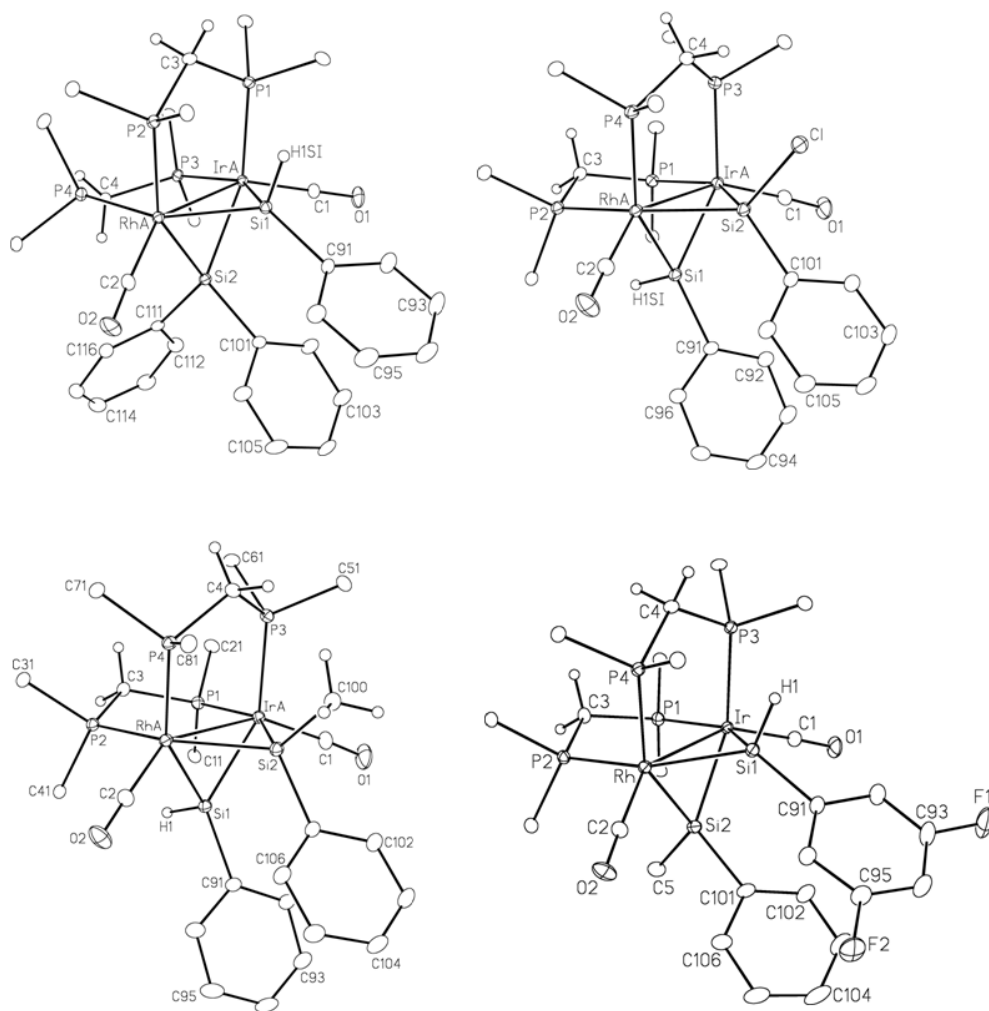


Figure 4.1: Perspective view of complexes **34** (top left), **35** (top right), **36** (bottom left) and **37** (bottom right) showing the atom labeling scheme. Non-hydrogen atoms are represented by Gaussian ellipsoids at the 20% probability level. Hydrogen atoms are shown arbitrarily small but are not shown for the phenyl groups. For the *dppm* phenyl groups, only the ipso carbons are shown. For all complexes the Rh and Ir metals are disordered, but the structures refined well with each metal site having a 50 % occupancy of Rh and Ir.

Si---Si distances (2.858(1) Å for **34**, 2.821(1) Å for **35**, 2.8755(8) Å for **36** and 2.865(1) Å for **37**) are longer than the longest known Si–Si single bond (2.69 Å),

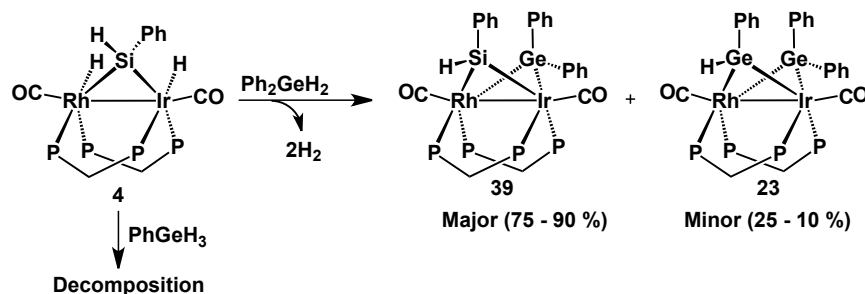
²⁸ although significantly shorter than the sum of the van der Waals radii of two Si atoms (4.20 Å).²⁹ In all cases, the μ -silylene groups are arranged having an aryl ring on each Si parallel and adjacent, taking advantage of π -stacking between the groups (centroid to centroid distance: 3.720 Å for **34**, 3.660 Å for **35**, 3.729 Å for **36**, and 3.552 Å for **37**). These ring separations are within the range of 3.3 Å and 3.8 Å generally considered to arise from favourable π -stacking interactions.^{21a} In this series, it is interesting to note that the centroid-to-centroid distance between phenyl rings becomes shorter when electron-withdrawing groups are introduced either on the phenyl ring (compound **37**) or directly on silicon (compound **35**). This is consistent with our previous studies in which we observed a significant decrease in centroid-to-centroid distance (from 3.736 to 3.551 Å) between parallel phenyl rings in bis(silylene)-bridged complexes, upon introduction of electron-withdrawing fluorines on the rings.^{9a} In contrast, when an electron-donating group (CH₃) is introduced on the bridging silylene of compound **36**, the centroid-to-centroid distance is now increased to 3.729 Å. Although the introduction of electron-withdrawing substituents on the phenyl rings significantly decreases the separation between the parallel aryl rings, the distance between the two corresponding silicon atoms changes surprisingly little, and in fact in one case increases slightly, as will be discussed in detail later.

4.4.2 (μ -silylene)/(μ -germylene) Complexes

In an attempt to obtain mixed (μ -silylene)/(μ -germylene) species the phenylsilylene-bridged compound **4** was first reacted with one equiv of phenylgermane, however, this reaction led to the formation of several unidentified

products, as evident in the $^{31}\text{P}\{^1\text{H}\}$ NMR spectrum. This behavior is reminiscent of our earlier reaction of the corresponding mono(phenylgermylene)-bridged Rh/Ir dihydride complex (**20**) with one equiv of phenylgermane, which also resulted in decomposition (see Chapter 3).^{9b} However, the reaction of **4** with one equiv of diphenylgermane successfully yields the first mixed silylene- and germylene-bridged complex, $[\text{RhIr}(\text{CO})_2(\mu\text{-SiHPh})(\mu\text{-GePh}_2)(\text{dppm})_2]$ (**39**), in approximately 90 % yield along with 10 % of the previously reported bis(germylene)-bridged complex, $[\text{RhIr}(\text{CO})_2(\mu\text{-GeHPh})(\mu\text{-GePh}_2)(\text{dppm})_2]$ (**23**) (Scheme 4.2).^{9b} When the reaction is carried out in the presence of excess

Scheme 4.2

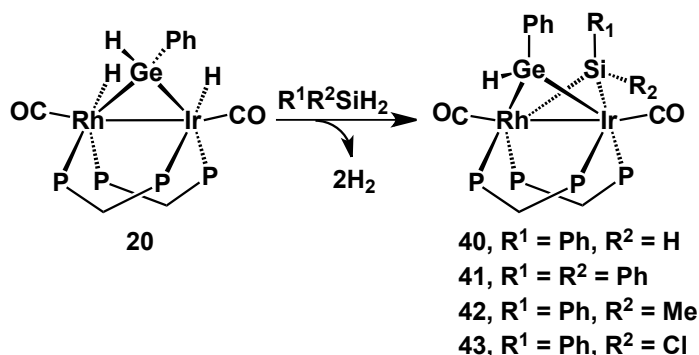


Ph_2GeH_2 , the yield of **23** increases (up to 25 %) with a corresponding drop in the yield of **39**. The mechanism for formation of **23** is not clear. Addition of excess (4 equiv) Ph_2GeH_2 to a 10:1 mixture of **39** and **23** leaves the ratio unchanged, indicating that **23** is not produced through the intermediacy of **39**; instead it is produced by a competing reaction.

Mixed (μ -silylene)/(μ -germylene) complexes can also be prepared by reaction of the mono-germylene-bridged complexes with silanes. For example, The reaction of the phenylgermylene-bridged dihydride complex,

[RhIr(H)₂(CO)₂(μ-GeHPh)(dppm)₂] (**20**), with phenylsilane leads to the formation of [RhIr(CO)₂(μ-SiHPh)(μ-GeHPh)(dppm)₂] (**40**) as the major product (70 %) along with some unidentified decomposition products. This is an interesting contrast to the reverse reaction of complex **4** with phenylgermane and of the previously reported reaction of **20** with phenylgermane, both of which lead only to decomposition.^{9b} The reaction of **20** with a series of secondary silanes yields the corresponding series of *mixed* (silylene)/(germylene)-bridged complexes, [RhIr(CO)₂(μ-SiR¹R²)(μ-GeHPh)(dppm)₂] (R¹ = R² = Ph (**41**); R¹ = Ph, R² = Me (**42**); R¹ = Ph, R² = Cl (**43**)) (Scheme 4.3).

Scheme 4.3



The NMR spectroscopic features and X-ray structures of these (μ-silylene)/(μ-germylene) complexes are similar to those of *mixed* bis(silylene)-bridged complexes mentioned above. The X-ray structures of complexes **39** (which co-crystallized with **23** in 3:1 ratio), **41** and **42** are shown in Figure 4.2, confirming the mixed (μ-silylene)/(μ-germylene) formulation. In each case the non-bonded distance between adjacent Ge and Si atoms of the two bridging units (2.9582(5) Å for compound **39**, 2.9255(6) Å for **41** and 2.9322(7) Å for **42**) is much longer than for a Si–Ge single bond (2.357(4) Å)³⁰ which appears to

preclude any significant interaction between these two atoms; however, these distances are again much shorter than the sum of the van der Waals radii (4.21 Å) of Si and Ge,²⁹ leaving some doubt about the nature of the Si---Ge interactions.

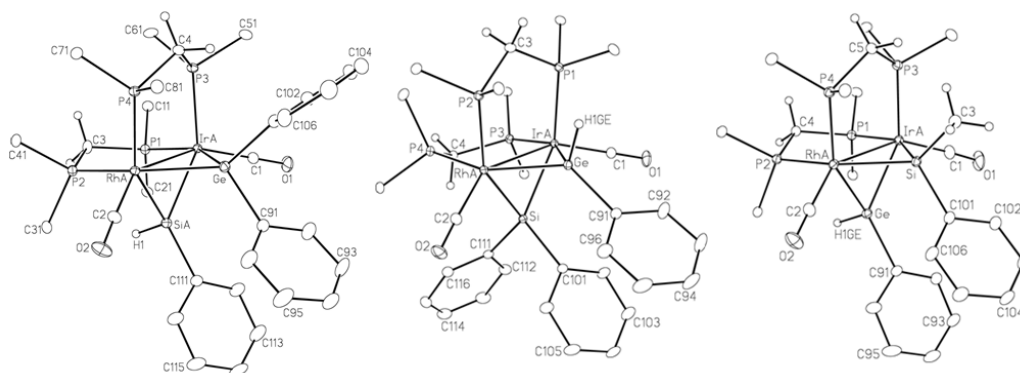


Figure 4.2: Perspective view of complex **39** (left), **41** (middle) and **42** (right) showing atom labeling scheme. Non-hydrogen atoms are represented by Gaussian ellipsoids at the 20 % probability level. Hydrogen atoms are shown arbitrarily small and are not shown for phenyl rings. For the *dppm* phenyl groups, only the ipso carbons are shown. For all complexes Rh(A) and Ir(A) were refined at 50 % occupancy. For compound **39**, the SiA position was refined with a site occupancy of Si_{0.75}Ge_{0.25} (see Experimental Section).

As noted for the *mixed* bis(silylene)-bridged complexes the silicon-germanium non-bonded distance in **42** is again slightly longer than in **41**, presumably due to the presence of the electron-donating methyl group in the former.

4.5 Discussion

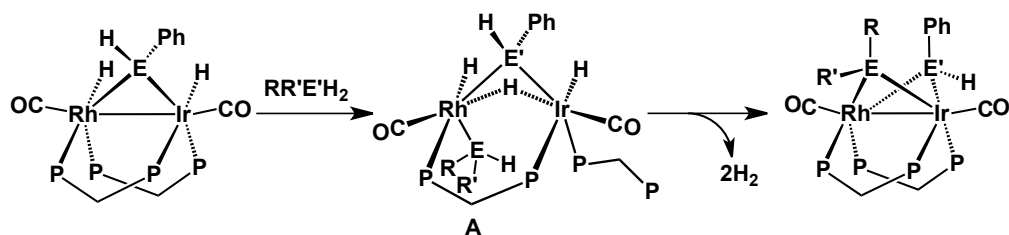
As noted in the Introduction, we had two major goals in this study: (1) to synthesize a series of *mixed* bis(μ -silylene) and (μ -silylene)/(μ -germylene) complexes which have potential applications for the coupling of the same elements having different substituents or for the coupling of Si- and Ge-

containing units; and (2) to study the influence of different silylene substituents and π -stacked aromatic rings on the Si---Si separation in such complexes, in order to obtain information about the nature of the interactions between bridging silylene units.

We were certainly successful in our first goal by taking advantage of stable mono-EHPPh-bridged dihydride complexes as precursors, which upon reaction with an equivalent of a different organosilane or an organogermane, yield a series of *mixed* bis(μ -silylene) and (μ -silylene)/(μ -germylene) complexes. All of the di-bridged complexes reported above are formed either at room temperature over extended periods (between 24 and 72 h) or require slightly elevated reaction temperatures. As a consequence, low-temperature studies failed to generate products, so intermediates in their formation could not be observed. However, during the formation of complex **42**, the presence of a small amount (*ca.* 5 %) of an intermediate species was detected in the $^{31}\text{P}\{^1\text{H}\}$ NMR spectra, in which four multiplets were observed at δ 25.2, 7.1, -6.1 and -28.2. Only the downfield peak displays Rh-P coupling while the most upfield peak corresponds to the free end of a pendent diphosphine, as has been previously observed in the formation of bis(μ -silylene) and bis(μ -germylene) complexes.^{3a,9a,9b} Although this pendent diphosphine species has not been characterized owing to its low abundance, we propose a structure like **A** as shown in Scheme 4.4, analogous to intermediates previously characterized by us in related chemistry.^{9a,9b}

The coordinative unsaturation necessary for reaction of mono-silylene or mono-germylene precursors with the second equivalent of silane can result either

Scheme 4.4



from dissociation of one arm of a diphosphine or by reductive elimination of a silylene and hydride unit from the more labile Rh centre to give an unsaturated Ir-bound silyl species. Certainly, in previous studies hydride exchange between Rh, Ir and Si/Ge⁹ was found to be facile.^{3a,7} Although hydride exchange was not pursued in detail in this study, we did observe that reaction of the mono(germylene)-bridged complex **20** with Ph₂SiD₂ results in the evolution of both HD and H₂ gas, as seen in the ¹H NMR spectrum along with the partial incorporation of deuterium in the germanium-bound proton position during the formation of the (μ-silylene)/(μ-germylene) complex (**41**), again suggesting a dynamic exchange process between these metal-bound hydrides and the germanium-bound protons. The ease of the hydride exchange noted above and in previous studies,^{3a,7,9} leads us to suggest that the reversible elimination of a silylene/hydride unit at one metal gives rise to the necessary coordinative unsaturation for reaction with additional substrate, which is subsequently facilitated by dissociation of the Rh-bound end of a diphosphine to ease the crowding within the inner coordination spheres of the metals. This proposal is supported by the failure of the phenylsilylene-bridged diiridium dihydride

analogue to react with a second equivalent of phenylsilane, combined with the absence of hydride exchange involving this less labile Ir₂ system.⁸

As noted above, another of our goals was to understand how the silylene substituents influence the Si---Si separation between the two bridging units, and to determine whether the variation in this separation with different substituents could tell something about the nature of the Si---Si interactions. In the three mixed bis(silylene)-bridged complexes (**34**, **35** and **36**) studied, all contain a common monosubstituted bridging-phenylsilylene unit (μ -SiPhH) and a different disubstituted bridging-silylene unit (μ -SiPhX; X = Ph (**34**), Cl (**35**) and Me (**36**); see Figure 4.3). A comparison of the Si---Si separations involving compounds **34**, **35**, **36** and a previously reported bis(phenylsilylene)-bridged complex in Chapter 2 (**8b** in Figure 4.3) shows that decreasing the electron-donating nature of the Si-

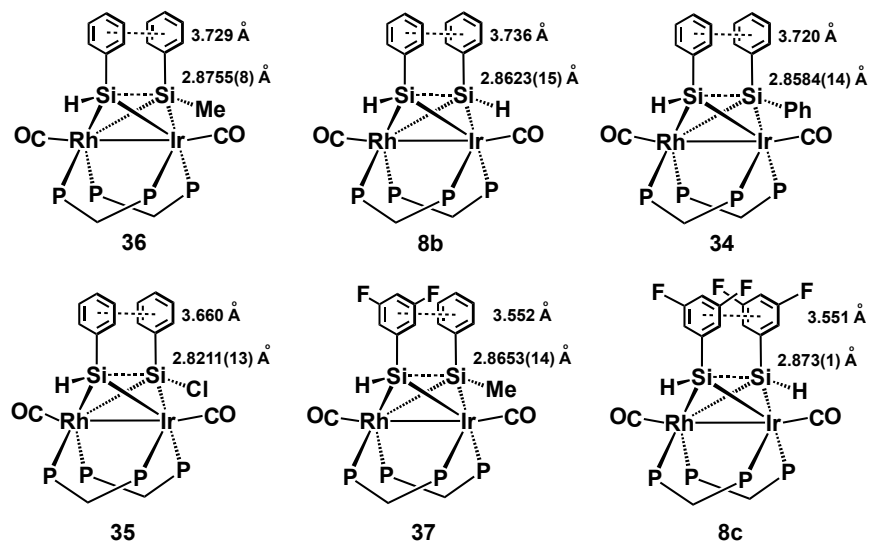


Figure 4.3: Representations of the bis(μ -silylene) complexes showing the separation between the parallel aryl rings and the pair of Si atoms.^{9a}

bound substituents gives rise to a decrease in the Si---Si separation. As shown in Figure 4.3 the Si---Si separation decreases in the order: X = Me (**36**); Si---Si = 2.8755(8) Å > X = H (**8b**); Si---Si = 2.8623(15) Å > X = Ph (**34**); Si---Si = 2.8584(14) Å > X = Cl (**35**); Si---Si = 2.8211(13). This decrease in Si---Si separation (ca. 0.055 Å) as the electron withdrawing nature of the Si-X bond increases is accompanied by a corresponding decrease (0.069 Å) in the separation between π -stacked aryl rings.

The influence of ring substituents can be seen in two sets of compounds. Compounds **8b** and **8c**^{9a} differ only in the aryl substituents with **8b** having parallel unsubstituted phenyl rings, while **8c** has electronegative fluorines in the meta positions of both rings. The two fluorine substituents give rise to a substantial decrease in separation between the ring centroids (by ca. 0.18 Å), while resulting in a slight *increase* (by 0.01 Å) in the Si---Si separation. Compounds **36** and **37**, each having a methyl substituent on one Si, can also be compared, differing only in the aryl substituents (this time on only one ring). Again fluorine substitution gives rise to a significant decrease in centroid-to-centroid distance of ca. 0.18 Å, but has little effect on the Si---Si separation which decreases marginally (0.01 Å). The decrease in separation between π -stacked aryl rings upon substitution by electron withdrawing groups is well established.²¹ However, we were surprised to observe that this closer approach of the aryl rings has little effect on the Si---Si separation. If the close approach of the pair of Si atoms in these bis-silylene-bridged compounds (in which the Si---Si separations are significantly less than van der Waals separations) were a consequence of nascent Si-Si bonding, we

would expect that reducing the repulsions between their attached π -stacked aryl groups, through the introduction of electronegative substituents on these groups, would allow the Si atoms to optimize their mutual bonding, leading to a shortening of the Si–Si separation. The observed insensitivity of this separation to fluorine substitution on the π -stacked rings indicates that closer approach of the pairs of Si atoms is not inhibited by van der Waals repulsion between the parallel aryl groups, and further suggests that mutual attraction by weak bonding interactions between the Si atoms is minimal.

On the basis of the above argument we suggest that the significant change in Si---Si separation upon changing the Si-bound substituents (in the series **36**, **8b**, **34** and **35**) might be attributed to a decrease in electron density at Si upon substitution by more electron-withdrawing groups ($\text{Me} < \text{H} < \text{Ph} < \text{Cl}$), leading to less van der Waals repulsion between these centers, therefore shorter separation. The accompanying decrease in aryl-aryl separation with the introduction of electron-withdrawing substituents on Si is presumably a result of accompanying withdrawal of electron density from these π -stacked rings leading to less repulsion between these groups. Both effects, resulting from direct substitution on Si, are most evident in **35**, having the very electronegative chlorine substituent.

In conclusion, we have developed a protocol for the synthesis of a wide variety of *mixed* bis(μ -silylene) complexes with different substituents on each bridging element and have extended this protocol for the synthesis of a series of novel (μ -silylene)/(μ -germylene) complexes of Rh and Ir. To our knowledge this latter accomplishment represents the first example of the selective incorporation

of two different bridging elements of group 14 into a bimetallic core. We have also been able to obtain crystallographic evidence of substituent effects on the Si--Si separation in the bis(μ -silylene) complexes involving substituents directly on Si or on the π -stacked aryl groups. Our conclusion from this part of the study is that the short separation between the silicon atoms is not the result of any nascent bonding interaction, but instead represents a close van der Waals separation enforced by the steric demands involving the bulky dppm groups.

4.6 References

- 1) (a) Ogino, H.; Tobita, H. *Adv. Organomet. Chem.* **1998**, *42*, 223 and reference therein. (b) Corey, J. Y.; Braddock-Wilking, J. *Chem. Rev.* **1999**, *99*, 175 and references therein. (c) Corey, J. Y. *Chem. Rev.* **2011**, *111*, 863 and references therein.
- 2) (a) Aitken, C. T.; Harrod, J. F.; Samuel, E. *J. Am. Chem. Soc.* **1986**, *108*, 4059. (b) Zarate, E.A.; Tessier-Youngs, C. A.; Youngs, W. J. *J. Am. Chem. Soc.* **1988**, *110*, 4068. (c) Zarate, E.A.; Tessier-Youngs, C. A.; Youngs, W. J. *J. Chem. Soc. Chem. Comm.* **1989**, 577. (d) Heyn, R. H.; Tilley, T. D. *J. Am. Chem. Soc.* **1992**, *114*, 1917. (e) Rosenberg, L.; Fryzuk, M. D; Rettig, S. J. *Organometallics* **1999**, *18*, 958. (f) Shimada, S.; Rao, M. L. N.; Hayashi, T.; Tanaka, M. *Angew. Chem. Int. Ed. Engl.* **2001**, *40*, 213. (g) Corey, J. Y. *Adv. Organomet. Chem.* **2004**, *51*, 1. (h) Tanabe, M.; Yumoto, R.; Osakada, K. *Chem. Comm.* **2012**, *48*, 2125.
- 3) (a) Wang, W. -D.; Eisenberg, R. *J. Am. Chem. Soc.* **1990**, *112*, 1833. (b) Takao, T.; Suzuki, H.; Tanaka, T. *Organometallics* **1994**, *13*, 2554. (c)

- Tanabe, M.; Jiang, J.; Yamazawa, H.; Osakada, K.; Ohmura, T.; Suginome, M. *Organometallics* **2011**, *30*, 3981.
- 4) (a) Shimada, S.; Li, Y. -H.; Choe, Y. -K.; Tanaka, M.; Bao, M.; Uchimaru, T. *Proc. Natl. Acad. Sci. U.S.A.* **2007**, *104*, 7758–7763. (b) Yamada, T.; Mawatari, A.; Tanabe, M.; Osakada, K.; Tanase, T. *Angew. Chem. Int. Ed. Engl.* **2009**, *48*, 568. (c) Arai, H.; Takahashi, M.; Nanjo, M.; Mochida, K. *Organometallics* **2011**, *30*, 917. (d) Tanabe, M.; Ishikawa, M.; Chiba, M.; Ide, T.; Osakada, K.; Tanase, T. *J. Am. Chem. Soc.* **2011**, *133*, 18598.
- 5) Chen, W.; Shimada, S.; Tanaka, M. *Science* **2002**, *295*, 308.
- 6) (a) Suzuki, H.; Takao, T. Tanaka, M.; Moro-oka, Y. *J. Chem. Soc. Chem. Commun.* **1992**, 476. (b) Shimada, S.; Tanaka, M.; Honda, K. *J. Am. Chem. Soc.* **1995**, *117*, 8289. (c) Sanow, L. M.; Chai, M.; McConnville, D. B.; Galat, K. J.; Simons, R. S.; Rinaldi, P. L.; Youngs, W. J.; Tessier, C. A. *Organometallics* **2000**, *19*, 192. (d) Braddock-Wilking, J.; Levchinsky, Y.; Rath, N. P. *Organometallics* **2001**, *20*, 474. (e) Takao, T.; Amako, M.; Suzuki, H. *Organometallics* **2003**, *22*, 3855. (f) Tanabe, M.; Mawatari, A.; Osakada, K. *Organometallics* **2007**, *26*, 2937. (g) Tanabe, M.; Ito, D.; Osakada, K. *Organometallics*, **2008**, *27*, 2258.
- 7) Wang, W. -D.; Hommeltoft, S. I.; Eisenberg, R. *Organometallics* **1988**, *7*, 2417.
- 8) McDonald, R.; Cowie, M. *Organometallics* **1990**, *9*, 2468.
- 9) (a) Mobarok, M. H.; Oke, O.; Ferguson, M. J.; McDonald, R.; Cowie, M. *Inorg. Chem.* **2010**, *49*, 11556. (b) Mobarok, M. H.; Ferguson, M. J.;

- McDonald, R.; Cowie, M. *Inorg. Chem.* **2012**, *51*, 4020. (c) Mobarok, M. H.; Ferguson, M. J.; Cowie, M. *Organometallics* **2012**, *31*, 4722.
10. (a) Anderson, A. B.; Shiller, P.; Zarate, E. A.; Tessier-Youngs, C. A.; Youngs, W. J. *Organometallics* **1989**, *8*, 2320. (b) Aullón, G.; Alemany, P.; Alvarez, S. *J. Organomet. Chem.* **1994**, *478*, 75. (c) Sakaki, S.; Yamaguchi, S.; Musashi, Y.; Sugimoto, M. *J. Organomet. Chem.* **2001**, *635*, 17. (d) Nakajima, S.; Yokogawa, D.; Nakao, Y.; Sato, H.; Sakaki, H. *Organometallics* **2004**, *23*, 4672.
11. Aitken, C.; Harrod, J. F.; Malek, A.; Samuel, E. *J. Organometal. Chem.* **1988**, *349*, 385.
12. (a) Bender (IV), J. E.; Litz, K. E.; Giarikos, D.; Wells, N. J.; Banaszak Holl, M. M.; Kampf, J. W. *Chem. Eur. J.* **1997**, *3*, 1793. (b) Tanabe, M.; Osakada, K.; *Organometallics* **2010**, *29*, 4702; and references therein.
13. (a) Yanemitsu, Y.; Suzuki, K.; Kyushin, K. S.; Matsumoto, H. *Phys. Rev. B* **1995**, *51*, 13103. (b) Miller, R. D. *Chem. Rev.* **1989**, *89*, 1359.
14. (a) Isaka, H.; Fujiki, M.; Fujino, M. Matsumoto, N. *Macromolecules* **1991**, *24*, 2647. (b) Shono, T.; Kashimura, S.; Murase, S. *J. Chem. Soc. Chem. Commun.* **1992**, 897. (c) Sutherland, D. G. J.; Xiong, J. Z.; Liu, Z.; Sham, T. K.; Bancroft, G. M.; Baines, K. M.; Tan, K. H. *Organometallics* **1994**, *13*, 3671. (d) Huang, K.; Vermeulen, L. A. *Chem. Commun.* **1998**, 247. (e) Nanjo, M.; Sekiguchi, A. *Organometallics* **1998**, *17*, 492.
15. (a) Pannell, K. H.; Sharma, S. *Organometallics* **1991**, *10*, 1655. (b) Koe, J. R.; Tobita, H.; Ogino, H.; *Organometallics* **1992**, *11*, 2479.

16. (a) Kim, Y. -J.; Lee, S. -C.; Park, J. -I. *Organometallics* **1998**, *17*, 4929.
(b) Shimada, S.; Li, Y. -H.; Rao, M. L. N.; Tanaka, M. *Organometallics* **2006**, *25*, 3796.
17. (a) Tanabe, M.; Ishikawa, N.; Osakada, K. *Organometallics* **2006**, *25*, 796.
(b) White, C. P.; Braddock-Wilking, J.; Corey, J. Y.; Xu, H.; Redekop, E.; Sedinkin, S.; Rath, N. P. *Organometallics* **2007**, *26*, 1996. (c) Tanabe, M.; Ishikawa, N.; Hanzawa, M.; Osakada, K. *Organometallics* **2008**, *27*, 5152.
(d) Adams, R. D.; Trufan, E. *Inorg. Chem.* **2009**, *48*, 6124.
18. (a) Suzuki, H.; Takao, T.; Tanaka, M.; Moro-oka, Y. *J. Chem. Soc. Chem. Comm.* **1992**, 476. (b) Fryzuk, M. D. Rosenberg, L.; Rettig, S. J. *Inorg. Chim. Acta* **1994**, *222*, 345. (c) Brittingham, K. A.; Gallaher, T. N.; Schreiner, S. *Organometallics* **1995**, *14*, 1070. (d) Fryzuk, M. D. Rosenberg, L.; Rettig, S. J. *Organometallics* **1996**, *15*, 2871. (e) Bourg, S.; Boury, B.; Carré, F.; Corriu, R. J. P. *Organometallics* **1997**, *16*, 3097. (f) Osakada, K.; Koizumi, T.; Yamamoto, T. *Angew. Chem. Int. Ed. Engl.* **1998**, *37*, 349. (g) Ohki, Y.; Kojima, T.; Oshima, M.; Suzuki, H. *Organometallics* **2001**, *20*, 2654.
19. Wang, W. -D.; Eisenberg, R. *Organometallics* **1992**, *11*, 908.
20. Braddock-Wilking, J.; Corey, J. Y.; White, C. P.; Xu, H.; Rath, N. P. *Organometallics* **2005**, *24*, 4113.
21. (a) Janiak, C. *J. Chem. Soc., Dalton Trans.* **2000**, 3885. (b) Meyer, E. A.; Castellano, R. K.; Diederich, F. *Angew. Chem. Int. Ed. Engl.* **2003**, *42*,

1210. (c) Salonen, L. M.; Ellermann, M. Diederich, F. *Angew. Chem. Int. Ed. Engl.* **2011**, *50*, 4808.
22. He, L.; Ma, D. X.; Duan, L.; Weo, Y. G.; Qiao, J.; Zhang, D. Q. Dong, G. F.; Wang, L.D.; Qiu, Y. *Inorg. Chem.* **2012**, *51*, 4502.
23. (a) Benkeser, R. A.; Landesman, H.; Foster, D. J. *J. Am. Chem. Soc.* **1952**, *74*, 648. (b) Minge, O.; Nogai, S.; Schmidbaur, H. *Z. Naturforsch. B* **2004**, *59*, 153. (c) Prince, P. D.; Bearpark, M. J.; McGrady, G. S.; Steed, G. W. *Dalton Trans.* **2008**, 271.
24. McDonald, R.; Cowie, M. *Inorg.Chem.* **1990**, *29*, 1564.
25. Programs for diffractometer operation, data collection, data reduction, and absorption. correction were those supplied by Bruker.
26. Beurskens, P. T.; Beurskens, G.; de Gelder, R.; Smits, J. M. M.; Garcia-Granda, S.; Gould, R. O. (2008). The *DIRDIF-2008* program system. Crystallography Laboratory, Radboud University Nijmegen, The Netherlands.
27. Sheldrick, G. M. *Acta Crystallogr.* **2008**, *A64*, 112.
28. Wiberg, N.; Schuster, H.; Simon, A.; Peter, K. *Angew. Chem.Int. Ed. Engl.* **1986**, *25*, 79.
29. Mantina, M.; Chamberlin, A. C.; Valero, R.; Cramer, C. J.; Truhlar, D. G. *J. Phys. Chem. A* **2009**, *113*, 5806.
30. (a) Baines, K. M.; Stibbs, W. G.; *Coord. Chem. Rev.* **1995**, *145*, 157. (b) Lee, V. Y.; Ichinohe, M.; Sekiguchi, A. *J. Organomet. Chem.* **2003**, *685*, 168.

Chapter 5

Multiple Si–H Bond Activations in a Bis(diethylphosphino)methane-bridged Complex of Rh and Ir: Synthesis of an Unusual Bis(silyl)/(μ -silylene) Complex.^V

5.1 Introduction

Transition metal complexes containing silyl or silylene ligands are effective catalysts in a number of reactions, including those involving industrially important silicon-carbon and silicon-silicon bond formation.¹⁻⁴ Recent investigations suggest that monometallic complexes containing both silyl and silylene ligands can act as intermediates in silicon–silicon bond formation, silane oligomerization, isomerization and redistribution.⁵⁻⁹ Among these transformations, Si–Si bond formation during silane oligomerization is proposed to occur via facile 1,2-silyl migration from the transition-metal centre to the silylene group within the coordination sphere of monometallic silyl/silylene complexes.⁵ There are precedents for metal-to-metal silyl migration in two heterobimetallic (Fe/Pt¹⁰ and Rh/Pt¹¹) complexes, and in both cases the silyl group migrates from the more labile to the less labile metal. It is of interest to determine whether such silyl migrations can take place within a bimetallic core from either metal to a bridging silylene ligand, instead of merely between metals; such reactivity has not been observed to date.

The nature of the pair of metals in such bimetallic compounds has been shown to exert a significant influence on the reactivity. In a previous study on silane activation by a diphosphine-bridged diiridium complex, our group

^V A version of this Chapter has been published. Mobarok, M. H.; Ferguson, M. J.; McDonald, R.; Cowie, M. *Organometallics* **2012** *3*, 4722.

demonstrated that one bridging SiR₂ unit could be incorporated through reactions of an Ir₂ precursor with primary and secondary silanes, but reaction with a second equivalent of silane was not observed.¹² In contrast, a related dirhodium system, studied by Eisenberg and coworkers, readily incorporates two bridging SiHR units in reactions involving primary silanes to produce bis(silylene)-bridged complexes.¹³ In the second Chapter of this thesis we described an unusual example of a heterobimetallic silyl/μ-silylene complex, [RhIr(H)(SiPh₂H)(CO)₃(κ¹-dppm)(μ-SiPh₂)(dppm)].¹⁴ An analogous germyl/μ-germylene complex, [RhIr(H)(GePh₂H)(CO)₃(κ¹-dppm)(μ-GePh₂)(dppm)], has also been prepared and discussed in the third Chapter of this work.¹⁵ This type of bimetallic complex, containing both bridging silylene and terminal silyl groups is not common.^{11, 14-16} As has been proposed in the second and third chapter, that dissociation of one end of a dppm ligand could play a pivotal role in the incorporation of the second Si- or Ge-containing fragment by generating the required coordinative unsaturation for oxidative addition of the second silane or germane and in easing the steric crowding at the metals. In the case of disubstituted silyl/μ-silylene or germyl/μ-germylene examples, the steric bulk of these groups combined with the bulk of the dppm ligands prevented recoordination of the pendent dppm group that resulted in addition of the second silane.^{14,15} In those studies, we had also observed significant differences in reactivity involving primary and secondary silanes or germanes, in which bis(μ-silylene), bis(μ-germylene) or μ-silylene/μ-germylene complexes could not be generated when both groups were disubstituted.^{14,15,17} Clearly, steric factors play a

significant role in the incorporation of two or more Si- or Ge-containing fragments into the bimetallic core. For this reason, we set out to investigate related chemistry involving bis(diethylphosphino)methane (dep_m = Et₂PCH₂PEt₂) instead of dp_{pm}, in order to determine what role this smaller diphosphine might play in this chemistry. In addition, in second Chapter, we had proposed the involvement of unobserved intermediates containing three Si-containing fragments during isomerization of *bis*(μ-silylene) complexes¹⁴ and set out to determine if such species could be observed with the smaller dep_m group as a bridging ligand. Finally, the incorporation of Si- and Ge-containing fragments was brought about by the multiple oxidative additions of Si–H and Ge–H bonds, which should also be more favourable in complexes involving the more basic dep_m ligand, adding further incentive for investigating this chemistry, the initial results of which are discussed in this chapter.

5.2 Experimental

5.2.1 General Comments

All solvents were dried (using appropriate drying agents), distilled before use, and stored under dinitrogen. Reactions were performed under an argon atmosphere using standard Schlenk techniques. Ph₂SiH₂ and PhSiH₃ were purchased from Sigma-Aldrich; while MesSiH₃ (Mes = mesityl) was prepared according to the literature method.¹⁸ Silanes were dried over CaH₂ and distilled under Ar before use. ¹³C-enriched CO (99.4%) was purchased from Cambridge Isotope Laboratories, while [RhIr(CO)₃(dep_m)₂] (**44**) was prepared as previously reported¹⁹ and kept as a benzene solution under Ar at –20 °C (**44** is unstable in

CH₂Cl₂ over extended periods of time even at –20 °C) but benzene was removed under high vacuum prior to the reactions carried out in other solvents. NMR spectra were recorded on Varian Inova-400 or Varian Unity-500 spectrometers operating at the resonance frequencies for the NMR nuclei as given in the spectral information. The ¹H, ¹³C{¹H} and ²⁹Si{¹H} NMR spectra were referenced internally to residual solvent proton signals relative to tetramethylsilane whereas ³¹P{¹H} spectra were referenced relative to external 85 % H₃PO₄. All spectra were recorded at 27 °C unless otherwise noted. Infrared spectra were obtained on a Nicolet Avatar 370 DTGS spectrometer. The elemental analyses were performed by the Microanalytical Laboratory in the department.

5.2.2 Preparation of Compounds

a. **[RhIr(H)₂(CO)₂(μ-SiHPh)(depm)₂] (45)**: A total of 53 mg of [RhIr(CO)₃(depm)₂] (**44**) (0.069 mmol) was taken into a 10 mL Schlenk tube in 2 mL of CH₂Cl₂ followed by the addition of 10 μL of phenylsilane (0.081 mmol) to the solution by a microliter syringe. The colour of the solution changed from dark red to orange within 30 min. After 1 h the ³¹P{¹H} NMR spectrum suggested quantitative formation of complex **45**. The solvent was removed under high vacuum, followed by dissolution of the compound in 0.5 mL of toluene. Slow addition of 5 mL of pentane yielded a brown powder of compound **45**. ³¹P{¹H} NMR (27 °C; C₇D₈, 161.8 MHz): δ 23.7 (Rh–P, bm, 1P), 8.2 (Rh–P, bm, 1P), –16.7 (Ir–P, bm, 1P), –23.9 (Ir–P, bm, 1P); ¹H NMR (27 °C; C₇D₈, 399.8 MHz): δ 7.1 (Si–H, b, 1H), 2.9 (CH₂, b, 2H), 2.4 (CH₂, b, 2H), –10.70 (Rh–H, m, 1H), –11.96 (Ir–H, m, 1H); ³¹P{¹H} NMR (–80 °C; CD₂Cl₂, 161.8 MHz): δ 25.3 (Rh–P,

bm, 1P), 8.3 (Rh–P, dd, $^1J_{\text{RhP}} = 108$ Hz, $^2J_{\text{PP}} = 138$ Hz), –15.3 (Ir–P, m, 1P), –23.7 (Ir–P, m, 1P); ^1H NMR (–80 °C; CD_2Cl_2 , 399.8): δ 7.30 (Si–H, bs, 1H, $^1J_{\text{SiH}} = 180$), 3.04 (PCH₂P, m, 1H), 2.80 (PCH₂P, m, 1H), 0.70 – 2.10 (C₂H₅, m, 40H), –10.63 (Rh–H, ddm, 1H, $^2J_{\text{trans-PH}} = 154.0$, $J_{\text{RhH}} = 12$ Hz), –11.85 (Ir–H, dm, 1H, $^2J_{\text{trans-PH}} = 122$ Hz); $^{13}\text{C}\{^1\text{H}\}$ NMR (–80 °C, C₇D₈, 100.5 MHz): δ 194.4 (Rh–CO, dt, 1C, $^1J_{\text{RhC}} = 70.0$ Hz), 181.4 (Ir–CO, t, 1C), 48.5 (PCH₂P, 1C, m), 43.8 (PCH₂P, 1C, m). $^{29}\text{Si}\{^1\text{H}\}$ NMR (–80 °C, C₇D₈, 78.5 MHz, DEPT): δ 134.3 (dt, $^1J_{\text{SiRh}} = 32$ Hz, $^2J_{\text{PSi}} = 70$ Hz).

b. [RhIr(H)₂(CO)₂(μ -SiHMes)(depm)₂] (46): 50 mg (0.065 mmol) of [RhIr(CO)₃(depm)₂] (**44**) was taken into a Schlenk flask and dissolved in 2 mL of toluene. 10.9 μL (0.065 mmol) of C₆H₂Me₃SiH₃ was added to the stirring solution by a microliter syringe. The reaction was allowed to stir for 3 h. Slow addition of 10 mL of pentane yielded a brown powder of compound **46** in 73 % isolated yield. Anal. calcd. for: C₂₉H₅₈IrO₂P₄RhSi: C, 39.29; H, 6.55. Found: C, 39.52; H, 6.71. $^{31}\text{P}\{^1\text{H}\}$ NMR (27 °C; CD_2Cl_2 , 161.8 MHz): δ 21.6 (Rh–P, bm, 1P), 6.9 (Rh–P, bm, 1P), –19.3 (Ir–P, bm, 1P), –25.0 (Ir–P, bm, 1P); ^1H NMR (27 °C; CD_2Cl_2 , 399.8 MHz): δ –10.54 (Rh–H, bm, 1H), –11.96 (Ir–H, bm, 1H); $^{31}\text{P}\{^1\text{H}\}$ NMR (–80 °C; CD_2Cl_2 , 161.8 MHz): δ 23.2 (Rh–P, ddm, $^1J_{\text{RhP}} = 94$ Hz, $^2J_{\text{PP}} = 120$ Hz), 6.9 (Rh–P, ddm, 1P, $^1J_{\text{RhP}} = 104$ Hz, $^2J_{\text{PP}} = 118$ Hz), –17.3 (Ir–P, dm, 1P, $^2J_{\text{PP}} = 120$ Hz), –24.9 (Ir–P, 1P, dm, $^2J_{\text{PP}} = 120$ Hz); ^1H NMR (–80 °C; CD_2Cl_2 , 399.8 MHz): δ 7.22 (Si–H, bs, 1H, $^1J_{\text{SiH}} = 180$ Hz), 7.00 (Ar–H, s, 2H), 3.43 (*o*-CH₃, bs, 6H), 2.94 (PCH₂P, m, 1H), 2.54 (PCH₂P, m, 1H), 2.31 (*p*-CH₃, m, 3H), 2.02 (PCH₂P, m, 1H), 1.94 (PCH₂P, m, 1H), 1.92 – 0.78 (C₂H₅, m, 40 H);

-10.60 (Rh-H, ddm, 1H, $^2J_{trans\ PH} = 155$ Hz, $^1J_{RhH} = 11$ Hz), -11.79 (Ir-H, dm, 1H, $^2J_{trans\ PH} = 126$); $^{13}C\{^1H\}$ NMR (27 °C; CD₂Cl₂, 100.5 MHz): δ 194.4 (Rh-CO, dm, 1C, $^1J_{RhC} = 65.0$ Hz), 181.0 (Ir-CO, bs, 1C), 48.2 (PCH₂P, m, 1C), 32.4 (PCH₂P, m, 1C). $^{29}Si\{^1H\}$ NMR (-80 °C; CD₂Cl₂, 78.5 MHz, DEPT): δ 104.0 (m).

c. **[RhIr(CO)₂(μ -SiHPh)₂(depm)₂](47)**: Under an atmosphere of Ar, 60 mg (0.079 mmol) of [RhIr(CO)₃(depm)₂] (**44**) was taken into a 10 mL Schlenk tube and dissolved in 5 mL of benzene followed by the addition of 39 μ L (0.32 mmol, 4 equiv) of phenylsilane by microliter syringe. The tube was set in an oil bath at 60 °C for 1h, during which time the dark red solution turned orange. Addition of 5 mL of ether resulted in the precipitation of a light brown powder in 53 % (40 mg) isolated yield. Single crystals of **47** were obtained by slow diffusion of ether into concentrated solution of benzene. However, due to extreme disorder, this structure could not be refined acceptably. Anal. calcd. for C₃₂H₅₆IrO₂P₄RhSi₂: C, 40.51; H, 5.91. Found: C, 40.79; H, 5.27. Compound **47** can also be prepared by reacting benzene solution of **45** (45 mg, 0.059 mmol) with excess phenylsilane (2 equiv, 15 μ L) at 60 °C within 1h. $^{31}P\{^1H\}$ NMR (27 °C; C₆D₆, 161.8 MHz): δ 18.3 (Rh-P, dm, 2P, $^1J_{RhP} = 102$ Hz), -15.4 (Ir-P, m, 2P); 1H NMR (27 °C; C₆D₆, 399.8 MHz): δ 6.48 (Si-H, m, 2H, $^1J_{SiH} = 161$ Hz), 2.92 (PCH₂P, m, 2H), 1.30 (PCH₂P, m, 2H) 1.90 – 0.85 (C₂H₅, m, 40 H); $^{13}C\{^1H\}$ NMR (27 °C; CD₂Cl₂, 100.5 MHz): δ 197.7 (Rh-CO, dm, 1C, $^1J_{RhC} = 73$ Hz), 184.9 (Ir-CO, bs, 1C), 33.4 (PCH₂P, m, 2C); $^{29}Si\{^1H\}$ NMR (27 °C; CD₂Cl₂, 79.5 MHz, DEPT): δ 115.3 (m).

d. [RhIr(CO)₂(μ-CO)(μ-SiHMes)(depm)₂] (48): Under an atmosphere of Ar, 60 mg (0.079 mmol) of [RhIr(CO)₃(depm)₂] (**44**) was dissolved in 2 mL of toluene in a Schlenk tube followed by the addition of 26 μL (0.16 mmol, 2 equiv) of mesitylsilane by microliter syringe. The tube was set in an oil bath at 60 °C overnight under dynamic CO atmosphere. During this time a light-yellow precipitate settled from the solution. The supernatant was removed by cannula and the solid was washed 3 times with 15 mL of pentane. The residual solvent was removed under high vacuum and analytically pure complex **48** was obtained in 63 % (45 mg) isolated yield. Anal. calcd. for C₃₀H₅₄IrO₃P₄RhSi: C, 39.48; H, 5.92. Found: C, 39.61; H, 6.09. Compound **48** can also be generated by purging CO through a toluene solution of complex **46**. ³¹P{¹H} NMR (27 °C; CD₂Cl₂, 201.6 MHz): δ 28.6 (Rh–P, ddd, 1P, ¹J_{RhP} = 102 Hz, ²J_{PP} = 281 Hz, ²J_{PP} = 24 Hz), 23.2 (Rh–P, 1P, ddd, ¹J_{RhP} = 97 Hz, ²J_{PP} = 185 Hz, ²J_{PP} = 20 Hz), –12.0 (Ir–P, dd, 1P, ²J_{PP} = 281 Hz, ²J_{PP} = 24 Hz), –12.2 (Ir–P, dd, 1P, ²J_{PP} = 185 Hz, ²J_{PP} = 20 Hz); ¹H NMR (27 °; CD₂Cl₂, 498.1 MHz): δ 6.77 (*m*-Ph–H, s, 2H), 5.17 (Si–H, m, 1H, ¹J_{SiH} = 167 Hz), 2.77 (PCH₂P, m, 1H), 2.67 (*o*-CH₃, m, 6H) 2.45 (PCH₂P, m, 2H), 2.23 (*p*-CH₃, m, 3H), 2.30 – 1.03 (C₂H₅, m, 40H), 0.70 (PCH₂P, m, 1H) ¹³C{¹H} NMR (27 °C; CD₂Cl₂, 125.7 MHz): δ 242.9 (μ-CO, dm, 1C, ¹J_{RhC} = 27 Hz), 194.4 (Rh–CO, dm, 1C, ¹J_{RhC} = 78 Hz), 182.5 (Ir–CO, bs, 1C), 32.1(PCH₂P, m, 1C), 24.2 (PCH₂P, m, 1C). ²⁹Si{¹H} NMR (27 °C; CD₂Cl₂, 78.5 MHz, DEPT): δ 52.2 (m).

e. [RhIr(H)₂(CO)₂(μ-SiPh₂)(depm)₂] (49): Under an atmosphere of Ar, 52 mg (0.068 mmol) of [RhIr(CO)₃(depm)₂] (**44**) was dissolved in a 1 mL of toluene in a

Schlenk tube followed by the addition of 12.6 μL (0.068 mmol) of diphenylsilane by microliter syringe. The reaction mixture was stirred for 3 h. Layering the toluene solution with 2 mL of pentane in an NMR tube yielded light yellow crystals (suitable for X-ray analysis) in 29 % (18 mg) isolated yield. $^{31}\text{P}\{^1\text{H}\}$ NMR (27 $^\circ\text{C}$; C_7D_8 , 161.9 MHz): δ 17.7 (Rh–P, m, 2P), –19.4 (Ir–P, m, 2P); ^1H NMR (27 $^\circ\text{C}$; C_7D_8 , 399.8 MHz): δ –10.51 (Rh–H, m, 1H), –12.05 (Ir–H, m, 1H); $^{31}\text{P}\{^1\text{H}\}$ NMR (–80 $^\circ\text{C}$, C_7D_8 , 161.8 MHz): δ 17.4 (Rh–P, dm, 1P, $^1J_{\text{RhP}} = 101$ Hz), 12.1 (Rh–P, dm, 1P, $^1J_{\text{RhP}} = 105$ Hz), –21.6 (Ir–P, m, 1P), –23.3 (Ir–P, m, 1P); ^1H NMR (–80 $^\circ\text{C}$; C_7D_8 , 399.8 MHz): δ 7.25–7.06 (Ph–H, m, 10 H), 2.87 (PCH₂P, m, 2H), 2.27 (PCH₂P, m, 2H), 1.87 – 0.28 (C₂H₅, m, 40H), –10.61 (Rh–H, ddm, 1H, $^2J_{\text{trans PH}} = 152$ Hz, $^1J_{\text{RhH}} = 11$ Hz), –12.06 (Ir–H, dm, 1H, $^2J_{\text{trans PH}} = 120$ Hz); $^{13}\text{C}\{^1\text{H}\}$ NMR (–80 $^\circ\text{C}$; C_7D_8 , 100.5 MHz): δ 198.1 (Rh–CO, dm, 1C, $^1J_{\text{RhC}} = 67$ Hz), 184.5 (Ir–CO, bs, 1C), 48.1 (PCH₂P, m, 1C), 30.2 (PCH₂P, m, 1C); $^{29}\text{Si}\{^1\text{H}\}$ NMR (27 $^\circ\text{C}$; C_7D_8 , 78.5 MHz, DEPT): δ 148.1 (m).

f. **[RhIr(H)(SiPh₂H)(CO)₃(κ^1 -dep μ)(μ -SiPh₂)(dep μ)] (50):** Under an atmosphere of Ar, 100 mg (0.131 mmol) of [RhIr(CO)₃(dep μ)₂] (**44**) was dissolved in a 5 mL of toluene in a Schlenk tube followed by the addition of 97 μL (0.52 mmol) of diphenylsilane by microliter syringe. The tube was set in an oil bath at 60 $^\circ\text{C}$ overnight under a dynamic CO atmosphere. During this time the colour of the solution changed from dark red to orange accompanied by the precipitation of a light green solid. The supernatant was separated by cannula and the solvent was removed to give a brown oil. The oil was further washed with 3 \times 5 mL of pentane and dried under high vacuum to give compound **50** in 47 % (69

mg) isolated yield. This complex could not be obtained analytically pure as the oil contained some unidentified impurities. The solid was identified to be compound **51** (described below). $^{31}\text{P}\{^1\text{H}\}$ NMR (27 °C; CD_2Cl_2 , 161.8 MHz): δ -3.9 (Rh-P, ddd, 1P, $^1J_{\text{RhP}} = 94$ Hz, $^2J_{\text{PP}} = 86$ Hz, $^3J_{\text{PP}} = 4$ Hz), -7.5 (Ir-P, dddd, 1P, $^2J_{\text{PP}} = 32$ Hz, $^2J_{\text{PP}} = 9$ Hz, $^3J_{\text{PP}} = 11$ Hz, $^3J_{\text{RhP}} = 5$ Hz), -27.1 (Ir-P, ddd, 1P, $^2J_{\text{PP}} = 86$ Hz, $^3J_{\text{PP}} = 11$ Hz, $^3J_{\text{PP}} = 4$ Hz, $^4J_{\text{PP}} = 5$ Hz), -35.0 (Pendent-P, dd, 1P, $^2J_{\text{PP}} = 32$ Hz, $^4J_{\text{PP}} = 5$); ^1H NMR (27 °C; CD_2Cl_2 , 399.8 MHz): δ 6.02 (Si-H, d, 1H, $^1J_{\text{SiH}} = 177$ Hz, $^3J_{\text{PH}} = 4$ Hz), 2.60 (PCH₂P, m, 1H), 1.92 (PCH₂P, m, 1H), 1.84 (PCH₂P, m, 1H), 1.14 (PCH₂P, m, 1H), 2.15 - 0.55 (C₂H₅, m, 40H), -11.93 (Ir-H, dd, 1H, $^2J_{\text{PH}} = 20$ Hz); $^{13}\text{C}\{^1\text{H}\}$ NMR (27 °C; CD_2Cl_2 , 100.5 MHz): δ 205.2 (Rh-CO, dd, 1C, $^1J_{\text{RhC}} = 56$ Hz, $^2J_{\text{PC}} = 10$ Hz), 202.4 (Rh-CO, dm, 1C, $^1J_{\text{RhC}} = 54$ Hz), 187.1 (Ir-CO, m, 1C), 54.3 (PCH₂P, m, 1C), 38.1 (PCH₂P, m, 1C); $^{29}\text{Si}\{^1\text{H}\}$ NMR (27 °C; CD_2Cl_2 78.5 MHz, gHSQC): δ -3.4 (m), 143.3 (m).

g. [RhIr(SiPh₂H)₂(CO)₂(μ -SiPh₂)(dep μ)] (51**):** Under an atmosphere of Ar, 200 mg (0.262 mmol) of [RhIr(CO)₃(dep μ)₂] (**44**) was dissolved in 7 mL of toluene in a Schlenk tube followed by the addition of 194 μL (1.048 mmol, 4 equiv) of diphenylsilane by microliter syringe. The tube was set in an oil bath at 80 °C overnight under dynamic CO atmosphere. During this time a light-green precipitate settled from solution. The supernatant was removed by cannula and the solid was washed 3 times with 15 mL of pentane. Removal of residual solvents under high vacuum yielded analytically pure compound **51** in 43 % (123 mg) isolated yield. Anal. calcd. for C₄₉H₅₄IrO₄P₄RhSi₃: C, 51.21; H, 4.70. Found: C, 51.49; H, 4.74. $^{31}\text{P}\{^1\text{H}\}$ NMR (27 °C; CD_2Cl_2 , 201.6 MHz): δ -1.9 (Rh-P, dd, 1P,

$^1J_{\text{RhP}} = 92$ Hz, $^2J_{\text{PP}} = 70$ Hz), -30.5 (Ir–P, d, 1P, $^1J_{\text{PP}} = 70$ Hz). ^1H NMR (27 °C; CD_2Cl_2 , 498.1 MHz): δ 7.75 – 6.99 (Ph–H, m, 30 H), 5.95 (Ir–Si–H, d, 1H, $^1J_{\text{SiH}} = 182$ Hz, $^3J_{\text{PH}} = 4$ Hz), 5.74 (Rh–Si–H, d, 1H, $^1J_{\text{SiH}} = 182$ Hz, $^3J_{\text{PH}} = 5$ Hz), 3.08 (PCH₂P, t, 2H, $^2J_{\text{PH}} = 11$ Hz), 1.79–0.93 (CH₃–CH₂, m, 20H); $^{13}\text{C}\{^1\text{H}\}$ NMR (27 °C; CD_2Cl_2 , 125.7 MHz): δ 202.5 (Rh–CO, dd, 2C, $^1J_{\text{RhC}} = 54$ Hz, $^2J_{\text{PC}} = 12$ Hz), 187.7 (Ir–CO, d, 2C, $^2J_{\text{PC}} = 11$ Hz), 45.5 (PCH₂P, m, 1C); $^{29}\text{Si}\{^1\text{H}\}$ NMR (27 °C; CD_2Cl_2 , 78.5 MHz, DEPT, gHSQC): δ 136.9 (μ -Si, m) -2.3 (Rh–Si, d, $^1J_{\text{RhSi}} = 23$), -23.1 (Ir–Si, s).

5.3 X-ray Data Collection and Structure Determination.

5.3.1 General considerations.

Single crystals suitable for X-ray diffraction were obtained by the slow diffusion of pentane into CH_2Cl_2 (**48** and **51**) and toluene (**49**) solutions of the compounds. Data were collected on either a Bruker D8/APEX II CCD diffractometer (**48**, **49**) or Bruker PLATFORM/APEX II CCD (**51**) diffractometer at -100 °C using Mo K α radiation.²⁰ Data were corrected for absorption through the use of Gaussian integration from indexing of the crystal faces. All structures were solved by direct methods (*SHELXS-97*).²¹ Refinement was carried out using the program *SHELXL-97*.²¹ Hydrogen atoms attached to carbons were assigned positions on the basis of the sp^2 or sp^3 hybridization geometries of their parent atoms and were given isotropic displacement parameters 20 % greater than the U_{eq} 's of their parent carbons. Metal-hydrides for **49** and Si-bound hydrogens for **48** and **51** were located from difference Fourier maps and treated as detailed

below. A listing of crystallographic experimental data is provided for all structures as Appendix IV.

5.3.2 Special refinement conditions.

i. Compound 48. One metal atom site [labeled Ir] was refined with a site occupancy of 67% Ir and 33% Rh; the other site [labeled Rh] was refined as 67% Rh and 33% Ir. The silicon-bound hydrogen atom was given an isotropic displacement parameter 20% greater than the silicon atom; and its coordinates were allowed to freely refine.

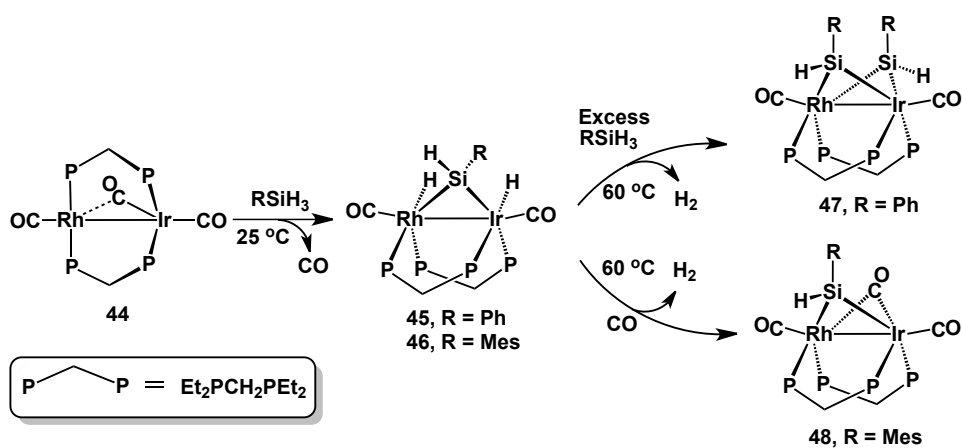
ii. Compound 49. Metal positions were refined with 50% site occupancy of Ir and Rh. The Ir- and Rh-bound hydrides were constrained to have a M–H distance of 1.60 Å and were given isotropic displacement parameters 20% greater than the metal atoms to which they are attached.

iii. Compound 51. The “IrRh(CO)₄(dep_m)” fragment of the molecule was found to be disordered about the crystallographic 2-fold rotation axis that passes through Si(2) and approximately bisects the Ir–Rh bond. Pairs of atoms [Ir and Rh, P(1) and P(2), O(1) and O(3), O(2) and O(4), C(1) and C(3), and C(2) and C(4)] that are pseudo-related by the rotation axis were refined with equivalent anisotropic displacement parameters. Additionally, the P(1)–C(5) and P(2)–C(5) distances were restrained to be approximately equal.

5.4 Results and Compound Characterizations

Reaction of the *bis*(diethylphosphino)methane-bridged complex, $[\text{RhIr}(\text{CO})_3(\text{dep}m)_2]$ (**44**) ($\text{dep}m = \text{Et}_2\text{PCH}_2\text{PEt}_2$) with one equiv of primary silanes (RSiH_3 , $\text{R} = \text{Ph}$ and Mes) yields the respective mono(silylene)-bridged dihydride complexes, $[\text{RhIr}(\text{H})_2(\text{CO})_2(\mu\text{-SiHR})(\text{dep}m)_2]$ (**45**, $\text{R} = \text{Ph}$; **46**, $\text{R} = \text{Mes}$) by double Si–H bond activation (Scheme 5.1) much as reported for the *dppm*-bridged systems.¹²⁻¹⁵ The rate of formation of **45** is slower than that for the

Scheme 5.1



previously reported *dppm* analogue, $[\text{RhIr}(\text{H})_2(\text{CO})_2(\mu\text{-SiHPh})(\text{dpp}m)_2]$ under similar reaction conditions.¹⁴ While the formation of $[\text{RhIr}(\text{H})_2(\text{CO})_2(\mu\text{-SiHPh})(\text{dpp}m)_2]$ was complete within 30 min, in the same time period conversion of **44** to **45** was only half complete. This slight rate inhibition in the *dep*m chemistry may result from the lower tendency for carbonyl loss from the more electron rich *dep*m species compared to the *dppm* analogue. Both **45** and **46** display fluxional behaviour at room temperature, as is evident by the broad and

unresolved peaks in the ^1H NMR and $^{31}\text{P}\{^1\text{H}\}$ NMR spectra, which upon cooling to $-80\text{ }^\circ\text{C}$ gives rise to well resolved peaks. This fluxionality resembles that of previously characterized dppm-bridged mono(μ -silylene) dihydride complexes of Rh_2 ¹³ and Rh/Ir ^{14,15} so was not investigated in this study. In the $^{31}\text{P}\{^1\text{H}\}$ NMR spectra at $-80\text{ }^\circ\text{C}$ both complexes display four multiplets, in which two downfield resonances are assigned to the Rh-bound ^{31}P -nuclei on the basis of the observed Rh–P coupling. The ^1H NMR spectra display two multiplets between $\delta -10.0$ to -12.0 for the metal-bound hydrides while the silicon-bound protons appear as a broad singlet at *ca.* $\delta 7.2$. A multiplet is observed in the $^{29}\text{Si}\{^1\text{H}\}$ NMR spectrum at *ca.* $\delta 134.3$ for **45** and 104.0 for **46** consistent with a bridging silylene unit.^{1b, 22}

Reaction of the phenylsilylene dihydride complex (**45**) with excess phenylsilane (2 equiv) at $60\text{ }^\circ\text{C}$ yields a bis(silylene)-bridged complex, $[\text{RhIr}(\text{CO})_2(\mu\text{-SiHPh})_2(\text{dep}m)_2]$ (**47**), incorporating a second bridging silylene unit, accompanied by the reductive elimination of two equiv of H_2 (Scheme 5.1). This reaction requires only 1 h for completion in contrast to the formation of the dppm analogue, $[\text{RhIr}(\text{CO})_2(\mu\text{-SiHPh})_2(\text{dpp}m)_2]$,¹³ which requires over 12 h to form under similar reaction conditions. In this case, the observed rate increase might be attributed to the lower steric demand and higher electron-donating ability of the depm ligand, which allows better substrate access to the metals and facilitates the oxidative addition of the Si–H bonds, respectively. Owing to higher symmetry of this complex compared to **45**, the $^{31}\text{P}\{^1\text{H}\}$ NMR spectrum of **47** displays only two multiplets in which the downfield resonance is again assigned to the Rh-bound ^{31}P nuclei. The two silicon-bound protons appear as a multiplet at

δ 6.48 in the ^1H NMR spectrum while in the $^{29}\text{Si}\{^1\text{H}\}$ NMR spectrum a multiplet is observed for the two chemically equivalent bridging silylene units at δ 115.3. The $^{13}\text{C}\{^1\text{H}\}$ NMR spectrum displays a doublet of multiplets (at δ 197.7) and a singlet (at δ 184.9) for Rh and Ir-bound carbonyls, respectively. We were unable to obtain X-ray structural information for compound **47** owing to extensive disorder in the crystals.

The reaction of **46** with CO at elevated temperature (60 °C) yields a carbonyl- and silylene-bridged complex, $[\text{RhIr}(\text{CO})_2(\mu\text{-CO})(\mu\text{-SiHMes})(\text{depM})_2]$ (**48**), in 63% yield (see Scheme 5.1). Interestingly, the reaction of **2** with CO under similar reaction conditions did not yield the phenylsilylene analogue, and increasing the reaction temperature to 80 °C led only to decomposition. Although the analogous phenylsilylene-bridged dppm species, $[\text{RhIr}(\text{H})_2(\text{CO})_2(\mu\text{-SiHPh})(\text{dppM})_2]$ did react with CO under similar conditions, the tricarbonyl product, $[\text{RhIr}(\text{CO})_2(\mu\text{-CO})(\mu\text{-SiHR})(\text{dppM})_2]$, was only obtained in very low yield (15 %).

The $^{31}\text{P}\{^1\text{H}\}$ NMR spectrum of **48** displays four multiplets at δ 28.6, 23.2, -12.0 and -12.2, for which the two downfield peaks display Rh-P coupling of 102 and 97 Hz, respectively. The $^{13}\text{C}\{^1\text{H}\}$ NMR spectrum displays three multiplets at δ 242.9 ($^1J_{\text{RhC}} = 27$ Hz), 194.4 ($^1J_{\text{RhC}} = 78$ Hz) and 182.5 corresponding to the bridging, Rh- and Ir-bound carbonyls, respectively. The Si-bound proton appears as a multiplet at δ 5.17 in the ^1H NMR spectrum while a multiplet is observed in the $^{29}\text{Si}\{^1\text{H}\}$ NMR spectroscopy for the bridging silylene unit at δ 52.2.

The structure of complex **48** is shown in Figure 5.1, confirming the formulation described above, in which the bridging-carbonyl is pseudo-trans to one bridging depm ligand while the bridging mesitylsilylene unit is pseudo-trans to the other. Although this type of silylene-carbonyl-bridged species was characterized by NMR in previously reported Rh₂¹³ and RhIr systems,¹⁴ they were not crystallographically characterized. The Rh–Ir distance (2.6961(2) Å) in **48**

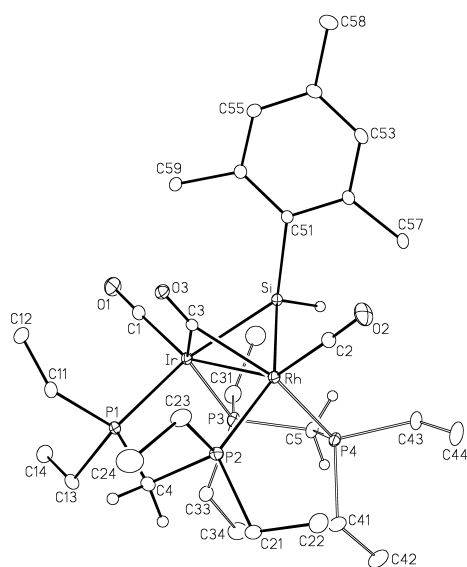


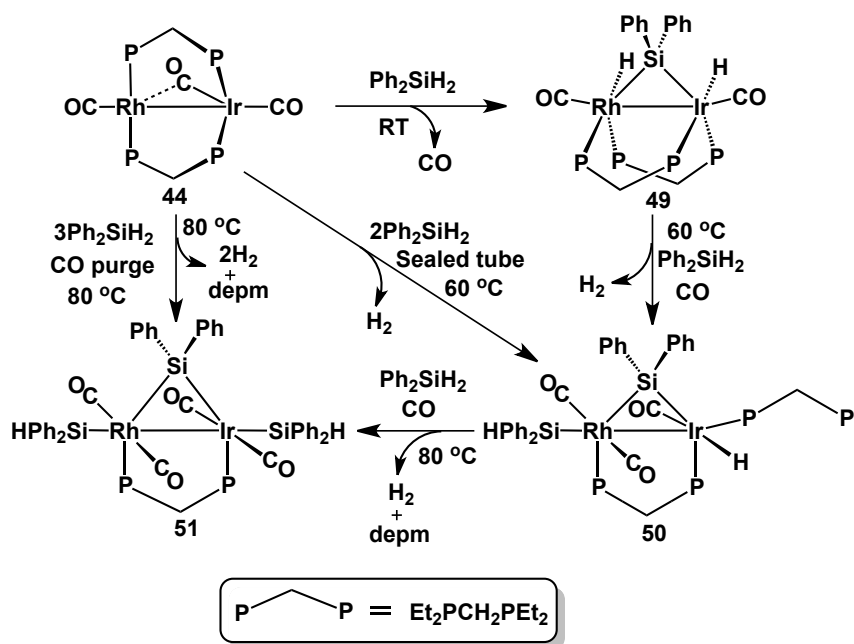
Figure 5.1: Perspective view of the major disordered form of compound **48** showing the numbering scheme. Non-hydrogen atoms are represented by Gaussian ellipsoids at the 20% probability level. Hydrogen atoms are shown arbitrarily small. One metal atom position was refined with a site occupancy of 67 % Ir/ 33 % Rh; the other was refined as 67 % Rh/ 33 % Ir.

is significantly shorter than the previously reported mono(μ -silylene), bis(μ -silylene) and silyl/(μ -silylene) complexes of Rh/Ir for which separations of *ca.* 2.83 to 2.86 Å were typical.¹⁴ As a consequence, the Ir–Si–Rh angle (68.95(2)°) is also more acute than those of previous determinations (*ca.* 72.0°).¹⁴ This shorter

separation and accompanying acute Rh–Si–Ir angle may reflect less crowded environments at the metals by virtue of the smaller diphosphines, or may be a function of the small accompanying bridging carbonyl group requiring a closer metal approach to optimize orbital overlap with the metals. However, the significantly longer Rh–Ir separation in a related structure (**49**, *vide infra*) appears to suggest that the shorter Rh–Ir separation in **48** is not solely steric in origin. Both carbonyl and silylene groups are symmetrically bridged. (Rh–C(3) = 2.061(2) Å, Ir–C(3) = 2.047(2) Å and Rh–Si = 2.3759(6) Å, Ir–Si = 2.3874(6) Å).

Reaction of one equiv of a secondary silane (Ph_2SiH_2) with complex **44** again yields a mono(silylene)-bridged product, $[\text{RhIr}(\text{H})_2(\text{CO})_2(\mu\text{-SiPh})(\text{depm})_2]$ (**49**) (Scheme 5.2), closely resembling complexes **45** and **46**. This product has

Scheme 5.2



been fully characterized by NMR and X-ray crystallography; owing to the similarity of the NMR parameters to those of **45** and **46** these data are not discussed further. The X-ray structure of this complex is shown in Figure 5.2. The Rh–Ir distance of this complex (2.8829(3) Å) is significantly longer than in complex **48**, but agrees well with previously characterized mono(silylene)-bridged complexes.¹³ Consistent with the longer Rh–Ir distance the Rh–Si–Ir angle (75.65(3)°) in this complex is also significantly larger than that of complex **48**.

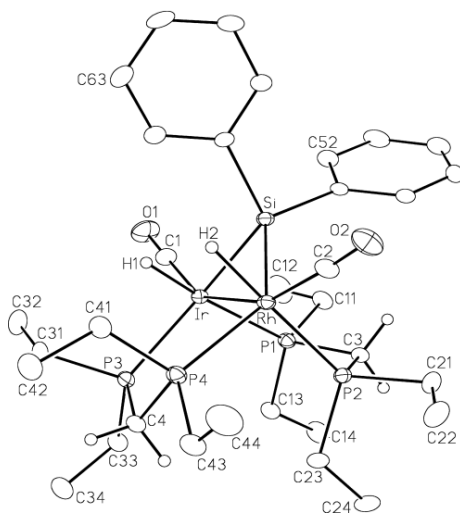


Figure 5.2: Perspective view of **49** showing the numbering scheme. Atom labeling scheme and thermal parameters are as described in Figure 5.1. the structure was refined each metal position as a 50 % mix of Rh and Ir.

These larger values compared to **48** suggest that the lower steric demands of the depm groups is in fact not a significant factor in determining the Rh–Ir separation.

Reaction of complex **44** with excess Ph_2SiH_2 (4 equiv) under a CO purge at 60 °C yields a mixture of a silyl/(μ -silylene) complex, $[\text{RhIr}(\text{H})(\text{SiPh}_2\text{H})(\text{CO})_3(\kappa^1\text{-depdm})(\mu\text{-SiPh}_2)(\text{depdm})]$ (**50**) and a bis(silyl)/(μ -silylene) complex,

[RhIr(SiPh₂H)₂(CO)₂(μ-SiPh₂)(dep_m)] (**51**) after 18 h in an approximate 60:40 ratio (based on isolated yield). Increasing the reaction temperature to 80 °C, but keeping all other reaction conditions the same, led to the quantitative formation of **51** after the same period. Complex **50** can be prepared from the reaction of **49** with 1 equiv of Ph₂SiH₂ in the presence of CO at 60 °C. It is interesting to note that the formation of **50** requires a higher temperature than for the dppm analogue, [RhIr(H)(SiPh₂H)(CO)₃(κ¹-dppm)(μ-SiPh₂)(dppm)],¹⁴ which readily forms at ambient temperature. To determine whether compounds **50** and **51** form by competing reaction pathways or whether **50** is an intermediate during the formation of **51**, the former was reacted with one equiv of Ph₂SiH₂ with a CO purge at 80 °C. The clean formation of **51** with the elimination of 1 equiv of dep_m (as evident from ³¹P NMR) and H₂ in this reaction suggests that **50** is an intermediate in the formation of **51**.

The NMR features of **50** are similar to those of the dppm analogue¹⁴ displaying four resonances in the ³¹P{¹H} NMR spectrum at δ -3.9, -7.5, -27.1, -35.0, in which only the resonance at δ -3.9 displays Rh-P coupling (94 Hz), confirming that only one phosphine arm of the diphosphines is coordinated to Rh. The most upfield resonance, showing the lowest multiplicity (a doublet of doublets, arising due to coupling to the two Ir-bound ³¹P nuclei), is assigned to the pendent end of dep_m. In the ¹H NMR spectrum the silyl hydrogen appears as a doublet at δ 6.02 (³J_{PH} = 4 Hz); although it displays no resolvable coupling to Rh, its collapse to a singlet only upon irradiation of the Rh-bound ³¹P resonance indicates that the silyl group is bound to Rh. The hydride ligand appears as a

doublet of doublets at $\delta -11.93$ showing equal coupling to both Ir-bound ^{31}P nuclei ($^2J_{\text{PH}} = 20$ Hz) as established by selective $^{31}\text{P}\{^1\text{H}\}$ decoupling experiments. The absence of Rh–H coupling further indicates that the hydride is terminally bound to Ir. In the $^{13}\text{C}\{^1\text{H}\}$ NMR spectrum two resonances, observed at $\delta 205.2$ ($^1J_{\text{RhC}} = 56$ Hz) and 202.4 Hz ($^1J_{\text{RhC}} = 54$ Hz), correspond to the Rh-bound carbonyls while the peak at $\delta 187.1$, having no Rh coupling, indicates that this CO is bound to Ir. Two multiplets were observed for the silyl and silylene groups in the $^{29}\text{Si}\{^1\text{H}\}$ NMR spectrum at $\delta -3.4$ and 143.3 , respectively.

Complex **51** has been fully characterized by multinuclear NMR spectroscopy and X-ray analysis. The $^{31}\text{P}\{^1\text{H}\}$ NMR spectrum displays a doublet of doublets $\delta -1.9$ ($^1J_{\text{RHP}} = 92$ Hz) and a doublet at $\delta -30.5$ for Rh- and Ir-bound ^{31}P -nuclei, respectively. Two doublet resonances are observed at $\delta 5.95$ and 5.74 in the ^1H NMR spectrum for the metal-bound silyl protons (displaying three-bond coupling to phosphorus of 4 and 5 Hz, respectively); both signals collapse to a singlet upon broadband ^{31}P decoupling. The depm ethyl protons display a cluster of multiplets between $\delta 1.79$ and 0.93 , and interestingly, integration of these signals indicates that only one depm is coordinated. The $^{29}\text{Si}\{^1\text{H}\}$ NMR spectrum displays a doublet at $\delta -2.3$ ($^1J_{\text{RhSi}} = 23$ Hz) and a singlet at $\delta -23.1$ for Rh-bound and Ir-bound silyl groups, respectively, while the bridging silylene group appears as a multiplet at $\delta 136.9$. A doublet of doublets at $\delta 202.5$ ($^1J_{\text{RhC}} = 54$ Hz) and a doublet at 187.7 are observed in the $^{13}\text{C}\{^1\text{H}\}$ NMR spectrum for Rh- and Ir-bound carbonyls.

The X-ray structure of complex **51** is shown in Figure 5.3 confirming the bis(silyl)/(μ -silylene) formulation in which the silylene-bridged bimetallic core is flanked by two terminal silyl ligands. The bridging silylene ligand resides opposite the bridging diphosphine, while the terminal silyl ligands lie opposite the metal–metal bond. Structurally, complex **51** is similar to the previously reported silane-bridged diruthenium species, $[\text{Ru}_2(\text{SiTol}_2\text{H})_2(\text{CO})_2(\mu\text{-}\eta^2\text{:}\eta^2\text{-H}_2\text{SiTol}_2)(\text{dppm})]$.²³ The Rh–Ir distance (2.897(1) Å) in **51** is slightly longer

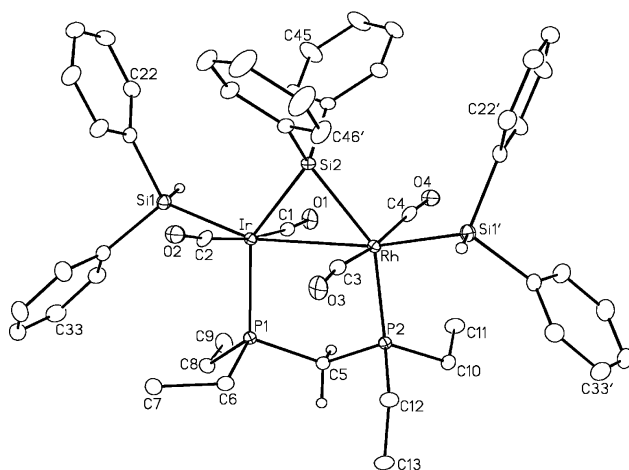


Figure 5.3: Perspective view of **51** showing the numbering scheme. Atom labeling scheme and thermal parameters are as described in Figure 5.1. Metal positions were refined with 50 % site occupancy of Rh and Ir. The primed atoms are related to the unprimed ones by the 2-fold rotation axis that passes through Si(2) and bisects the Ir–Rh bond (see Experimental Section).

than in complex **48** and other previously reported mono(μ -silylene) and bis(μ -silylene) complexes¹⁴ while the metal–silicon distances in the terminal and bridging silicon moieties are quite similar (Ir–Si(1) = 2.413(1) Å, Ir–Si(2) = 2.401(1) Å; Rh–Si(1') = 2.410(3) Å, Rh–Si(2') = 2.399(2) Å). The carbonyls on

each metal are approximately mutually trans ($C(1)-Ir-C(2) = 171.9(9)^\circ$ and $C(3)-Rh-C(4) = 166.5(9)^\circ$), with those on one metal being staggered with respect to those on the other ($OC-Ir-Rh-CO$ torsion angles between $13.3(9)^\circ$ and $19.0(10)^\circ$).

5.5 Discussion

As noted in the Introduction, the purpose of this study was to compare the reactivity of the depm-bridged complex, $[RhIr(CO)_3(dep_m)_2]$ (**44**), with silanes to that previously reported for the dppm-bridged analogue. While we see many similarities in the reactions of primary and secondary silanes in these two systems, some reactivity differences are also evident. The relative rates of these reactions involving the depm and dppm can be expected to depend on a number of factors. The smaller size of depm favours silane access to the metals while the greater basicity of this diphosphine should favour silane oxidative addition at both metals; both factors should lead to an increased rate for the depm system. However, the smaller depm should have less tendency for dissociation, which has been proposed to be a factor in generating the required coordinative unsaturation,¹⁴ while CO dissociation and H_2 reductive elimination should also be less facile for this more basic system (due to greater π back donation to CO and favouring the higher oxidation state, respectively); both of these factors should lead to a slower rate for depm. It is also possible that both systems (dep_m or dppm) generate coordinative unsaturation by different mechanisms, although the observation of the pendent-depm species, $[RhIr(H)(SiPh_2H)(CO)_3(\kappa^1-depm)(\mu-SiPh_2)(dep_m)]$ (**50**), analogous to the previously reported dppm species suggests a proclivity for phosphine dissociation in both systems. In this study we see that although the

reactivities of **44** with one equivalent of primary silanes proceeds with the formation of the respective mono-silylene-bridged dihydride complexes, much as reported in the dppm chemistry, the rate of formation of these complexes is found to be slower. This decrease in rate might be attributed to the slow dissociation of CO, which is necessary for the double Si–H bond activation of the first equiv of silane. For the incorporation of the second silylene group the relative reactivities are reversed such that the rate in the depm system is approximately 10 times *faster* than for dppm, indicating that for this transformation substrate accessibility and/or the greater tendency for oxidative addition dominate. The high yield of a carbonyl- and silylene-bridged complex (**48**) upon reacting **46** with CO is also in contrast to the previously reported dppm chemistry with the Rh/Ir metal combination, for which the reaction of $[\text{RhIr}(\text{H})_2(\text{CO})_2(\mu\text{-SiHPh})(\text{dppm})_2]$ (**4**) with CO under similar reaction conditions only yielded the carbonyl-adduct (**6**) in low yield, which could not be isolated.¹⁴ The reason for this difference is not clear, particularly since a “ $\text{Rh}_2(\text{dppm})_2$ ” analogue cleanly yielded the related carbonyl- and silylene-bridged product.^{13a,b}

The reactivity of **44** with diphenylsilane also displays similarities with the dppm chemistry initially yielding a mono-silylene-bridged dihydride product (**49**) followed by dissociation of one end of a diphosphine ligand, elimination of H_2 and addition of a second equiv of silane and carbonyl ligand to give the silyl/ μ -silylene complex, $[\text{RhIr}(\text{H})(\text{SiPh}_2\text{H})(\text{CO})_3(\kappa^1\text{-dep})_2(\mu\text{-SiPh}_2)(\text{dep})]$ (**50**). However, in contrast to the dppm analogue, complex **50** reacts further with a third equiv of diphenylsilane to produce a novel bis(silyl)/(μ -silylene) complex **51**, by

loss of the pendent depm ligand (see Scheme 5.2). Complete diphosphine loss was not previously observed in related dppm chemistry, arguing against a dissociative pathway for which loss of the bulkier dppm ligand should be favoured. Possibly the lower steric bulk of depm allows substrate access promoting phosphine dissociation in this case. In Chapter 2 we had observed the isomerization of a bis(phenylsilylene)-bridged complex, $[\text{RhIr}(\text{CO})_2(\mu\text{-SiHPh})_2(\text{dppm})_2]$ (**8a** to **8b**), from the kinetic isomer in which a phenyl ring on one silylene group was adjacent to a hydrogen on the other, to the thermodynamic product in which the phenyl groups on each silylene unit were adjacent and parallel.¹⁴ This isomerization occurred only in the presence of excess phenylsilane, suggesting an unobserved intermediate in which three Si-containing fragments were incorporated. The observation of the bis(silyl)/(μ -silylene) product **51** confirms that such species can exist.

5.6 References

- 1) (a) Corey, J. Y.; Braddock-Wilking, J. *Chem. Rev.* **1999**, *99*, 175 (b) Corey, J. Y. *Chem. Rev.* **2011**, *111*, 863 (c) Marciniak, B. *Silicon Chem.* **2002**, *1*, 155. (d) Roy, A. K. *Adv. Organomet. Chem.* **2007**, *55*, 1.
- 2) (a) Watermann, R.; Hayes, P. G.; Tilley, T. D. *Acc. Chem. Res.* **2007**, *40*, 712. (b) Takao, T.; Suzuki, H. *Organometallics* **1994**, *13*, 2554. (c) Calimano, E.; Tilley T. D. *J. Am. Chem. Soc.* **2009**, *131*, 11161. (d) Glaser, P. B.; Tilley T. D. *J. Am. Chem. Soc.* **2003**, *125*, 13640.

- 3) (a) Aitken, C. T.; Harrod, J. F.; Samuel, E. *J. Am. Chem. Soc.* **1986**, *108*, 4059. (b) Tilley, T. D. *Acc. Chem. Res.* **1993**, *26*, 22. (c) Corey, J. Y. *Adv. Organomet. Chem.* **2004**, *51*, 1.
- 4) (a) Zarate, E. A.; Tessier-Youngs, C. A.; Youngs, W. J. *J. Am. Chem. Soc.* **1988**, *110*, 4068. (b) Zarate, E. A.; Tessier-Youngs, C. A.; Youngs, W. J. *J. Chem. Soc., Chem. Commun.* **1989**, 577.
- 5) Tobita, H.; Matsuda, A.; Hashimoto, H.; Ueno, K.; Ogino, H. *Angew. Chem. Int. Ed. Engl.* **2004**, *43*, 221.
- 6) Ogino, H. *Chem. Rec.* **2002**, *2*, 291.
- 7) Okazaki, M.; Tobita, H.; Ogino, H. *Dalton Trans.* **2003**, 493.
- 8) Sharma, H. K.; Pannell, K. H. *Chem. Rev.* **1995**, *95*, 1351.
- 9) Pannell, K. H.; Cervantes, J.; Hernandez, C.; Cassias, J.; Vincenti, S. P. *Organometallics* **1986**, *5*, 1056.
- 10) (a) Bodensieck, U.; Braunstein, P.; Deck, W.; Faure, T.; Knorr, M.; Stern, C. *Angew. Chem. Int. Ed. Engl.* **1994**, *33*, 2440. (b) Braunstein, P.; Faure, T.; Knorr, M. *Organometallics* **1999**, *18*, 1791. (c) Braunstein, P.; Knorr, M.; Reinhard, G.; Schubert, U.; Stährfeldt, T. *Chem. Eur. J.* **2000**, *6*, 4265. (d) Schuh, W.; Braunstein, P.; Benard, M.; Rohmer, M. M.; Welter, R. *J. Am. Chem. Soc.* **2005**, *127*, 10250.
- 11) Tanabe, M.; Osakada, K. *Inorg. Chim. Acta* **2003**, *350*, 201.
- 12) McDonald, R.; Cowie, M. *Organometallics* **1990**, *9*, 2468.

- 13) (a) Wang, W. -D.; Hommeltoft, S. I.; Eisenberg, R. *Organometallics* **1988**, 7, 2417. (b) Wang, W. -D.; Eisenberg, R. *J. Am. Chem. Soc.* **1990**, 112, 1833. (c) Wang, W. -D.; Eisenberg, R. *Organometallics* **1992**, 11, 908.
- 14) Mobarok, M. H.; Oke, O.; Ferguson, M. J.; McDonald, R.; Cowie, M. *Inorg. Chem.* **2010**, 49, 11556.
- 15) Mobarok, M. H.; Ferguson, M. J.; McDonald, R.; Cowie, M. *Inorg. Chem.* **2012**, 51, 4020.
- 16) Shimada, S.; Rao, M. L. N.; Hayashi, T.; Tanaka, M. *Angew. Chem. Int. Ed. Engl.* **2001**, 40, 213.
- 17) Mobarok, M. H.; Ferguson, M. J.; McDonald, R.; Cowie, M. *Submitted for Publication*.
- 18) Minge, O.; Nogai, S.; Schmidbaur, H. *Z. Naturforsch. B* **2004**, 59, 153.
- 19) Slaney, M. E.; Anderson, D. J.; Ferguson, M. J.; McDonald, R.; Cowie, M. *Organometallics* **2012**, 31, 2286.
- 20) Programs for diffractometer operation, data collection, data reduction, and absorption correction were those supplied by Bruker.
- 21) Sheldrick, G. M. *Acta Crystallogr.* **2008**, A64, 112.
- 22) Ogino, H.; Tobita, H. *Adv. Organomet. Chem.* **1998**, 42, 223.
- 23) Hashimoto, H.; Aratani, I.; Kabuto, C.; Kira, M. *Organometallics* **2003**, 22, 2199.

Chapter 6

Conclusions

6.1 Concluding Remarks

6.1.1 Roles of metals in Si–H bond activation

As noted in the Introduction of this thesis, interests in bimetallic complexes involving bridging silylene or germylene complexes were driven, particularly in the last two decades, by the anticipation of unique reactivities involving these bridging groups.¹ In particular, the possible interaction between a pair of bridging ER_2 units ($E = Si, Ge$) in bimetallic complexes has been of interest owing to the possibility that such species might lead to $E-E$ ($E = Si$ or Ge) bond formation. When I started working on this project there were already a number of examples of silylene- and germylene-bridged bimetallic (mostly homobimetallic) complexes, a portion of which were synthesized by the $E-H$ ($E = Si, Ge$) bond activations of organosilanes or organogermanes at preorganized bimetallic cores.¹ However, little was understood about the roles of the adjacent metals during the activation processes of multiple $E-H$ bonds in such complexes, particularly when two or more Si-containing groups were incorporated. One of the research endeavors in the Cowie group has been to develop an understanding of the roles of adjacent metals in binuclear complexes in substrate binding, activation and in the subsequent transformations, and by the time I started working, there had been significant progress in this regard. The cooperative involvement of adjacent metals had successfully been demonstrated in numerous research projects such as C–C

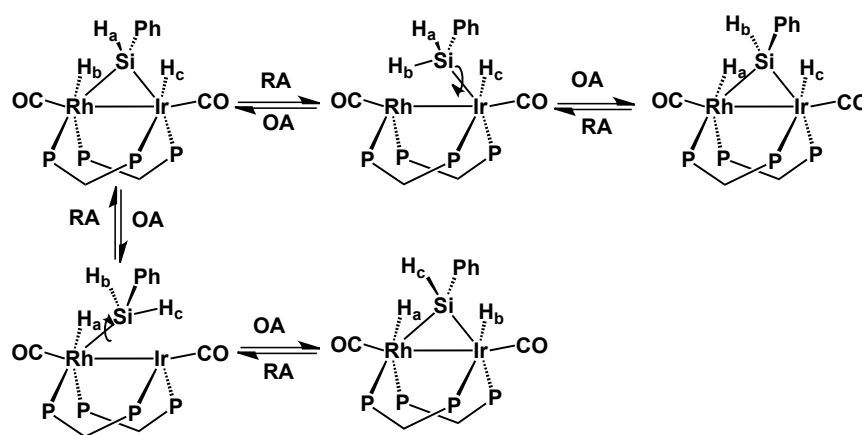
bond formation through the coupling of methylene units,² and multiple C–H³ and C–F⁴ bond activation of olefins and fluoroolefins.

At the outset of this research project the main goal was to understand how multiple E–H bond activations proceed in bimetallic complexes involving Group 9 metals to produce bridging ER₂-containing complexes. And as noted previously, our rationale behind choosing the Rh/Ir combination of metals for this purpose was to exploit the stronger tendency of low-valent Ir to undergo oxidative addition and the greater resulting bond strengths involving this metal, combined with the greater lability at Rh. This combination also takes advantage of the useful NMR characteristics of Rh as an aid in characterization of labile intermediates, which we anticipated would assist in determining the roles of the different metals in the stepwise activation of E–H bonds. Our other goal was to assess whether such ER₂-containing complex could promote unique transformations such as E–E bond formation by the coupling of such fragments, analogous to methylene coupling for C–C bond formation. In addition, we were also interested in exploring further reactivity of such complexes with small molecules.

In the second Chapter of this thesis, we investigated Si–H bond activation of a number of primary and secondary silanes and made substantial progress towards the understanding of multiple of Si–H bond activation by isolating and characterizing a few models of key intermediates. These models were obtained by the use of a variety of silanes that reacted to different degrees owing to steric differences. In addition to the models of intermediates, mechanistic details were obtained mainly by using low temperature NMR spectroscopy to monitor the

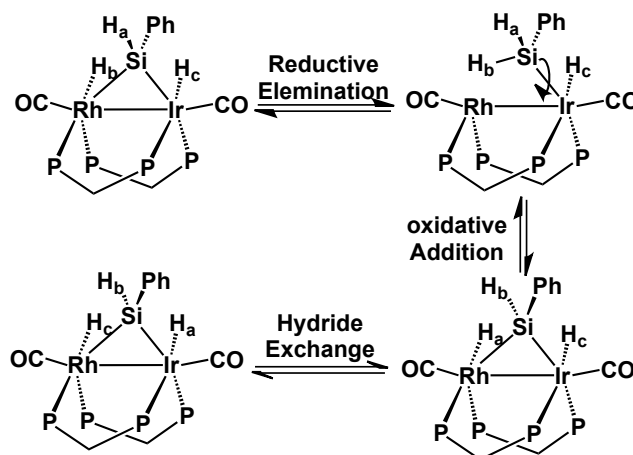
stepwise transformations from reactants through products. Reactions of 1 equiv of primary silanes with the neutral complex, $[\text{RhIr}(\text{CO})_3(\text{dppm})_2]$ (**1**), at $-80\text{ }^\circ\text{C}$, proceed with single Si–H bond cleavage at Rh as indicated by the characterization of the silyl/hydride intermediate, $[\text{RhIr}(\text{H})(\text{SiH}_2\text{Ph})(\text{CO})_2(\mu\text{-CO})(\text{dppm})_2]$ (**3**), followed by the activation of a second Si–H bond of the coordinated silyl group upon warming to $-20\text{ }^\circ\text{C}$ to give a mono(μ -silylene) dihydride complex **4**. This complex exhibits fluxional behavior at ambient temperature in which the metal-bound hydrides are in continuous exchange with each other and with a Si-bound hydrogen; this exchange process is operative even at temperature as low as $-50\text{ }^\circ\text{C}$. An STD NMR experiment at this temperature clearly shows that the exchange rate is twice as fast at Rh than at Ir. Two mechanistic possibilities were proposed to explain this exchange phenomenon: 1) sequential reductive elimination /oxidative addition (RE/OA) of a silylene and hydride unit, in which the faster exchange rate at Rh can be attributed to the greater lability at this metal (Scheme 6.1); alternatively 2) the RE/OA process is only operative at the more labile Rh

Scheme 6.1



centre, accompanied by slower migration of the hydrides between the metals (Scheme 6.2). Although we do not have evidence to rule out either of these mechanistic proposals, the second proposal is consistent with the observation

Scheme 6.2



that the Ir₂ analogue exhibits no fluxional behavior at ambient temperature,⁵ while the Rh₂ analogues, [Rh₂(H)₂(CO)₂(μ-SiRH)(dppm)] (R = Ph, Hex, Et), exhibit fluxionality much like our RhIr species. However, in this latter case, the RE/OA pathway is equally plausible at both metal centres.⁶ The facility of reductive elimination at the pair of Rh centres in the Eisenberg study is further demonstrated by the exchange of one bridging silylene unit upon reaction with 1 equiv of a different primary or secondary silane.^{6c} In contrast, as has been demonstrated in Chapter 4 of this thesis, such exchange reactions do not proceed for the RhIr species, [RhIr(H)₂(CO)₂(μ-SiPhH)(dppm)], which upon reacting with 1 equiv of a different primary and secondary silanes leads to the clean formation of mixed bis(μ-silylene) complexes by the incorporation of another bridging-

silylene unit. These observations suggest a lower tendency for Ir–Si cleavage during the fluxional process involving $[\text{RhIr}(\text{H})_2(\text{CO})_2(\mu\text{-SiPhH})(\text{dppm})_2]$ (**4**).

The coordinative unsaturation necessary to activate Si–H bonds of the second equivalent of primary or secondary silane in the coordinatively saturated mono(silylene)-bridged dihydride complexes may be created either by phosphine dissociation from the Rh end, as suggested by the characterization of complexes such as $[\text{RhIr}(\text{CO})_3(\kappa^1\text{-dppm})(\mu\text{-SiHPh})_2(\text{dppm})]$ (**7**) and $[\text{RhIr}(\text{H})(\text{SiPh}_2\text{H})(\text{CO})_3(\kappa^1\text{-dppm})(\mu\text{-SiPh}_2)(\text{dppm})]$ (**12**) having a pendent diphosphine group or by the reductive elimination of the Si–H bond from Rh as proposed for the fluxional process that exchange the Si- and metal-bound hydrogens. In this regard it is significant that, we did not observe evidence of reversible phosphine dissociation in the mono(silylene)-bridged dihydride complexes (**4**, **5** and **9**) at ambient temperature. On the other hand, the reversible elimination of the Si–H unit from the metal centres of mono(silylene)-bridged dihydride complexes is clearly occurring as indicated by SST and STD NMR experiment (*vide infra*). These observations suggest that the latter process is primarily responsible for generating the necessary coordinative unsaturation for subsequent reactivity.

Although the process involving the isomerization of the bis(phenylsilylene)-bridged complex **8a** (in which one silylene phenyl substituent is axial while the other is equatorial) to **8b** (in which both silylene phenyl groups are axial) is not fully understood, a control experiment suggests that the presence of a third equivalent of phenylsilane is necessary for this transformation to occur.

Presumably, it proceeds through an intermediate containing three Si-containing units, and the necessary coordinative unsaturation for the activation of the third equiv of phenylsilane presumably takes place via phosphine dissociation from Rh. Evidence in support of the incorporation of three Si units is seen in the fifth chapter of this thesis in which we were able to isolate and crystallographically characterize a bis(silyl)/(μ -silylene) complex (**51**) containing two silyl and silylene group, by using the smaller depm ligand as a bridging group.

The reactivity pattern of Si–H bonds in the cationic complex, $[\text{RhIr}(\text{CH}_3)(\text{CO})_2(\text{dppm})_2][\text{OTf}]$ (**2**) is markedly different than for the neutral complex **1**. Whereas complex **1** possesses a 16e/18e configuration in which Rh is coordinatively unsaturated, complex **2** possesses a 16e/16e configuration in which both metals are coordinatively unsaturated. This fact became obvious during the Si–H bond activation of silanes in complex **1**, in which reaction was initiated at the unsaturated Rh centre while for complex **2**, Si–H bond activation was initiated at Ir. In the latter case, the greater tendency of the third-row transition metal for oxidative addition favours addition at this centre. The observation of a silyl-bridged complex $[\text{RhIr}(\text{CH}_3)(\text{CO})_2(\mu\text{-H})(\mu\text{-}\eta^1\text{:}\eta^2\text{-SiPh}_2\text{H})(\text{dppm})_2][\text{CF}_3\text{SO}_3]$ (**15**) at $-20\text{ }^\circ\text{C}$, containing an agostic Si–H interaction during the reaction of **2** with diphenylsilane, is another important difference from the reactivity of silanes with complex **1**. Such intermediates were only observed in the cationic system (**2**), presumably due to the lower tendency for the cationic species to undergo Si–H oxidative addition. Intermediates such as this provide an snapshot of how the

Si–H bond of a silyl group coordinated to one metal can swing towards the second metal leading to its activation.

6.1.2 Nature of Si---Si interaction

In the bis(μ -silylene) species, discussed in Chapter 2, the substantially shorter separation between the two Si atoms in **8a** compared to **8b** suggests a somewhat stronger interaction between these atoms and certainly “nascent” Si---Si bonding had been suggested in such complexes.⁷ In order to address the question related to the nature of the Si---Si interactions a series of mixed bis(μ -silylene) complexes (containing different substituents on silylene units) were prepared and crystallographically characterized in Chapter 4. The purpose of the synthesis of such series of complexes was to determine how substituents could influence the separation between two Si atoms of bridging silylene units and to determine what could be discovered about the nature of the Si---Si interactions by varying the silylene substituents. In this series, substituents were introduced either directly on silicon or on the aryl rings of bridging silylene groups.

As demonstrated (in Chapter 4) that changing substituents directly on Si of bridging silylene units can modulate the Si---Si separation, in which the Si---Si separation decreases with the increasing electron-withdrawing nature of the substituents. On the other hand, although ring substitution has a significant influence on the separation between parallel aryl groups (with electron withdrawing groups dramatically reducing the ring centroid-to-centroid distance while donor groups have the opposite effect), this closer approach of the aryl rings has little effect on the Si---Si separation. This observation demonstrates that

closer approach of the pairs of Si atoms is not inhibited by van der Waals repulsion between the parallel aryl groups and indicates that mutual attraction by a weak bonding interaction between the Si atoms is minimal. The substantial change in Si---Si separation upon changing the Si-bound substituents might be attributed to a decrease in electron density at Si upon substitution by electron-withdrawing groups leading to less repulsion therefore shorter separation.

6.1.3 Ge–H bond activation

As a natural extension of the Si–H bond activation chemistry, the third Chapter of this thesis discusses the reactivity of primary and secondary germanes with the Rh/Ir complexes **1** and **2**. In addition to probing the roles of the different metals in Ge–H bond activation, compared to that of Si–H bonds, we were also interested in discovering if the study with the germanes would yield additional information not obtained with silanes. Again, low-temperature studies allowed us to establish details about the stepwise activation processes involved, and to determine the natures of some intermediates. Similar to the Si–H bond activation chemistry discussed above, the initial site for the activation of first Ge–H bond is decided by the nature of the starting complex (**1** or **2**). Activation of germanes with **1** occurs at the coordinatively unsaturated Rh (complex **18** and **19**) whereas reaction of **2** with germanes occurs at Ir (complex **26**).

Incorporation of a second germanium-containing fragment in the germylene-bridged products has also been observed. Surprisingly, the incorporation of a second equivalent of phenylgermane into the phenylgermylene-bridged product, $[\text{RhIr}(\text{H})_2(\text{CO})_2(\mu\text{-GeHPh})(\text{dppm})_2]$ (**20**) is only observed at low

temperature as indicated by the characterization of the intermediate, $[\text{RhIr}(\text{H})_2(\text{GeH}_2\text{Ph})(\text{CO})_2(\kappa^1\text{-dppm})(\mu\text{-H})(\mu\text{-GeHPh})(\text{dppm})]$ (**22**). This intermediate decomposes above $-40\text{ }^\circ\text{C}$ and does not lead to the formation of a stable bis(μ -phenylgermylene) product. This is in contrast to the reactivity of Si–H bond activation chemistry, in which reaction of the mono(μ -phenylsilylene) dihydride complex, $[\text{RhIr}(\text{H})_2(\text{CO})_2(\mu\text{-SiPhH})_2(\text{dppm})]$, with phenylsilane leads to a stable bis(μ -phenylsilylene) complex. This apparent instability of the bis(μ -phenylgermylene) complex is presumably a result of elimination of hydrogen (observed by NMR spectroscopy) by the further activation of the remaining Ge–H bonds of the putative bis(μ -phenylgermylene) intermediate owing to the weaker nature of these bonds, although the nature of such bond activation is not clear from this study. Interestingly, however, the reaction of $[\text{RhIr}(\text{H})_2(\text{CO})_2(\mu\text{-GePhH})(\text{dppm})_2]$, with one equiv of diphenylgermane leads to the formation of the first mixed bis (μ -germylene) complex, $[\text{RhIr}(\text{CO})_2(\mu\text{-GeHPh})(\mu\text{-GePh}_2)(\text{dppm})_2]$ (**23**) incorporating both mono- and disubstituted bridging-germylene units.

The observation of this mixed bis(μ -germylene) complex suggested the possibility of generating complexes incorporating both Si- and Ge-containing moiety in the bimetallic core to give the first examples of (μ -silylene)/(μ -germylene) complexes. In the Chapter 4 of this thesis, a series of (μ -silylene)/(μ -germylene) complexes were described through the reaction of either a mono(μ -silylene) dihydride complex with a corresponding germane or a mono(μ -germylene) dihydride complex with a corresponding silane.

The reaction of the diphenylgermylene-bridged complex, $[\text{RhIr}(\text{H})_2(\text{CO})_2(\mu\text{-GePh}_2)(\text{dppm})_2]$ (**24**) with another equivalent of diphenylgermane (in Chapter 3) leads to decomposition; however, the same reaction under a CO atmosphere leads to the formation of $[\text{RhIr}(\text{H})(\text{GeHPh}_2)(\text{CO})_3(\kappa^1\text{-dppm})(\mu\text{-GePh}_2)(\text{dppm})]$ (**25**). This product is closely related to **22** (apart from the different substituents on Ge), in which two hydride ligands have been replaced by CO. Presumably, when the initial trihydride, diphenylgermyl intermediate in the reaction of **24** with diphenylgermane (analogous to **22**), loses H_2 , oxidative addition of the germyl–H bond, to give a *bis*-diphenylgermylene-bridged product analogous to **23** is inhibited, owing to the greater bulk of the disubstituted germyl and germylene groups (see Scheme 3.8). In addition, the pendent dppm is too bulky to recoordinate, decomposition occurs in the absence of an additional ligand required to alleviate the unsaturation. However, under CO the stable tricarbonyl species **25** is formed, having both metals coordinatively saturated.

The exclusive formation of the $(\mu\text{-germylene})(\mu\text{-hydride})$ complex, $[\text{RhIr}(\text{CO})_2(\mu\text{-GePh}_2)(\mu\text{-H})(\text{dppm})_2][\text{CF}_3\text{SO}_3]$ (**28**), by the reaction of one equiv of diphenylsilane with cationic complex, **2** is an important difference compared to the Si–H bond activation in the same complex. As demonstrated in Chapter 2, the reaction of **2** with 1 equiv of diphenylsilane under similar reaction condition led to the two different products: an analogous $\mu\text{-silylene}/\mu\text{-hydride}$ complex, $[\text{RhIr}(\text{CO})_2(\mu\text{-SiPh}_2)(\mu\text{-H})(\text{dppm})_2][\text{CF}_3\text{SO}_3]$ (**17**), the result of reductive elimination of methane from the silyl-bridged intermediate (**15**), and a $(\mu\text{-silylene})/\text{acetyl}$ complex, $[\text{RhIr}(\text{CO})_2(\text{H})(\text{C}(\text{CH}_3)\text{O})(\mu\text{-H})(\mu\text{-$

$\text{SiPh}_2(\text{dppm})_2[\text{CF}_3\text{SO}_3]$ (**16**), formed by methyl migration to a carbonyl ligand in competition to methane loss from **15**. This latter result, which was not duplicated in the germyl analogue, demonstrates the greater trans labilizing effect of the silyl group compared to the germyl ligand, which promoted the migratory-insertion reaction.

In Chapter 3 we were also able to demonstrate the reactivity of the cationic (μ -germylene)(μ -hydride) complex, $[\text{RhIr}(\text{CO})_2(\mu\text{-GePh}_2)(\mu\text{-H})(\text{dppm})_2][\text{CF}_3\text{SO}_3]$ (**28**) with the substrates, H_2 , Ph_2SiH_2 , H_2O , MeOH and HCl . Among these, H_2 activation was found to be reversible. The reactivity of the analogous (μ -silylene)(μ -hydride) complex (**17**) (see Chapter 2) was not studied due our inability to isolate this species from the mixture of **16** and **17**. Further reactivity of silylene- or germylene-bridged bimetallic complexes is less common compared to the monometallic silylene- or germylene complexes presumably due to the better back-donation from the symmetry adapted metal *d* orbitals of both metals into the empty *p* orbitals of the silylene or germylene ligands (which may effectively reduce the polarity of the M–E bonds in such complexes) and due to the poorer access of substrates to the sterically protected silylene or germylene units in a bimetallic environment. It is not clear how the activation of H_2 and HX ($\text{X} = \text{OH}$, OMe , Cl) proceeds in this germyl-bridged complex, as low temperature NMR spectroscopy failed to produce any detectable intermediate. There are two mechanistic possibilities that can be envisioned for these types of activation processes: 1) metal-mediated (either at Rh or Ir) activation of the H–H or H–X bonds followed by migration of the H or X functionality to the electron deficient

Ge centre; or 2) activation of the H–H bond by the electron-deficient germylene unit, in which bond activation is initiated by σ -donation from the H–H bond to the empty p orbital of the germylene unit, followed by the back-donation from the symmetry adapted metal (Rh/Ir) d orbitals into the σ^* -orbital of H_2 leading to its cleavage. This latter mechanism is analogous to the activation of the H–H bond by a singlet carbene,⁸ with the exception of back-donation from the metal d -orbital instead of the sp^2 orbital of the germylene unit, which is already engaged in donation to the empty metal orbitals. The bridging-germylene unit in $[RhIr(CO)_2(\mu\text{-GePh}_2)(\mu\text{-H})(dppm)_2][CF_3SO_3]$ (**28**), should be more electron deficient than its neutral analogue owing to the less backdonation from the positively charged metal centres, so should be more susceptible to nucleophilic attack. In this case, Reaction of H–X (X = OH, OMe, Cl) could occur by nucleophilic attack by HX on the bridging germylene unit, followed by proton migration to the metals.

6.1.4 Effect of bridging diphosphine on Si–H bond activation

In the fifth Chapter of this thesis the influence of the sterically smaller and electronically richer bridging ligand (dep m) in Si–H bond activations was investigated. Recent investigations from our group demonstrated that the use of this bridging ligand can have a dramatic effect on olefinic C–H and C–F activation.^{9,10} The more basic nature of dep m compared to dpp m ligand should facilitate oxidative addition at the bimetallic core, while the smaller size of this ligand should be advantageous for easier substrate access. However, the more

electron-donating nature of this ligand might also reduce the dissociative tendency of the ancillary ligands.

This latter effect is obvious in the slower rate of formation of mono(μ -silylene) dihydride complex (**45**) from the reaction of $[\text{RhIr}(\text{CO})_3(\text{dep}m)_2]$ upon reacting with 1 equiv of phenylsilane. The slower rate may be attributed to the slower rate of CO loss. Phosphine dissociation from Rh was also found to be less facile as indicated by the requirement of higher temperature during the formation of $[\text{RhIr}(\text{H})(\text{SiPh}_2\text{H})(\text{CO})_3(\kappa^1\text{-dep}m)(\mu\text{-SiPh}_2)(\text{dep}m)]$ (**50**) having a pendent diphosphine presumably due to the greater basicity of depm which leads to stronger interaction with metal; the analogous dppm complex forms at ambient temperature. However, the formation of the bis(μ -silylene) complex, $[\text{RhIr}(\text{CO})_2(\mu\text{-SiPhH})_2(\text{dep}m)_2]$ (**47**) is much faster compared to its dppm analogue presumably due to easier substrate access. The most unusual result obtained from depm chemistry is the formation of a bis(silyl)/(μ -silylene) complex, $[\text{RhIr}(\text{SiPh}_2\text{H})_2(\text{CO})_2(\mu\text{-SiPh}_2)(\text{dep}m)]$ (**51**), which incorporates *three* Si-containing units into the bimetallic core, accompanied by the complete dissociation of one depm ligand. Complete dissociation of diphosphine ligand, from both Rh and Ir was never observed in the dppm series. Since this is the opposite to the expectation of more facile loss of the more bulky phosphine, it is presumably a result of better substrate access, which subsequently facilitates such dissociation.

6.2 Future Directions

Much of the research in this work has focused on the development of a better understanding of how multiple Si- or Ge-containing units can be incorporated into the bimetallic system involving two Group 9 metals. As noted above, this study was quite successful in this regard. However, our attempts to exploit multiple silicon- or germanium-containing species such as bis(μ -silylene) or silyl/(μ -silylene) complexes for promoting coupling of these fragments were unsuccessful. One strategy was attempted in the fourth Chapter, in which an electron donating group was introduced into one bridging silylene unit and an electron-withdrawing group on other, to produce a mixed bis(μ -silylene) complex, in order to determine whether the electron rich silylene might transfer to the electron-deficient silylene in the presence of CO or other donor ligands; however, that approach was unsuccessful. Monometallic silyl/silylene complexes are known to promote Si-Si coupling via 1,2 silyl migration. Such migration did not occur in our silyl/(μ -silylene) species under the conditions investigated. It would be interesting to determine whether such migration is possible in our system upon the introduction of electron-donating substituents on the silyl unit to make it electron rich and to introduce electron-withdrawing groups in the μ -silylene unit to make it electron poor. Such a strategy could facilitate silyl group migration to the silylene unit, analogous to alkyl migration to a CO ligand. The fluxional behavior of the μ -silylene dihydride complexes, frequently observed throughout this study, can be viewed as hydride migration to the electron-deficient bridging-silylene unit in which hydride functions as a nucleophile. Certainly, as alluded to earlier, an SiR_3

unit has much in common with a hydrogen atom, suggesting that silyl-to-silylene migration should be possible.

One of the main reasons behind the failure of the bis(μ -silylene) or silyl/ μ -silylene complexes of Rh/Ir in promoting Si–Si bond formation appears to be the strength of nature of the M–Si bonds. Initially it had been anticipated that the presence of the more labile Rh might make such a transformation possible while the stronger nature of the Ir–Si bond would help to retain the Si–Si coupled product. However, the Rh–Si bond appears to be too strong to allow the migration from this metal. One possible future direction of this work could be to investigate the Rh/Co or Ir/Co combinations in order to exploit the greater lability of the first-row metal. An analogous heterobimetallic $[\text{RhCo}(\text{CO})_3(\text{dppm})_2]$ has been synthesized and reported.¹¹ Although not reported, the analogous $[\text{IrCo}(\text{CO})_3(\text{dppm})_2]$ should be easily prepared by an analogous synthetic procedure.

6.3 References

- 1) 1) (a) Ogino, H.; Tobita, H. *Adv. Organomet. Chem.* **1998**, *42*, 223 (b) Shimada, S.; Rao, M. L. N.; Hayashi, T.; Tanaka, M. *Angew. Chem. Int. Ed. Engl.* **2001**, *40*, 213.
- 2) Trepanier, S. J.; Dennett, J. N. L.; Sterenberg, B. T.; McDonald, R.; Cowie, M. *J. Am. Chem. Soc.* **2004**, *126*, 8046.
- 3) Ristic-Petrovic, D.; Torkelson, J. R.; Hiltz, R. W.; McDonald, R.; Cowie, M. *Organometallics.* **2000**, *19*, 4432.

- 4) Slaney, M. E.; Anderson, D. J.; Ferguson, M. J.; McDonald, R.; Cowie, M. *J. Am. Chem. Soc.* **2011**, *132*, 16544. (b) Anderson, D. J.; McDonald, R.; Cowie, M. *Angew. Chem. Int. Ed. Engl.* **2007**, *46*, 3741.
- 5) McDonald, R.; Cowie, M. *Organometallics* **1990**, *9*, 2468.
- 6) (a) Wang, W. -D.; Eisenberg, R. *J. Am. Chem. Soc.* **1990**, *112*, 1833. (b) Wang, W. -D.; Hommeltoft, S. I.; Eisenberg, R. *Organometallics* **1988**, *7*, 2417. (c) Wang, W. -D.; Eisenberg, R. *Organometallics* **1991**, *10*, 2222.
- 7) (a) Mobarok, M. H.; Oke, O.; Ferguson, M. J.; McDonald, R.; Cowie, M. *Inorg. Chem.* **2010**, *49*, 11556. (b) Zarate, E.A.; Tessier-Youngs, C. A.; Youngs, W. J. *J. Chem. Soc. Chem. Comm.* **1989**, 577. (c) Nikonov, G. I. *Angew. Chem. Int. Ed. Engl.* **2003**, *42*, 1335.
- 8) Frey, G. D.; Lavallo, B.; Donnadiu, B.; Schoeller, W. W; Bertrand, G. *Science* **2007**, *316*, 439.
- 9) Slaney, M. E.; Ferguson, M. J.; McDonald, R.; Cowie, M. *Organometallics* **2012**, *31*, 1384.
- 10) Slaney, M. E.; Anderson, D. J.; Ferguson, M. J.; McDonald, R.; Cowie, M. *Organometallics* **2012**, *31*, 2286.
- 11) Antonelli, D. M.; Cowie, M. *Organometallics* **1990**, *9*, 1818.

Appendices

Appendix I – For Chapter 2

Table A.1. Crystallographic Experimental Details for Compounds 4, 5 and 12

Compound	4 • C ₆ D ₆	5 • 0.25 CH ₂ Cl ₂	12 • 1.5 C ₆ D ₆
Formula	C ₆₄ H ₅₈ IrO ₂ P ₄ RhSi	C _{61.25} H _{58.5} Cl _{0.5} IrO ₂ P ₄ Si ₂	C ₈₆ H ₇₅ IrO ₃ P ₄ RhSi ₂
formula weight	1306.18	1291.39	1631.63
crystal dimens (mm)	0.38 × 0.35 × 0.19	0.65 × 0.57 × 0.14	0.33 × 0.12 × 0.08
crystal system	orthorhombic	monoclinic	triclinic
space group	<i>P</i> 2 ₁ 2 ₁ 2 ₁ (No. 19)	<i>P</i> 2 ₁ / <i>c</i> (No. 14)	<i>P</i> $\bar{1}$ (No. 2)
unit cell parameters			
<i>a</i> (Å)	12.6419(8)	23.3576 (8)	13.3971 (6)
<i>b</i> (Å)	18.0672(11)	19.2433 (7)	15.8618 (7)
<i>c</i> (Å)	24.7646 (16)	24.8837 (8)	20.9238 (12)
α (deg)			97.730 (4)
β (deg)		100.4443 (4)	104.590 (4)
γ (deg)			113.895 (4)
<i>V</i> (Å ³)	5656.3 (6)	10999.3 (7)	3791.0 (3)
<i>Z</i>	4	8	2
ρ_{calcd} (g cm ⁻³)	1.534	1.560	1.429
μ (mm ⁻¹)	2.820	2.923	6.587
diffractometer	Bruker D8/APEX II CCD ^a		SiemensP4/RA ^b
radiation (λ [Å])	graphite-monochromated Mo K α (0.71073)		Cu K α (1.54178)
temperature (°C)	-100	-100	-60
scan type	ω scans (0.3°) (20s exposures)	ω scans (0.3°) (20 s exposures)	θ -2 θ
2 θ_{max} (deg)	52.90	54.96	115.00
total data collected	45409 (-15 ≤ <i>h</i> ≤ 15, -22 ≤ <i>k</i> ≤ 22, - 30 ≤ <i>l</i> ≤ 31)	95522(-30 ≤ <i>h</i> ≤ 30, -24 ≤ <i>k</i> ≤ 24, -32 ≤ <i>l</i> ≤ 32)	10485 (0 ≤ <i>h</i> ≤ 14, -16 ≤ <i>k</i> ≤ 15, -22 ≤ <i>l</i> ≤ 22)
Independ reflns (<i>R</i> _{int})	11626 (0.0293)	25177 (0.0156)	9993 (0.0761)
obsd reflns [<i>I</i> ≥ 2 σ (<i>I</i>)]	11232	22869	8438
restraints/params	0 / 674	0 / 1313	10 / 877
Flack abs struct parameter	0.007(4)		
goodness-of-fit (<i>S</i>) ^c	1.095	1.039	1.052
final <i>R</i> indices ^d			
<i>R</i> ₁ [<i>I</i> ≥ 2 σ (<i>I</i>)]	0.0202	0.0179	0.0531
<i>wR</i> ₂ [all data]	0.0463	0.0473	0.1470
largest diff peak, hole (e Å ⁻³)	0.596, -0.389	0.691, -0.639	1.981, -2.348

a. Programs for diffractometer operation, data collection, data reduction and absorption correction were those supplied by Bruker.

b. Programs for diffractometer operation, data collection, data reduction and absorption correction were those supplied by Siemens.

c. $S = [\sum w(F_o^2 - F_c^2)^2 / (n - p)]^{1/2}$ (*n* = number of data; *p* = number of parameters varied; $w = [\sigma^2(F_o^2) + (0.0227P)^2 + 8.1710P]^{-1}$ where $P = [\text{Max}(F_o^2, 0) + 2F_c^2]/3$).

d. $R_1 = \sum ||F_o| - |F_c|| / \sum |F_o|$; $wR_2 = [\sum w(F_o^2 - F_c^2)^2 / \sum w(F_o^4)]^{1/2}$

Table A.2. Crystallographic Experimental Details for Compounds **8a**, **8b** and **8c**

Compound	8a • CH ₂ Cl ₂	8b • 2 C ₄ H ₈ O	8c • 2 CH ₂ Cl ₂
Formula	C ₆₅ H ₅₈ Cl ₂ IrO ₂ P ₄ RhSi ₂	C ₇₂ H ₇₂ IrO ₄ P ₄ RhSi ₂	C ₆₆ H ₅₆ Cl ₄ F ₄ IrO ₂ P ₄ RhSi ₂
formula weight	1417.18	1476.47	1574.08
crystal dimens (mm)	0.59 × 0.24 × 0.04	0.27 × 0.19 × 0.03	0.29 × 0.18 × 0.13
crystal system	triclinic	monoclinic	monoclinic
space group	<i>P</i> $\bar{1}$ (No. 2)	<i>P</i> 2 ₁ / <i>n</i> (No. 14)	<i>P</i> 2 ₁ / <i>n</i> (No. 14)
unit cell parameters			
<i>a</i> (Å)	13.5659(8)	17.9511(12)	12.5479 (13)
<i>b</i> (Å)	13.9983(9)	15.0138(10)	22.295 (2)
<i>c</i> (Å)	17.3524	24.0458(16)	22.699 (2)
<i>α</i> (deg)	81.0505(7)		
<i>β</i> (deg)	74.4767(7)	96.7210(10)	95.854 (1)
<i>γ</i> (deg)	67.2656(7)		
<i>V</i> (Å ³)	1692923.3(3)	6436.1	6316.9 (11)
<i>Z</i>	2	4	4
ρ_{calcd} (g cm ⁻³)	1.610	1.524	1.655
μ (mm ⁻¹)	2.843	25.08	2.731
diffractometer	Bruker D8/APEX II CCD ^a		
radiation (λ [Å])	graphite-monochromated Mo K α (0.71073)		
temperature (°C)	-100	-100	-100
scan type	ω scans (0.3°) (20s exposures)	ω scans (0.3°) (20s exposures)	ω scans (0.3°) (20s exposures)
2 θ_{max} (deg)	55.14	53.56	55.02
total data collected	25911(-17 ≤ <i>h</i> ≤ 17, -18 ≤ <i>k</i> ≤ 18, -22 ≤ <i>l</i> ≤ 22)	52248(-22 ≤ <i>h</i> ≤ 22, -18 ≤ <i>k</i> ≤ 18, -30 ≤ <i>l</i> ≤ 30)	56206 (-16 ≤ <i>h</i> ≤ 16, -28 ≤ <i>k</i> ≤ 28, -29 ≤ <i>l</i> ≤ 29)
Independ reflns (<i>R</i> _{int})	13346 (0.0239)	13711(0.0683)	14510 (0.0162)
obsd reflns [<i>I</i> ≥ 2 σ (<i>I</i>)]	11060	10053	11832
restraints/params	0 / 701	0 / 715	12 ^d / 787
goodness-of-fit (<i>S</i>) ^b	1.038	0.964	1.058
final <i>R</i> indices ^c			
<i>R</i> ₁ [<i>I</i> ≥ 2 σ (<i>I</i>)]	0.0364	0.0366	0.0338
<i>wR</i> ₂ [all data]	0.1020	0.0838	0.1011
largest diff peak, hole (e Å ⁻³)	2.672, -1.406	1.041, -1.185	1.464, -1.904

a. Programs for diffractometer operation, data collection, data reduction and absorption correction were those supplied by Bruker.

b. $S = [\sum w(F_o^2 - F_c^2)^2 / (n - p)]^{1/2}$ (*n* = number of data; *p* = number of parameters varied; $w = [\sigma^2(F_o^2) + (0.0227P)^2 + 8.1710P]^{-1}$ where $P = [\text{Max}(F_o^2, 0) + 2F_c^2]/3$).

c. $R_1 = \sum ||F_o| - |F_c|| / \sum |F_o|$; $wR_2 = [\sum w(F_o^2 - F_c^2)^2 / \sum w(F_o^4)]^{1/2}$.

d. The C–Cl and Cl⋯Cl distances within the disordered solvent dichloromethane molecules were restrained to by 1.800(3) and 2.800(5) Å, respectively.

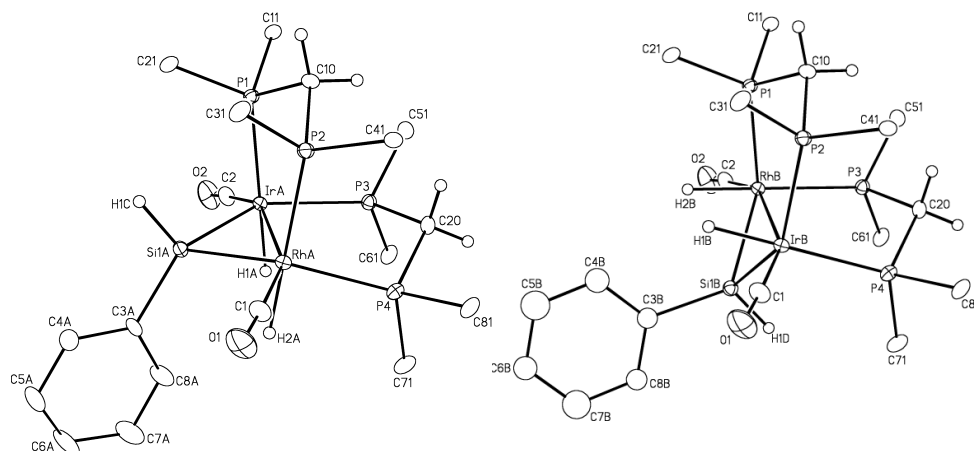


Figure A.1: Perspective views of $[\text{RhIr}(\text{H})_2(\text{CO})_2(\mu\text{-SiHPh})(\text{dppm})_2]$ (**4**) with major (left) and minor (right) orientation of disordered phenylsilylene group. Non-hydrogen atoms are represented by the Gaussian ellipsoids at the 20% probability level. For the dppm phenyl groups, only the ipso carbons are shown

Table A.3: Selected bond distances (\AA) of **4**

Ir–Rh	2.848(3)	Rh–P(4)	2.354(8)
Ir–P(1)	2.344(7)	Rh–Si(1A)	2.317(1)
Ir–P(3)	2.348(8)	Rh–Si(1B)	2.435(4)
Ir–Si(1A)	2.355(1)	Rh–H(1)	1.549(3)
Ir–Si(1B)	2.299(4)	Rh–C(1)	1.869(4)
Ir–H(1)	1.550(3)	C(1)–O(1)	1.153(4)
Ir–C(2)	1.862(4)	C(2)–O(2)	1.150(4)
Rh–P(2)	2.335(8)		

Table A.4: Selected bond angles ($^\circ$) of **4**

Rh–Ir–P(2)	93.04(1)	Ir–Rh–Si(1A)	53.06(3)
Rh–Ir–P(3)	91.58(2)	Ir–Rh–Si(1B)	50.88(1)
Ir–Rh–P(2)	90.44(2)	Rh–Ir–C(2)	157.40(1)
Ir–Rh–P(4)	91.53(2)	Ir–Rh–C(1)	156.79(1)
Rh–Ir–Si(1A)	51.84(3)	P(1)–Ir–P(3)	97.75(3)
Rh–Ir–Si(1B)	55.24(1)	P(2)–Rh–P(4)	99.199(16)

Table A.5: Selected bond distances (Å) of **5** (molecule A)

Ir–Rh	2.851(1)	Rh–Si(1)	2.383(5)
Ir–P(1)	2.347(4)	Rh–H(1)	1.480(3)
Ir–P(3)	2.356(5)	Rh–C(2)	1.867(2)
Ir–Si(1)	2.359(5)	C(1)–O(1)	1.151(2)
Ir–H(1)	1.560(3)	C(2)–O(2)	1.148(2)
Ir–C(1)	1.861(2)	Si(1)–H(1SI)	1.520(2)
Rh–P(2)	2.341(4)	Si(1)–H(1)*	2.604(3)

* = Non-bonded distances

Table A.6: Selected bond angles (°) of **5** (molecule A)

Rh–Ir–P(1)	90.86(1)	Si(1)–Rh–H(2)	64.30(1)
Rh–Ir–P(3)	93.42(1)	Si(1)–Ir–H(1)	80.40(9)
Ir–Rh–P(2)	91.14(1)	P(1)–Ir–Si(1)	94.96(2)
Ir–Rh–P(4)	87.39(1)	P(3)–Ir–Si(1)	145.08(2)
Rh–Ir–Si(1)	53.41(1)	P(4)–Rh–Si(1)	129.52(2)
Ir–Rh–Si(1)	52.67(1)	P(2)–Rh–Si(1)	109.69(2)
Rh–Ir–H(1)	79.70(1)	P(2)–Rh–P(4)	99.20(2)
Ir–Rh–H(2)	85.90(1)	P(1)–Ir–H(1)	170.50(1)
P(1)–Ir–P(3)	96.28(2)	P(2)–Rh–H(2)	173.90(1)
Rh–Ir–C(1)	154.34(6)	P(3)–Ir–H(1)	83.20(9)
Ir–Rh–C(2)	157.32(6)	P(4)–Rh–H(2)	86.00(1)

Table A.7: Selected bond distances (Å) of **5** (molecule B)

Ir–Rh	2.843(1)	Rh–Si(1)	2.364(5)
Ir–P(1)	2.348(4)	Rh–H(1)	1.520(3)
Ir–P(3)	2.338(5)	Rh–C(2)	1.867(2)
Ir–Si(1)	2.366(5)	C(1)–O(1)	1.144(2)
Ir–H(1)	1.540(2)	C(2)–O(2)	1.149(2)
Ir–C(1)	1.866(2)	Si(1)–H(2SI)	1.447(2)
Rh–P(2)	2.347(4)	Si(1)–H(1)*	2.631(3)
Rh–P(4)	2.352(5)	Si(1)–H(2)*	2.247(3)

* = Non-bonded distances

Table A.8: Selected bond angles ($^{\circ}$) of **5** (molecule B)

Rh–Ir–P(1)	91.82(1)	Si(1)–Rh–H(2)	66.60(1)
Rh–Ir–P(3)	93.61(1)	Si(1)–Ir–H(1)	81.70(9)
Ir–Rh–P(2)	91.14(1)	P(1)–Ir–Si(1)	93.79(2)
Ir–Rh–P(4)	88.54(1)	P(3)–Ir–Si(1)	145.63(2)
Rh–Ir–Si(1)	53.04(1)	P(4)–Rh–Si(1)	133.82(2)
Ir–Rh–Si(1)	53.08(1)	P(2)–Rh–Si(1)	106.84(2)
Rh–Ir–H(1)	78.10(9)	P(2)–Rh–P(4)	97.40(2)
Ir–Rh–H(2)	83.70(1)	P(1)–Ir–H(1)	169.90(9)
P(1)–Ir–P(3)	96.78(1)	P(2)–Rh–H(2)	173.30(1)
Rh–Ir–C(1)	157.59(6)	P(3)–Ir–H(1)	83.30(9)
Ir–Rh–C(2)	153.90(6)	P(4)–Rh–H(2)	86.80(1)

Table A.9: Selected bond distances (\AA) of **8c**

Ir–Rh	2.825(4)	Rh–Si(2)	2.371(1)
Ir–P(1)	2.373(9)	Ir–C(1)	1.859(4)
Ir–P(3)	2.343(9)	Rh–C(2)	1.854(5)
Ir–Si(1)	2.362(1)	C(1)–O(1)	1.151(5)
Ir–Si(2)	1.353(1)	C(2)–O(2)	1.175(6)
Rh–P(2)	2.361(9)	Si(1)–H(1)	1.41(4)
Rh–P(4)	2.366(9)	Si(1)–H(2)	1.40(4)
Rh–Si(1)	2.348(1)	Si(1)–Si(2)	2.873(1)

Table A.10: Selected bond angles ($^{\circ}$) of **8c**

Rh–Ir–Si(1)	52.94(3)	Rh–Ir–P(1)	94.04(3)
Rh–Ir–Si(2)	53.57(3)	Rh–Ir–P(3)	93.92(3)
Ir–Rh–Si(1)	53.35(3)	Ir–Rh–P(2)	94.73(3)
Ir–Rh–Si(2)	52.97(3)	Ir–Rh–P(4)	94.14(3)
Si(1)–Ir–Si(2)	75.09(4)	P(1)–Ir–Si(1)	83.47(4)
Si(1)–Rh–Si(2)	74.99(3)	P(3)–Ir–Si(2)	84.43(3)
Rh–Si(1)–Ir	73.71(3)	P(2)–Rh–Si(1)	82.71(3)
Rh–Si(2)–Ir	73.46(3)	P(4)–Rh–Si(2)	85.58(3)

Table A.11: Selected bond distances (Å) of **12**

Ir–Rh	2.8594(6)	Rh–Si(1)	2.427(2)
Ir–P(1)	2.341(2)	Rh–Si(2)	2.398(2)
Ir–P(3)	2.273(2)	Rh–C(2)	1.904(10)
Ir–Si(1)	2.338(2)	Rh–C(3)	1.878(10)
Ir–H(1)	1.65	C(1)–O(1)	1.141(11)
Ir–C(1)	1.905(11)	C(2)–O(2)	1.146(10)
Rh–P(2)	2.372(2)	C(2)–O(2)	1.151(10)

Table A.12: Selected bond angles (°) of **12**

Rh–Ir–P(1)	91.09(5)	Rh–Ir–C(1)	93.60(2)
Rh–Ir–P(3)	156.46(5)	Ir–Rh–C(2)	92.80(2)
Ir–Rh–P(2)	93.57(5)	Ir–Rh–C(3)	93.20(2)
Rh–Ir–Si(1)	54.55(5)	Rh–Si(1)–Ir	73.73(6)
Ir–Rh–Si(1)	51.72(5)	Ir–P(3)–C(5)	114.00(3)
Ir–Rh–Si(2)	165.33(6)	Rh–P(2)–C(4)	110.00(3)
Rh–Ir–H	99.5	Ir–P(1)–C(4)	109.90(3)

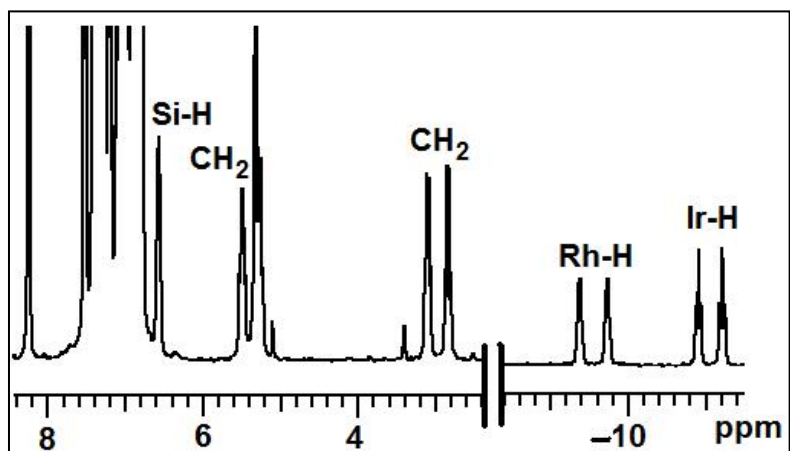


Figure A.2: $^1\text{H-NMR}$ spectrum of $[\text{RhIr}(\text{H})_2(\text{CO})_2(\mu\text{-SiHPh})(\text{dppm})_2]$ (**4**) at $-50\text{ }^\circ\text{C}$

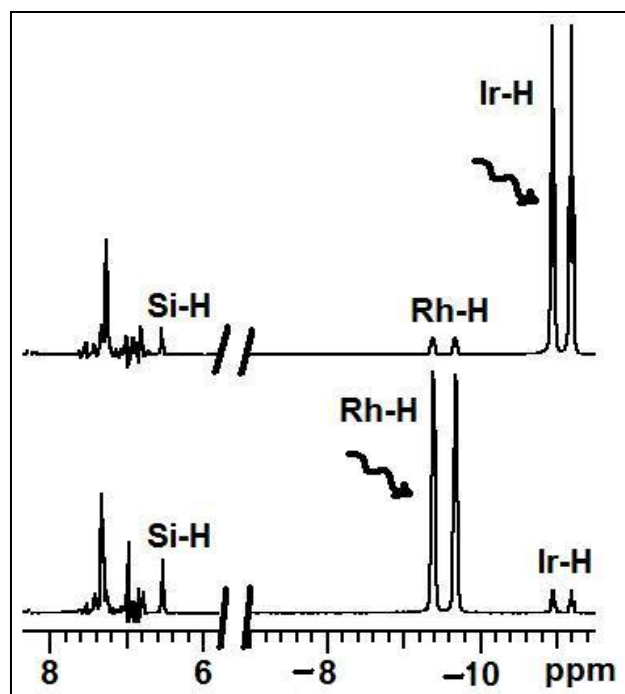


Figure A.3: STD-NMR spectrum of complex **4** at $-50\text{ }^\circ\text{C}$. The resonance irradiated is indicated by the oscillating arrow sign.

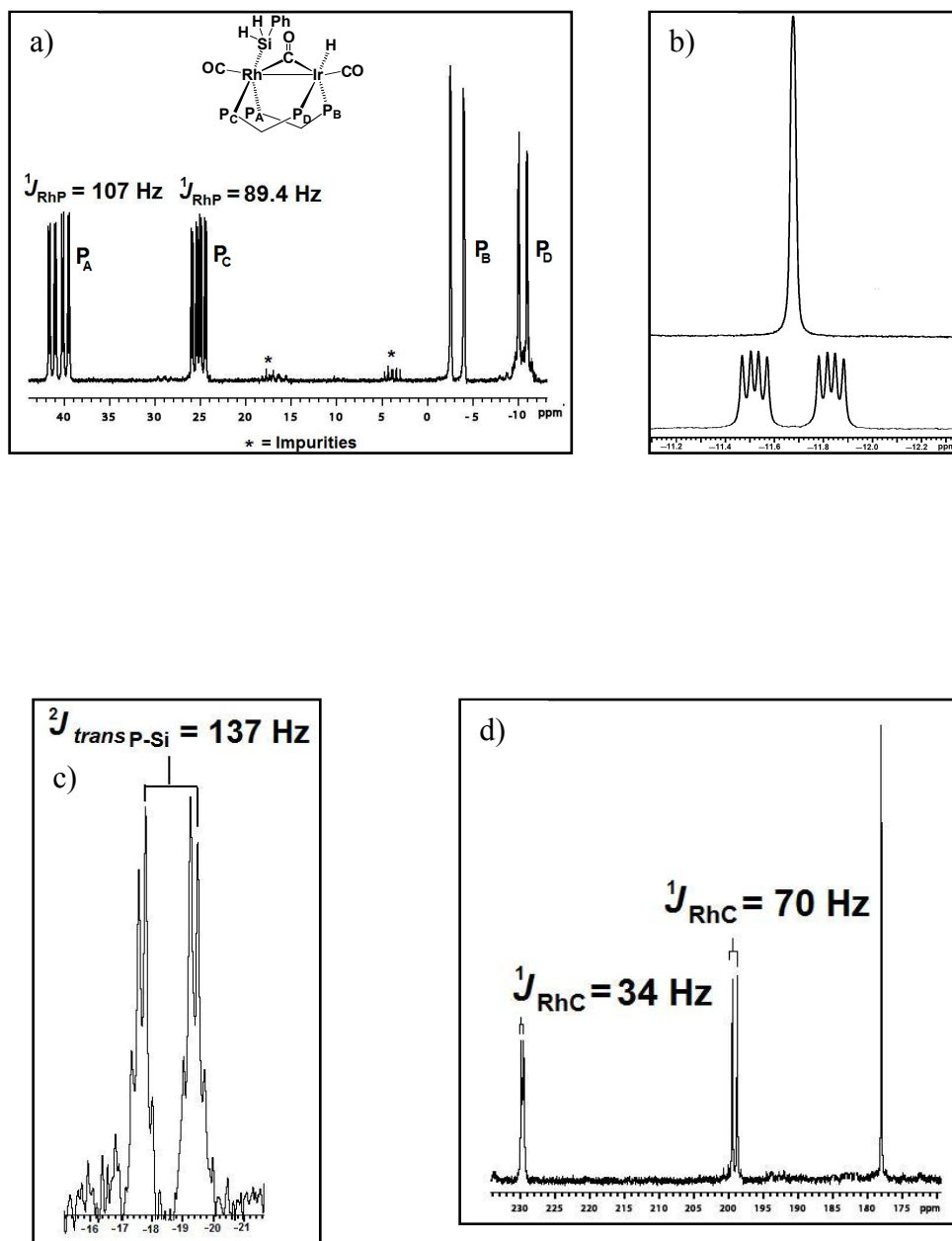


Figure A.4: Selected NMR spectra of $[\text{RhIr}(\text{H})(\text{SiH}_2\text{Ph})(\text{CO})_2(\mu\text{-CO})(\text{dppm})_2]$ (**2**) at $-80 \text{ }^\circ\text{C}$: a) ${}^{31}\text{P}\{^1\text{H}\}$ NMR spectrum; b) Iridium-bound hydride resonance in the ${}^1\text{H}$ NMR (below) and ${}^1\text{H}\{\text{broadband } {}^{31}\text{P}\}$ NMR spectra (above); c) ${}^{29}\text{Si}\{^1\text{H}\}$ -NMR spectrum; and d) ${}^{13}\text{C}\{^1\text{H}, {}^{31}\text{P}\}$ NMR spectrum showing three CO resonances.

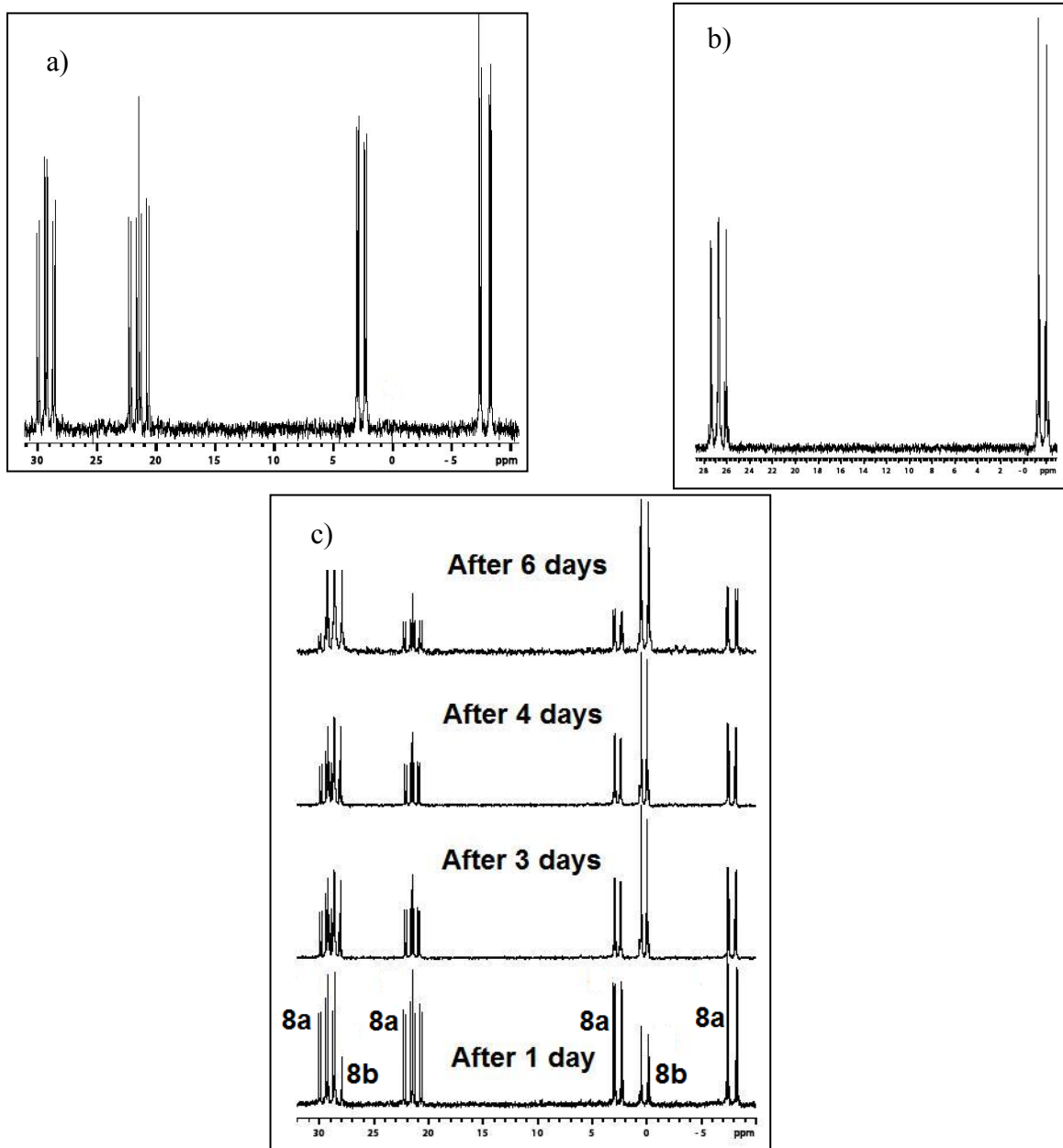


Figure A.5: a) $^{31}\text{P}\{^1\text{H}\}$ NMR spectra of a) $ax/eq-[RhIr(CO)_2(\mu\text{-SiHPh})_2(dppm)_2]$ (**8a**) b) $ax/ax-[RhIr(CO)_2(\mu\text{-SiHPh})_2(dppm)_2]$ (**8b**) c) mixture of **8a** and **8b** showing the slow conversion of former to latter at room temperature.

Appendix II – For Chapter 3

Table A.13. Crystallographic Experimental Details for Compounds **20**, **21** and **23**

Compound	20 •C ₆ H ₆	21 •CH ₂ Cl ₂	23 •CH ₂ Cl ₂
Formula	C ₆₄ H ₅₈ GeIrO ₂ P ₄ Rh	C ₅₇ H ₅₈ Cl ₂ GeIrO ₂ P ₄ Rh	C ₇₁ H ₆₂ Cl ₂ Ge ₂ IrO ₂ P ₄ Rh
formula weight	1350.68	1337.51	1582.28
crystal dimens (mm)	0.39 × 0.32 × 0.21	0.71 × 0.55 × 0.28	0.22 × 0.21 × 0.14
crystal system	orthorhombic	orthorhombic	monoclinic
space group	P2 ₁ 2 ₁ 2 ₁ (No. 19)	P2 ₁ 2 ₁ 2 ₁ (No. 19)	P2 ₁ /n (No. 14)
unit cell parameters			
<i>a</i> (Å)	12.6582(5)	12.3318 (7)	19.0061(10)
<i>b</i> (Å)	18.0565(7)	17.7653 (10)	15.3895(8)
<i>c</i> (Å)	24.8261(10)	25.2646 (15)	21.6357(11)
<i>α</i> (deg)			
<i>β</i> (deg)			91.0052(8)
<i>γ</i> (deg)			
<i>V</i> (Å ³)	5674.3(4)	5534.9 (6)	6327.2(6)
<i>Z</i>	4	4	4
ρ_{calcd} (g cm ⁻³)	1.581	1.605	1.661
μ (mm ⁻¹)	3.309	3.485	3.525
diffractometer	Bruker D8/APEX II CCD ^a		
radiation (λ [Å])	graphite-monochromated Mo K α (0.71073)		
temperature (°C)	-100	-100	-100
scan type	ω scans (0.3°) (15 s exposures)	ω scans (0.3°) (15 s exposures)	ω scans (0.3°) (20 s exposures)
$2\theta_{\text{max}}$ (deg)	55.18	54.98	52.82
total data collected	50979(-16 ≤ <i>h</i> ≤ 16, -23 ≤ <i>k</i> ≤ 23, -22 ≤ <i>l</i> ≤ 32)	48239 (-15 ≤ <i>h</i> ≤ 16, -23 ≤ <i>k</i> ≤ 23, -32 ≤ <i>l</i> ≤ 32)	50313 (-23 ≤ <i>h</i> ≤ 23, -19 ≤ <i>k</i> ≤ 27, -26 ≤ <i>l</i> ≤ 27)
Independ reflns (R _{int})	13100 (0.0353)	12595 (0.0197)	12962(0.0616)
obsd reflns [I ≥ 2σ(I)]	12714	12378	10058
restraints/params	5 / 676	6 / 612	0/753
goodness-of-fit (S) ^c	1.154	1.074	1.019
final <i>R</i> indices ^d			
<i>R</i> ₁ [I ≥ 2σ(I)]	0.0200	0.0188	0.0318
<i>wR</i> ₂ [all data]	0.0456	0.0526	0.0724
largest diff peak, hole (e Å ⁻³)	0.555, -0.384	1.018, -0.781	1.017, -1.013

a. Programs for diffractometer operation, data collection, data reduction and absorption correction were those supplied by Bruker.

b. $S = [\sum w(F_o^2 - F_c^2)^2 / (n - p)]^{1/2}$ (*n* = number of data; *p* = number of parameters varied; $w = [\sigma^2(F_o^2) + (a_0P)^2 + a_1P]^{-1}$ where $P = [\text{Max}(F_o^2, 0) + 2F_c^2]/3$ and the values of *a*₀ and *a*₁ are optimized during refinement; for **20**, *a*₀ = 0.0047, *a*₁ = 2.4481; for **21**, *a*₀ = 0.0290, *a*₁ = 2.5187; for **23**, *a*₀ = 0.0269, *a*₁ = 6.9795.

c. $R_1 = \sum ||F_o| - |F_c|| / \sum |F_o|$; $wR_2 = [\sum w(F_o^2 - F_c^2)^2 / \sum w(F_o^4)]^{1/2}$.

Table A.14. Crystallographic Experimental Details for Compounds **24**, **25** and **28**.

Compound	24•2CH₂Cl₂	25•1.5C₆H₅F	28•3C₄H₈O
Formula	C ₆₆ H ₆₀ Cl ₄ GeIrO ₂ P ₄ Rh	C ₈₆ H _{73.5} F _{1.5} Ge ₂ IrO ₃ P ₄ Rh	C ₁₀₀ H ₈₇ BGeIrO ₃ P ₄ Rh
formula weight	1518.52	1747.62	1883.18
crystal dimens (mm)	0.31 × 0.21 × 0.05	0.71 × 0.56 × 0.34	0.39 × 0.29 × 0.04
crystal system	trigonal	triclinic	triclinic
space group	<i>P</i> 3 ₁ (No. 144)	<i>P</i> $\bar{1}$ (No. 2)	<i>P</i> $\bar{1}$ (No. 2)
unit cell param.			
<i>a</i> (Å)	13.0777(6)	13.4862 (5)	11.4112 (12)
<i>b</i> (Å)		15.7589 (6)	18.4332 (19)
<i>c</i> (Å)	32.0219(14)	20.9542 (8)	20.728 (2)
α (deg)		97.4832 (4)	81.9654(12)
β (deg)		104.7670 (4)	89.8087(12)
γ (deg)		113.7850 (4)	89.6227(12)
<i>V</i> (Å ³)	4742.9(4)	3801.4 (3)	4310.0 (8)
<i>Z</i>	3	2	2
ρ_{calcd} (g cm ⁻³)	1.595	1.527	1.449
μ (mm ⁻¹)	3.143	2.878	2.200
diffractometer	Bruker D8/APEX II CCD ^a		Bruker PLATFORM/SMART 1000CCD ^a
radiation (λ Å)	graphite-monochromated Mo <i>K</i> α (0.71073)		
temperature(°C)	-100	-100	-100
scan type	ω scans (0.3°) (20 s exposures)	ω scans (0.3°) (20 s exposures)	ω scans (0.3°) (20 s exposures)
$2\theta_{\text{max}}$ (deg)	54.96	55.22	52.90
total data coll.	42144(-16 ≤ <i>h</i> ≤ 16, -16 ≤ <i>k</i> ≤ 16 -41 ≤ <i>l</i> ≤ 41)	34726 (-17 ≤ <i>h</i> ≤ 17, -20 ≤ <i>k</i> ≤ 20, -27 ≤ <i>l</i> ≤ 27)	34713 (-14 ≤ <i>h</i> ≤ 14, -23 ≤ <i>k</i> ≤ 23, -25 ≤ <i>l</i> ≤ 25)
Independ reflns (R _{int})	14411(0.0186)	17540 (0.0095)	17703 (0.0303)
obsd reflns [I ≥ 2σ(I)]	14242	16703	13808
restraints/param	33 / 672	12 / 850	20 / 994
goodness-of-fit (S) ^c	1.222	1.035	1.038
final <i>R</i> indices ^d			
<i>R</i> ₁ [I ≥ 2σ(I)]	0.0520	0.0187	0.0349
<i>wR</i> ₂ [all data]	0.1179	0.0537	0.0878
largest diff peak, hole (e Å ⁻³)	1.193, -1.965	1.317, -1.074	0.968, -1.202

a. Programs for diffractometer operation, data collection, data reduction and absorption correction were those supplied by Bruker.

b. $S = [\sum w(F_o^2 - F_c^2)^2 / (n - p)]^{1/2}$ (*n* = number of data; *p* = number of parameters varied; $w = [\sigma^2(F_o^2) + (a_0P)^2 + a_1P]^{-1}$ where $P = [\text{Max}(F_o^2, 0) + 2F_c^2]/3$ and the values of *a*₀ and *a*₁ are optimized during refinement; for **24**, *a*₀ = 0, *a*₁ = 31.9801; for **25**, *a*₀ = 0.0298, *a*₁ = 2.5341; for **28**, *a*₀ = 0.0362, *a*₁ = 4.7526.

c. $R_1 = \sum ||F_o| - |F_c|| / \sum |F_o|$; $wR_2 = [\sum w(F_o^2 - F_c^2)^2 / \sum w(F_o^4)]^{1/2}$.

Table A.15. Crystallographic Experimental Details for Compounds **29**, **30** and **31**.

Compound	29 •4 C ₄ H ₈ O	30 •1.5 CH ₂ Cl ₂	31 •1.5 CH ₂ Cl ₂ •0.5 C ₄ H ₁₀ O
Formula	C ₁₀₄ H ₁₀₉ BGeIrO ₆ P ₄ Rh	C _{66.5} H ₆₀ F ₃ GeIrO ₆ P ₄ RhS	C _{69.5} H ₆₇ F ₃ GeIrO ₇ P ₄ RhS
formula weight	1957.30	1642.14	1693.22
crystal dimens (mm)	0.34 × 0.22 × 0.11	0.28 × 0.17 × 0.17	0.29 × 0.15 × 0.12
crystal system	triclinic	monoclinic	monoclinic
space group	<i>P</i> $\bar{1}$ (No. 2)	<i>P</i> 2 ₁ / <i>c</i> (No. 14)	<i>P</i> 2 ₁ / <i>n</i> (No. 14)
unit cell param.			
<i>a</i> (Å)	14.1513(4)	13.0611(7)	17.0440(6)
<i>b</i> (Å)	16.7686(5)	22.6927(12)	24.1520(12)
<i>c</i> (Å)	20.6792(6)	22.6651(12)	17.5193(9)
α (deg)	96.1547(3)		
β (deg)	108.3519(3)	100.7033(7)	98.4450(10)
γ (deg)	97.5944(4)		
<i>V</i> (Å ³)	4558.6(2)	6600.9(6)	7133.6(6)
<i>Z</i>	2	4	4
ρ_{calcd} (g cm ⁻³)	1.426	1.652	1.577
μ (mm ⁻¹)	2.087	3.019	2.797
diffractometer	Bruker D8/APEX IICCD ^a	Bruker PLATFORM/APEX II CCD ^a	
radiation (λ Å)	graphite-monochromated Mo K α (0.71073)		
temperature(°C)	-100	- 100	- 100
scan type	ω scans (0.3°) (20 s exposures)	ω scans (0.3°) (20 s exposures)	ω scans (0.3°) (20 s exposures)
$2\theta_{\text{max}}$ (deg)	55.00	52.96	55.66
total data coll.	40961(-18 ≤ <i>h</i> ≤ 18, -21 ≤ <i>k</i> ≤ 21, -26 ≤ <i>l</i> ≤ 26)	52762((-16 ≤ <i>h</i> ≤ 16, -28 ≤ <i>k</i> ≤ 28, -28 ≤ <i>l</i> ≤ 28)	63884(-22 ≤ <i>h</i> ≤ 22, -31 ≤ <i>k</i> ≤ 31, -22 ≤ <i>l</i> ≤ 23)
Independ reflns (R _{int})	20835 (0.0167)	13627(0.0391)	16865(0.0424)
obsd reflns [I ≥ 2σ(I)]	18288	11342	13522
restraints/param	5 / 985	0/805	10 / 821
goodness-of-fit (S) ^c	1.070	1.056	1.068
final <i>R</i> indices ^d			
<i>R</i> ₁ [I ≥ 2σ(I)]	0.0252	0.0411	0.0338
<i>wR</i> ₂ [all data]	0.0759	0.0968	0.0962
largest diff peak, hole (e Å ⁻³)	0.763, -0.446	1.839, -1.516	1.753, -1.004

a. Programs for diffractometer operation, data collection, data reduction and absorption correction were those supplied by Bruker.

b. $S = [\sum w(F_o^2 - F_c^2)^2 / (n - p)]^{1/2}$ (*n* = number of data; *p* = number of parameters varied; $w = [\sigma^2(F_o^2) + (a_0P)^2 + a_1P]^{-1}$ where $P = [\text{Max}(F_o^2, 0) + 2F_c^2]/3$ and the values of *a*₀ and *a*₁ are optimized during refinement; for **29**, *a*₀ = 0.0455, *a*₁ = 0.7951; for **30**, *a*₀ = 0.0370, *a*₁ = 18.3210; for **31**, *a*₀ = 0.0434, *a*₁ = 15.1816).

c. $R_1 = \sum ||F_o| - |F_c|| / \sum |F_o|$; $wR_2 = [\sum w(F_o^2 - F_c^2)^2 / \sum w(F_o^4)]^{1/2}$.

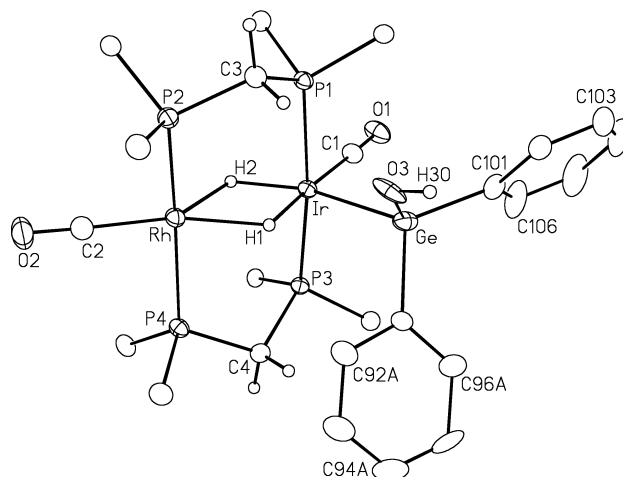


Figure A.6: Perspective view of the complex cation of **30** showing the numbering scheme. Non-hydrogen atoms are represented by Gaussian ellipsoids at the 20% probability level. Hydrogen atoms are shown arbitrarily small. For the *dppm* phenyl groups only the ipso carbons are shown.

Table A.16: Selected bond distances (\AA) of **20**

Ir(A)–Rh(A)	2.8691(2)	Rh(A)–P(4)	2.3354(7)
Ir(A)–P(1)	2.3343(7)	Rh(A)–Ge(A)	2.4000(4)
Ir(A)–P(3)	2.3443(7)	Rh(B)–Ge(B)	2.4023(15)
Ir(A)–Ge(A)	2.4234(1)	Rh(A)–H(1)	1.55 ^a
Ir(B)–Ge(B)	2.4951(15)	Rh(A)–C(2)	1.868(4)
Ir(A)–H(1)	1.55	C(1)–O(1)	1.160(4)
Ir(A)–C(1)	1.860(3)	C(2)–O(2)	1.154(4)
Rh(A)–P(2)	2.3439(8)		

Table A.17: Selected bond angles ($^\circ$) of **20**

Rh(A)–Ir(A)–P(1)	91.33(2)	Ge(A)–Rh(A)–P(2)	137.66(2)
Rh(A)–Ir(A)–P(3)	93.002(18)	Ge(A)–Rh(A)–P(4)	103.31(2)
Ir(A)–Rh(A)–P(2)	91.26(2)	Ir(A)–Rh(A)–C(2)	156.99(1)
Ir(A)–Rh(A)–P(4)	90.050(19)	Rh(A)–Ir(A)–C(1)	157.45(10)
Ge(A)–Ir(A)–P(1)	143.11(2)	P(1)–Ir(A)–P(3)	97.93(3)
Ge(A)–Ir(A)–P(3)	93.93(2)	P(2)–Rh(A)–P(4)	99.41(3)
Ir(A)–Ge(A)–Rh(A)	72.998(12)		

Table A.18: Selected bond distances (\AA) of **21**

Ir–Rh	2.8736(2)	Rh–P(4)	2.3382(8)
Ir–P(1)	2.3445(7)	Rh–Ge	2.4294(3)
Ir–P(3)	2.3452(7)	Rh–H(2)	1.55
Ir–Ge	2.4303(3)	Rh–C(2)	1.867(3)
Ir–H(1)	1.55	C(1)–O(1)	1.155(4)
Ir–C(1)	1.861(3)	C(2)–O(2)	1.142(4)
Rh–P(2)	2.3351(7)		

Table A.19: Selected bond angles ($^\circ$) of **21**

Rh–Ir–P(1)	93.356(18)	Ge–Rh–P(2)	101.411(19)
Rh–Ir–P(3)	91.971(19)	Ge–Rh–P(4)	136.31(2)
Ir–Rh–P(2)	89.592(18)	Ir–Rh–C(2)	158.75(10)
Ir–Rh–P(4)	89.341(19)	Rh–Ir–C(1)	157.33(10)
Ge–Ir–P(1)	91.413(19)	P(1)–Ir–P(3)	97.14(2)
Ge–Ir–P(3)	145.17(2)	P(2)–Rh–P(4)	100.67(3)
Ir–Ge–Rh	72.501(10)		

Table A.20: Selected bond distances (\AA) of **23**

Ir(A)–Rh(A)	2.8070(3)	Rh(A)–P(4)	2.3476(11)
Ir(A)–P(1)	2.3494(11)	Rh(A)–Ge(1)	2.4320(5)
Ir(A)–P(3)	2.3484(10)	Rh(A)–Ge(2)	2.4436(5)
Ir(A)–Ge(1)	2.4516(5)	Rh(A)–C(2)	1.862(4)
Ir(A)–Ge(2)	2.4857(5)	C(1)–O(1)	1.150(5)
Ir(A)–C(1)	1.868(4)	C(2)–O(2)	1.151(5)
Rh(A)–P(2)	2.3252(11)	Ge(1)–Ge(2)	2.9921(6) ^a

a = non-bonded distance

Table A.21: Selected bond angles ($^\circ$) of **23**

Rh(A)–Ir(A)–P(1)	92.17(3)	Ge(1)–Rh(A)–P(2)	82.28(3)
Rh(A)–Ir(A)–P(3)	96.42(3)	Ge(1)–Rh(A)–P(4)	145.423
Ir(A)–Rh(A)–P(2)	96.36(3)	Ge(2)–Rh(A)–P(2)	151.40(3)
Ir(A)–Rh(A)–P(4)	90.77(3)	Ge(2)–Rh(A)–P(4)	91.06(3)
Ge(1)–Ir(A)–P(1)	81.58(3)	Ir(A)–Ge(1)–Rh(A)	70.166(13)
Ge(1)–Ir(A)–P(3)	150.64(3)	Ir(A)–Ge(2)–Rh(A)	69.416(13)
Ge(2)–Ir(A)–P(1)	146.31(3)	P(1)–Ir(A)–P(3)	106.59(4)
Ge(2)–Ir(A)–P(3)	84.77(3)	P(2)–Rh(A)–P(4)	97.03(4)
Ge(1)–Ir(A)–Ge(2)	74.601(15)	Ge(1)–Rh(A)–Ge(2)	75.714(16)

Table A.22: Selected bond distances (Å) of **24**

Ir(A)–Rh(A)	2.8790(6)	Rh(A)–P(4)	2.346(2)
Ir(A)–P(1)	2.335(2)	Rh(A)–Ge	2.4372(10)
Ir(A)–P(3)	2.325(2)	Rh(A)–H(1)	1.598(10) ^b
Ir(A)–Ge	2.4365(10)	Rh(A)–C(2)	1.844(10)
Ir(A)–H(1)	1.597(10)	C(1)–O(1)	1.167(12)
Ir(A)–C(1)	1.835(10)	C(2)–O(2)	1.144(12)
Rh(A)–P(2)	2.317(2)		

Table A.23: Selected bond angles (°) of **24**

Rh(A)–Ir(A)–P(1)	83.20(6)	Ge–Rh(A)–P(2)	135.78(6)
Rh(A)–Ir(A)–P(3)	95.10(5)	Ge–Rh(A)–P(4)	105.11(6)
Ir(A)–Rh(A)–P(2)	94.96(5)	Ir(A)–Rh(A)–C(2)	153.7(4)
Ir(A)–Rh(A)–P(4)	83.32(6)	Rh(A)–Ir(A)–C(1)	151.8(4)
Ge–Ir(A)–P(1)	106.23(6)	P(1)–Ir(A)–P(3)	100.45(8)
Ge–Ir(A)–P(3)	134.77(6)	P(2)–Rh(A)–P(4)	100.30(8)
P(1)–Ir(A)–H(1)	164(3)	P(2)–Rh(A)–H(2)	82(2)
Ir(A)–Ge–Rh(A)	72.42(3)		

Table A.24: Selected bond distances (Å) of **25**

Ir–Rh	2.85754(18)	Rh–Ge(1)	2.4923(3)
Ir–P(1)	2.3207(5)	Rh–Ge(2)	2.4665(3)
Ir–P(3)	2.2774(5)	Rh–C(2)	1.903(2)
Ir–Ge(1)	2.4103(2)	Rh–C(3)	1.883(2)
Ir–H(1)	1.55(3)	C(1)–O(1)	1.137(3)
Ir–C(1)	1.902(2)	C(2)–O(2)	1.138(3)
Rh–P(2)	2.3582(5)	C(2)–O(2)	1.143(3)

Table A.25: Selected bond angles (°) of **25**

Rh–Ir–P(1)	90.870(12)	Rh–Ir–C(1)	93.41(6)
Rh–Ir–P(3)	156.349(13)	Ir–Rh–C(2)	92.62(6)
Ir–Rh–P(2)	93.719(13)	Ir–Rh–C(3)	92.43(6)
Rh–Ir–Ge(1)	55.696(6)	Rh–Ge(1)–Ir	71.28(7)
Ir–Rh–Ge(1)	53.023(6)	Ir–P(3)–C(5)	113.86(7)
Ir–Rh–Ge(2)	164.796(8)	Rh–P(2)–C(4)	110.07(6)
Rh–Ir–H(1)	84.7(11)	Ir–P(1)–C(4)	110.54(6)

Table A.26: Selected bond distances (Å) of **28**

Ir(A)–Rh(A)	2.8337(3)	Rh(A)–P(4)	2.3060(10)
Ir(A)–P(1)	2.3243(10)	Rh(A)–Ge	2.4875(5)
Ir(A)–P(3)	2.3267(10)	Rh(A)–H(1)	1.77(4)
Ir(A)–Ge	2.5088(5)	Rh(A)–C(2)	1.843(4)
Ir(A)–H(1)	1.75(4)	C(1)–O(1)	1.147(5)
Ir(A)–C(1)	1.842(4)	C(2)–O(2)	1.160(5)
Rh(A)–P(2)	2.3220(10)		

Table A.27: Selected bond angles (°) of **28**

Rh(A)–Ir(A)–P(1)	92.99(2)	Ge–Rh(A)–P(2)	102.03(3)
Rh(A)–Ir(A)–P(3)	90.29(2)	Ge–Rh(A)–P(4)	94.88(3)
Ir(A)–Rh(A)–P(2)	91.02(2)	Ir(A)–Rh(A)–C(2)	168.56(14)
Ir(A)–Rh(A)–P(4)	93.90(2)	Rh(A)–Ir(A)–C(1)	167.44(14)
Ge–Ir(A)–P(1)	96.48(3)	P(1)–Ir(A)–P(3)	160.90(4)
Ge–Ir(A)–P(3)	100.81(3)	P(2)–Rh(A)–P(4)	162.19(3)
Ir(A)–Ge–Rh(A)	69.105(12)		

Table A.28: Selected bond distances (Å) of **29**

Ir–Rh	3.0273(2)	Rh–P(4)	2.3275(6)
Ir–P(1)	2.3065(6)	Rh–Ge	2.6106(3)
Ir–P(3)	2.3186(6)	Rh–H(2)	1.96(3)
Ir–Ge	2.5228(3)	Rh–H(3)	1.85(3)
Ir–H(1)	1.58(4)	Rh–C(2)	1.846(3)
Ir–H(2)	1.67(3)	C(1)–O(1)	1.142(3)
Ir–C(1)	1.885(3)	C(2)–O(2)	1.154(3)
Rh–P(2)	2.3335(6)		

Table A.29: Selected bond angles (°) of **29**

Rh–Ir–P(1)	87.166(15)	Ge–Ir–H(1)	176.3(13)
Rh–Ir–P(3)	90.921(15)	C(1)–Ir–H(2)	177.0(11)
Ir–Rh–P(2)	91.995(16)	Ge–Rh–C(2)	159.17(8)
Ir–Rh–P(4)	90.013(15)	H(1)–Ir–H(2)	84.5(17)
Ge–Ir–P(1)	99.142(17)	Ir–Rh–C(2)	148.28(8)
Ge–Ir–P(3)	97.900(16)	Rh–Ir–C(1)	145.67(9)
Ge–Rh–P(2)	92.767(17)	P(1)–Ir–P(3)	157.76(2)
Ge–Rh–P(4)	93.124(17)	P(2)–Rh–P(4)	173.78(2)
Ir–Ge–Rh	72.253(8)		

Table A.30: Selected bond distances (\AA) of **30**

Ir–Rh	2.8646(4)	Rh–P(2)	2.2996(13)
Ir–P(1)	2.3451(12)	Rh–P(4)	2.3053(13)
Ir–P(3)	2.3500(12)	Rh–H(1)	1.86(4)
Ir–Ge	2.4835(6)	Rh–H(2)	1.91(5)
Ir–H(1)	1.63(4)	Rh–C(2)	1.828(6)
Ir–H(2)	1.63(5)	C(1)–O(1)	1.145(6)
Ir–C(1)	1.867(5)	C(2)–O(2)	1.136(7)

Table A.31: Selected bond angles ($^\circ$) of **30**

Rh–Ir–P(1)	89.29(3)	Ge–Ir–H(2)	154.1(18)
Rh–Ir–P(3)	87.64(3)	H(2)–Ir–C(1)	106.4(18)
Ir–Rh–P(2)	93.61(3)	H(1)–Rh–C(2)	157.7(14)
Ir–Rh–P(4)	94.40(3)	H(2)–Rh–C(2)	137.4(16)
Ge–Ir–P(1)	89.92(3)	Ir–Rh–C(2)	170.1(2)
Ge–Ir–P(3)	97.70(3)	Rh–Ir–C(1)	145.80(16)
Ge–Ir–H(1)	77.3(15)	P(1)–Ir–P(3)	172.38(4)
		P(2)–Rh–P(4)	160.83(5)

Table A.32: Selected bond distances (\AA) of **31**

Ir–Rh	2.8605(3)	Rh–P(2)	2.3137(11)
Ir–P(1)	2.3440(10)	Rh–P(4)	2.3134(11)
Ir–P(3)	2.3423(10)	Rh–H(1)	2.04(5)
Ir–Ge	2.4925(5)	Rh–H(2)	1.89(4)
Ir–H(1)	1.67(5)	Rh–C(2)	1.823(4)
Ir–H(2)	1.68(4)	C(1)–O(1)	1.151(5)
Ir–C(1)	1.877(4)	C(2)–O(2)	1.145(5)

Table A.33: Selected bond angles ($^\circ$) of **31**

Rh–Ir–P(1)	91.09(3)	Ge–Ir–H(2)	72.2(15)
Rh–Ir–P(3)	88.02(3)	H(2)–Ir–C(1)	176.8(15)
Ir–Rh–P(2)	93.05(3)	H(1)–Rh–C(2)	138.0(15)
Ir–Rh–P(4)	93.16(3)	H(2)–Rh–C(2)	152.5(13)
Ge–Ir–P(1)	92.81(3)	Ir–Rh–C(2)	172.98(16)
Ge–Ir–P(3)	93.60(3)	Rh–Ir–C(1)	143.66(13)
Ge–Ir–H(1)	156.1(18)	P(1)–Ir–P(3)	173.40(4)
		P(2)–Rh–P(4)	167.01(4)

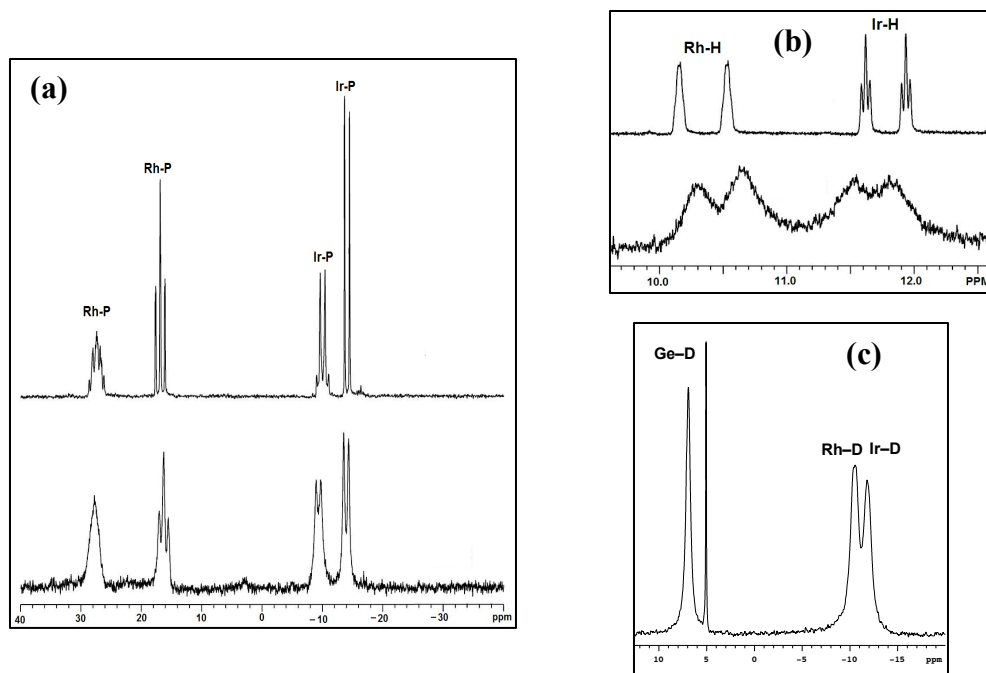


Figure A.7: a) $^{31}\text{P}\{^1\text{H}\}$ NMR spectra of compound **20** in CD_2Cl_2 at 27°C (below) and at -80°C (above). b) Hydride region of ^1H NMR spectra of complex **20** at 27°C (below) and at -80°C (above). c) ^2H NMR spectrum of **20-D₃** in CH_2Cl_2 showing M-D (M = Ir and Rh) and Ge-D.

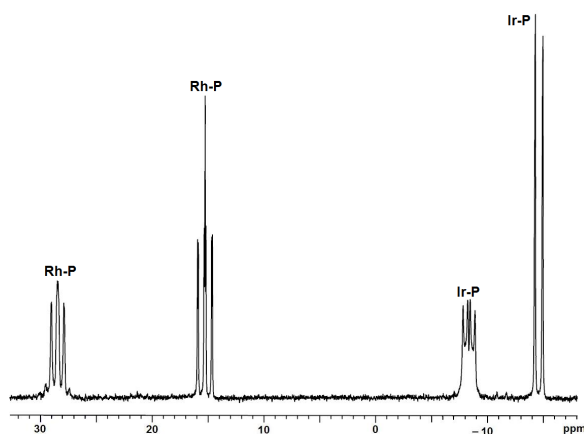


Figure A.8: $^{31}\text{P}\{^1\text{H}\}$ NMR spectrum of Compound **21** in CD_2Cl_2 at 27°C . The spectrum remain unchanged at -80°C

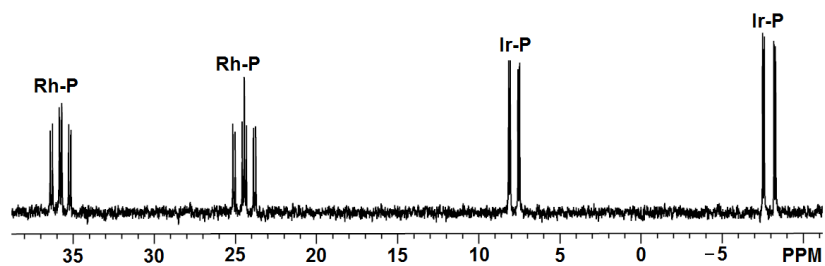


Figure A.9: $^{31}\text{P}\{^1\text{H}\}$ NMR spectrum of compound **23** in CD_2Cl_2 at 27°C .

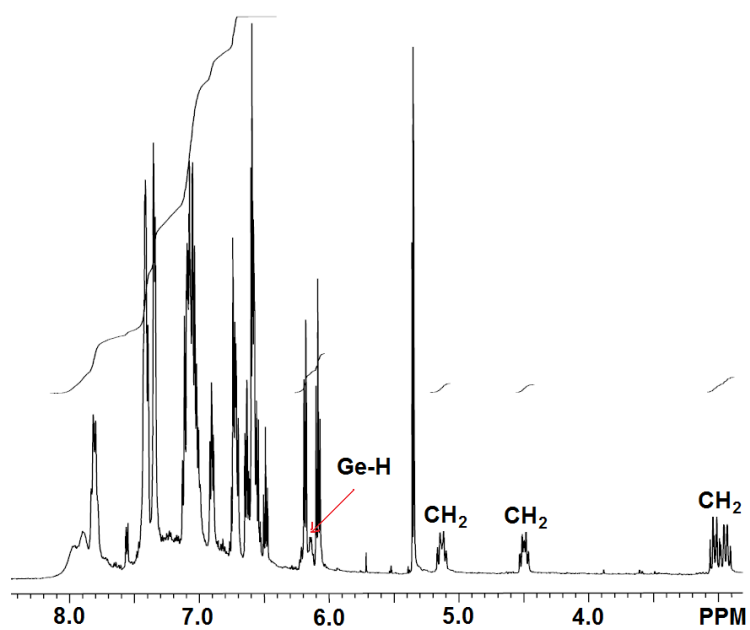


Figure A.10: ^1H NMR spectrum of compound **23** in CD_2Cl_2 at 27°C .

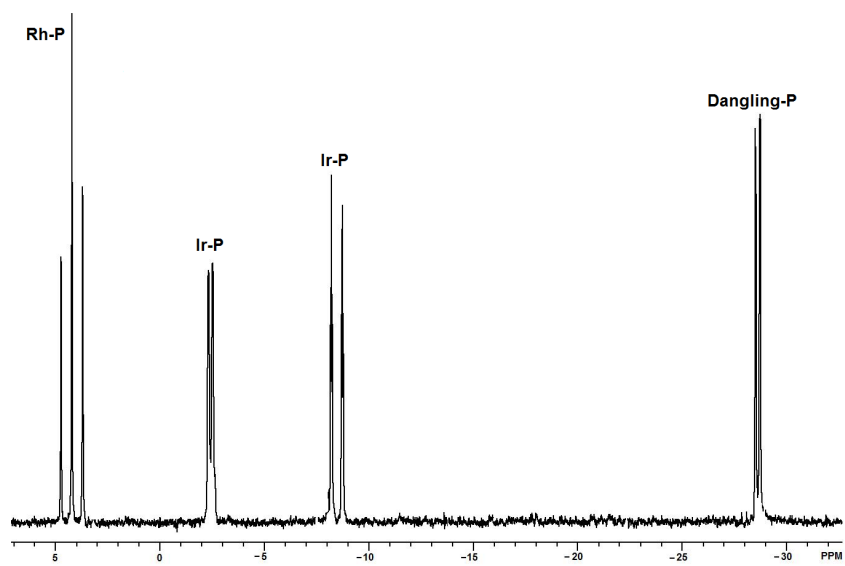


Figure A.11: $^{31}\text{P}\{^1\text{H}\}$ NMR spectrum of compound **25** in C_6D_6 at 27°C .

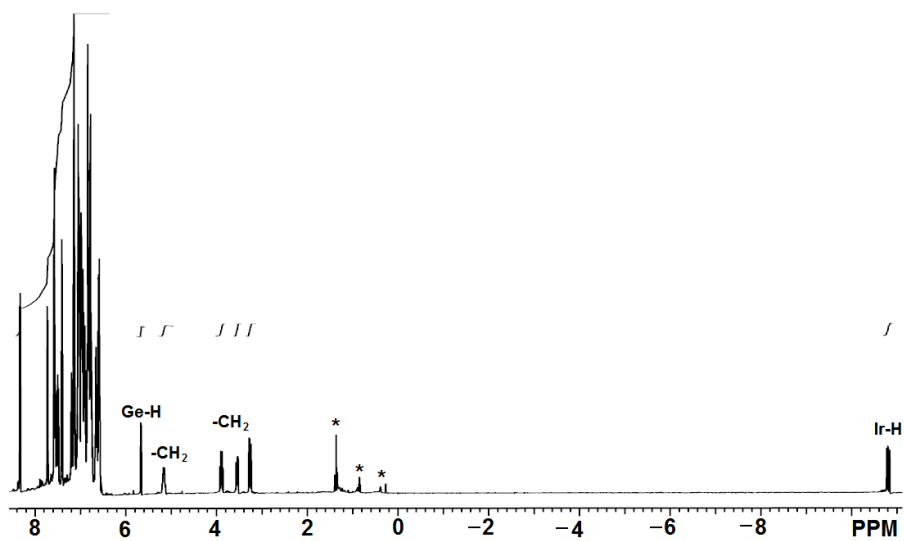


Figure A.12: ^1H NMR spectrum of compound **25** in C_6D_6 at 27°C . Asterisks denote the residual solvents.

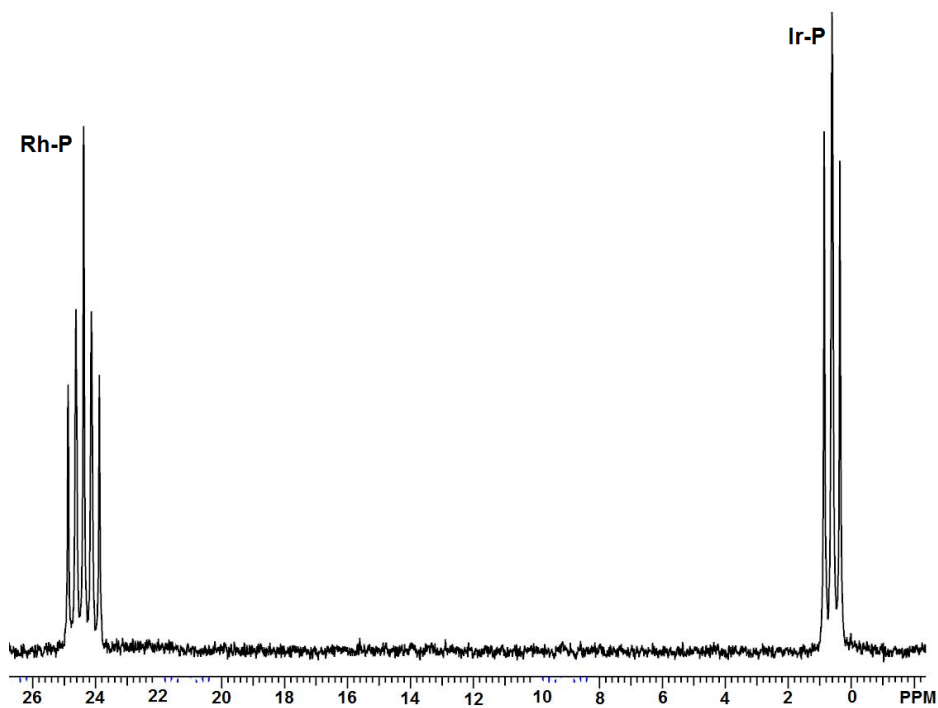


Figure A.13: $^{31}\text{P}\{^1\text{H}\}$ NMR spectrum of Compound **28** in CD_2Cl_2 at 27°C .

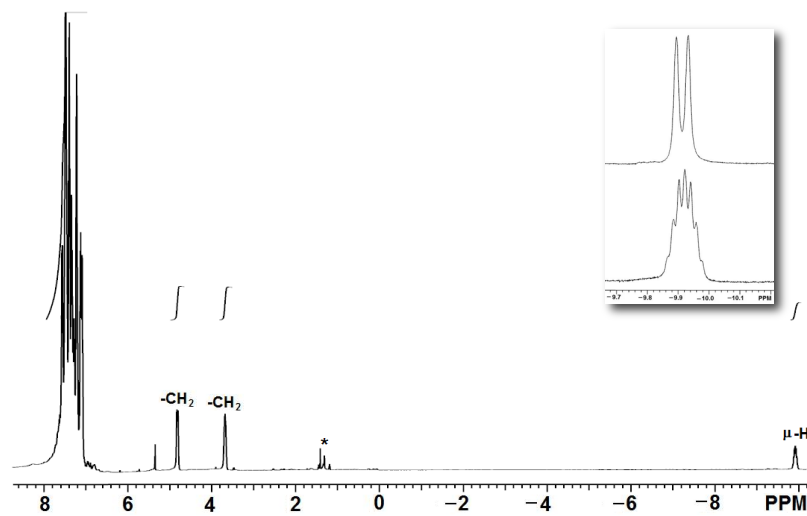


Figure A.14: ^1H NMR spectrum of Compound **28** in CD_2Cl_2 at 27°C . Inset shows the ^1H -NMR resonance of the $\mu\text{-H}$ moiety (below) with broadband ^{31}P -decoupling (above) for **28**. Asterisk denotes the residual solvents.

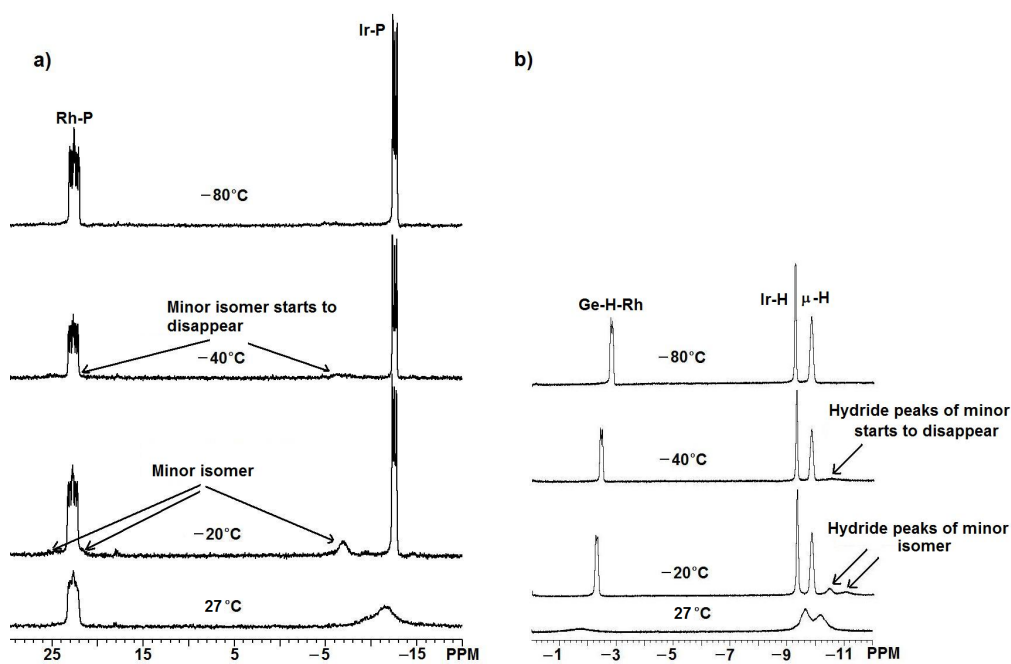


Figure A.15: Variable temperature a) $^{31}\text{P}\{^1\text{H}\}$ NMR spectrum and b) Hydride region of ^1H NMR spectrum of complex **29**. The major set of peaks corresponds to compound **29** and the indicated minor set of peaks at -20°C and -40°C is due to **29a**.

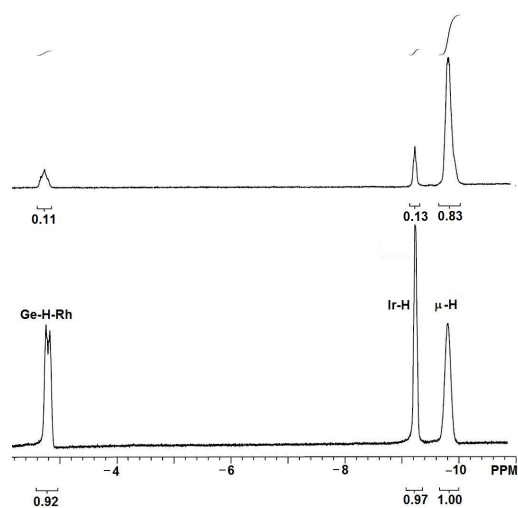


Figure A.16: Hydride region of ^1H NMR spectrum of complex **29** (below) and isotopologue **14-D₂** (above; the NMR spectrum was taken within 30 min of reacting compound **28** with D_2).

Appendix III – For Chapter 4

Table A.34. Crystallographic Experimental Details for Compounds 34, 35 and 36

Compound	34•CH ₂ Cl ₂	35•2 PhMe	36•2.5 C ₆ H ₆
Formula	C ₇₁ H ₆₂ Cl ₂ IrO ₂ P ₄ RhSi ₂	C ₇₈ H ₇₁ ClIrO ₂ P ₄ RhSi ₂	C ₈₀ H ₇₃ IrO ₂ P ₄ RhSi ₂
formula weight	1493.28	1550.97	1541.55
crystal dimens (mm)	0.19 × 0.18 × 0.09	0.41 × 0.15 × 0.13	0.39 × 0.31 × 0.25
crystal system	monoclinic	monoclinic	monoclinic
space group	<i>P</i> 2 ₁ / <i>n</i> (No. 14)	<i>C</i> 2/ <i>c</i> (No. 15)	<i>C</i> 2/ <i>c</i> (No. 15)
unit cell param.			
<i>a</i> (Å)	19.1085(9)	20.1970 (8)	20.1338 (8)
<i>b</i> (Å)	15.2861(7)	23.1105 (10)	22.4680 (9)
<i>c</i> (Å)	21.5289 (10)	29.3930 (12)	30.3133 (12)
β (deg)	90.6052(7)	96.3869 (5)	96.4988 (4)
<i>V</i> (Å ³)	6288.1 (5)	13634.4 (10)	13624.6 (9)
<i>Z</i>	4	8	8
ρ_{calcd} (g cm ⁻³)	1.577	1.511	1.503
μ (mm ⁻¹)	2.648	2.408	2.371
diffractometer	Bruker D8/APEX IICCD ^a		
radiation (λ Å)	graphite-monochromated Mo K α (0.71073)		
temperature(°C)	-100	-100	-100
scan type	ω scans (0.3°) (20s exposures)	ω scans (0.3°) (20 s exposures)	ω scans (0.3°) (20 s exposures)
2 θ_{max} (deg)	52.90	52.84	55.04
total data coll.	49929 (-23 ≤ <i>h</i> ≤ 23, -19 ≤ <i>k</i> ≤ 19, -26 ≤ <i>l</i> ≤ 26)	54580(-25 ≤ <i>h</i> ≤ 25, -28 ≤ <i>k</i> ≤ 28, -36 ≤ <i>l</i> ≤ 36)	59862 (-26 ≤ <i>h</i> ≤ 26, -29 ≤ <i>k</i> ≤ 29, -39 ≤ <i>l</i> ≤ 39)
Independ reflns (R _{int})	12939 (0.0293)	14019 (0.0384)	15662 (0.0248)
obsd reflns [I ≥ 2 σ (I)]	10206	11967	14009
restraints/param	0 / 753	12/ 722	0 / 817
goodness-of-fit (S) ^c	1.020	1.041	1.039
final <i>R</i> indices ^d			
<i>R</i> ₁ [I ≥ 2 σ (I)]	0.0312	0.0299	0.0216
<i>wR</i> ₂ [all data]	0.0720	0.0763	0.0530
largest diff peak, hole (e Å ⁻³)	1.017, -0.961	1.708, -1.220	0.974, -0.360

a. Programs for diffractometer operation, data collection, data reduction and absorption correction were those supplied by Bruker.

b. $S = [\sum w(F_o^2 - F_c^2)^2 / (n - p)]^{1/2}$ (*n* = number of data; *p* = number of parameters varied; $w = [\sigma^2(F_o^2) + (a_0P)^2 + a_1P]^{-1}$ where $P = [\text{Max}(F_o^2, 0) + 2F_c^2]/3$.

c. $R_1 = \sum |F_o| - |F_c| / \sum |F_o|$; $wR_2 = [\sum w(F_o^2 - F_c^2)^2 / \sum w(F_o^4)]^{1/2}$.

Table A.35. Crystallographic Experimental Details for Compounds 37 and 39.

Compound	37•2CH ₂ Cl ₂	39•CH ₂ Cl ₂
Formula	C ₆₇ H ₆₀ Cl ₄ F ₂ IrO ₂ P ₄ RhSi ₂	C ₇₁ H ₆₂ Cl ₂ Ge _{1.25} IrO ₂ P ₄ RhSi _{0.75}
formula weight	1552.12	1548.90
crystal dimens (mm)	0.31 × 0.28 × 0.11	0.43 × 0.29 × 0.21
crystal system	monoclinic	monoclinic
space group	<i>P</i> 2 ₁ / <i>n</i>	<i>P</i> 2 ₁ / <i>n</i> (No. 14)
unit cell param.		
<i>a</i> (Å)	12.5539(10)	19.0572(8)
<i>b</i> (Å)	22.3572(18)	15.3723(6)
<i>c</i> (Å)	22.6809(18)	21.6764(9)
β (deg)	96.4640(10)	91.0874(4)
<i>V</i> (Å ³)	6325.4(9)	6349.0(4)
<i>Z</i>	4	4
ρ_{calcd} (g cm ⁻³)	1.630	1.620
μ (mm ⁻¹)	2.722	3.179
diffractometer	Bruker D8/APEX IICCD ^a	Bruker PLATFORM/APEX II CCD ^a
radiation (λ Å)	Graphite-monochromated Mo K α (0.71073)	
temperature(°C)	-100	-100
scan type	ω scans (0.3°) (20 s exposures)	ω scans (0.3°) (20s exposures)
$2\theta_{\text{max}}$ (deg)	55.00	55.28
total data coll.	55252 ($-16 \leq h \leq 16$, $-28 \leq k \leq 29$, $-29 \leq l \leq 29$)	56287 ($-24 \leq h \leq 24$, $-20 \leq k \leq 20$, $-28 \leq l \leq 28$)
Independ reflns (<i>R</i> _{int})	14459(0.0348)	14740 (0.0177)
obsd reflns [<i>I</i> ≥ 2 σ (<i>I</i>)]	12515	13634
restraints/param	6/758	0 / 752
goodness-of-fit (<i>S</i>) ^c	1.018	1.049
final <i>R</i> indices ^d		
<i>R</i> ₁ [<i>I</i> ≥ 2 σ (<i>I</i>)]	0.0336	0.0222
<i>wR</i> ₂ [all data]	0.896	0.0574
largest diff peak, hole (e Å ⁻³)	2.352 and -1.422	1.077, -1.017

a. Programs for diffractometer operation, data collection, data reduction and absorption correction were those supplied by Bruker.

b. $S = [\sum w(F_o^2 - F_c^2)^2 / (n - p)]^{1/2}$ (*n* = number of data; *p* = number of parameters varied; $w = [\sigma^2(F_o^2) + (a_0P)^2 + a_1P]^{-1}$ where $P = [\text{Max}(F_o^2, 0) + 2F_c^2]/3$.

c. $R_1 = \sum |F_o| - |F_c| / \sum |F_o|$; $wR_2 = [\sum w(F_o^2 - F_c^2)^2 / \sum w(F_o^4)]^{1/2}$.

Table A.36. Crystallographic Experimental Details for Compounds **41** and **42**.

Compound	41 •CH ₂ Cl ₂	42 •2.5 C ₆ H ₆
Formula	C ₇₁ H ₆₂ Cl ₂ GeIrO ₂ P ₄ RhSi	C ₈₀ H ₇₃ GeIrO ₂ P ₄ RhSi ₂
formula weight	1537.78	1586.05
crystal dimens (mm)	0.19 × 0.17 × 0.10	0.20 × 0.15 × 0.12
crystal system	monoclinic	monoclinic
space group	<i>P2</i> ₁ / <i>n</i> (No. 14)	<i>C2/c</i> (No. 15)
unit cell param.		
<i>a</i> (Å)	19.0881(4)	20.1747 (7)
<i>b</i> (Å)	15.3613(3)	22.4687 (8)
<i>c</i> (Å)	21.5716(4)	30.2707 (11)
β (deg)	90.6440(3)	96.4467 (5)
<i>V</i> (Å ³)	6324.8 (2)	13634.9 (8)
<i>Z</i>	4	8
ρ_{calcd} (g cm ⁻³)	1.615	1.545
μ (mm ⁻¹)	3.080	2.784
diffractometer	Bruker PLATFORM/APEX II CCD ^a	Bruker D8/APEX IICCD ^a
radiation (λ Å)	Graphite-monochromated Mo K α (0.71073)	
temperature(°C)	-100	-100
scan type	ω scans (0.3°) (20s exposures)	ω scans (0.3°) (20s exposures)
$2\theta_{\text{max}}$ (deg)	55.14	55.10
total data coll.	55977 ($-24 \leq h \leq 24$, $-19 \leq k \leq 19$, $-27 \leq l \leq 28$)	59858 ($-26 \leq h \leq 25$, $-29 \leq k \leq 28$, $-39 \leq l \leq 39$)
Independ reflns (<i>R</i> _{int})	14586(0.0303)	15693 (0.0356)
obsd reflns [$I \geq 2\sigma(I)$]	12836	13333
restraints/param	0 / 755	0/ 817
goodness-of-fit (<i>S</i>) ^c	1.026	1.088
final <i>R</i> indices ^d		
<i>R</i> ₁ [$I \geq 2\sigma(I)$]	0.0205	0.0247
<i>wR</i> ₂ [all data]	0.0471	0.0677
largest diff peak, hole (e Å ⁻³)	0.658, -0.618	0.644, -0.776

a. Programs for diffractometer operation, data collection, data reduction and absorption correction were those supplied by Bruker.

b. $S = [\sum w(F_o^2 - F_c^2)^2 / (n - p)]^{1/2}$ (*n* = number of data; *p* = number of parameters varied; $w = [\sigma^2(F_o^2) + (a_0P)^2 + a_1P]^{-1}$ where $P = [\text{Max}(F_o^2, 0) + 2F_c^2]/3$.

c. $R_1 = \sum |F_o| - |F_c| / \sum |F_o|$; $wR_2 = [\sum w(F_o^2 - F_c^2)^2 / \sum w(F_o^4)]^{1/2}$.

Table A.37: Selected bond distances (\AA) of **34**

Ir(A)–Rh(A)	2.7868(3)	Rh(A)–P(4)	2.3698(10)
Ir(A)–P(1)	2.3667(10)	Rh(A)–Si(1)	2.3506(10)
Ir(A)–P(3)	2.3672(9)	Rh(A)–Si(2)	2.3684(10)
Ir(A)–Si (1)	2.3693(10)	Rh(A)–C(2)	1.862(4)
Ir(A)–Si (2)	2.4130(10)	C(1)–O(1)	1.153(4)
Ir(A)–C(1)	1.861(4)	C(2)–O(2)	1.149(4)
Rh(A)–P(2)	2.3439(10)	Si(1)–Si(2)	2.8584(14) ^a

Table A.38: Selected bond angles ($^\circ$) of **34**

Rh(A)–Ir(A)–P(1)	92.36(2)	Si(1)–Rh(A)–P(2)	82.30(3)
Rh(A)–Ir(A)–P(3)	96.71(2)	Si(1)–Rh(A)–P(4)	144.27(3)
Ir(A)–Rh(A)–P(2)	96.53(2)	Si(2)–Rh(A)–P(2)	150.58(3)
Ir(A)–Rh(A)–P(4)	90.86(2)	Si(2)–Rh(A)–P(4)	91.88(3)
Si(1)–Ir(A)–P(1)	81.58(3)	Ir(A)–Si(1)–Rh(A)	72.38(3)
Si(1)–Ir(A)–P(3)	149.99(3)	Ir(A)–Si(2)–Rh(A)	71.30(3)
Si(2)–Ir(A)–P(1)	145.47(3)	P(1)–Ir(A)–P(3)	105.83(3)
Si(2)–Ir(A)–P(3)	86.07(3)	P(2)–Rh(A)–P(4)	96.64(3)

Table A.39: Selected bond distances (\AA) of **35**

Ir(A)–Rh(A)	2.7955(3)	Rh(A)–P(4)	2.3549(9)
Ir(A)–P(1)	2.3526(8)	Rh(A)–Si(1)	2.3766(9)
Ir(A)–P(3)	2.3674(9)	Rh(A)–Si(2)	2.3705(9)
Ir(A)–Si (1)	2.3668(9)	Rh(A)–C(2)	1.860(4)
Ir(A)–Si (2)	2.3450(9)	C(1)–O(1)	1.150(4)
Ir(A)–C(1)	1.866(4)	C(2)–O(2)	1.149(4)
Rh(A)–P(2)	2.3929(8)	Si(1)–Si(2)	2.8211(13) ^a
Si(1)–H	1.35(3)	Si(2)–Cl	2.1401(12)

Table A.40: Selected bond angles ($^\circ$) of **35**

Rh(A)–Ir(A)–P(1)	96.33(2)	Si(1)–Rh(A)–P(2)	81.64(3)
Rh(A)–Ir(A)–P(3)	91.35(2)	Si(1)–Rh(A)–P(4)	150.89(3)
Ir(A)–Rh(A)–P(2)	92.59(2)	Si(2)–Rh(A)–P(2)	145.22(3)
Ir(A)–Rh(A)–P(4)	97.21(2)	Si(2)–Rh(A)–P(4)	88.51(3)
Si(1)–Ir(A)–P(1)	82.64(3)	Ir(A)–Si(1)–Rh(A)	72.22(3)
Si(1)–Ir(A)–P(3)	144.91(3)	Ir(A)–Si(2)–Rh(A)	72.71(3)
Si(2)–Ir(A)–P(1)	149.39(3)	P(1)–Ir(A)–P(3)	97.40(3)
Si(2)–Ir(A)–P(3)	91.51(3)	P(2)–Rh(A)–P(4)	103.82(3)

Table A.41: Selected bond distances (\AA) of **36**

Ir(A)–Rh(A)	2.80107(16)	Rh(A)–P(4)	2.3403(5)
Ir(A)–P(1)	2.3491(5)	Rh(A)–Si(1)	2.3673(5)
Ir(A)–P(3)	2.3637(5)	Rh(A)–Si(2)	2.4126(5)
Ir(A)–Si (1)	2.3598(6)	Rh(A)–C(2)	1.860(2)
Ir(A)–Si (2)	2.3801(5)	C(1)–O(1)	1.155(3)
Ir(A)–C(1)	1.854(2)	C(2)–O(2)	1.151(3)
Rh(A)–P(2)	2.3835(5)	Si(1)–Si(2)	2.8755(8) ^a
Si(1)–H	1.38(9)	Si(2)–C(100)	1.911(2)

Table A.42: Selected bond angles ($^\circ$) of **36**

Rh(A)–Ir(A)–P(1)	96.270(13)	Si(1)–Rh(A)–P(2)	82.523(17)
Rh(A)–Ir(A)–P(3)	91.082(13)	Si(1)–Rh(A)–P(4)	150.849(19)
Ir(A)–Rh(A)–P(2)	92.560(12)	Si(2)–Rh(A)–P(2)	145.998(18)
Ir(A)–Rh(A)–P(4)	97.478(13)	Si(2)–Rh(A)–P(4)	86.369(18)
Si(1)–Ir(A)–P(1)	83.686(18)	Ir(A)–Si(1)–Rh(A)	72.677(16)
Si(1)–Ir(A)–P(3)	144.658(18)	Ir(A)–Si(2)–Rh(A)	71.523(15)
Si(2)–Ir(A)–P(1)	150.546(18)	P(1)–Ir(A)–P(3)	98.265(18)
Si(2)–Ir(A)–P(3)	88.532(18)	P(2)–Rh(A)–P(4)	104.184(17)

Table A.43: Selected bond distances (\AA) of **37**

Ir(A)–Rh(A)	2.8144(3)	Rh(A)–P(4)	2.3593(9)
Ir(A)–P(1)	2.3435(9)	Rh(A)–Si(1)	2.3586(10)
Ir(A)–P(3)	2.3843(9)	Rh(A)–Si(2)	2.3790(10)
Ir(A)–Si (1)	2.3575(10)	Rh(A)–C(2)	1.870(4)
Ir(A)–Si (2)	2.3953(10)	C(1)–O(1)	1.154(5)
Ir(A)–C(1)	1.858(4)	C(2)–O(2)	1.145(5)
Rh(A)–P(2)	2.3614(9)	Si(1)–Si(2)	2.8653(14) ^a
Si(1)–H	1.43(2)		

Table A.44: Selected bond angles ($^\circ$) of **37**

Rh(A)–Ir(A)–P(1)	94.96(2)	Si(1)–Rh(A)–P(2)	146.53(3)
Rh(A)–Ir(A)–P(3)	93.03(2)	Si(1)–Rh(A)–P(4)	81.11(3)
Ir(A)–Rh(A)–P(2)	93.38(2)	Si(2)–Rh(A)–P(2)	89.41(3)
Ir(A)–Rh(A)–P(4)	95.94(2)	Si(2)–Rh(A)–P(4)	149.07(3)
Si(1)–Ir(A)–P(1)	148.29(3)	Ir(A)–Si(1)–Rh(A)	73.28(3)
Si(1)–Ir(A)–P(3)	81.30(3)	Ir(A)–Si(2)–Rh(A)	72.24(3)
Si(2)–Ir(A)–P(1)	88.73(3)	P(1)–Ir(A)–P(3)	100.93(3)
Si(2)–Ir(A)–P(3)	146.18(3)	P(2)–Rh(A)–P(4)	101.29(3)

Table A.45: Selected bond distances (Å) of **39**

Ir(A)–Rh(A)	2.80310(19)	Rh(A)–P(4)	2.3685(6)
Ir(A)–P(1)	2.3282(6)	Rh(A)–Si*	2.4041(5)
Ir(A)–P(3)	2.3671(6)	Rh(A)–Ge	2.4900(3)
Ir(A)–Si*	2.3831(5)	Rh(A)–C(2)	1.867(2)
Ir(A)–Ge	2.4475(3)	C(1)–O(1)	1.153(3)
Ir(A)–C(1)	1.863(2)	C(2)–O(2)	1.151(3)
Rh(A)–P(2)	2.3529(6)	Si*–Ge	2.95(8) ^a
Si*–H	1.35(3)		

* Si position was refined with a site occupancy of Si_{0.75}Ge_{0.25}

Table A.46: Selected bond angles (°) of **39**

Rh(A)–Ir(A)–P(1)	96.473(14)	Si*–Rh(A)–P(2)	81.619(18)
Rh(A)–Ir(A)–P(3)	90.940(14)	Si*–Rh(A)–P(4)	149.922(18)
Ir(A)–Rh(A)–P(2)	92.219(14)	Ge–Rh(A)–P(2)	146.475(16)
Ir(A)–Rh(A)–P(4)	96.434(14)	Ge–Rh(A)–P(4)	84.808(16)
Si*–Ir(A)–P(1)	82.264(18)	Ir(A)–Si*–Rh(A)	71.680(13)
Si*–Ir(A)–P(3)	144.840(18)	Ir(A)–Ge–Rh(A)	69.176(7)
Ge–Ir(A)–P(1)	151.596(16)	P(1)–Ir(A)–P(3)	97.16(2)
Ge–Ir(A)–P(3)	91.166(16)	P(2)–Rh(A)–P(4)	106.49(2)

* Si position was refined with a site occupancy of Si_{0.75}Ge_{0.25}

Table A.47: Selected bond distances (Å) of **41**

Ir(A)–Rh(A)	2.79851(15)	Rh(A)–P(4)	2.3543(5)
Ir(A)–P(1)	2.3739(5)	Rh(A)–Si	2.3713(5)
Ir(A)–P(3)	2.3489(5)	Rh(A)–Ge	2.4360(2)
Ir(A)–Si	2.4166(6)	Rh(A)–C(2)	1.866(2)
Ir(A)–Ge	2.4360(2)	C(1)–O(1)	1.156(3)
Ir(A)–C(1)	1.863(2)	C(2)–O(2)	1.150(3)
Rh(A)–P(2)	2.3514(5)	Si–Ge	2.9255(6) ^a
Ge–H	1.44(6)		

Table A.48: Selected bond angles (°) of **41**

Rh(A)–Ir(A)–P(1)	92.393(13)	Ge–Rh(A)–P(2)	82.227(14)
Rh(A)–Ir(A)–P(3)	96.663(13)	Ge–Rh(A)–P(4)	145.486(14)
Ir(A)–Rh(A)–P(2)	96.399(13)	Si–Rh(A)–P(2)	150.354(19)
Ir(A)–Rh(A)–P(4)	90.708(13)	Si–Rh(A)–P(4)	91.706(19)
Ge–Ir(A)–P(1)	81.625(14)	Ir(A)–Si–Rh(A)	71.528(15)
Ge–Ir(A)–P(3)	151.146(14)	Ir(A)–Ge–Rh(A)	69.790(7)
Si–Ir(A)–P(1)	145.370(18)	P(1)–Ir(A)–P(3)	106.015(19)
Si–Ir(A)–P(3)	85.979(19)	P(2)–Rh(A)–P(4)	96.713(19)

Table A.49: Selected bond distances (Å) of **42**

Ir(A)–Rh(A)	2.8061(2)	Rh(A)–P(4)	2.3207(7)
Ir(A)–P(1)	2.3488(6)	Rh(A)–Si	2.4118(7)
Ir(A)–P(3)	2.3451(7)	Rh(A)–Ge	2.4437(3)
Ir(A)–Si	2.3780(7)	Rh(A)–C(2)	1.860(3)
Ir(A)–Ge	2.4421(3)	C(1)–O(1)	1.154(4)
Ir(A)–C(1)	1.856(3)	C(2)–O(2)	1.151(3)
Rh(A)–P(2)	2.3861(6)	Si–Ge	2.9322(7) ^a
Ge–H	1.49(3)		

Table A.50: Selected bond angles (°) of **42**

Rh(A)–Ir(A)–P(1)	96.349(17)	Ge–Rh(A)–P(2)	82.741(17)
Rh(A)–Ir(A)–P(3)	90.967(17)	Ge–Rh(A)–P(4)	152.038(19)
Ir(A)–Rh(A)–P(2)	92.420(17)	Si–Rh(A)–P(2)	145.75(2)
Ir(A)–Rh(A)–P(4)	97.376(18)	Si–Rh(A)–P(4)	86.21(2)
Ge–Ir(A)–P(1)	83.960(18)	Ir(A)–Si–Rh(A)	71.722(19)
Ge–Ir(A)–P(3)	145.791(19)	Ir(A)–Ge–Rh(A)	70.106(8)
Si–Ir(A)–P(1)	150.56(2)	P(1)–Ir(A)–P(3)	98.37(2)
Si–Ir(A)–P(3)	88.34(2)	P(2)–Rh(A)–P(4)	104.29(2)

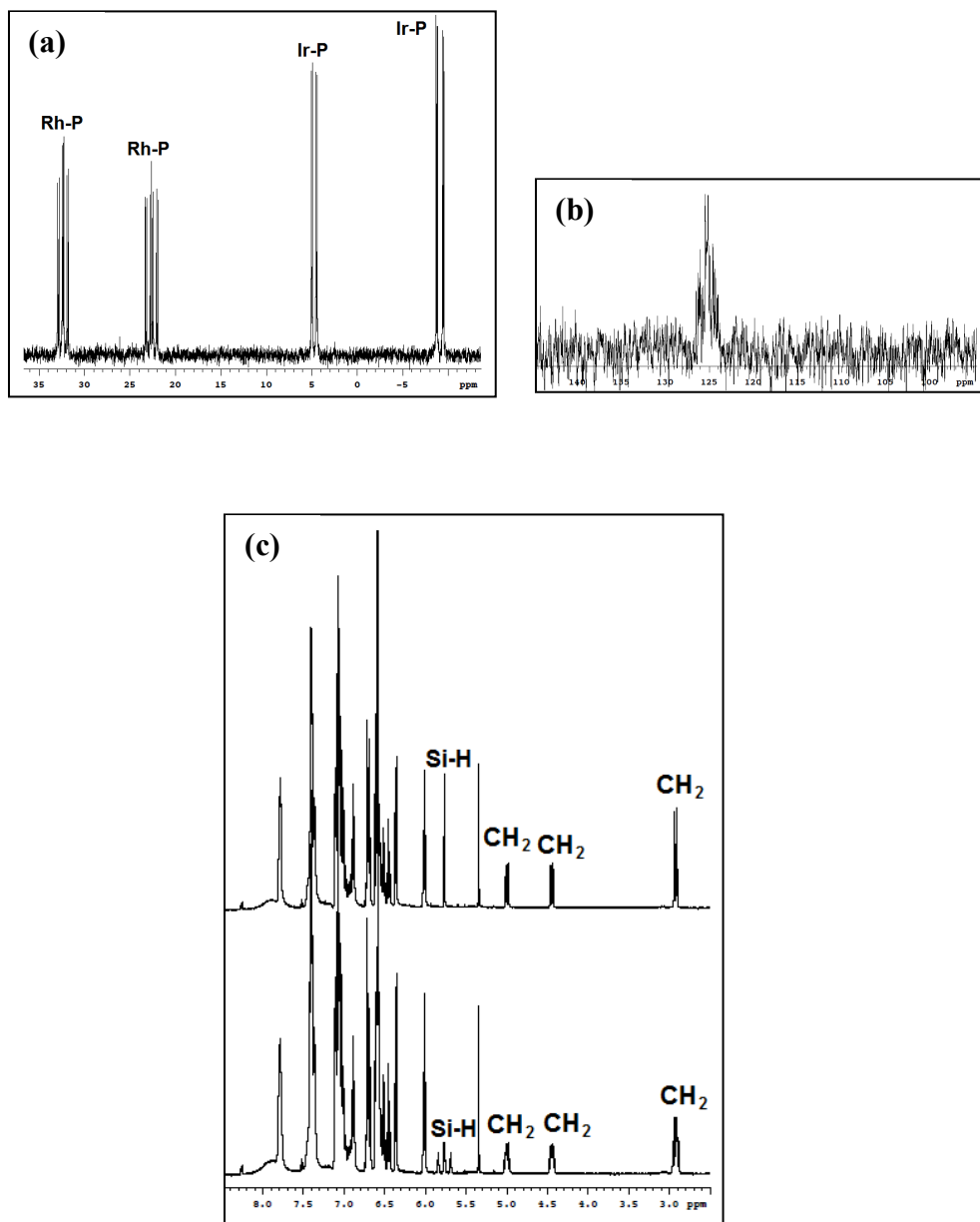


Figure A.17: (a) $^{31}\text{P}\{^1\text{H}\}$ NMR spectrum of compound **34** in CD_2Cl_2 at 27°C . (b) $^{29}\text{Si}\{^1\text{H}\}$ NMR spectrum for complex **34** at 27°C . (c) ^1H (below) and $^1\text{H}\{^{31}\text{P}\}$ (above) NMR spectrum of **34** in CH_2Cl_2 .

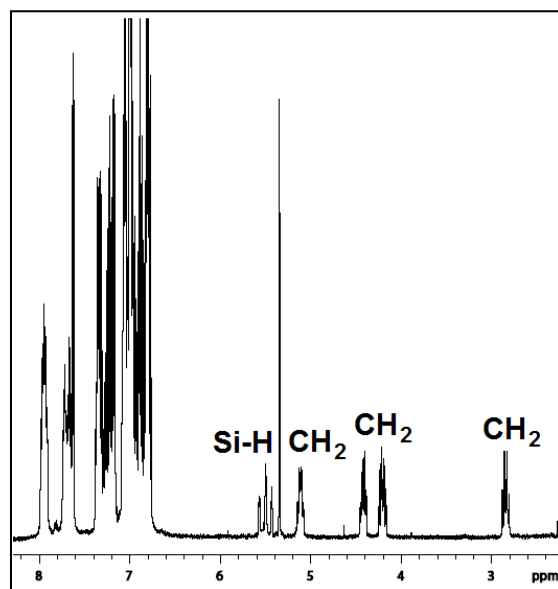
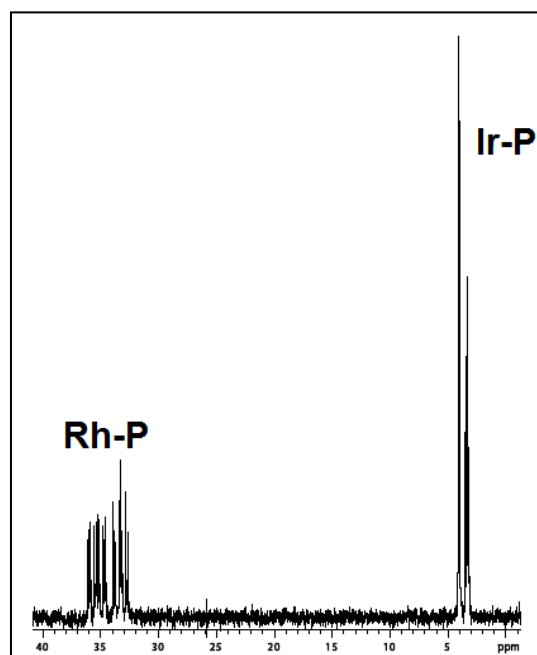


Figure A.18: $^{31}\text{P}\{^1\text{H}\}$ (above) and ^1H NMR (below) spectrum of compound **35** in CD_2Cl_2 at 27°C .

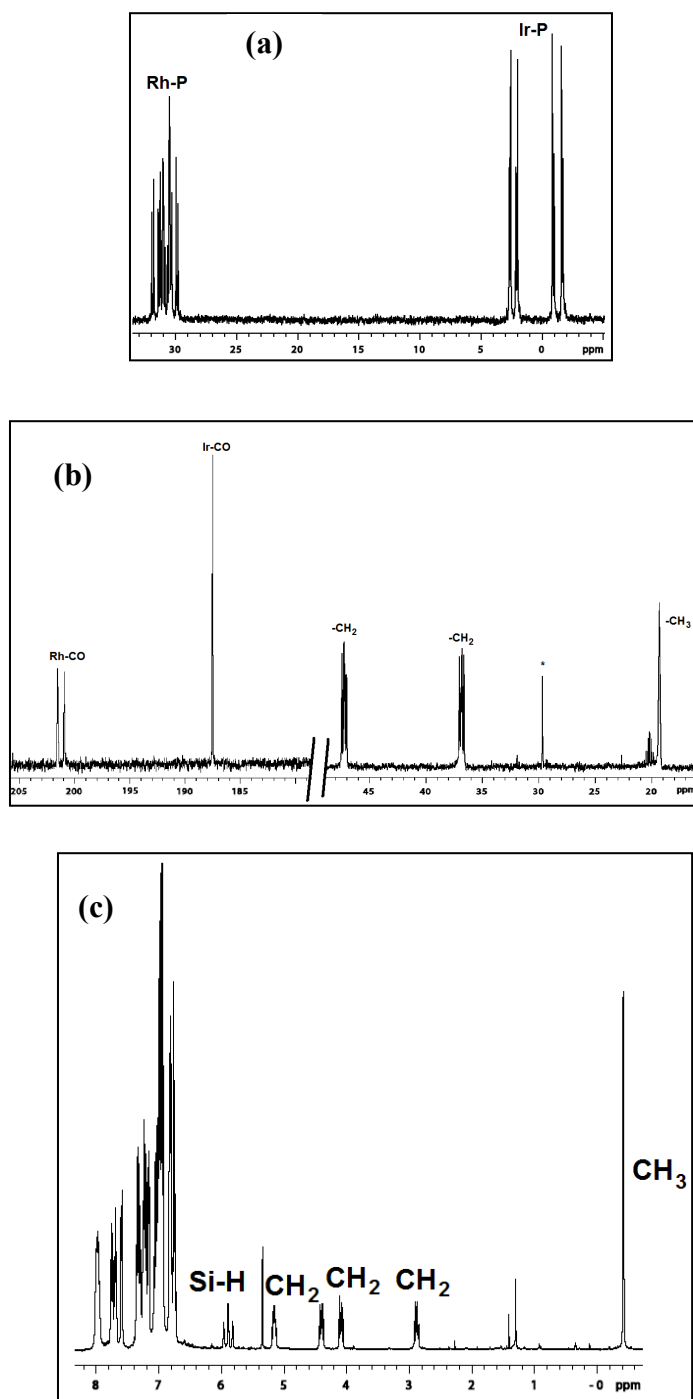


Figure A.19: (a) $^{31}\text{P}\{^1\text{H}\}$ NMR spectrum of compound **36** in CD_2Cl_2 at 27°C . (b) Selected regions of the $^{13}\text{C}\{^1\text{H}\}$ NMR spectrum of compound **36** in CD_2Cl_2 at 27°C . (c) ^1H NMR spectrum of compound **36** in CD_2Cl_2 at 27°C .

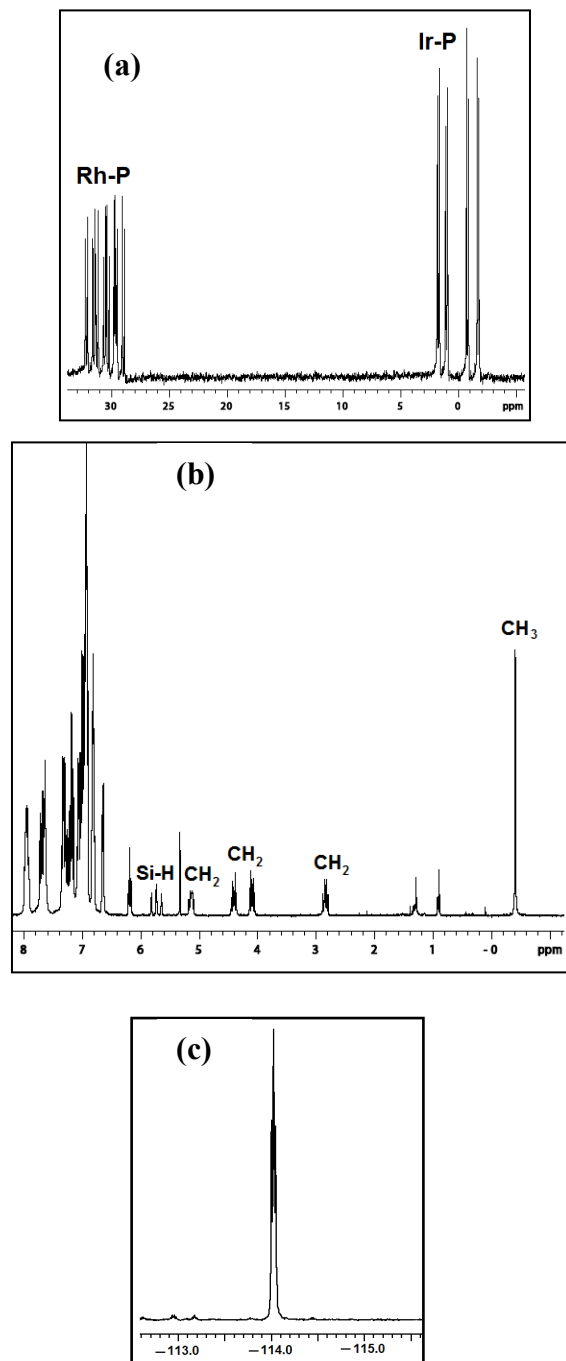


Figure A.20: (a) $^{31}\text{P}\{^1\text{H}\}$; (b) ^1H NMR; and (c) ^{19}F NMR spectra of compound 37 in CD_2Cl_2 at 27 $^\circ\text{C}$.

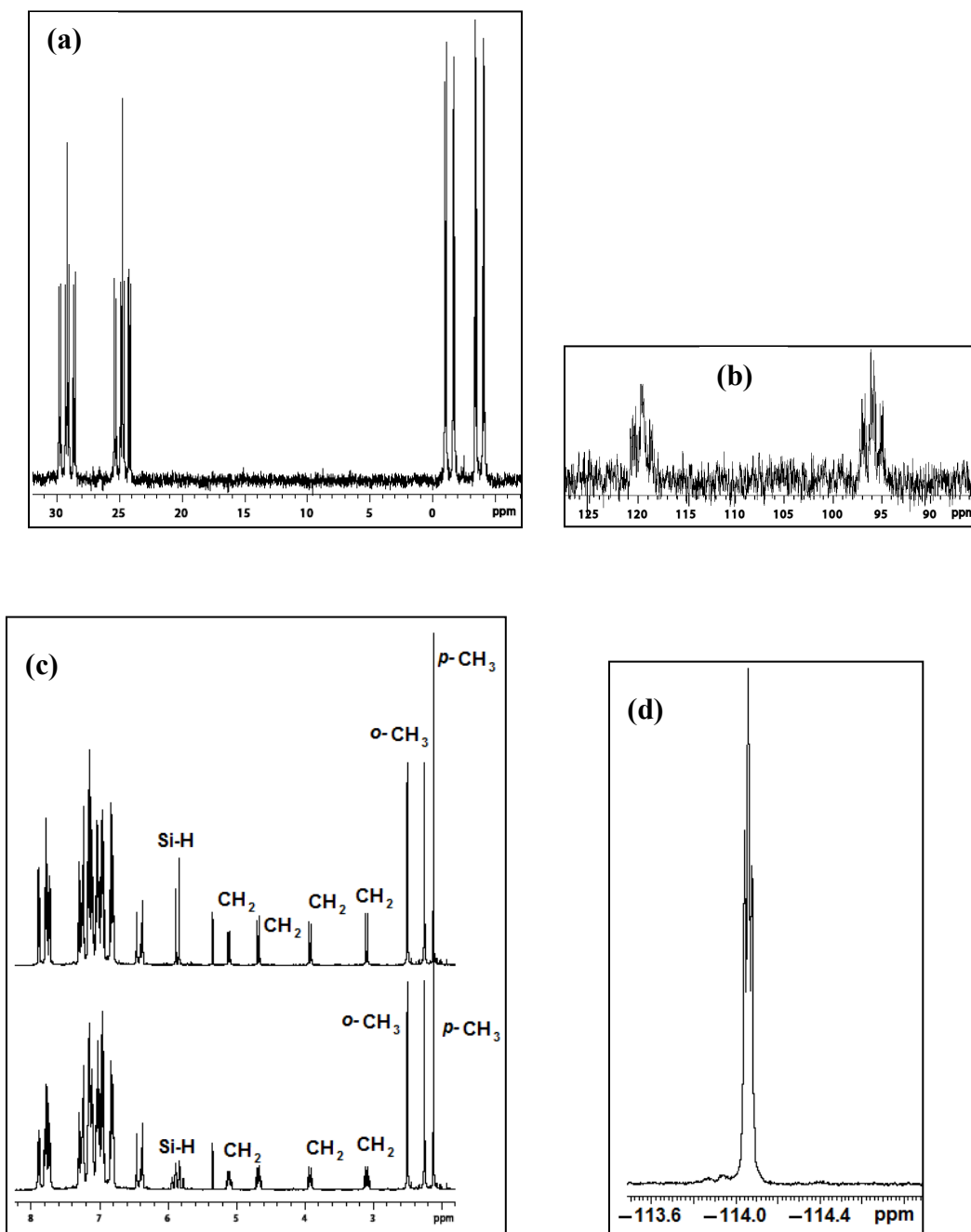


Figure A.21: (a) $^{31}\text{P}\{^1\text{H}\}$; (b) $^{29}\text{Si}\{^1\text{H}\}$; (c) ^1H (below) and $^1\text{H}\{^{31}\text{P}\}$ (above); (d) ^{19}F NMR spectra of compound **38** in CD_2Cl_2 at 27°C .

Appendix IV – For Chapter 5

Table A.51. Crystallographic Experimental Details for Compounds 48, 49 and 51.

	48	49	51
Formula	C ₃₀ H ₅₆ IrO ₃ P ₄ RhSi	C ₃₂ H ₅₆ IrO ₂ P ₄ RhSi	C ₄₉ H ₅₄ IrO ₄ P ₂ RhSi ₃
formula weight	911.83	919.85	1148.24
crystal dimens (mm)	0.42 × 0.30 × 0.15	0.35 × 0.112 × 0.09	0.46 × 0.25 × 0.16
crystal system	monoclinic	monoclinic	monoclinic
space group	<i>P</i> 2 ₁ / <i>n</i> (No. 14)	<i>P</i> 2 ₁ / <i>n</i> (No. 14)	<i>I</i> 2/ <i>a</i> (No. 15)
unit cell parameters			
<i>a</i> (Å)	11.5032 (4)	10.0265 (4)	20.6418 (9)
<i>b</i> (Å)	17.1496 (6)	15.2613 (7)	10.9486 (5)
<i>c</i> (Å)	18.5262 (6)	24.6102 (11)	20.9305 (9)
β (deg)	97.0573 (4)	93.7340 (10)	92.8670 (10)
<i>V</i> (Å ³)	3627.1 (2)	3757.8 (3)	4724.3 (4)
<i>Z</i>	4	4	4
ρ_{calcd} (g cm ⁻³)	1.670	1.626	1.614
μ (mm ⁻¹)	4.358	4.205	3.350
diffractometer	Bruker D8/APEX II CCD ^a		Bruker PLATFORM/APEX II CCD ^a
radiation (λ [Å])	graphite-monochromated Mo K α (0.71073)		
temperature (°C)	-100	-100	-100
scan type	ω scans (0.3°) (20s exposures)	ω scans (0.3°) (20 s exposures)	ω scans (0.3°) (20 s exposures)
$2\theta_{\text{max}}$ (deg)	54.96	52.92	55.02
total data collected	31560 ($-14 \leq h \leq 22$, $-22 \leq k \leq 22$, $-23 \leq l \leq 23$)	30044 ($-12 \leq h \leq 12$, $-19 \leq k \leq 19$, $-30 \leq l \leq 30$)	20792 ($-26 \leq h \leq 26$, $-14 \leq k \leq 14$, $-27 \leq l \leq 27$)
Independ reflns (<i>R</i> _{int})	8293 (0.0161)	7746 (0.0291)	5423 (0.0115)
obsd reflns [<i>I</i> ≥ 2 σ (<i>I</i>)]	7933	6424	4895
restraints/params	0 / 367	0/ 370	1/ 334
goodness-of-fit (<i>S</i>) ^b	1.107	1.026	1.039
final <i>R</i> indices ^c			
<i>R</i> ₁ [<i>I</i> ≥ 2 σ (<i>I</i>)]	0.0178	0.0262	0.0171
<i>wR</i> ₂ [all data]	0.0450	0.0617	0.0434
largest diff peak, hole (e Å ⁻³)	0.572, -0.471	1.508, -1.023	0.771, -0.475

a. Programs for diffractometer operation, data collection, data reduction and absorption correction were those supplied by Bruker.

b. $S = [\sum w(F_o^2 - F_c^2)^2 / (n - p)]^{1/2}$ (n = number of data; p = number of parameters varied; $w = [\sigma^2(F_o^2) + (a_0P)^2 + a_1P]^{-1}$ where $P = [\text{Max}(F_o^2, 0) + 2F_c^2]/3$.

c. $R_1 = \sum ||F_o| - |F_c|| / \sum |F_o|$; $wR_2 = [\sum w(F_o^2 - F_c^2)^2 / \sum w(F_o^4)]^{1/2}$.

Table A.52: Selected bond distances (\AA) of **48**

Ir–Rh	2.69614(16)	Rh–P(4)	2.3677(5)
Ir–P(1)	2.3655(6)	Rh–Si	2.3759(6)
Ir–P(3)	2.3608(6)	Rh–C(3)	2.061(2)
Ir–Si	2.3874(6)	Rh(A)–C(2)	1.875(2)
Ir–C(3)	2.047(2)	C(1)–O(1)	1.148(3)
Ir–C(1)	1.877(2)	C(2)–O(2)	1.143(3)
Rh–P(2)	2.3510(6)	C(3)–O(3)	1.190(3)

Table A.53: Selected bond angles ($^\circ$) of **48**

Rh(A)–Ir(A)–P(1)	93.866(14)	Si–Rh(A)–P(2)	151.07(2)
Rh(A)–Ir(A)–P(3)	94.406(14)	Si–Rh(A)–P(4)	89.15(2)
Ir(A)–Rh(A)–P(2)	96.704(14)	C(3)–Rh(A)–P(2)	84.76(6)
Ir(A)–Rh(A)–P(4)	94.882(14)	C(3)–Rh(A)–P(4)	143.62(6)
Si–Ir(A)–P(1)	147.95(2)	Ir(A)–Si–Rh(A)	68.946(16)
Si–Ir(A)–P(3)	91.07(2)	Ir(A)–C(3)–Rh(A)	82.05(8)
C(3)–Ir(A)–P(1)	82.71(6)	P(1)–Ir(A)–P(3)	100.92(2)
C(3)–Ir(A)–P(3)	143.58(6)	P(2)–Rh(A)–P(4)	103.12(2)

Table A.54: Selected bond distances (\AA) of **49**

Ir(A)–Rh(A)	2.8829(3)	Rh(A)–P(4)	2.3464(9)
Ir(A)–P(1)	2.3448(9)	Rh(A)–Si	2.3526(9)
Ir(A)–P(3)	2.3645(9)	Rh(A)–H(1)	1.58(8)
Ir(A)–Si	2.3485(9)	Rh(A)–C(2)	1.843(4)
Ir(A)–H(1)	1.59(3)	C(1)–O(1)	1.141(5)
Ir(A)–C(1)	1.864(4)	C(2)–O(2)	1.157(5)
Rh(A)–P(2)	2.3314(9)		

Table A.55: Selected bond angles ($^\circ$) of **49**

Rh(A)–Ir(A)–P(1)	93.10(2)	Si–Rh(A)–P(2)	103.71(3)
Rh(A)–Ir(A)–P(3)	94.87(3)	Si–Rh(A)–P(4)	132.68(3)
Ir(A)–Rh(A)–P(2)	88.66(2)	Ir(A)–Rh(A)–C(2)	153.43(11)
Ir(A)–Rh(A)–P(4)	89.06(3)	Rh(A)–Ir(A)–C(1)	153.50(12)
Si–Ir(A)–P(1)	93.96(3)	P(1)–Ir(A)–P(3)	104.73(3)
Si–Ir(A)–P(3)	143.36(3)	P(2)–Rh(A)–P(4)	100.72(3)
Ir(A)–Si–Rh(A)	75.65(3)		

Table A.56: Selected bond distances (Å) of **51**

Ir(A)–Rh(A)	2.8973(14)	Rh(A)–Si(1')	2.410(3)
Ir(A)–P(1)	2.3889(14)	Rh(A)–Si(2)	2.3989(19)
Ir(A)–Si(1)	2.4134(13)	Rh(A)–C(3)	1.981(11)
Ir(A)–Si(2)	2.4009(10)	Rh(A)–C(4)	1.80(2)
Ir(A)–C(1)	1.885(8)	C(1)–O(1)	1.22(3)
Ir(A)–C(2)	1.92(2)	C(2)–O(2)	1.16(3)
Rh(A)–P(2)	2.3608(17)	C(3)–O(3)	1.09(3)
		C(4)–O(4)	1.13(3)

Table A.57: Selected bond angles (°) of **51**

Rh(A)–Ir(A)–P(1)	89.20(8)	Si(1')–Rh(A)–P(2)	99.86(11)
Rh(A)–Ir(A)–Si(1)	160.58(3)	Si(2)–Rh(A)–P(2)	147.86(13)
Rh(A)–Ir(A)–Si(2)	52.84(3)	Si(1)–Ir(A)–Si(2)	110.72(3)
Ir(A)–Rh(A)–Si(1')	159.27(7)	Si(1')–Rh(A)–Si(2)	110.90(5)
Ir(A)–Rh(A)–Si(2)	52.90(5)	C(1)–Ir(A)–C(2)	171.9(9)
Si(1)–Ir(A)–P(1)	108.35(8)	C(2)–Rh(A)–C(4)	166.5(9)
Si(2)–Ir(A)–P(1)	140.79(9)		

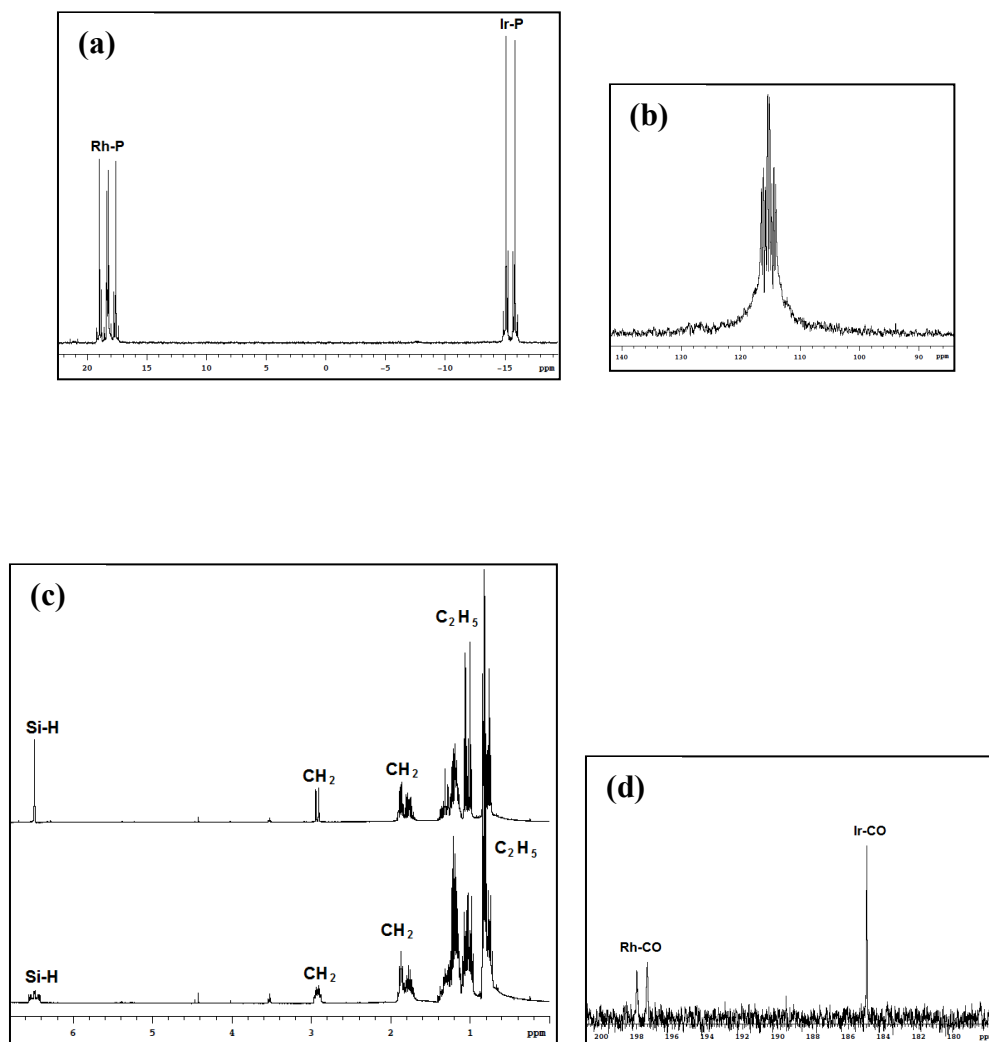


Figure A.22: (a) $^{31}\text{P}\{^1\text{H}\}$ NMR spectrum of Compound 47 in C_6D_6 at 27°C ; (b) $^{29}\text{Si}\{^1\text{H}\}$ NMR spectrum for complex 47 in C_6D_6 at 27°C ; (c) ^1H (below) and $^1\text{H}\{^31\text{P}\}$ (above) NMR spectra of 47 in C_6D_6 at 27°C ; and (d) Selected region of $^{13}\text{C}\{^1\text{H}\}$ NMR spectrum of compound 47 in C_6D_6 at 27°C displaying CO peaks.

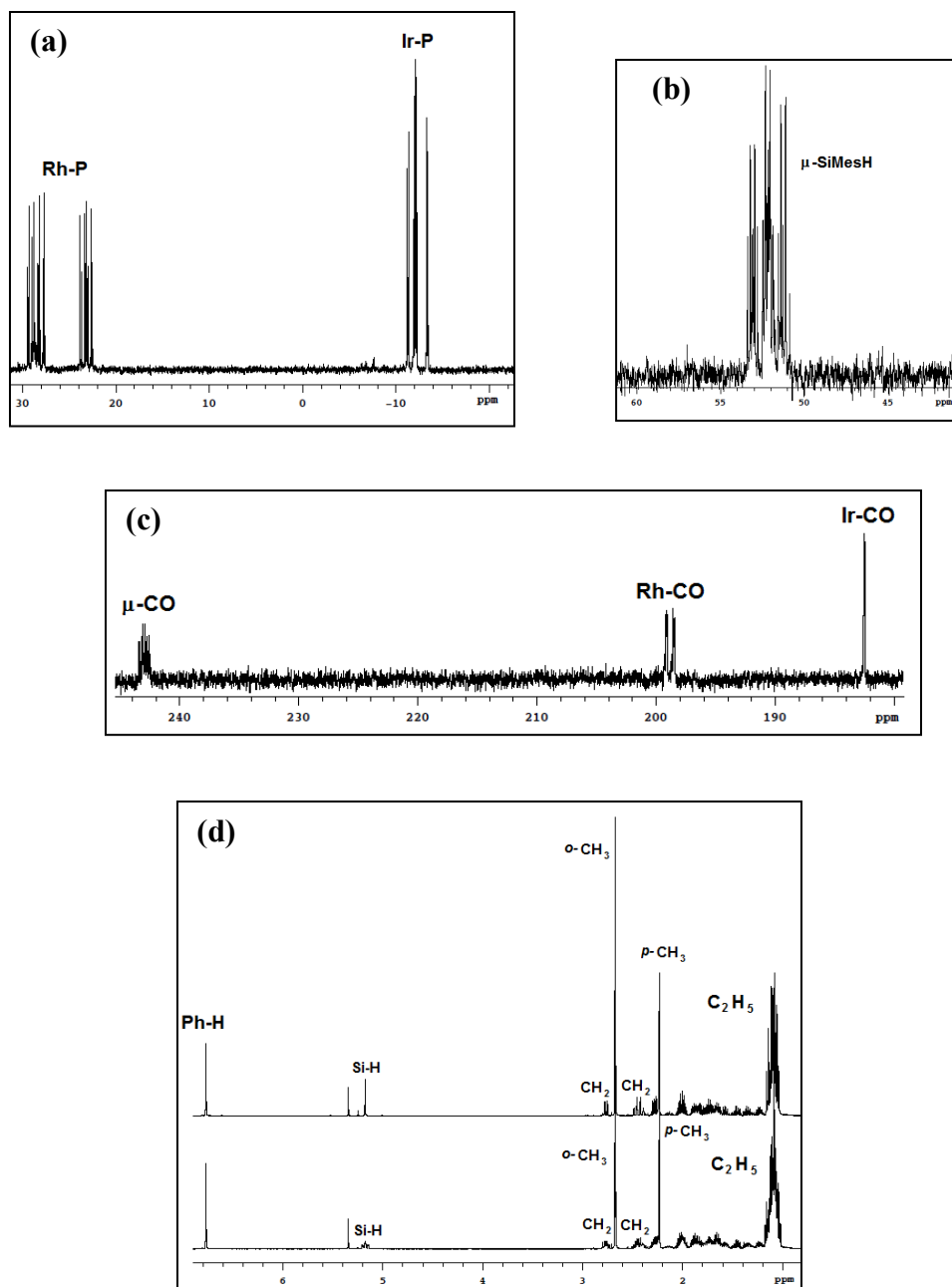


Figure A.23: (a) $^{31}\text{P}\{^1\text{H}\}$ NMR spectrum of compound **5** in CD_2Cl_2 at 27°C ; (b) $^{29}\text{Si}\{^1\text{H}\}$ NMR spectrum for complex **48** in CD_2Cl_2 at 27°C ; (c) Selected region of $^{13}\text{C}\{^1\text{H}\}$ NMR spectrum of compound **48** in CD_2Cl_2 at 27°C displaying CO peaks; and (d) ^1H (below) and $^1\text{H}\{^{31}\text{P}\}$ (above) NMR spectra of **48** in CD_2Cl_2 at 27°C .

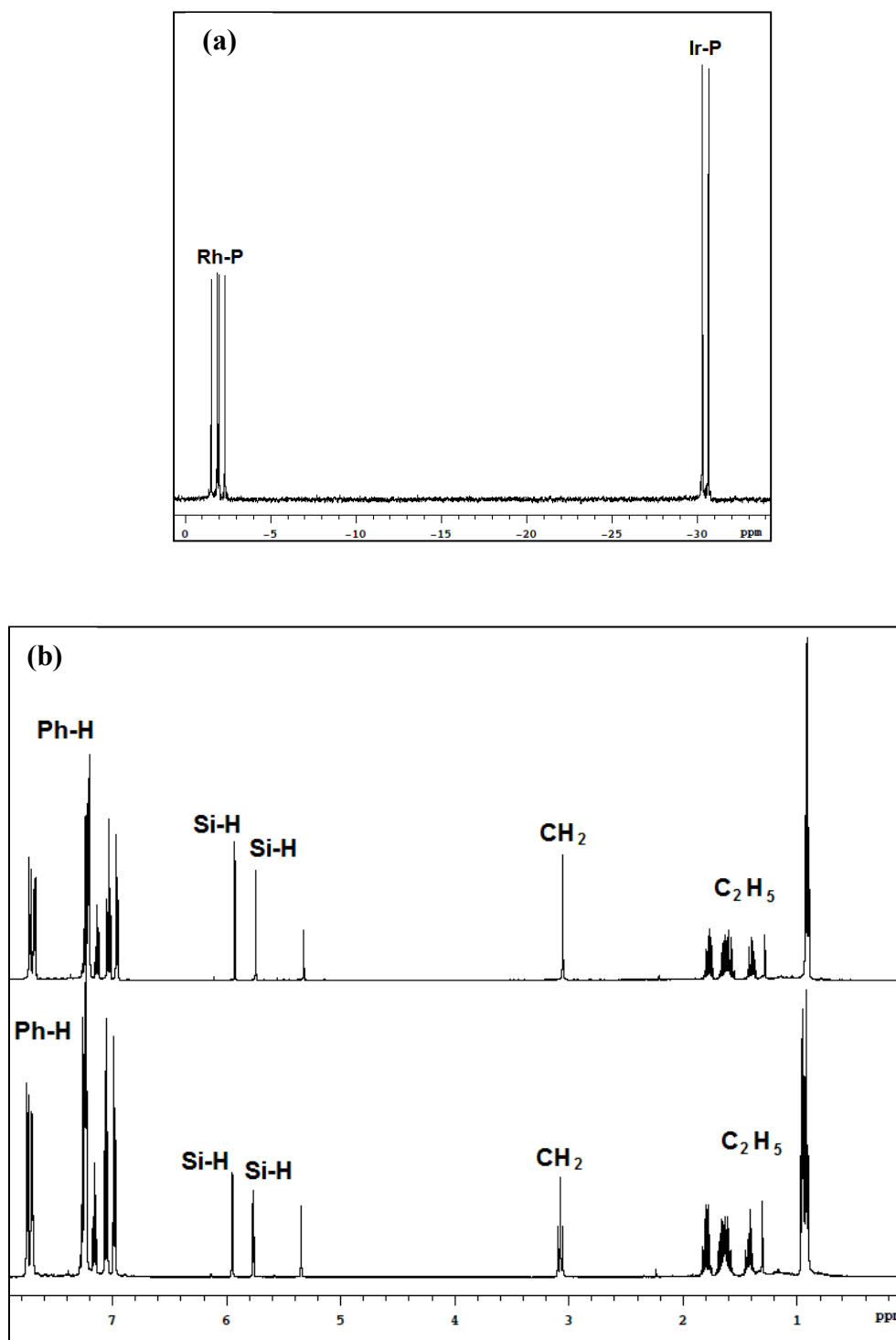


Figure A.24: (a) $^{31}\text{P}\{^1\text{H}\}$ NMR spectrum of compound **51** in CD_2Cl_2 at 27°C ; and (b) ^1H (below) and broadband $^1\text{H}\{^{31}\text{P}\}$ (above) NMR spectra of **51** in CD_2Cl_2 at 27°C .

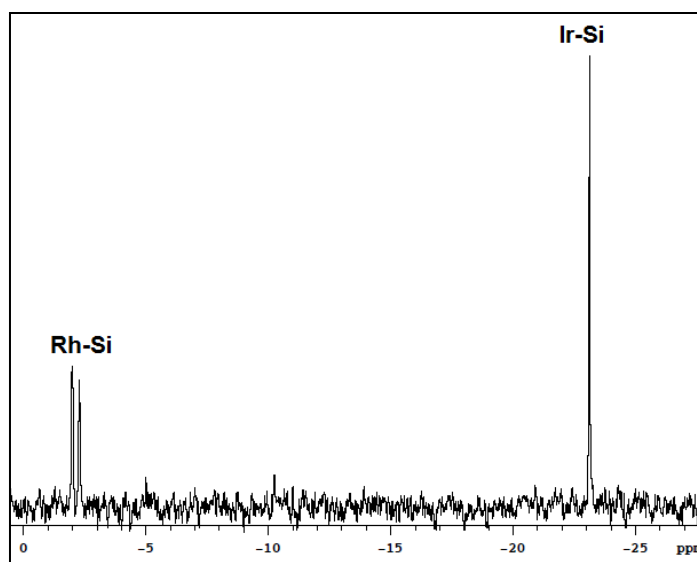
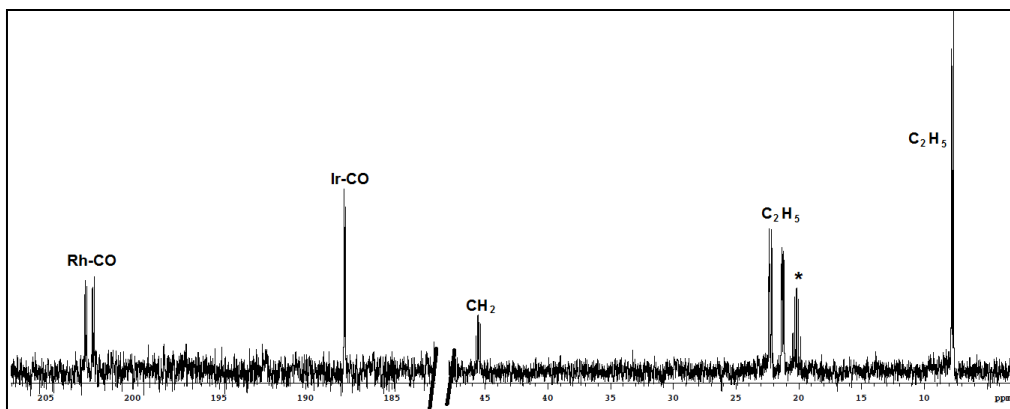


Figure A.25: (a) Selected region of $^{13}\text{C}\{^1\text{H}\}$ NMR spectrum of compound **51** in CD_2Cl_2 at 27°C displaying CO and depm carbon peaks; and (b) Selected region of $^{29}\text{Si}\{^1\text{H}\}$ NMR spectrum for complex **51** in CD_2Cl_2 at 27°C displaying terminal silyl groups.

Appendix V – Crystallographic Data

Structure reports, crystallographic information files (CIFs) and Check CIF reports for the structures shown in Chapters 2 – 5 can be obtained free of charge by contacting either Dr. Robert McDonald or Dr. Michael J. Ferguson at the address below and quoting the internal reference number(s) for the appropriate compound(s) provided below:

X-ray Crystallography Laboratory (Room E 3–13)
Department of Chemistry, University of Alberta
11227 Saskatchewan Drive NW
Edmonton AB Canada T6G 2G2
Tel: 1 780 492 2485 Fax: 1 780 492 8231
E-mail: bob.mcdonald@ualberta.ca
michael.ferguson@ualberta.ca

Chapter 2	
Compound Number	Internal Reference Code
4	Cow0837
5	Cow0922
8a	Cow1003
8b	Cow1005
8c	Cow1026
12	Cow9804

Chapter 3	
Compound Number	Internal Reference Code
20	Cow1035
21	Cow1029
23	Cow1127
24	Cow1105
25	Cow1106
28	Cow1110
29	Cow1115
30	Cow1109
31	Cow1120

Chapter 4	
Compound Number	Internal Reference Code
34	Cow1131
35	Cow1132
36	Cow1135
37	Cow1201
39	Cow1128
41	Cow1129
42	Cow1146

Chapter 5	
Compound Number	Internal Reference Code
48	Cow1143
49	Cow1141
51	Cow1126

Appendix VI – Drying Agents for Solvents

Solvents

Acetone

Acetonitrile

Benzene

Dichloromethane

Diethyl ether

Fluorobenzene

Methanol

n-Pentane

Tetrahydrofuran

Toluene

Drying Agents

calcium chloride/benzophenone

calcium hydride

sodium metal (Na)/benzophenone

phosphorus pentoxide

sodium metal (Na)/benzophenone

sodium metal (Na)/benzophenone

magnesium sulphate

calcium hydride

sodium metal (Na)/benzophenone

sodium metal (Na)/benzophenone

Appendix VII – Acknowledgements

Chapter 1 Acknowledgements

Martin Cowie assisted with editing and revising.

Chapter 2 Acknowledgements

Okemona Oke initiated the reactivity study of diphenylsilane with Complex **1** and **2**. Robert McDonald and Michael J. Ferguson carried out crystallographic analysis. Albin Otter, Mark Miskolzie and Nupur Dabral assisted with low-temperature NMR analysis. Martin Cowie supervised the project and assisted with revising and editing.

Chapter 3 Acknowledgements

Michael J. Ferguson and Robert McDonald carried out crystallographic analysis. Mark Miskolzie and Nupur Dabral assisted with low-temperature NMR analysis. Martin Cowie supervised the project and assisted with revising and editing.

Chapter 4 Acknowledgements

Michael J. Ferguson and Robert McDonald carried out crystallographic analysis. Martin Cowie supervised the project and assisted with revising and editing.

Chapter 5 Acknowledgements

Michael J. Ferguson carried out crystallographic analysis. Martin Cowie supervised the project and assisted with revising and editing.

Chapter 6 Acknowledgements

Martin Cowie assisted with revising and editing.